Photoinduced Charge-Transfer Processes in Redox Cascades based on Triarylamine Donors and the Perchlorinated Triphenylmethyl Radical Acceptor

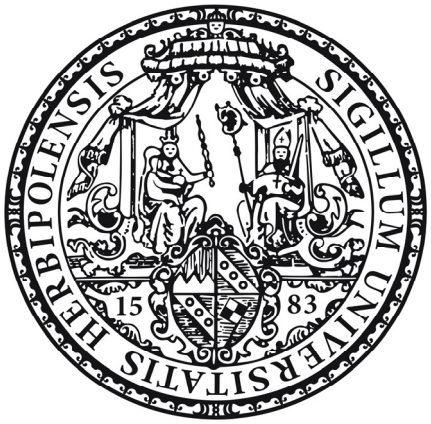

Dissertation zur Erlangung des
naturwissenschaftlichen Doktorgrades
der Julius-Maximillians-Universität Würzburg

vorgelegt von
Nina Dürrbeck
aus Bad Kissingen

Würzburg 2013

Eingereicht am: _____

bei der Fakultät für Chemie und Pharmazie

1.Gutachter: _____

2.Gutachter: _____

der Dissertation

1. Prüfer: _____

2. Prüfer: _____

3. Prüfer: _____

des öffentlichen Promotionskolloquiums

Tag des öffentlichen Promotionskolloquiums: _____

Doktorkunde ausgehändigt am: _____

Die vorliegende Arbeit wurde in der Zeit von November 2007 bis Oktober 2013
am Institut für Organische Chemie der Universität Würzburg angefertigt.

Mein besonderer Dank gilt

Herrn Prof. Dr. Christoph Lambert

für die Überlassung des äußerst vielseitigen und interessanten Themas und
das mit vielen Anregungen verbundene Interesse an dieser Arbeit.

Table of Contents

List of Abbreviations

AlO_x	neutral aluminium oxide
^{t}BME	*t*-butyl methyl ether
CT	charge transfer
CS	charge separated
CV	cyclic voltammetry
dba	dibenzylideneacetone
DDQ	2,3-dichloro-5,6-dicyano-1,4-benzoquinone
DMF	*N*,*N*-dimethylformamide
DMSO	dimethylsulfoxide
DPP	diketopyrrolopyrrole
DPPH	2,2-diphenyl-1-picrylhydrazyl
ESI	electrospray ionisation
ESR	electron spin resonance
ET	electron transfer
EtOAc	ethyl acetate
EtOH	ethanol
Fc	ferrocene
GPC	gel permeation chromatography
HOMO	highest occupied molecular orbital
HT	hole transfer
IVCT	intervalence charge transfer
LDA	lithium di-*i*-propyl amine
LUMO	lowest unoccupied molecular orbital
MALDI	matrix assisted laser desorption/ionisation
MeCN	acetonitrile
MeOH	methanol
MOROF	metal organic radical open framework
NIR	near infrared
NMR	nuclear magnetic resonance
OD	optical density
OFET	organic field effect transistor
OLED	organic light emitting diode
OPV	organic photovoltaic device
PCA	*p*-chloranil
PCDM	perchlorodiphenylmethane

PCTM	perchlorotriphenylmethane
PCPF	perchloro-9-phenylfluorene
PE	petrol ether
PES	potential energy surface
PET	photoinduced electron transfer
PhCN	benzonitrile
POROF	pure organic radical open framework
RT	room temperature
SAM	self-assembled monolayer
SEC	spectroelectrochemistry
SET	single electron transfer
SOMO	singly occupied molecular orbital
TCTM	tris(2,4,6-trichlorophenyl)methane
TFA	trifluoroacetic acid
THF	tetrahydrofurane
TMS	tetramethylsilane
TMSA	trimethylsilylacetylene
TosOH	*p*-toluenesulfonic acid
$T^{i}PSA$	tri-*i*-propylsilylacetylene
UV	ultraviolet
vis	visible

1 Introduction

Photoinduced charge transfer is probably one of the most fundamental reactions in chemical science. It plays a vital role in diverse fields such as organic syntheses, biological processes or optoelectronic devices. For this reason, great effort has been made over the past few decades to increase the current scientific knowledge concerning this topic.[1-8]

The most popular representatives in the subject of devices are certainly organic light-emitting diodes (OLEDs)[9], organic photovoltaic devices (OPVs)[10], and organic field-effect transistors (OFETs)[11]. The working principle of an OLED can be described as the transformation of electrical energy into light, whereas in OPVs electrical energy is gained by conversion of energy from sunlight. The main goal of an OFET is the voltage-driven control of the conductivity by means of organic semiconducting materials.[12-19]

In order to control and optimise the performance of devices, an understanding of the basic principles is essential. Therefore, investigation of processes like charge-separation, -transport, and -recombination in artificial systems is of immense current interest. For the successful design of such artificial structures, some important features have to be kept in mind: Especially in view of OPVs, absorption over a wide range of the solar spectrum is crucial to ensure harnessing of a great energy amount. In addition, a fast charge-separation process with a high quantum yield is desirable. The energy content of the charge-separated state should be as high as possible. Above all, charge-recombination processes should be impeded to guarantee a lifetime of the charge-separated state that is high enough to carry out chemical work (μs – ms).[20-23] Possibly lifetimes < μs may also be sufficient.

The dynamics of charge-transfer processes can be influenced by the electronic coupling between the redox centres, reorganisation energies, and the relative energies among the different states. The last two directly are responsible for whether the processes are located in the *Marcus*-normal or in the *Marcus*-inverted region. Another important aspect for the control of such processes is the phenomenon of spin correlation.[24-28]

The most straightforward strategy to study charge-transfer processes is probably the preparation of small molecules, for example the arrangement of suitable redox centres and chromophores in a dyad. Starting with rather simple systems combines several advantages. Generation of small entities provides an effortless and expeditious route of synthesis. Through implementation of an appropriate spacer unit, a defined geometry within the molecules can be realised. Furthermore, specific modifications concerning the distance between the redox centres are easily attainable. In contrast to large molecules and complex materials, small systems often are associated with simple spectral and electrochemical features that enable a straightforward interpretation. Albeit, in view of a realistic mimicry of natural processes, an enlargement of the systems from dyads to triads, tetrads, pentads, or even dendritic structures might be

appropriate, in spite of a probable increasing complexity in synthesis and/or photoinduced processes. To avoid this extra effort, self-assembly strategies might provide an alternative option.[29,30]

In order to design materials that fulfil the above mentioned requirements for an almost ideal performance, it is essential to be familiar with the rudimental basics. For a better understanding, some of the theoretical aspects that are necessary for an appropriate description of these phenomena will be presented in the next paragraph.

2 Theory

2.1 *Marcus*-Theory

A simple electron transfer (ET) process between a donor (D) and an acceptor (A) can occur either by thermal or optical activation or through a photoinduced pathway. In the latter, electron transfer takes place, when either the donor or the acceptor is in an excited state.

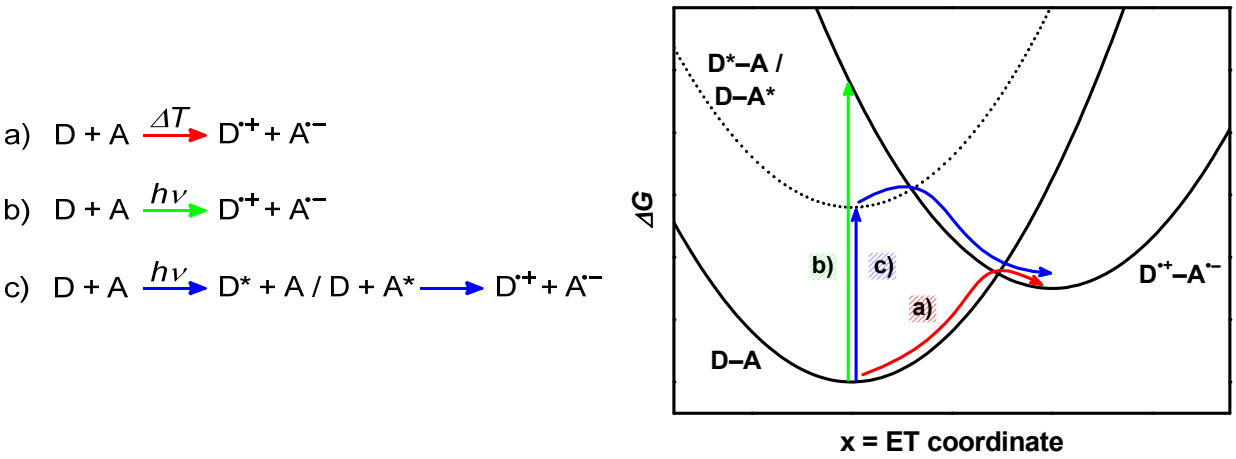

Figure 2.1: Schematic (left) and graphic (right) representation of a) thermal, b) optical and c) photoinduced electron transfer between D and A. It must be noted, that the thermal process depicted here is thermodynamically unfavoured.

Up to now, the most commonly used classical model to describe electron transfer reactions is certainly the *Marcus*-theory.[31-35] Initially, it was developed for the description of thermally activated outer-sphere electron transfer reactions and is based on the transition state theory. The classical *Marcus*-theory refers to processes taking place in the diabatic regime, where the electronic coupling V_{el} between the reactant and product state is small compared to the thermal energy ($V_{el} < k_B T$).[1] V_{el} roughly represents the amount of orbital interaction between D and A. Furthermore, diffusion processes are neglected, i.e. the reaction partners are located at fixed distances. Based on the assumption that the system is in quasi-equilibrium with its environment during the whole process, vibrational and solvent relaxation should be fast compared to the actual ET reaction. For this reason, the potential-energy surface (PES) of a charge-separation process can be represented by two diabatic Gibbs free energy profiles (blue curve in Figure 2.2), which stand for the electronic configurations of the reactant (D–A) and product ($D^{\bullet+}$–$A^{\bullet-}$) state. In order to reduce the multidimensional energy surface to a one-dimensional profile, a reaction coordinate is introduced, describing changes in the solvent orientation and the D–A

[1] The ET is said to take place adiabatically if $V_{el} > k_B T$ (with the Boltzmann constant k_B and the temperature T).

geometry. As the solvent is treated as a dielectric continuum, the PES of reactant and product depend quadratic on the reaction coordinate and are therefore represented by parabolas with equal force constants. In a thermal process, electron transfer occurs at the intersection point of the two parabolas.[32,36,37]

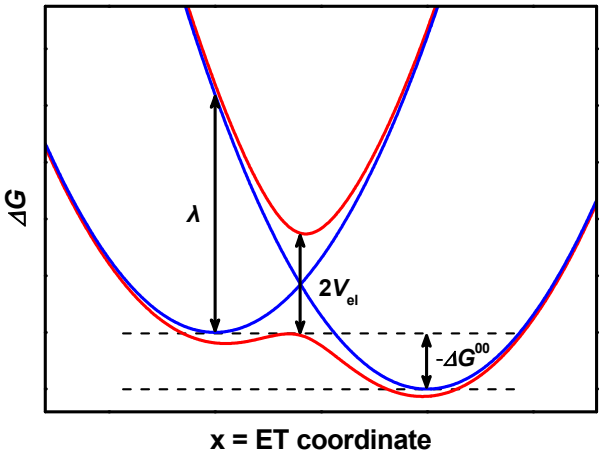

Figure 2.2: Diabatic Gibbs free energy surfaces for a diabatic and adiabatic electron transfer.

In an adiabatic process, mixing of the two harmonic potentials results in an avoided crossing (red curve in Figure 2.2), with an energy gap of $2V_{el}$. As $V_{el} > k_B T$, the ET reaction remains on the lower surface. In accordance with transition state theory, the rate of diabatic electron transfer k_{ET} can be derived by an *Arrhenius*-type equation:

$$k_{ET} = \kappa_{el} \nu_{el} \exp\left(-\frac{\Delta G^*}{k_B T}\right) \tag{1}$$

κ_{el} is the electronic transmission coefficient and represents the probability of an electron transfer through the intersection region. It can be obtained within the framework of the *Landau-Zener* treatment of avoided crossings.[38] For a diabatic process $\kappa_{el} \sim 1$, and the electronic frequency factor ν_{el} is proportional to V_{el}^2. In case of an adiabatic process $\kappa_{el} \ll 1$, and ν_{el} is replaced by the nuclear frequency factor ν_N, showing the rate dependence on the nuclear motion.[19] Assuming harmonic potentials for the nuclear distortion that is required for a charge-separation process, the thermal activation barrier ΔG^* is given by equation (2):

$$\Delta G^* = \frac{(\Delta G^{00} + \lambda)^2}{4\lambda} \tag{2}$$

ΔG^{00} is the difference in Gibbs free energy between the reactants and products equilibrium configurations. λ is the total reorganisation energy (force constant of the harmonic potentials) which is required for the distortion of the product state to reach the equilibrium geometry of the reactant. Generally, it is divided into two parts: a solvent independent internal term λ_i, which arises from structural differences between the relaxed nuclear geometries of reactant and

product, and a solvent reorganisation term λ_o, referring to differences in the orientation and polarisation of the solvent molecules surrounding reactant and product.

$$\lambda = \lambda_i + \lambda_o \tag{3}$$

λ_i is usually treated harmonically and can be calculated from the force constants for all molecular vibrations of the reactant and the product state.[39] Corresponding to an ith vibration, Δq_i is the difference in the equilibrium bond length between reactant and product state and f_i is a reduced force constant.

$$\lambda_i = \frac{1}{2}\sum_i f_i(\Delta q_i)^2 \tag{4}$$

In a two-sphere model, λ_o can be derived from the *Born*-equation[40,41] (5), if the surrounding medium is treated as a dielectric continuum:

$$\lambda_o = \frac{e^2}{4\pi\varepsilon_0}\left(\frac{1}{2r_D}+\frac{1}{2r_A}-\frac{1}{R_{DA}}\right)\left(\frac{1}{\varepsilon_{opt}}-\frac{1}{\varepsilon_{stat}}\right) \tag{5}$$

with the elementary charge e and the vacuum permittivity ε_0. ε_{stat} and ε_{opt} are the static and the optical[1] dielectric constant, respectively. R_{DA} denotes the centre-to-centre distance between donor and acceptor, r_D and r_A their corresponding spherical radii.

According to equation (1) and (2), the rate of the electron transfer can be derived by the classical *Marcus*-equation:

$$k_{ET} = 4\pi^2 hc^2 V_{el}^2 \sqrt{\frac{1}{4\pi hc\lambda_o k_B T}} \exp\left(-\frac{hc(\Delta G^{00}+\lambda_o+\lambda_i)^2}{4\lambda_o k_B T}\right) \tag{6}$$

In this equation, h is the Planck constant and c the speed of light *in vacuo*. It is important to note that the relationship of $k_{ET} \sim V_{el}^2$ is only valid in the weak coupling limit ($V_{el} < k_B T$).

As can be seen from equation (2), λ and ΔG^* exhibit a quadratic relationship. Hence, different kinetic regimes can be defined. No significant driving force ($\Delta G^{00} = 0$) is present in the case of a self-exchange reaction and $\Delta G^* = \lambda/4$ (Figure 2.3 A). In the *Marcus*-normal region, $-\Delta G^{00} < \lambda$ (Figure 2.3 B) and the activation barrier progressively decreases with increasing exergonicity. Simultaneously, the rate k_{ET} increases until it becomes maximum at $-\Delta G^{00} = \lambda$ ($\Delta G^* = 0$) (Figure 2.3 C). In the inverted region (Figure 2.3 D), a further increase of $-\Delta G^{00}$ ($-\Delta G^{00} > \lambda$) leads to a renewed increase of ΔG^* and therefore to a decrease in k_{ET}.

The inverted region effect on k_{ET} was confirmed by the experimental results of *Closs* and *Miller* in 1984,[42] but it was found to be less pronounced than predicted by the theory. Obviously, λ has a great influence on k_{ET}. Considering charge separation to occur in the *Marcus*-normal region and charge recombination in the *Marcus*-inverted region, like it is found

[1] $\varepsilon_{opt} = n^2$, n is the refractive index of the solvent.

for many compounds, a small λ, for example, accelerates the charge-separation process and slows down the charge recombination.

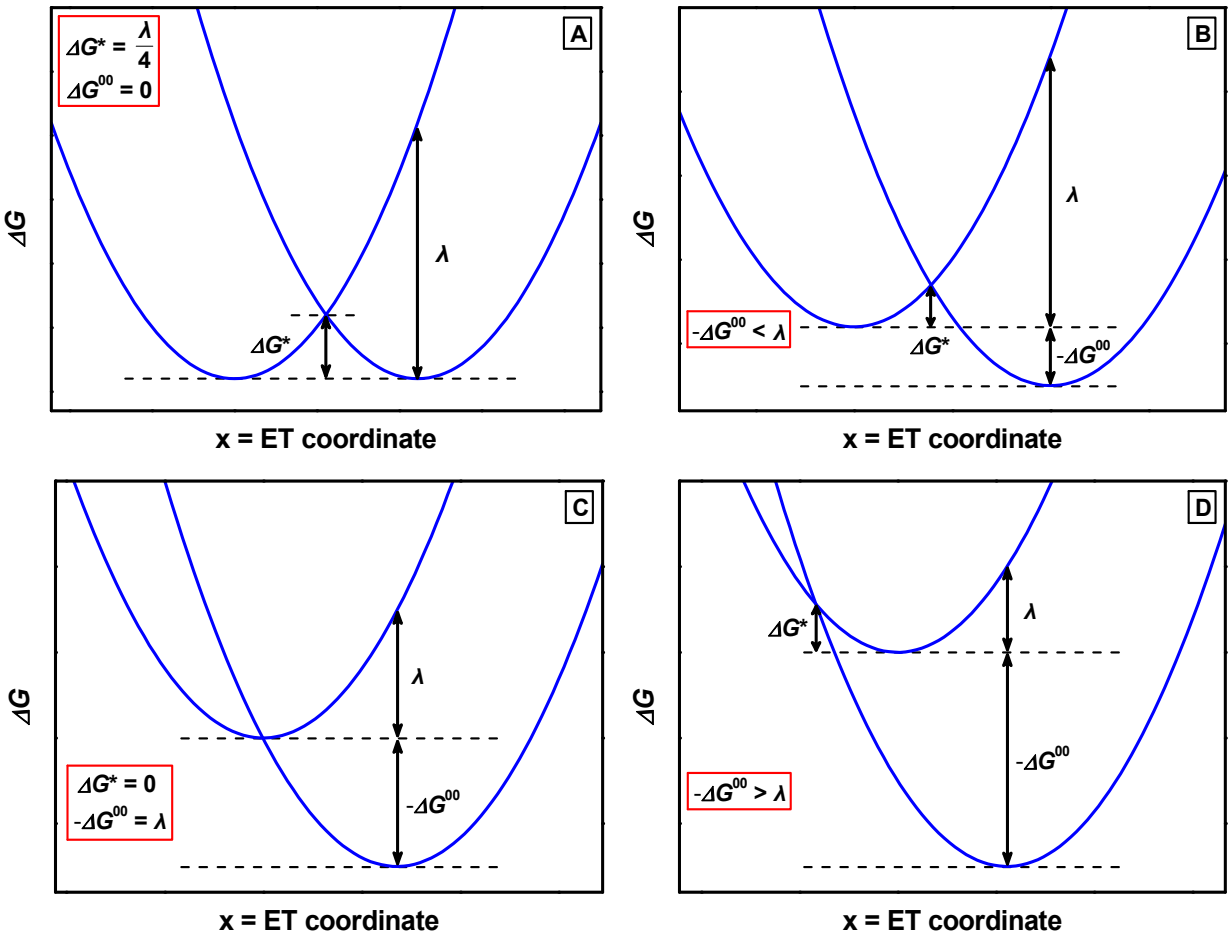

Figure 2.3: Schematic diabatic potentials of a self-exchange reaction (A), the *Marcus*-normal region (B), optimal conditions (C), and the *Marcus*-inverted region (D).

2.2 *Jortner*-Theory

The classical *Marcus*-theory only works well for diabatic electron transfer. Nevertheless, in systems that show a very weak electronic coupling ($V_{el} \rightarrow 0$) ET processes could also be observed. An explanation for this phenomenon can be found in semi-classical *Marcus*-theories, where quantum-mechanical tunnelling-processes are taken into account.

In the theory developed by *Bixon* and *Jortner*, ET may be described as a diabatic, radiationless transition.[43-47] The probability for a transition between the initial (i) and final (f) state is calculated by means of *Franck-Condon* factors. The corresponding rate is then given by a *Fermi's* golden rule expression:

$$k_{ET} \propto \frac{2\pi}{h} V_{if}^2 FCWD. \tag{7}$$

The electronic coupling energy between the initial and final state is represented by V_{if}. *FCWD* stands for the *Franck-Condon* weighted density of the final states at the initial energy and is given by

$$FCWD \propto \sum_v \sum_w \rho_{fw} \left| \langle \chi_{iv} \mid \chi_{fw} \rangle \right|^2 \delta(E_{iv} - E_{fw}). \tag{8}$$

w and v denote the vibrational levels of the initial and final state, ρ_{fw} is the population density of the reactant and E_{iv} and E_{fw} are the vibrational energy levels. The matrix element, which describes the overlap of the nuclear wavefunctions χ_{iv} and χ_{fw} is called the nuclear *Franck-Condon* factor. In the semi-classical *Jortner*-theory, a simplification of this factor was achieved by application of equation (9),

$$\left| \langle \chi_{iv} \mid \chi_{fw} \rangle \right|^2 = \frac{e^{-S} S^w}{w!} \tag{9}$$

with the *Huang-Rhys* factor:

$$S = \frac{\lambda_i}{\tilde{\nu}_v}. \tag{10}$$

For the solvent vibrations, a classical treatment is used as they usually occur at low frequencies. On the contrary, the high-energetic molecular vibrations are treated quantum mechanically and are replaced by a single average mode $\tilde{\nu}_v$. The rate of the electron transfer can therefore be obtained from equation (11), in which the sum is extended over the number of quanta *j* of the average mode in the product state:

$$k_{ET} = 4\pi^2 hc^2 V_{el}^2 \sum_{j=0}^{\infty} \frac{e^{-S} S^j}{j!} \sqrt{\frac{1}{4\pi hc\lambda_o k_B T}} \exp\left(- \frac{hc(\Delta G^{00} + \lambda_o + j\tilde{\nu}_v)^2}{4\lambda_o k_B T} \right). \tag{11}$$

The results for k_{ET} derived from quantum mechanical and classical models match very well in the *Marcus*-normal region, but differ strongly in the inverted region. The crucial point is that nuclear tunnelling allows an electronic transition at energies lower than the intersection point. Therefore, the decrease of k_{ET} in the inverted region was found to be rather linear than parabolic. At the high-temperature limit $S \gg 1$ and $k_B T > h\nu$. For this reason, equation (11) reduces to the classical diabatic *Marcus*-equation (6).

The *Jortner*-model provides a good possibility for estimating the electron transfer parameters from spectral data.[48,49] Least-square fits of equation (12) to experimental data derived from absorption or emission spectra allow a separate evaluation of the four electron transfer parameters $-\Delta G^{00}$, λ_o, λ_i and $\tilde{\nu}_v$,

$$\frac{I_{fl}}{\tilde{\nu}^3} = \frac{16\times10^6\pi^3}{3\varepsilon_0}\frac{n^2(n+2)^2}{9}\mu_{fl}^2\sum_{j=0}^{\infty}\frac{e^{-S}S^j}{j!}\sqrt{\frac{1}{4\pi hc\lambda_o k_B T}}\exp\left(-\frac{hc(\Delta G^{00}+\lambda_o+j\tilde{\nu}_v)^2}{4\lambda_o k_B T}\right) \tag{12}$$

where μ_{fl} is the fluorescence transition-moment and can be determined by the *Stickler-Berg* equation[50] (13), which correlates μ_{fl} with the rate constant of the fluorescence k_{fl} with the aid of the averaged cubic fluorescence energy

$$k_{fl} = \frac{16\times10^6\pi^3}{3h\varepsilon_0}\frac{n^2(n+2)^2}{9}\frac{g_g}{g_e}\left\langle\tilde{\nu}_{fl}^{-3}\right\rangle_{av}^{-1}\mu_{fl}^2. \tag{13}$$

Here g denotes the degeneracy of the ground (g) and excited (e) state.

In general, a successful *Jortner*-analysis is only possible for asymmetrical bands. The band shape is determined by the *Huang-Rhys* factor S (eq. 10), which is a measure for the number of vibrations occurring during the vertical transition. As large values of S provide symmetrical bands, an application of the *Jortner*-model is therefore only valid for systems with small *Huang-Rhys* factors.

3 State of the Art

3.1 General Aspects

The theoretical overview given in the previous chapter only deals with some aspects that control the electron transfer dynamics. For a better understanding of the complexity of such processes, the pivotal facts will briefly be summarised below, followed by some examples for elucidation.

First of all, the nature of donor and acceptor obviously plays an important role. Suitable adaption of the redox potentials directly influences the relative energies of the reactant and product states, which are clearly decisive for any interaction between the reaction centres. Besides, reorganisation energies of the surrounding medium, as well as of the donor-acceptor system itself are vital factors, with regard to the activation barrier and driving force in charge-separation and charge-recombination processes.

Additionally, interconversion between states with different spin multiplicities might be of great significance concerning charge-separation and -recombination. As such processes are spin-forbidden, they should be substantially slower than the corresponding spin-allowed ones. The relative state energies for their part, may further be affected by solvent effects.

The nature of the bridging unit mainly determines the spatial distance between the redox centres as well as the electronic coupling V_{el} of the reactant and product states. At close distances of D and A, one has to distinguish between a through-bond and a through-space (through-solvent) charge-transfer. In the latter case, charge transfer is expected to be rather slow at distances greater than 6 Å. An active involvement of the bridge into the charge-transfer may in general be described by two alternative mechanisms: First, the superexchange, which is commonly regarded as a strongly distance-dependent tunnelling process, and second, the weakly distance-dependent sequential process, called (thermally activated) hopping. According to the strong distance dependence, superexchange is not expected to occur to D–A-distances exceeding 15 Å, whereas charge transport *via* the incoherent hopping mechanism was observed up to ~50 Å.[20,51]

3.2 Artificial Systems for the Study of Charge-Transfer Processes

For a successful design of artificial systems that fulfil the above-mentioned criteria, some key points have to be taken into account. Obviously, a simple route of synthesis is desirable. The implemented donor and acceptor moieties should show a high chemical and photophysical stability, additionally to an easily attainable possibility of modification. Furthermore, reversible redox processes are important to exclude decomposition during the electron transfer. For the detailed investigation of stepwise charge-transfer processes, donor and acceptor moieties as well as their radical ions should possess characteristic spectral features. Frequently applicated donors are, for example porphyrins (P)[52-55], phenothiazines (PT)[56,57], ferrocenes (Fc)[58-60], tetrathiafulvalenes (TTF)[61-63] or triarylamines (TAA)[64-69]. The most popular acceptor moieties are probably fullerenes, especially C_{60}.[70-72] Furthermore quinones (Q)[73,74], borondipyrromethanes (BODIPY)[75-80], naphthalene-1,8:4,5-bis(dicarboximides) (NDI)[81-83] or pyrromellitimides (PI)[84,85] are commonly used.

Controlling the distance and orientation of the chromophores and/or redox centres is essential for designing suitable model compounds. In case of compound **AA**, rigid norbornylogous bridges were used to connect a strong *N*,*N*-dimethylaniline (DMA) donor with a weaker 1,4-dimethoxynaphthalene (DMN) donor and a strong 2,2-dicyanovinyl (DCV) acceptor (Figure 3.1). Two different isomers (*syn* and *anti*) were synthesised and investigated in view of their long-range charge-separation and -recombination processes.[1]

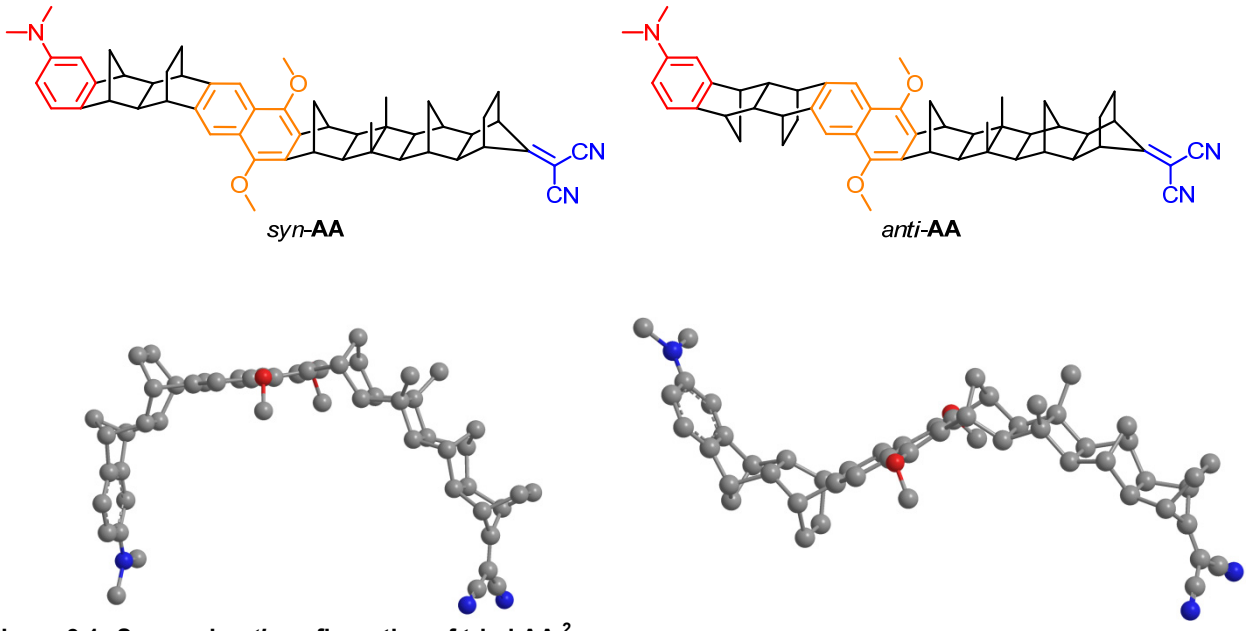

Figure 3.1: *Syn*- and *anti*-configuration of triad AA.[2]

[1] Transient absorption measurements were performed in solvents with various polarity. For simplification, only the results in less polar environment ($^{n}Bu_2O$) will be discussed here.

[2] Optimization was performed by means of force field MM2 in ChemBio3D Ultra 11.0.1, CambridgeSoft 2007.

After excitation of the DMN, a first electron transfer step generates the initial charge-separated (CS) state DMA–DMN$^{\bullet+}$–DCV$^{\bullet-}$ within 8 ps for both isomers. In case of *syn*-**AA,** conversion of the initial to the final CS state DMA$^{\bullet+}$–DMN–DCV$^{\bullet-}$ was found to be faster (70 ps) than for *anti*- **AA** (100 ps), which is in agreement with the different driving forces found for both compounds. For *anti*-**AA**, a lifetime of 73 ns was found. Remarkably, the lifetime of *syn*-**AA** was only ~200 ps. Assuming that the through-bond coupling should be similar in both compounds, the authors supposed a through-space or through-solvent mechanism for the charge recombination in *syn*-**AA**. Measurements in different solvents revealed a strong dependence of the charge-recombination rates on the solvent polarity, due to inverted-region effects. In contrast to DMA–DMN–DCV, the corresponding dyad DMN–DCV revealed a charge-separation within 10 – 20 ps and a lifetime of the CS state of 49 ns. This example clearly demonstrates the importance of a rigid bridging unit. Furthermore a possible prolongation of the lifetime of the charge-separated state by extension of a dyad to a triad was demonstrated.[86-92]

Within the scope of designing multichromophoric systems with large spatial distances, extremely long-lived CS states were realised in cooperation of *Fukuzumi*, *Imahori,* and *Guldi*. A ferrocene (Fc) donor was connected to a C_{60} acceptor through a bridge containing two porphyrin (P) moieties (Figure 3.2). Adjacent to the C_{60} unit, either a free-base porphyrin (tetrad **AB**) or a second zinc porphyrin (tetrad **AC**) was attached.

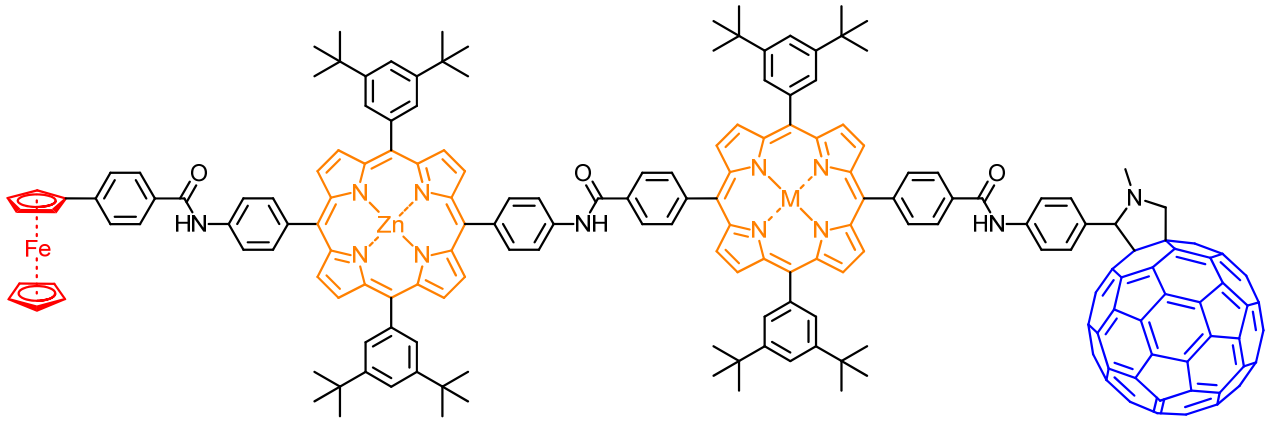

Figure 3.2: Tetrads AB and AC.

In case of **AB,** an edge-to-edge distance of 48.9 Å was reported by the authors. ET processes were investigated by transient absorption spectroscopy in the ps-regime. After excitation of the porphyrin to its singlet excited state, formation of the CS state (Fc$^{\bullet+}$–P–P–$C_{60}^{\bullet-}$) occurred on the ps- to ns-timescale. Quantum yields for the full charge-separation of 24 and 17 % in DMF were reported for **AB** and **AC**, respectively. Decay kinetics obtained by electron spin resonance (ESR) measurements were found to be only moderately temperature dependent, excluding a stepwise charge-recombination process. In frozen DMF at 163 K, the fully CS states showed lifetimes of 34 ms for **AB** and 1.6 s for **AC**. Furthermore, **AC** showed a lifetime of 1.3 s in DMF even at 295 K. A direct connection of the two porphyrin moieties by removing the central amide unit,

reduced the lifetime to 83 μs (DMF, 295 K).[93-96] Even though the presented results concerning generation of a long-lived CS state are remarkable, further investigations (e.g. time-resolved ESR(TRESR)) seem to be required to enlighten e.g. possible effects of spin correlation.

Detailed investigations concerning spin correlation were presented for the triad **AD** by *Wasielewski et al.*. In the rodlike structure, a 1,4-piperazine bridge was used for the connection of a *p*-methoxyaniline (MeOAn) donor and a 1,8-naphthalene dicarboximide (NI) acceptor. Attachment of the secondary acceptor, naphthalene-1,8:4,5-bis(dicarboximide) (NDI), was achieved through a 2,5-diphenylmethyl spacer (Figure 3.3).

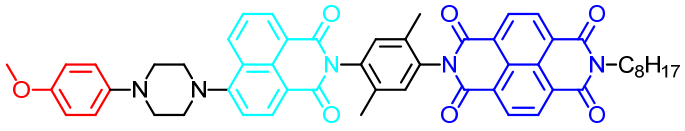

AD

Figure 3.3: Triad AD.

Photoexcitation of NI into the lowest excited singlet state ^{1}*NI was followed by charge separation to MeOAn$^{\bullet+}$–NI$^{\bullet-}$–NDI with a risetime of 8 ps. A subsequent charge shift from NI to the NDI acceptor occurred within 430 ps. The overall quantum yield for the formation of the fully CS state MeOAn$^{\bullet+}$–NI–NDI$^{\bullet-}$ was 92 % (toluene), with an energy storage of ~2 eV. Transient absorption kinetics of the triad **AD** in degassed solutions revealed a biexponential decay with a fast component of ~310 ns and a slow one of ~42 μs. Nondegassed samples did not obtain the slow component and decayed within 2 μs. The fast decay was therefore associated with the lifetime of the final CS state ^{1}[MeOAn$^{\bullet+}$–NI–NDI$^{\bullet-}$]. The slow decay component represents the decay of a localised triplet species MeOAn–NI–^{3}*NDI to the ground state. Formation of the localised triplet state was possible on account of a radical-pair intersystem-crossing (RP-ISC) from ^{1}[MeOAn$^{\bullet+}$–NI–NDI$^{\bullet-}$] to ^{3}[MeOAn$^{\bullet+}$–NI–NDI$^{\bullet-}$], driven by hyperfine interactions between the unpaired electrons and the nuclear spins. This was confirmed by TRESR spectroscopy in the nematic phase of a liquid crystal.[96-102]

The phenomenon of spin correlation might be a promising attempt to impede charge recombination, since the decay from the ^{3}CS state to ground state is spin-forbidden. Ideally, the ^{3}CS should constitute the lowest triplet state, to avoid spin-allowed decay to localised triplet states, as it was found for **AD**. However, one has to keep in mind that, the lower the energy of the ^{3}CS state is, the less energy is stored, what is clearly unfavourable.

Carbonera et al. also reported about a triad (**AE**), in which spin control played an important role. Linkage of a tetrathiafulvalene (TTF) donor to a C_{60} acceptor was achieved by implementation of a free-base porphyrin (P) (Figure 3.4). In solution (2-methyl-THF), the final charge separated state, TTF$^{\bullet+}$–P–$C_{60}^{\bullet-}$, showed a lifetime of 660 ns. A prolongation of the lifetime to ~8 μs was observed in the corresponding isotropic glass at 10 K. In the nematic phase of a liquid crystal at 295 K, two lifetimes point out to a singlet-born (~1 μs) and a triplet-born (~7 μs) radical pair, respectively. Assuming that the difference in the lifetimes can be ascribed to spin

dynamic effects in the magnetic field, such artificial reaction centres might be switched magnetically.[103]

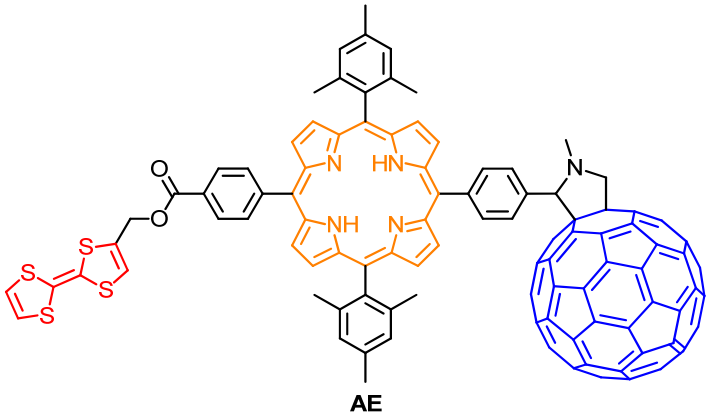

Figure 3.4: Triad AE.

An approach to mimic the charge-separation and light-harvesting functions of photosynthetic reaction centre proteins is the design of self-assembled chromophores. As the synthesis of large, covalently bound structures is often time-consuming, development of non-covalent strategies might be a promising alternative. One suitable model compound may be chlorophyll. Chlorophylls are able to absorb light over a wide range of the visible spectrum and can act as electron donors as well as acceptors, which is supported by their tuneable redox properties. *Wasielewski et al.* presented the photoinduced charge-transfer properties of triad **AF** (Figure 3.5 left) and its corresponding cyclic tetramer (schematic representation in Figure 3.5 right). A modified zinc chlorophyll (Chl) donor was attached to a pyrromellitimide (PI) acceptor, equipped with two naphthalene-1,8:4,5-bis(dicarboximide) (NDI) secondary acceptors.

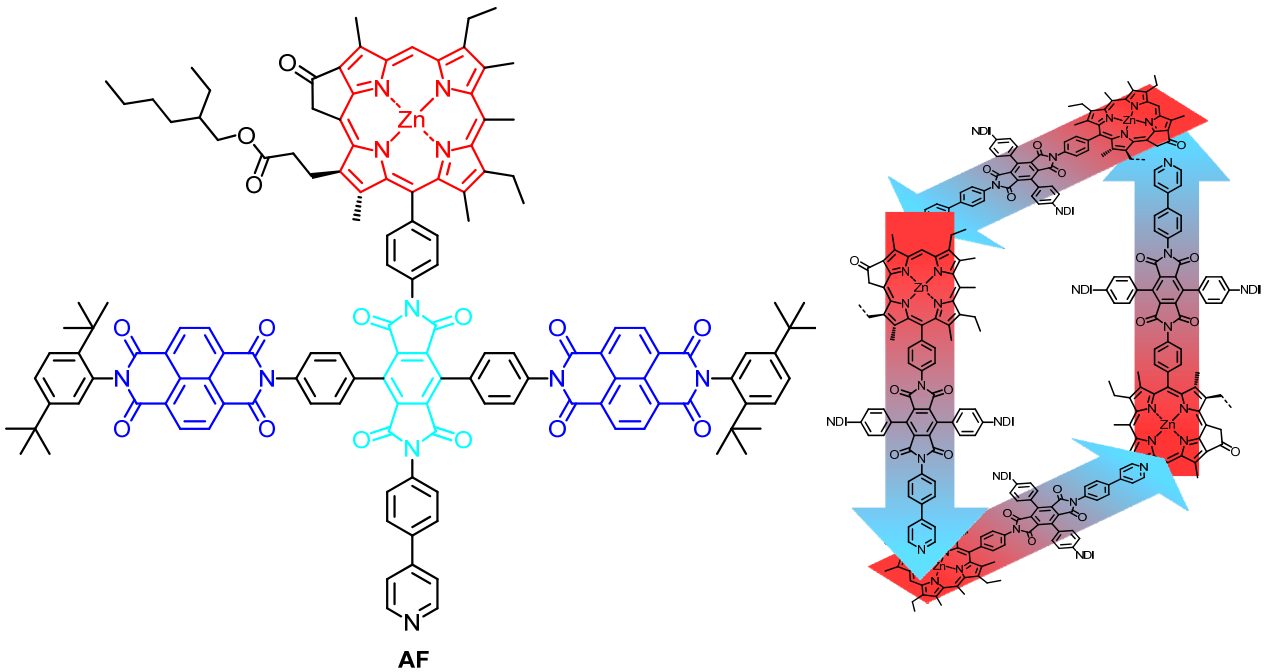

Figure 3.5: Tetrad AF.

A pyridine moiety additionally was connected to the PI, to promote self-assembly by intermolecular metal-ligand interaction with the Zn-Chl. Selective excitation of Chl (Chl → ^{1}*Chl) led to the formation of NDI–PI$^{\bullet-}$–Chl$^{\bullet+}$, and in a second ET step to the fully CS state NDI$^{\bullet-}$–PI–Chl$^{\bullet+}$, with an overall quantum yield of about 60 % for both, monomer and tetramer. The authors were able to demonstrate a prolongation of the overall charge-recombination (CR) lifetimes in the tetramer (30 ns in toluene) by a factor of about 3 compared to the monomer (10 ns in toluene/1 % pyridine). This observation strengthens the strategy of tuning charge-transfer dynamics by self-assembly of molecular building blocks.[85]

In nature, antenna systems comprise many chromophores, especially porphyrins. Therefore, investigations concerning artificial, light-harvesting multiporphyrin arrays were intensively performed, such as in a work of *Gust et al.*.

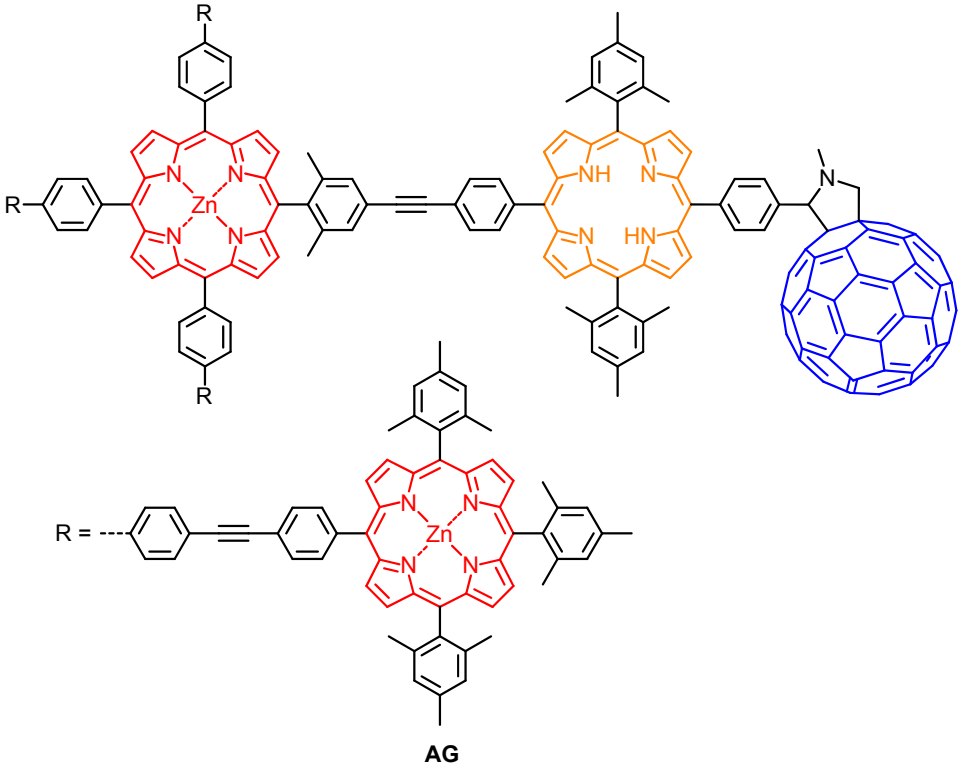

AG

Figure 3.6: Artificial antenna system AG.

Four covalently bound zinc tetraarylporphyrins (ZnP_p)$_3$–ZnP_c[1] were connected to a free-base-porphyrin-C_{60} dyad (P–C_{60}) to combine a light-harvesting array with a reaction centre capable of charge separation (ZnP_p)$_3$–ZnP_c–P–C_{60} (**AG**) (Figure 3.6). Energy transfer (EnT) from ZnP_p to the ZnP_c occurred within 50 ps ((ZnP_p)$_3$–^{1}*ZnP_c–P–C_{60}), followed by a second EnT to generate (ZnP_p)$_3$–ZnP_c–^{1}*P–C_{60} in 32 ps. Subsequently, an electron is transferred from ^{1}*P to C_{60} on a timescale of 25 ps, yielding the CS state (ZnP_p)$_3$–ZnP_c–P$^{\bullet+}$–$C_{60}^{\bullet-}$ with a quantum yield of 98 %. A likewise high quantum yield (~90 %) was found for the formation of the second CS state (ZnP_p)$_3$–$ZnP_c^{\bullet+}$–P–$C_{60}^{\bullet-}$ (380 ps), which showed a lifetime of 240 ns.[104,105]

[1] p stands for peripheral, c for central

3.3 The Perchlorinated Triphenylmethyl (PCTM) Radical Acceptor

In the preceding section, several acceptor units were shown, which differ in structure, size and reduction potential. One class of organic molecules that might offer an access to further suitable acceptor units is the one of stable free radicals. The beginning of organic free radical chemistry started with the synthesis of the triphenylmethyl radical **BA** by *Gomberg* in 1904.[106] Since then, a great variety of persistent or stable radicals has been synthesised, in spite of their often high reactivity.[107] A small selection is given in Figure 3.7. Dimerisation, hydrogen abstraction, disproportionation or reaction with O_2 are certainly some of the main reaction pathways. Dealing with the thermal and chemical stability of such species, two key criteria have to be taken into account: resonance effects and steric shielding of the unpaired electron.

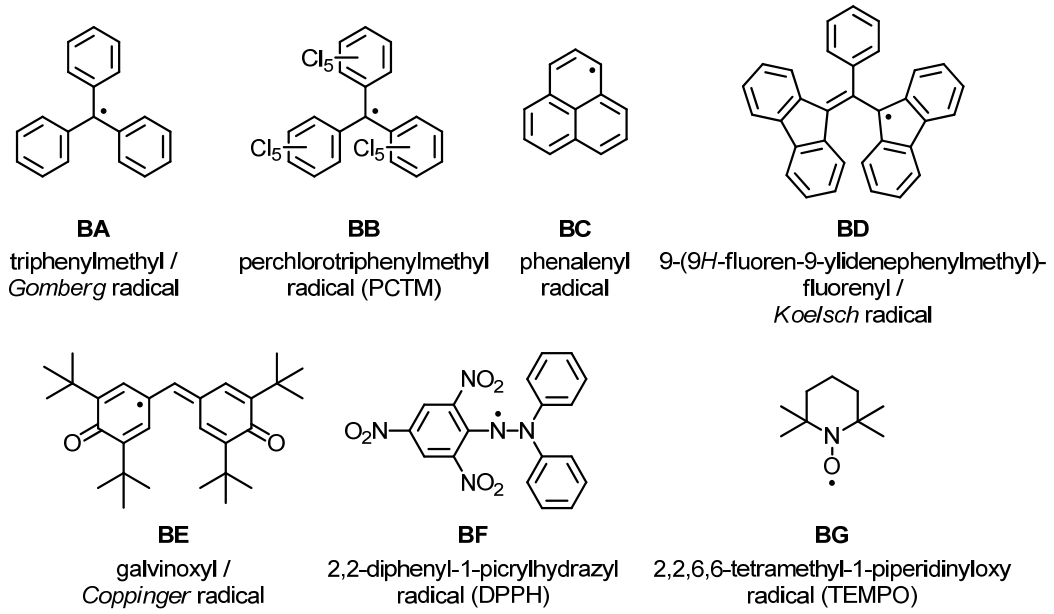

BA triphenylmethyl / *Gomberg* radical

BB perchlorotriphenylmethyl radical (PCTM)

BC phenalenyl radical

BD 9-(9*H*-fluoren-9-ylidenephenylmethyl)-fluorenyl / *Koelsch* radical

BE galvinoxyl / *Coppinger* radical

BF 2,2-diphenyl-1-picrylhydrazyl radical (DPPH)

BG 2,2,6,6-tetramethyl-1-piperidinyloxy radical (TEMPO)

Figure 3.7: Examples of persistent or stable radicals.[107]

3.3.1 Perchlorinated Triphenylmethyl Radicals - Synthesis, Structure & Reactivity

A species, which perfects the above-mentioned criteria is the perchlorinated analogue to the *Gomberg* radical, the perchlorotriphenylmethane (PCTM) radical **BB** (Figure 3.8).[108-110] Perchlorination of organic compounds was already in focus of chemists in the middle of the 19th century. Despite of great efforts, almost no progress in this research field was made during the next century. The high steric and electronic claim of this kind of molecules hindered the exhaustive chlorination, especially in case of alkylaromatic hydrocarbons. Perchlorination of toluene, for example, provided only quasi-perchlorinated species or led to side-chain chlorinolysis. Nevertheless, perchlorotoluene was the first "fully" perchlorinated alkylaromatic

hydrocarbon, synthesised by *Ballester* and *Molinet*.[111,112] Similar to a previously described method of *Silberrad*,[113,114] these authors developed the so-called BMC (*Ballester*/*Molinet*/*Castañer*) reagent, resulting from a mixture of aluminium trichloride and sulphur monochloride in sulphuryl chloride. The actual chlorinating species is assumed to be the trichlorosulphonium ion SCl_3^+, which was first obtained by *Ruff et al.* in 1924.[115] Scheme 3.1 shows the proposed mechanism for the formation of the chlorinating species SCl_3^+.

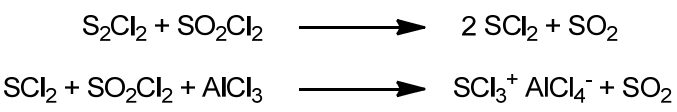

Scheme 3.1: Proposed mechanism for the generation of the BMC reagent.[109]

The BMC method was decisive in the synthesis of a great number of perchlorinated aromatic and alkylaromatic compounds, like the perchlorinated triphenylmethane **BB**, which serves as a precursor for the above-mentioned PCTM radical. *Ballester et al.* first isolated this so-called "inert free radical" in 1971.[116] Starting from the perchlororinated hydrocarbon, the first step was the generation of the corresponding anion using NaOH in DMSO/Et_2O solution. Subsequent oxidation was performed with a surplus of I_2. Since then, different bases and/or oxidising reagents have been investigated. A commonly used reaction mixture is $^nBu_4NOH$ in combination with *p*-chloranil (PCA) in THF.[117]

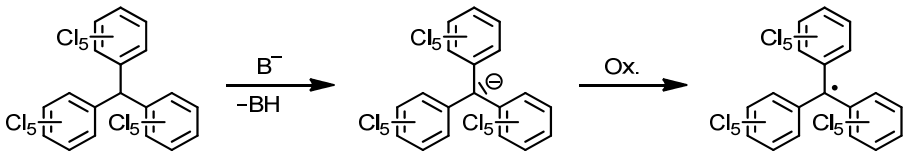

Scheme 3.2: Generation of the PCTM radical from the corresponding *α*-H precursor.

Like the triphenylmethyl radical **BA**, **BB** is a *π*-radical with a propeller-like geometry, existing in two atropisomeric forms, M and P, with a rotation barrier of ~90 kJ mol^{-1}.[110] Replacement of all hydrogens by chlorine atoms increases the dihedral angles to ~50°,[118-121] compared to ~30° in its non-chlorinated counterpart. Therefore, the *α*-carbon is highly shielded by the bulky chlorine atoms, as shown in the space-filling model in Figure 3.8 (only the atropisomer M is shown). Furthermore, the great distortion hinders an overlap of the ring *π*-orbitals and the *p*-orbital of the *α*-C, resulting in a low electron-spin delocalization. Reactions on sites other than the central carbon are prevented, leading to a remarkable stability. Contrary to many other organic radicals, the PCTM radical is unreactive to typical radical reagents and scavengers like e.g. NO, N_2O, hydroquinone and boiling toluene. It is also stable against O_2, Cl_2, Br_2 and concentrated acids like H_2SO_4 and HNO_3. Thermal decomposition in air in the solid state is observed at temperatures around 300°C.[122]

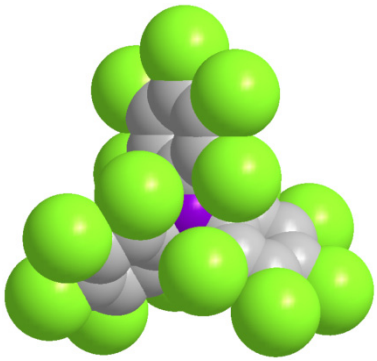

Figure 3.8: Space-filling model of the PCTM radical BB.[1] Colours are depicted as follows: C, grey; α-C, violet; Cl, green.

Compound **BB** is a dark red solid and exhibits characteristic absorption and emission bands in the visible range of the spectra. Fluorescence quantum yields are found to be dependent on the excitation wavelength and range between 1.5 and 0.25 %.[123] According to its octupolar character, it exhibits large NLO (non-linear optical) responses, which is interesting for the design of multifunctional materials.[124,125] Albeit, the PCTM radical is light sensitive in solution and undergoes ring-closure reactions to the perchloro-9-phenylfluorenyl (PCPF) radical **BH** (Scheme 3.3).[126]

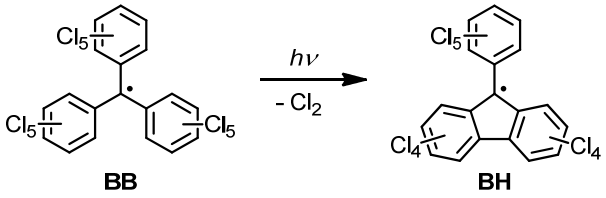

Scheme 3.3: Light induced ring closure of the PCTM radical.

First reported by *Luckhurst* and *Ockwell* in 1968,[127] the ring-closing process was further investigated by *Fox et al.*, employing steady state and time-resolved methods.[128] These authors reported a sequential process after excitation to ^{2}PCTM*. The first intermediate was found to be lower in energy and may possess an internal charge-transfer character. A ring-closed structure with disrupted aromaticity was supposed to be the second intermediate. The loss of two chlorine atoms irreversibly lead to the PCPF radical. Similar reactions also were found for the perchlorodiphenylmethyl (PCDM) radical,[123] as well as for the non-chlorinated analogue of the PCTM radical **BA**. Corresponding processes were also observed for triarylamine cations, which are isoelectric species to the triarylmethyl radicals.[129,130]

Compound **BB** is an electroactive species, which can reversibly be turned into its corresponding carbanion and carbocation, respectively. Furthermore, it undergoes single electron transfer (SET) reactions with a great variety of suitable reaction partners.[116,122] Apart from electrochemical oxidation, the carbocationic species can easily be attained by reaction of

[1] Optimization was performed by means of force field MM2 in ChemBio3D Ultra 11.0.1, CambridgeSoft 2007.

the PCTM radical with $AlCl_3$ in CH_2Cl_2, or $SbCl_5$ in SO_2Cl_2.[131,132] Although the resulting hexachloroantimonate salt can be isolated,[133] the carbocation is highly reactive in solution. With H_2O, for example, it does not react at the *α*-C, but in *p*-position of one of the phenyl rings, to give perchlorofuchsone. Similar reactions were observed with alcohols or amines. With oleum or fuming HNO_3, the PCTM radical undergoes SET reactions to the carbocation as well. [134]

In Et_2O, alkali metals, such as Na or K, reduce the PCTM radical to the corresponding carbanion. The thus obtained salts are quite stable in solution but cannot be isolated in pure form, for they are extremely strong reducing species.[135] Stabilisation with suitable crown ethers however is possible.[136] In polar solvents, such as THF and DMSO, a reduction of the PCTM radical by ascorbic acid was observed.[137] Remarkably, treatment of the PCTM radical with aqueous solutions of $^n Bu_4NOH$ also resulted in the quantitative formation of the PCTM anion.[116] This phenomenon was discovered earlier using NaOH or KOH solutions in DMSO/Et_2O or HMPA[1], respectively.[138] The fast SET was ascribed to the formation of a *p*-*π*-charge-transfer (CT) complex between the perchlorinated radical and the hydroxide ion.[139] Several examples proving the one-electron donor abilities of the hydroxide ion can be found in the literature.[140,141] With regard to the above-mentioned application of bases such as $^n Bu_4NOH$ in the synthesis of the PCTM radical, these SET transfer reactions might be problematic. During the reaction, the desired product might be converted back to the starting material, resulting in a diminished yield of the desired radical species. In contrast to the PCTM carbocation, the carbanion is stable in solution in the presence of H_2O. This is a major advantage compared to its cationic counterpart. In addition, the reduction is easier accessible, due to the electron withdrawing effects of the chlorine atoms.

During the last 50 years, a great variety of substituted PCTM radicals has been synthesised and investigated. In Figure 3.9 a selection of those examples that show single substitution in the *p*-position of one phenyl ring is given.[122,142] Substitution is not limited to this special case. Furthermore, exchanges of more than one chlorine atom are possible.

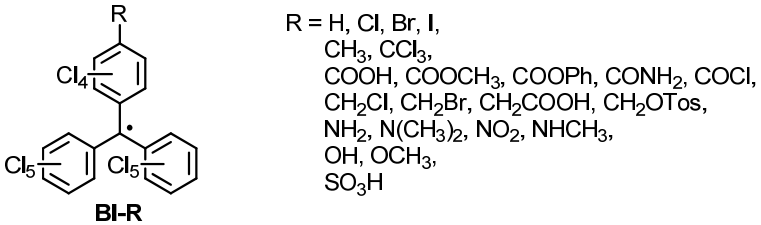

Figure 3.9: Examples of monofunctionalised PCTM radicals.

In principle, functionalisation can be attained in two different ways. On the one hand, appropriate synthesis of the α-H precursor and subsequent radicalisation is conceivable. On the other hand, the outstanding stability of the PCTM radical and its substituted analogues makes the inverse route of synthesis feasible: radicalisation is hereby followed by a substitution of one to three

[1] Hexamethylphosphoramide

chlorine atoms in *p*-position of the phenyl rings. One functionalisation worth mentioning is the implementation of one or more –COOH groups, which provides access to a wide range of possible applications (some examples will be shown in the following), for example the spin labelling of amino acids.[143]

The chemical inertness of the radicals is in most cases not affected by subsequent reactions of the substituents. Thus, conversions between the different functional groups are easily attainable. During the history of the organic free radicals, the focus mostly lay on the substituents effect on the radical character, whereas the functionalised PCTM radicals were additionally intensively studied with regard to the so-called "reverse effect".[144-146] This effect represents the influence of the free radical character on the reactivity of the substituents. The investigated reactions all show moderate to high increase of the reaction rate. A nice example is the reaction of the PCTM radical with Me_2NH. Besides SET from the Me_2NH to the radical centre, a nucleophlic aromatic substitution of one or two chlorine atoms takes place. This reaction is not observable in case of the nonradicalised counterpart. The authors attribute this effect to a stabilisation of the relevant transition states by the orbital of the unpaired electron.[147]

3.3.2 Perchlorinated Bi- and Polyradicals

3.3.2.1 Magnetic and Electronic Interactions in Radicals and Radical Ions connected by Covalent Bridges

The preceding section gave an overview over the easy accessibility of substituted PCTM radicals. Investigations regarding their electronic, magnetic and optical properties are important, especially in view of possible multifunctional molecular materials. A first step in this direction was the linkage of two or more PCTM radical centres.

Ballester et al. published a series of representative compounds in the middle of the 1980s, where two PCTM moieties were directly linked with each other (**CA**).[138,148] As depicted in Figure 3.10, the diradical, dication and dianion as well as the radical cation and the radical anion were synthesised.

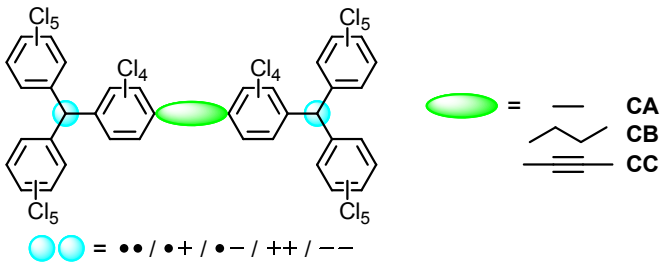

Figure 3.10: Diradicals with different spacers and their corresponding ionic and diionic species.

The absorption spectrum of the diradical is almost coincident to that of the PCTM radical, showing no presence of a biphenyl "conjugation band" at around 300 nm. This observation indicates an almost perpendicular orientation of the two directly connected aromatic rings (~87°), as it was found for other biphenyl systems with bulky substituents in *o*-position.[149] Hindering an overlap of the *π*-orbitals, this fact excludes a quinoidal structure of the diradical. Consequently, no spin-spin exchange was observed. However, in both radical ions of **CB**, an intramolecular spin-charge exchange takes place, which was confirmed by ESR measurements. The same observation was made for the radical anion of compound **CC**, where a saturated bridge was implemented. Therefore, the spin-charge exchange was supposed to take place along *σ*-bond paths. An intermolecular SET could be excluded, due to the fact that such processes are found to be rather slow.[150] The mixed-valence compounds of **CA** and **CB** both belong to the Robin-Day class II. A study of *Castañer et al.* showed a significant resonance interaction for the acetylene-bridged radical anion of **CC**, which classified it to be a class III species (V_{el} = 17.5 kcal/mol ≈ 6130 cm^{-1}).[151-155]

As already discussed before, the bridge plays an important role in intramolecular CT processes. An insight into the effect of the bridge topology was provided by investigations of **CD** and **CE** (Figure 3.11), as well as their one- and twofold reduced species.[117,156] Both compounds showed almost no magnetic interaction. The highly twisted vinylene-phenylene-vinylene spacer hinders an effective electronic conjugation, which could be confirmed by cyclic voltammetry. One reversible reduction wave was found for both diradicals, indicating a weak electronic interaction.

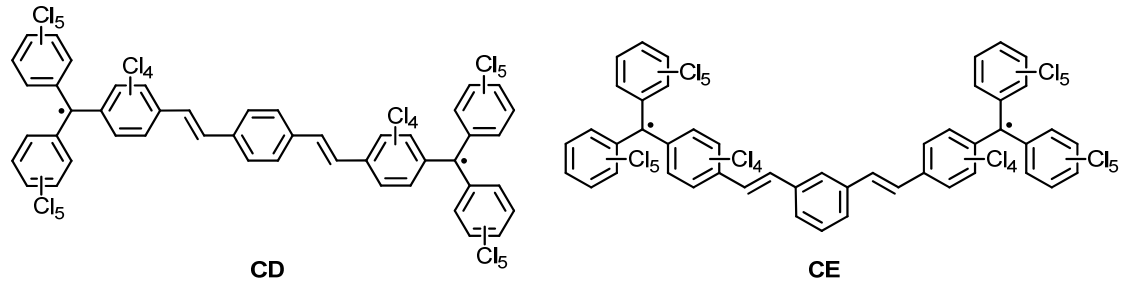

Figure 3.11: *p*- (CD) and *m*-connection (CE) of PCTM diradicals by a vinylene-phenylene-vinylene spacer.

The reduction processes to the mono- and dianionic species were monitored by spectroelectrochemistry. During the first reduction step of **CD**, the development of an IVCT (inter-valence charge-transfer) band was observable. The intramolecular electron transfer (ET) was also thermally accessible for this compound. An effective electronic coupling of 121 cm^{-1} was determined. In contrast, the *meta*-connected compound **CE** showed no indication of an intramolecular ET, neither optically nor thermally, which can be ascribed to a more localised electronic structure. UV/vis spectra of both compounds confirm this assumption, since bathochromic band shifts and enhanced absorptivities are present for **CD**.

Not only the electronic nature of the bridge, but also the distance of the redox centres plays an important role in ET processes. In compound **CF** (Figure 3.12), the two PCTM radical moieties are separated by a spacer, with a through-bond distance of about 40 Å.[157]

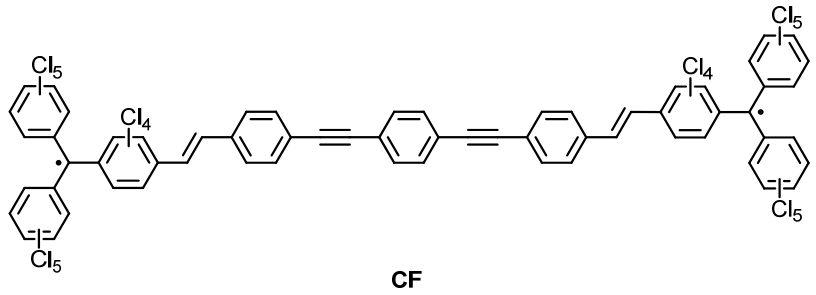

CF

Figure 3.12: Diradical CF with an acetylene bridge.

It shows a weak electronic interaction, like it was found for **CD**. Spectroelectrochemical and ESR measurements of its monoanion brought no evidence for an optical or thermally activated ET process. The excellent electron acceptor ability of the PCTM moiety hinders an effective long-range electron transfer *via* the acetylene bridge, keeping the extra electron localised on one side of the molecule.

To gain a better insight into the distance dependence of ET processes, a series of PCTM diradicals with *p*-phenylenevinylene bridges was synthesised by *Veciana et al.* (Figure 3.13).[158,159] The distance between both *α*-carbons was calculated to lie in a range of 19 – 45 Å.

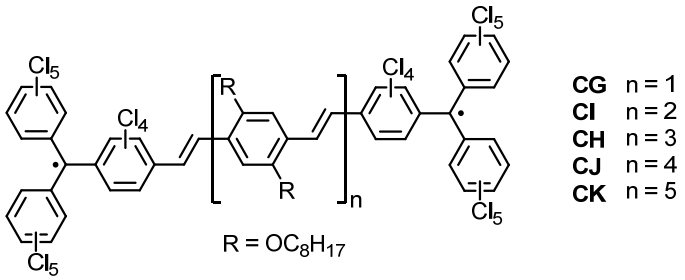

Figure 3.13: Diradicals CG – CK with *p*-phenylenevinylene bridges.

An optical induced electron transfer was observable for the radical anions of **CG** and **CH** *via* superexchange, with effective electronic couplings V_{el} of 109 and 52 cm^{-1}, respectively. Since the coupling is comparable to that of **CD**, effects of the ring substituents are supposed to be rather small. All mixed-valence species showed thermally induced ET in 1,2-dichlorobenzene, except **CK**. With increasing n, the rate of the ET, k_{ET} decreases. Two different regimes at high and low temperature indicated the presence of different ET processes. At higher temperatures, the hopping mechanism dominates, while at low temperatures superexchange is preferred. Depending on the length of the bridge, both mechanisms occur to different extents.

Some other di- and triradicals (**CL**, **CM**) were presented by *Veciana et al.*, using *m*-phenylene units as intramolecular ferromagnetic couplers (Figure 3.14).[160-168] Both compounds show high thermal and chemical stabilities and are high-spin molecules in the ground state.

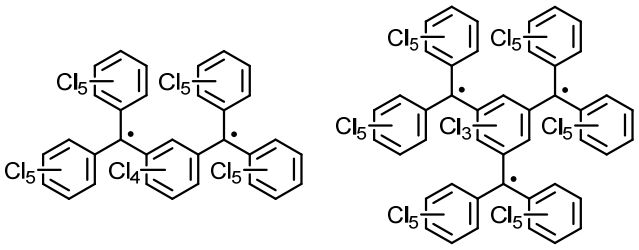

CL **CM**

Figure 3.14: Di- (CL) and triradical (CM) with *m*-phenylene bridge.

The rotation barriers are comparable to that of the PCTM radical. Reversible stepwise reduction processes to the corresponding anionic species were observed. Spectroelectrochemical measurements of **CM** revealed intramolecular ET for both monoanionic and dianionic species. The electronic couplings V_{el} were determined to be 320 and 392 cm^{-1} for $\mathbf{CM^{2\bullet-}}$ and $\mathbf{CM^{\bullet 2-}}$, respectively. The synthesis of other phenylene-bridged dendritic polyradicals with higher generations, was unsuccessful, due to the increasing steric strain.[169,170]

Another example for a stable organic radical is the polychlorinated tris(2,4,6-trichlorophenyl)methyl (TCTM) radical **CN** (Figure 3.15).[118]

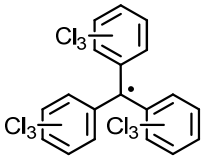

CN

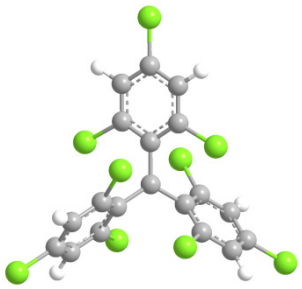

Figure 3.15: The polychlorinated tris(2,4,6-trichlorophenyl)methyl radical CN.[1] Colours are depicted as follows: C, grey; H, white; Cl, green.

Like its perchlorinated counterpart, it is inert to a variety of chemical reagents, due to the shielding of the radical centre by the *o*-chlorine atoms. It also shows characteristic absorption an emission bands and a high NLO response.[124,125] The reduction potential of the TCTM radical is shifted of about –450 mV compared to the PCTM radical.[171] Studies about light-induced ring-closure reactions have not been reported so far. Nevertheless, such reactions also seem to be probable for the TCTM radical. All compounds synthesised and investigated during the scope of this work are derivatives of the PCTM radical. For this reason, only a few examples of the TCTM radical will be presented in the following. The exact position of the chlorine atoms (2,4,6) will not be depicted in the illustrations for simplification.

Juliá et al. published polyradicals with dendritic structure based on the TCTM radical (Figure 3.16).[172] Connection was achieved by the implementation of amide bonds. The synthetic approach differs to the above applicated procedures, as radicalisation of **CO** was not performed

[1] Optimization was performed by means of force field MM2 in ChemBio3D Ultra 11.0.1, CambridgeSoft 2007.

in the last step. Condensation of already radicalised precursors lead to the formation of the desired dendritic structure. Weak antiferromagnetic interactions between the radical centres were shown. CV measurements of **CO** revealed two separated quasi-reversible reduction processes. On the contrary, oxidation took place, at the same potential for all radical centres.

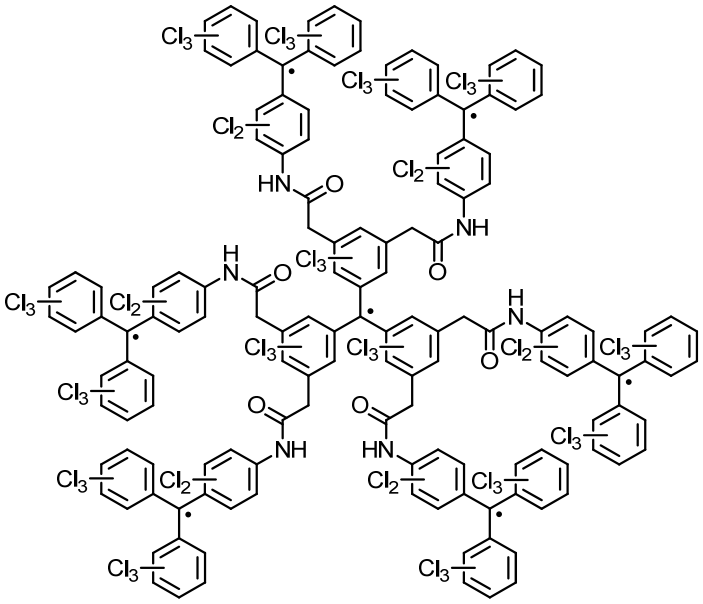

CO

Figure 3.16: Polyradical CO connected *via* amide bridges. The chlorine atoms are situated in *o*- and *p*-position to the C_{ipso} radical centre.

3.3.2.2 Magnetic and Electronic Interactions in Radicals and Radical Ions connected by Non-Covalent Bridges

As shown above, magnetic and electronic interactions between two or more PCTM radicals can be observed through covalent bridges. Interestingly, similar interactions were found for systems connected *via* coordinative or weak bonds (e.g. hydrogen bonds), respectively. In case of compound **DA** (Figure 3.17), ferrocene (Fc) acts as an intramolecular ferromagnetic coupler. The characteristic fine structure of a triplet species was observed in the ESR spectrum of DA in a frozen mixture of CH_2Cl_2/toluene (1/1).[173,174]

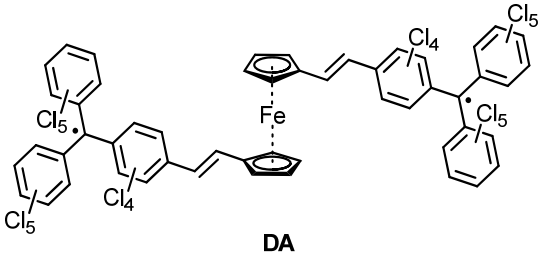

DA

Figure 3.17: Ferrocene-bridged PCTM radicals.

Cyclovoltammetric measurements showed one reversible process for the oxidation of the Fc moiety and one for the reduction of the PCTM radical, respectively. A very weak electronic interaction between the two radical moieties is suggested, since a strong interaction would provide two clearly separated reduction peaks. Instead, an intervalence charge transfer from the ferrocene to the radical unit was revealed by observation of an IVCT band in the NIR range of the absorption spectra. Further studies of ET processes between ferrocene derivatives and PCTM radicals will be presented more detailed in chapter 3.3.3.

A vivid example for a magnetic interaction through hydrogen bonds is the dimer of compound **DB** (Figure 3.18).[175-178] Isomerisation of the *Schiff*-base *trans*-**DB** results in the formation of the *cis*-configurated species, which undergoes dimerisation. This process can occur thermally or photoinduced, whereas the latter only occurs in nonpolar solvents.

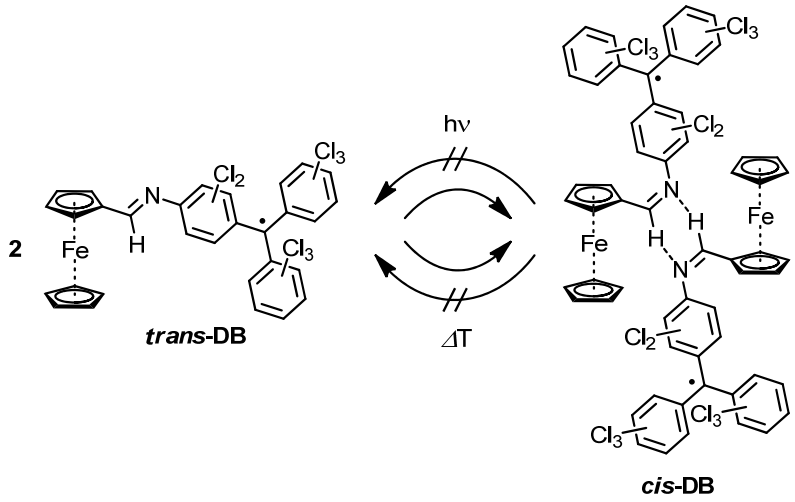

Figure 3.18: Photoinduced *cis*-*trans*-isomerisation of DB .

Strong intermolecular antiferromagnetic interactions were observable between the two electrons of the TCTM radicals. The stabilisation of the *cis*-isomer through hydrogen bonds hinders a reversion of the process in both ways.

Suppression of the dimerisation was achieved by replacing the Fc by its nonamethyl substituted counterpart *trans*-**DC** (Figure 3.19), due to the high steric strain of the additional methyl groups.[178] In contrast to *trans*-**DB** an intramolecular electron transfer between ferrocene and TCTM could be observed in *trans*-**DC**. Further information to the electron transfer phenomena in comparable dyads will be given in chapter 3.3.3.

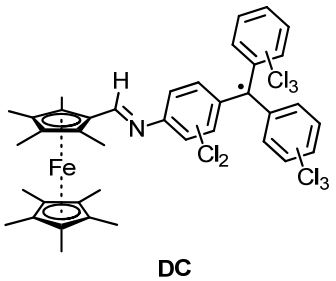

Figure 3.19: Nonamethyl-substituted dyad DC.

Another possibility to study magnetic interactions through hydrogen bonds is provided by PCTM radicals, substituted with –COOH functional groups. Compound **DD**, for example, forms dimeric structures, which show efficient magnetic interactions through their hydrogen bonds in the solid state (Figure 3.20). These interactions strongly depend on the crystallisation conditions. Solids derived from aprotic solvents, such as CH_2Cl_2, show ferromagnetic interactions, whereas in solids derived from protic solvents, e.g. EtOH, such interactions are suppressed, due to the intercalation of solvent molecules. In solution, aggregates formed through Cl···Cl and $\pi\cdots\pi$ interactions are present in a particular concentration range.[179]

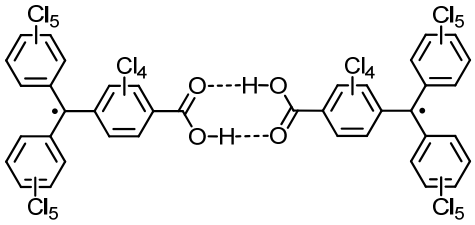

DD

Figure 3.20: Dimer of DD through hydrogen bonds.

Implementation of an additional carboxylic group results in the formation of pure organic radical open frameworks (POROFs) in the crystalline state.[180-184] Regarding the twofold substituted PCTM radical **DE**, the linkage through hydrogen bonds forms a hexameric repetitive unit. The presence of the second –COOH group enables the connection of several hexamers, resulting in two-dimensional layers (Figure 3.21).

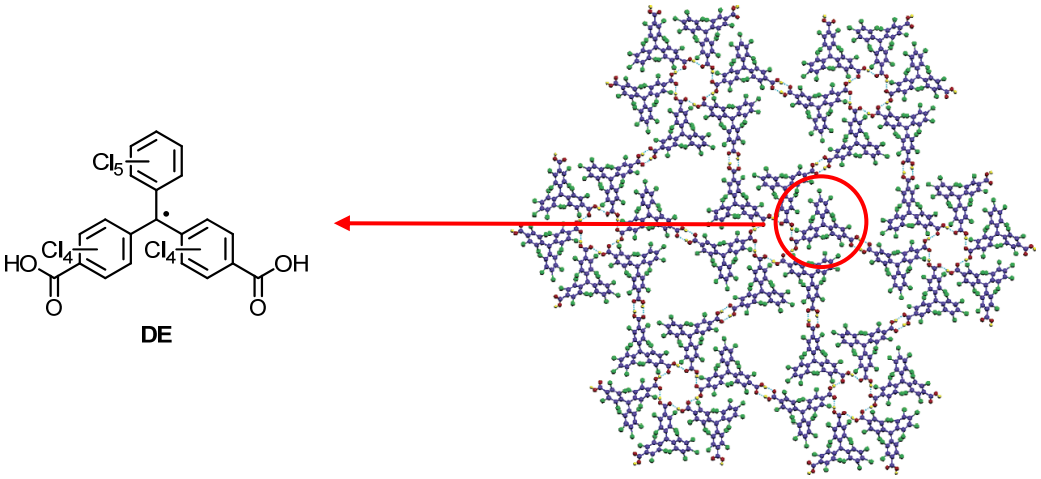

DE

Figure 3.21: Monomeric structure of DE (left) and 2D hydrogen bonded layer of POROF-1 (right).[1]

Self assembly through Cl···Cl interactions generates secondary three-dimensional structures (POROF-1), which possess large hydrophobic cavities. Changing the number and position of the substituents leads to different nanoporous structures with varying magnetic properties. The hydrophilic nanoporous architecture, high thermal stability and long-range magnetic ordering, may be of interest in the development of new multifunctional materials.

[1] Reprinted (adapted) with permission from [180]. Copyright 2004 American Chemical Society.

The above-mentioned abilities of the carboxylic acid substituted PCTM radicals gave rise to the investigation of possible magnetic interactions through coordinative bonds, like they were found for the Fc-bridged compounds. The mono-substituted species **DD**, proved to be an excellent coordinating ligand in complexes with transition metals such as Co(II), Ni(II), Cu(II) and Zn(II).[185-188] Furthermore, a series of lanthanide complexes was presented.[189] Mostly mono- and dinuclear complexes have been synthesised. Two examples with Cu(II) are given in Figure 3.22.

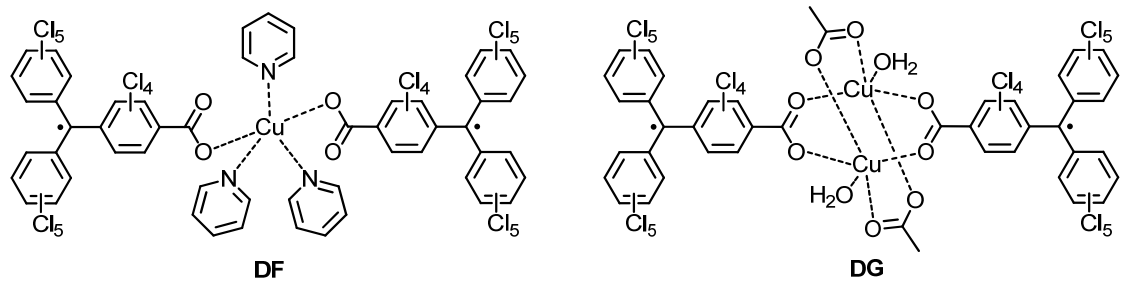

Figure 3.22: Mononuclear (left) and dinuclear Cu(II)/PCTM complex (right).

Complex **DF** shows a slightly distorted square pyramidal geometry and antiferromagnetic exchange coupling interactions between the PCTM subunits, as it was found for most of the mononuclear transition-metal complexes. Complex **DG** crystallises in a paddle-wheel Cu(II) dimeric structure, exhibiting strong antiferromagnetic interactions among the two Cu(II) ions and between the Cu(II) ions and the coordinated PCTM radicals. Since it represents a spin-frustrated system, it possesses a degenerate ground state. In the same line, the substitution of the carboxylic acid group by a sulfonate group was investigated. In comparison to the coordination *via* –COOH groups, the complexes with $–SO_3H$ groups provided a weaker antiferromagnetic behaviour between the PCTM radical moieties.[190]

In contrast to the above shown structure of POROF-1, connection of the PCTM radicals **DE** through coordination bonds to either Cu(II) or Co(II) led to the formation of chain-like structures with antiferromagnetic interactions (Figure 3.23).[191] The formation of 2D supramolecular layers was observed, due to Cl···Cl short contacts.

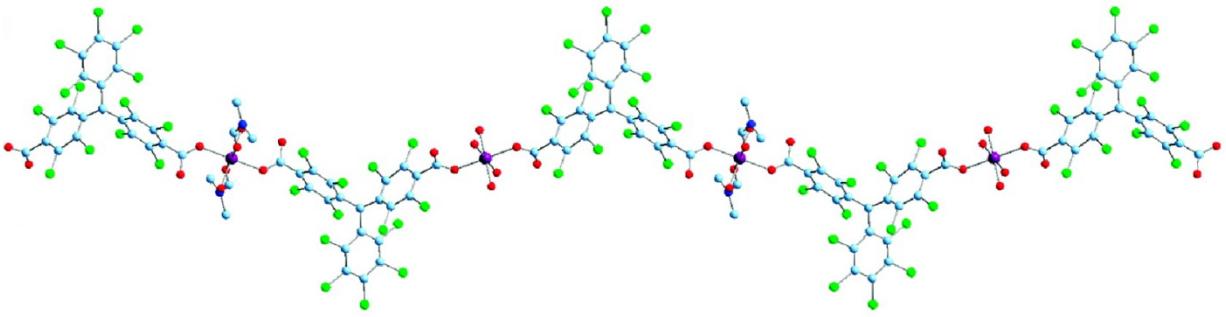

Figure 3.23: Chain-like structure of $[Co(DE)_2(DMF)_2(H_2O)_6] \cdot 5H_2O$.[1] Colours are depicted as follows: C, light blue; Cl, green; O, red; Co(II) violet; N, dark blue.

[1] Reprinted (adapted) with permission from [191]. Copyright 2010 American Chemical Society.

Application of the three-fold substituted PCTM radical **DH** (Figure 3.24) in complexes containing Cu(II) or Co(II) metal ions finally leads to the formation of metal-organic radical open frameworks (MOROFs). One of the first examples was MOROF-1 ([Cu_3(**DH**)$_2$(pyridine)$_6$(EtOH)$_2$(H_2O)]), synthesised by *Veciana et al.* in 2003.[192] The crystal structure revealed 2D honeycomb networks that show antiferromagnetic interactions. Arrangement of the planar layers resulted in very large hexagonal nanopores, which measure 3.1 and 2.8 nm between opposite vertices.

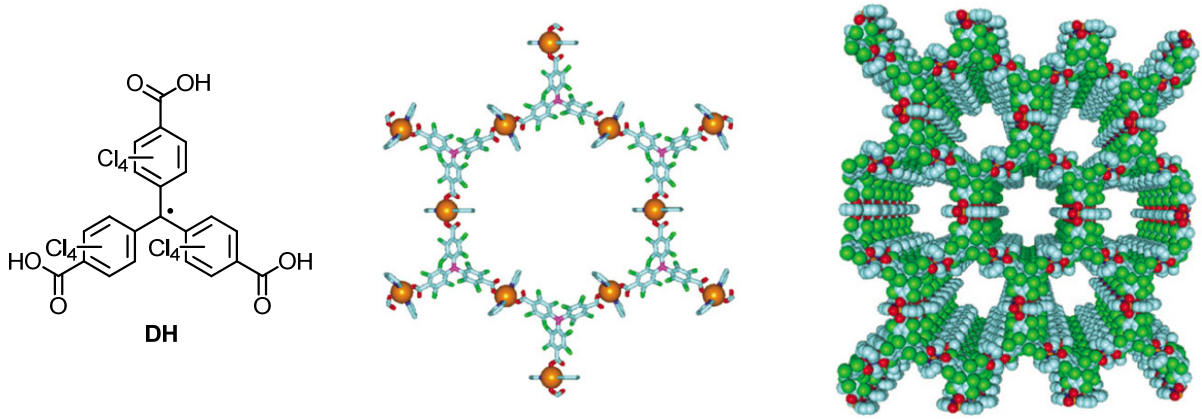

Figure 3.24: Left: Monomeric structure of DH. Middle: Hexagonal pores of MOROF-1.[1] DH units are located in the vertices of the hexagons. The Cu(II) ions are located in the middle of hexagon sides. Right: Distribution of the nanopores in the open framework.[2] Colours are depicted as follows: C, light blue; *α*-C, violet; Cl, green; O, red; Cu(II), orange.

Upon removal from the solution, MOROF-1 becomes an amorphous material, rapidly losing solvent guest molecules (EtOH, H_2O) even at RT. Exposure to EtOH or MeOH, respectively, resulted in a size-recovery up to 90 %. This reversible "shrinking-breathing" can be monitored by X-ray diffraction or changes in the magnetic properties.[193] Two different frameworks including Co(II) metal cores have been developed, named MOROF-2[2] and MOROF-3[3].[194-196] MOROF-2 showed similar antiferromagnetic behaviour as MOROF-1. However, MOROF-3 exhibits mixed ferro- and antiferromagnetic exchange interactions, due to monodentate and bidentate coordination modes between the PCTM radicals and the Co(II) ions. The phenomenon of reversible uptake and release of solvent molecules was not present for both frameworks. *Veciana et al.* published a series of chain-like structures and MOROFs containing lanthanide ions. Magnetic interactions are throughout found to be smaller than in comparable transition metal species.[197-199]

[1] Reprinted (adapted) with permission from [192]. Copyright 2003 Nature Publishing Group.
[2] ([Co(**DH**)$_2$(4,4'-bipyridine)(H_2O)$_3$] • 6EtOH • 2H_2O)
[3] ([Co_6(**DH**)$_4$(pyridine)$_{17}$(H_2O)$_4$(EtOH)])

3.3.2.3 Surface Grafting and Self-Assembly

As apparent from the preceding section, the –COOH substitution of PCTM radicals gave rise to a variety of ordered hydrogen-bonded networks. Particular interest exists in the study of such molecular functional organisations on metal surfaces. *Grillo et al.* investigated the formation of self-assembled supramolecular structures of the three-fold substituted PCTM radical **DH** (Figure 3.25) on Au (111).[200]

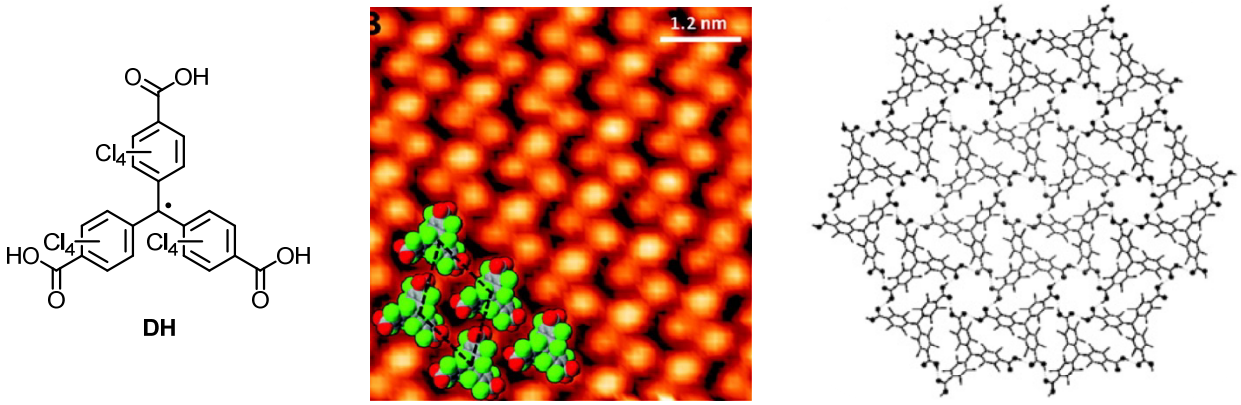

Figure 3.25: DH (left), RT-STM topographic image of DH on Au (111)[1] (middle) and hexameric 2D hydrogen bonded layer of POROF-2[2] for comparison (right).

EPR spectra showed a typical asymmetrical signal for the immobilised PCTM radical derivative, giving evidence to a remaining paramagnetic character of the multilayer after physisorption. Compared to the corresponding single crystals of **DH**, an alternative 2D ordering on the surface is energetically preferred in the absence of interlayer interactions. Racemic assemblies are found in alignment with the high symmetry directions of the Au (111). The authors assumed the intermolecular packing to arise from an interplay of attractive OH···H and repulsive Cl···Cl interactions.

Such Cl···Cl as well as $\pi\cdots\pi$ and van der Waals interactions are decisive in the self-assembly of functionalised PCTM radicals on highly oriented pyrolytic graphite (HOPG), as it was shown for **EA**.[201] As apparent from Figure 3.26, the long alkyl chains in **EA** support the formation of spin-bearing molecular ladders, with weak antiferromagnetic interactions. The neighbouring radical rows consist of head-to-head dimers and are thereby separated by the "diamagnetic" character of the alky chains. Cyclic voltammetry showed one reversible process, attributed to the reduction of the PCTM radical to the corresponding anion.

[1] Reprinted (adapted) with permission from [200]. Copyright 2012 American Chemical Society.
[2] Reprinted (adapted) with permission from [184]. Copyright 2006 Elsevier Ltd.

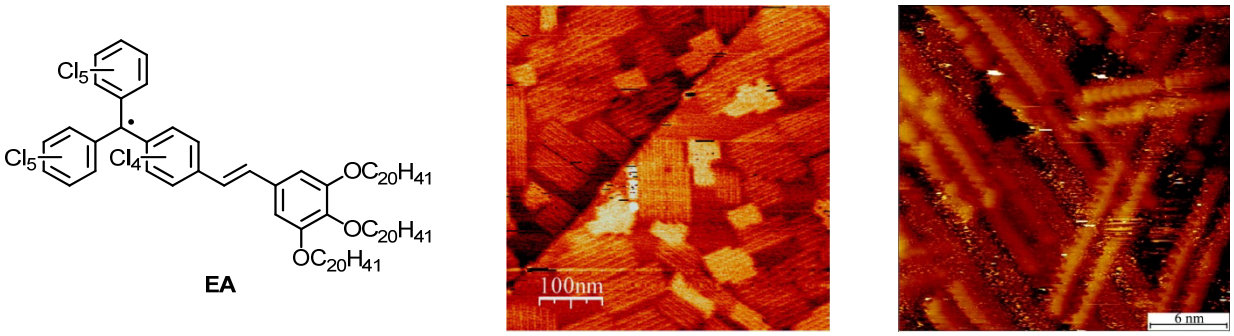

Figure 3.26: Monomeric structure EA (left), AFM image (middle) and RT-STM image of the multilayer on HOPG (right).[1]

Interestingly, the self-organisation of **EA** is not restricted to take place on surfaces. Precipitation from solutions with different polarity revealed the formation of highly ordered microscale objects, which exhibit magnetic properties, fluorescence and superhydrophobicity.[202] Possible applications of such superhydrophob objects are currently the engineering of self-cleaning surfaces.

After physisorption on a surface, the magnetic and electronic properties of the PCTM radical remain unchanged. In order to study these properties, self-assembled monolayers (SAMs) on varying substrates were prepared. Different anchoring groups were used for the chemisorption process of the PCTM radical.[203]

First attempts were reported by *Rovira et al.* in 2007 (Figure 3.27).[204] The PCTM radical was grafted on SiO_2 either by covalent bonds (**EB**) or electrostatic interactions (**EC**). In case of **EB**, the paramagnetic and fluorescent radical was reversibly turnable into its diamagnetic and nonfluorescent anionic species. The system therefore behaves as a chemical switch with a magnetic and an electronic response. Preparation of multifunctional patterned surfaces of **EB** and **EC** by microcontact printing shows the possibility to locally address the PCTM molecules (Figure 3.27 right).

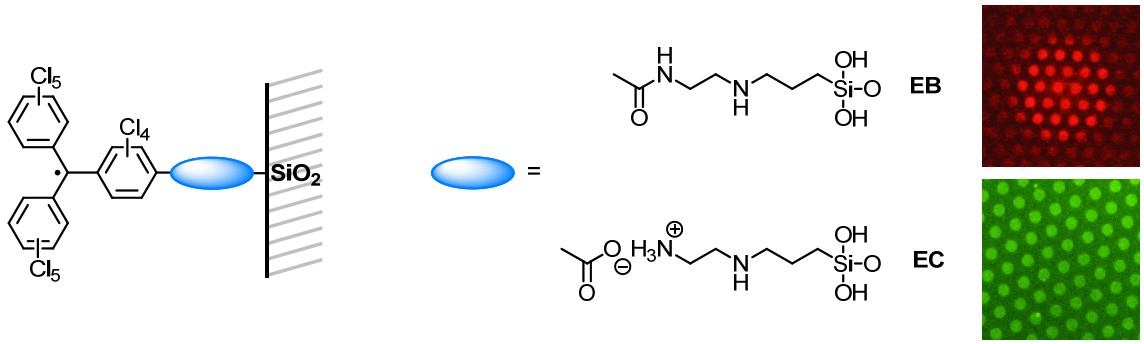

Figure 3.27: Left: Chemisorption of the PCTM radical on SiO_2. Right: Laser scanning confocal microscopy of EB (top) and fluorescence microscopy of EC (bottom).[2]

[1] Reprinted (adapted) with permission from [201]. Copyright 2009 American Chemical Society.
[2] Reprinted (adapted) with permission from [204]. Copyright 2007 Wiley VCH Verlag GmbH & Co. KGaA.

An elastomeric stamp was prepared, consisting of poly(dimethylsiloxane), possessing dots of **DD** or the corresponding carboxylic acid chloride (diameter 5 or 10 *μ*m) in a hexameric pattern. This stamp was brought in contact with a SAM of either the protonated or the neutral form of the alkylic chain shown in Figure 3.27. The fluorescent dots of PCTM radicals on the surface replicate the hexagonal pattern of the stamp, as can be seen by laser scanning confocal microscopy (Figure 3.27 top right) or fluorescence microscopy (Figure 3.27 bottom right).

An additional approach focused on the chemisorption of PCTM radical on Au (111) substrates (**ED**, **EE**, **EF**) (Figure 3.28).[205-209] A reversible redox behaviour was found for the PCTMs grafted on the surface, independently of the nature of the anchoring group. EPR spectra showed characteristic signals of immobilised PCTM radicals. Similar results were found for (SAMs) built on ITO (indium tin oxide) substrates, with silane-substituted alky chains as anchoring groups.[210]

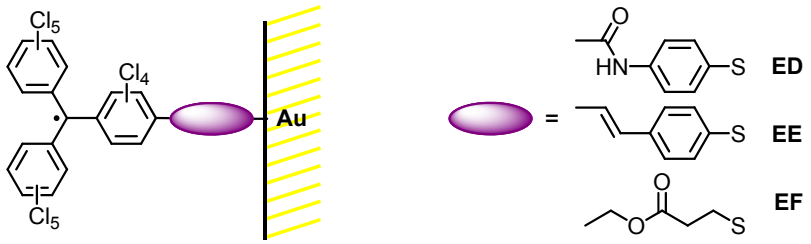

Figure 3.28: Chemisorption on a Au (111) substrate, mediated through different anchoring groups.

Another interesting opportunity for the grafting of PCTM radicals on Au (111) is the formation of SAMs by using Cu(II) metal ions as linkers.[211,212] For this purpose both radical and surface were substituted with –COOH groups, since their coordination ability has been studied before in complexes as well as in MOROFs (chapter 3.3.2.2). NEXAFS measurements[1] clearly show a paramagnetic character of the SAMs. The reported results might be a step towards the growth of MOROFs on surfaces.

3.3.3 Dyads based on the PCTM Radical Acceptor

The preceding section dealed with the intramolecular ET processes between two or more PCTM or TCTM radicals and their corresponding ionic species. As both radicals are excellent electron acceptors, their connection to suitable donors in order to form dyads and triads is obvious.

In dyad **FA**, for example, a ferrocene moiety is linked to the PCTM radical *via* an ethylene bridge.[173,174,213-219] Investigations of the intramolecular electron transfer properties were performed, also in view of a variation of the donor strength of the Fc (**FB**, **FC**) (Figure 3.29). The

[1] Near edge X-ray absorption fine structure measurements

crystal structure of **FA** revealed an almost eclipsed configuration of the cyclopentadienyl rings and the typical propeller-like geometry for the PCTM radical. The directly connected ring is twisted by an angle of ~45° with respect to the ethylene bridge, which shows *trans*-configuration. Interestingly, temperature-dependent Mössbauer spectroscopy demonstrated the coexistence of a neutral and a zwitterionic form in the crystalline phase in a wide temperature range. This phenomenon was ascribed to the bistability of the crystals, induced by electrostatic intermolecular interactions in the charge separated state.[215]

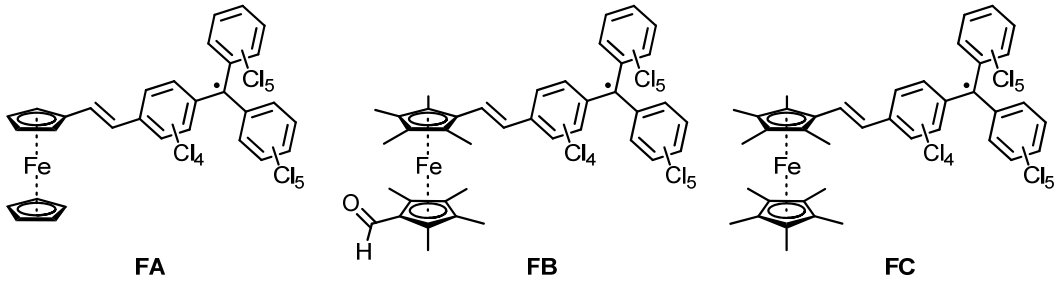

Figure 3.29: Different PCTM based dyads with ethylene-bridged ferrocene donors.

In cyclovoltammetric measurements, reversible redox processes were found for the donor and the acceptor moieties, as expected. Additional to the characteristic bands of the PCTM radical, absorption spectra revealed the presence of an IVCT band in the NIR range, indicating a charge transfer between donor and acceptor. Variation of the solvent polarity showed a positive solvatochromism, which becomes more marked with increasing donor strength of the Fc moiety (**FA** → **FC**). In addition, for **FC** the IVCT bands exhibit throughout the highest intensities, due to a higher degree of charge delocalisation. Despite their optical transitions occur at different energies, **FA** and **FC** both belong to the Robin-Day Class II, showing quite similar, moderate electronic coupling strengths of about 450 cm^{-1}. A LSER (linear solvent energy relationship) analysis of the spectroscopic data showed a linear correlation of the solvent polarity and the ET energies, whereas the latter are furthermore sensitive to the hydrogen-bond donor abilities of the surrounding media. Electrochemical measurements in different solvents were applied to estimate the electron transfer parameters. The authors reported a shift from the normal to the *Marcus*-inverted region with increasing solvent polarity for both compounds. The kinetics of the charge-recombination step of the charge-separated state were studied by the use of picosecond transient absorption measurements, revealing similar recombination rates for both compounds (~10^{12} s^{-1}).[216]

To gain further insight into the influence of a spacer with an extended conjugated systems, compound **FD** was synthesised (Figure 3.30).[220] Compared to the ethylene bridge, connected to one of the cyclopentadienyl rings in **FA**, the acetylene moiety exerts an enhanced electron withdrawing effect on the ferrocene donor. Differently as expected by the authors, this seemed to have a greater influence on the ET than the extension of the spacer.

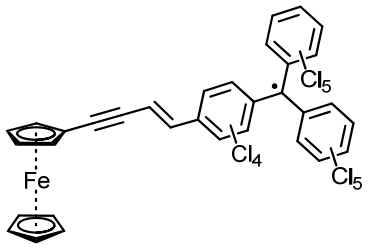

FD

Figure 3.30: PCTM based dyad with an extended spacer.

Apart from ferrocene donors, other examples for neutral open shell dyads based on the PCTM radical are presented in the literature. In compound **FE** (Figure 3.31), the Fc unit is replaced by tetrathiafulvalene (TTF), which is also known to be an excellent electron donor. **FE** exhibits intramolecular electron transfer processes in solution, leading to the formation of self-assembled dimeric species *via* the TTF moiety. Such dimers are found to be ESR-silent in polar solvents, indicating antiferromagnetic couplings. Moreover, variation of the solvent polarity enables reversible switching between the neutral and zwitterionic state. Comparable observations were already reported for a dyad similar to **FC**.[221,222]

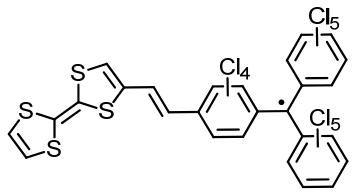

FE

Figure 3.31: PCTM based dyad FE with TTF as an electron donor.

As already mentioned above, the PCTM radical can easily be reduced to its corresponding anion and is therefore an excellent electron acceptor. The work of *Ito et al.* demonstrated the PCTM anion to act as an electron donor, when covalently bound to stronger acceptors, e.g. C_{60} (Figure 3.32).[223]

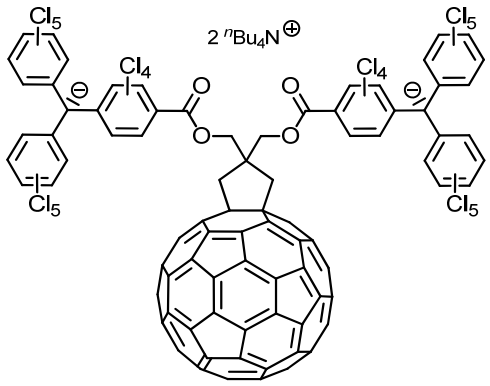

FF

Figure 3.32: PCTM anion as an electron donor connected to C_{60}.

As expected, one reversible oxidation process for the PCTM anions and two reversible reduction processes for C_{60} were observed by cyclic voltammetry. Charge-separation processes were investigated using time-resolved fluorescence spectroscopy and transient absorption measurements. Photoinduced charge separation at RT was proposed to occur *via* two intermediates, C_{60}–^{1}(PCTM$^-$)*(PCTM$^-$) and $^1C_{60}$*–(PCTM$^-$)$_2$, independent on solvent polarity. A possible pathway *via* ISC to the $^3C_{60}$*–(PCTM$^-$)$_2$ could be excluded, because the quantum yields of the charge separation were found to be almost unity in all solvents. A lifetime of the CS state $C_{60}^{\bullet-}$–(PCTM$^\bullet$)(PCTM$^-$) of 81 ns in toluene was reported, which is, according to the authors, comparable to other C_{60} based dyads.

A class of donor moieties that is already commonly used in optoelectronic and electrochromic devices are triarylamines. Upon oxidation, they form stable radical cations, which makes them suitable for the application as hole-transporting materials.[16] The redox potential of triarylamines, as well as their stability can easily be tuned by variation of the substituents in *p*-position of the phenyl rings.[224] For this reason, a series of D-A compounds, based on a PCTM radical acceptor and a triarylamine with varying donor strength was synthesised by our group (Figure 3.33).[225-227]

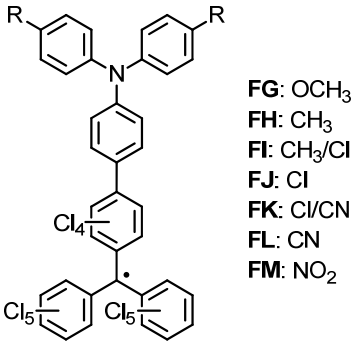

Figure 3.33: Dyads, composed of a triarylamine donor with varying donor strength and a PCTM radical acceptor.

All compounds were investigated in view of their photophysical properties. ET parameters were determined by a detailed band shape analysis of the absorption or fluorescence bands by employing the *Jortner*-model. Absorption spectra of all compounds showed the presence of IVCT bands in the NIR range. With increasing donor strength the IVCT bands showed a bathochromic shift, as it was already reported for comparable compounds, e.g. **FA**. The same trend was observable for the emission bands. As already described above, the bulky chlorine atoms in *o*-position cause a strong twist of the phenyl rings in the biaryl system. As a consequence, the electronic coupling was expected to be relatively small. The resulting slow back electron transfer process from the excited CT state to the ground state leads to an enhancement of the fluorescence quantum yields up to 40 %, which is quite high, compared to other emissive organic *π*-radicals. Transient absorption measurements in the ns time regime

revealed fluorescence to occur from the lowest lying CT state. Increasing strength of the donor caused a decrease in the excited state lifetimes.

Appropriate modification of compound **FG** (**FN**-**FP**) (Figure 3.34) allowed investigation of an influence on the electron transfer by changing the nature of the bridge.[227-229] Similar to the above-presented dyads, an optically induced ET could be proved by the presence of IVCT bands in the NIR range of the absorption spectra. An almost comparable electronic coupling was found for **FN** and **FP** (V_{el} ~2600 cm^{-1}), regardless of the solvent polarity, whereas it was clearly lower in case of **FO** (V_{el} ~2300 cm^{-1}).

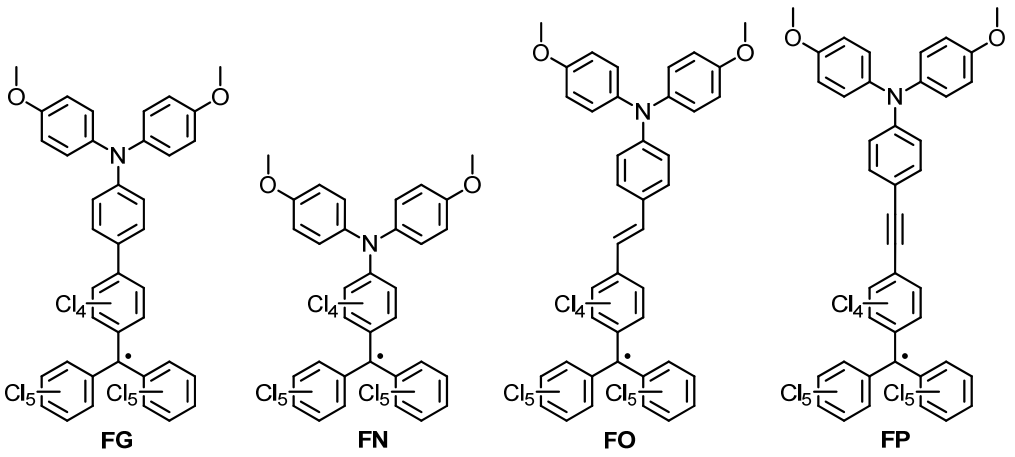

Figure 3.34: Dyads composed of triarylamine donors and PCTM radical acceptors with varying bridges.

This observation is contrary to a comparable bistriarylamine radical-cation, connected by either an acetylene or ethylene moiety, where the electronic coupling was reported to be higher in the latter case. The minor electronic coupling in **FO**, compared to **FP**, was also supported by the throughout lower extinction coefficient of the IVCT band. A twist of the ethylene moiety, caused by steric effects of the chlorine atoms, might explain this observation. In case of **FG**, a fit of the IVCT band was only possible in nonpolar solvents, which excluded a proper evaluation of V_{el}. However, the extinction coefficients of the IVCT bands were found to be smaller than the ones for **FP** and **FO**, pointing towards to a smaller electronic coupling. This is supported by the above mentioned twisting of the two aromatic rings in the biaryl moiety. Detailed analyses of the excited-state dynamics were performed for all compounds except **FN**, but will not be presented here.[226,230]

In view of a possible application in electronic devices, polymer **FQ** (Figure 3.35) was synthesised in our group.[231] This polymer represents the first polymeric neutral mixed-valence compound. Like the monomer **FO**, it exhibits an intramolecular CT, which is located on one of the donor/acceptor moieties. Polymer **FQ** formed air-stable amorphous films and was therefore tested in OFETs. Though the charge-carrier mobilities were found to be rather low, the synthesis of **FQ** was a first step towards the application of neutral MV polymers in organic devices.

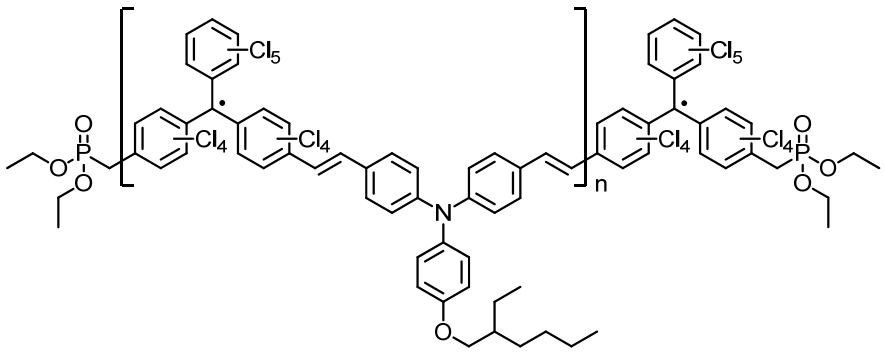

FQ

Figure 3.35: A polymer (FQ) consisting of a triarylamine donor and a PCTM radical acceptor.

Juliá et al. synthesised a series of dyads based on the TCTM radical directly linked to a carbazole donor moiety.[232-235] A variation of the optical and electrochemical properties was achieved, changing the donor strength of the carbazole by implementation of suitable substituents (Figure 3.36).

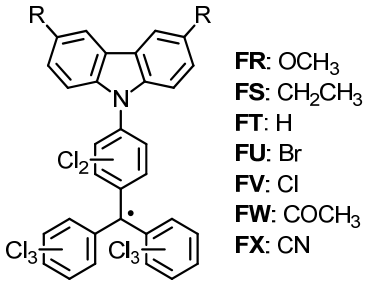

FR: OCH_3
FS: CH_2CH_3
FT: H
FU: Br
FV: Cl
FW: $COCH_3$
FX: CN

Figure 3.36: TCTM radical based series of dyads with carbazole donors with varying donor strength.

Altogether, the absorption bands at lower energy show a bathochromic shift with increasing donor strength, confirming an intramolecular CT between the carbazole and the TCTM radical, which is most pronounced for the methoxy-substituted compound **FR**. Emission maxima covered the red spectral band of the visible spectrum and exhibited a similar trend as the absorption bands at lower energy. As the fluorescence quantum yields decrease with increasing CT character of the transition, no fluorescence could be observed for the methoxy-substituted compound. Furthermore, reduced quantum yields were obtained in more polar solvents. Implementation of more than one carbazole moiety attached to the TCTM radical core led to an enhancement of the CT bands and to a greater red-shift of the absorption maxima. However, no detailed studies concerning the ET parameters of those systems were carried out.

A similar behaviour concerning the absorption and emission characteristics was found for the indole-substituted dyad **FY** (Figure 3.37). Interestingly, DSC (differential scanning calorimetry) measurements of **FT** and **FY** revealed the formation of stable amorphous glasses. A study of the charge transport properties showed high mobility values for both, electrons and holes, which might provide an access for a possible application in organic devices, e.g. OFETs.[236,237]

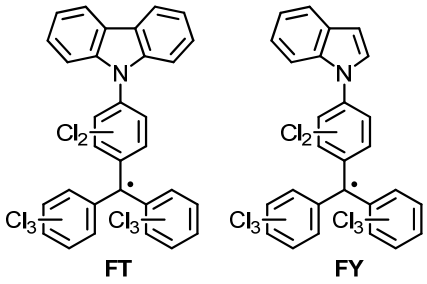

Figure 3.37: Carbazole-based (FT) and indole-based (FY) dyads forming amorphous glasses.

3.4 1,2,3-Triazoles as Versatile Linkers

The preceding sections focused on the PCTM radical acceptor and ET reactions with suitable donor species. The ET behaviour in such donor acceptor compounds is strongly influenced by the way both units are connected. There has been great effort on the development and investigation of new bridging units. One field that provides access to a great number of possible spacers is click chemistry. Disregarding the nature of building blocks or reaction conditions, click reactions are believed to be easy to perform and should result in high yields of the desired product species. Processes, that fulfil these criteria of a click reaction are, for example, hetero *Diels-Alder* reactions or 1,3-dipolar cycloadditions. A well-known example for the latter is the reaction of acetylenes and azides to 1,2,3-triazoles. First reported by *Michael* in 1893, such reactions were intensively studied by *Huisgen* and co-workers.[238,239] The lack of regioselectivity and the need of elevated temperatures limited the possible applications at first. In 2001, the groups of *Meldal* and *Sharpless* independently reported about the implementation of Cu(I) catalysts into such reactions.[240,241] Relative to the thermally activated process, exclusively 1,4-regioisomers are formed due to the drastic change of the reaction mechanism.[1] Moreover, reaction rates were increased by a factor of up to 10^7. The copper-catalyzed acetylene azide cycloaddition (CuAAC) can be performed in solvents with variable polarity and is mostly unaffected by the nature of the building blocks, hence tolerating many functional groups. During the last decade, a wide range of experimental conditions has been reported. The application of several different catalysts, ligands and additives was studied to overcome problems like the formation of copper aggregates or the oxidative coupling of two acetylenes.[243-254]

Detailed investigations including computational methods were performed to analyse the mechanistic details of CuAAC.[255,256] Up to now, several different reaction mechanisms were proposed, but no precise statements concerning especially the active acetylene copper species were made. First approaches focused on reaction pathways provided by mononuclear Cu(I) acetylides. However, several studies of the reaction kinetics revealed a second order rate dependence on the catalyst concentration. Nowadays it is clear that the mechanism is much more complex, also because of multiple equilibria steps during the catalytic cycle. *Fokin et al.* proposed a catalytic model including two Cu atoms, reinforced by *in situ* calorimetry and metal isotope crossover methods (Scheme 3.4). Upon combination of an isotopically pure ^{63}Cu(I) catalyst with a Cu(I) acetylide with a naturally isotopic distribution (^{63}Cu/^{65}Cu 69:31), the authors observed a change in the isotopic ratio (^{63}Cu/^{65}Cu 85:15 after the reaction). Precise investigations revealed the redistribution to take place within the cycloaddition step.

[1] Meanwhile the direct synthesis of the corresponding 1,5-regioisomeric triazoles was developed by application of Ru(II) catalysts.[242]

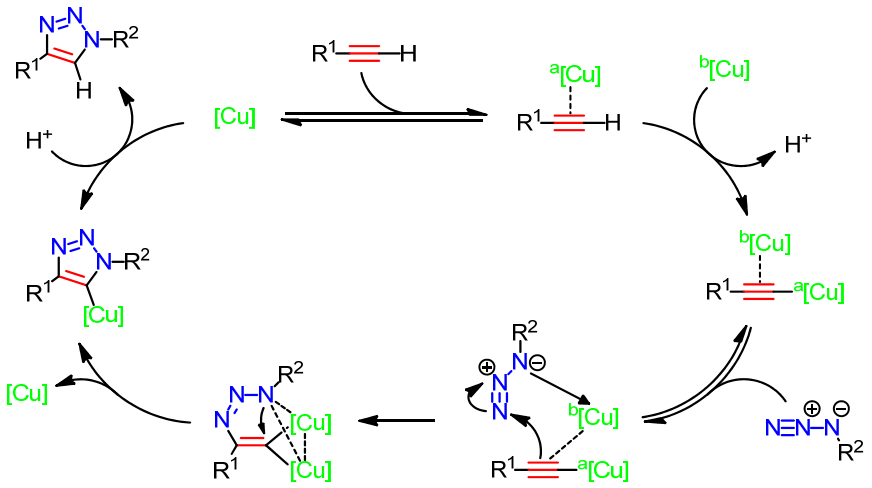

Scheme 3.4: Proposed catalytic model for the CuAAC reaction with two Cu ions. [a][Cu] denotes a Cu(I) species with naturally isotope distribution (^{63}Cu/^{65}Cu 69:31); [b][Cu] an isotopically pure ^{63}Cu(I) species.[233]

Indeed, varying catalyst systems with different ligands, additives and solvents may exclude one definite mechanism. Hence, further investigations will be necessary for a better understanding of the Cu(I)-catalysed formation of 1,4-disubstituted 1,2,3-triazoles.

The high chemical stability (e.g. against hydrolysis, oxidation and reduction), as well as their aromatic character and the strong dipolemoment (5.2 – 5.6 D) led to numerous applications of triazoles,[257-266] e.g. in drug discovery,[267] as two-photon absorbers,[268] organic semiconductors (**IA**),[269] tunable light emitters (**IB**)[270] or linkers in donor-acceptor compounds (**IC**)[271] (Figure 3.38).

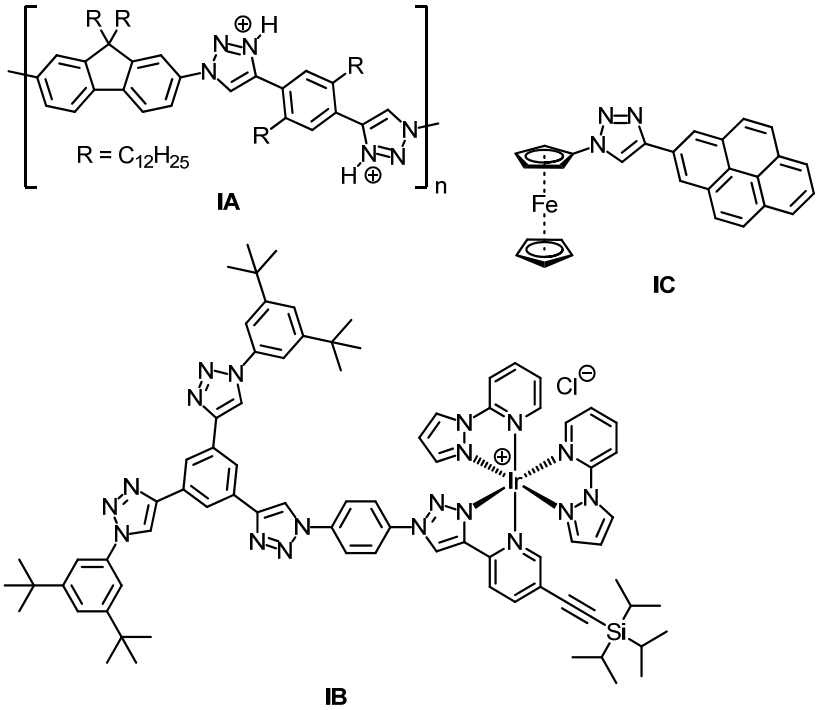

Figure 3.38: Application of triazole linkers.

4 Project Aim

4.1 Synthesis and Investigation of Redox Cascades

The most direct way to investigate charge-transfer processes in artificial systems is probably the synthesis of small molecules. In addition to an easy synthesis, such systems may provide a defined geometry and simple spectral and electrochemical features, which are important for a detailed interpretation of the results.

The aim of this project is the synthesis of redox cascades, focusing on the investigation of the photophysical and electrochemical properties. The basic structure of the herein synthesised compounds (Figure 4.1) resembles other cascades already investigated in our group.[272,273] All cascades comprise two donor units D1 and D2, covalently attached to an acceptor moiety A, and possess a downhill-directed redox gradient from D1 to D2. Additionally, reference compounds consisting of an acceptor A and only one donor D1 shall be synthesised, to allow a detailed interpretation of the results obtained from the measurements.

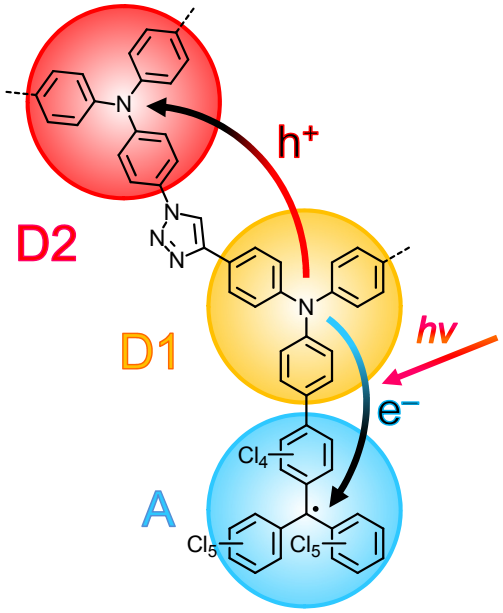

Figure 4.1: Generalised representation of triarylamine-based redox cascades and corresponding photoinduced charge-transfer processes.

Triarylamines are excellent electron donors and are well known as hole-transporting materials e.g. in OLEDs.[16] The redox potentials of triarylamines can easily be tuned by adequate substituents in the *p*-position of the phenyl rings.[224,274-276] Functionalisation of the *p*-position also increases the stability of the triarylamines, due to the prevention of dimerisation processes during oxidation.[277] In the herein synthesised compounds, the easy tunability of the triarylamines provides an opportunity to adjust the internal redox gradient.

Bridging of the triarylamine donors D1 and D2 was achieved by introduction of a 1,2,3-triazole unit *via* click chemistry. As already mentioned in chapter 3.4, triazoles show an aromatic character and are highly stable. For this reason, they are widely used as spacer units in versatile compounds. Two triarylamines connected by a triazole bridge show a moderate electronic coupling of about 710 cm^{-1},[278] which should guarantee a charge-separation process between D1 and D2 with high efficiency.

As an electron acceptor, the PCTM radical was chosen. It can easily be reduced in a reversible process and is highly stable against a variety of chemical reagents. The diversity of the PCTM radical and its application as an acceptor was already presented in chapter 3.3.3 in detail. The PCTM radical acceptor was linked to the triarylamine donor D1 by a biphenyl spacer. The almost perpendicular orientation of the two adjacent phenyl rings, due to the high steric claim of the chlorine atoms should ensure a small electronic coupling V_{el}. This was already demonstrated for a series of donor-acceptor dyads **FG** – **FM** (Figure 3.33) published by our group.[225] The results obtained for **FG** – **FM** showed the formation of a CT state between A and D1 upon excitation. This observation is important for the cascades synthesised within this work, since the formation of a CT state is the basis for a following population of other states.

Keeping the aforementioned facts in mind, the following scenario is expected to take place in the herein synthesised cascades upon excitation: First, a charge-transfer (^{2}CT) state between A and D1 is formed. Ideally, this will be followed by an efficient hole transfer from D1 to D2, resulting in the population of a charge-separated (^{2}CS) state. As already mentioned in Chapter 1, investigation of charge-separation, -transfer, and -recombination processes in small compounds is the key for mimicking biological systems, and for an optimisation of device performance. For this reason, the main goal of this work is the photophysical study of such processes in the herein synthesised compounds. An important aspect of the investigations of the charge-recombination processes is the influence of spin correlation *vs*. inverted-region effects. As already discussed in Chapter 2.1 and 3.2, the inverted-region effects are often less pronounced than expected.[28] Some authors therefore ascribe the observation of long-lived charge-separated states to the phenomenon of spin correlation. In the herein synthesised cascades, the investigated states are expected to be doublets. For this reason, intersystem crossing (ISC) between singlet and triplet states should not be present here and can therefore be excluded. The dynamics of the charge-transfer process may be attributed to inverted-region effects and/or the electronic coupling V_{el}, respectively.

Systems containing unpaired electrons have been reported in several publications to this point. Albeit, the focus of these publications mainly lies on investigations concerning the influence of an additional spin on charge-transfer dynamics, radical-induced quenching of locally excited states or spin polarisation as a result from three-spin mixing.[279-283] To this date, no detailed study concerning the excited-state dynamics of open-shell cascades has been published.

Synthesis of the cascades will mainly be focused on the application of transition-metal-catalysed cross-coupling reactions. Introduction of the PCTM radical acceptor will be performed by radicalisation of the corresponding *α*-H precursor in the last step. A full characterisation of the herein synthesised open-shell compounds shall be guaranteed by means of several optical, e.g. absorption and emission spectroscopy, and electrochemical measurements. Cyclic voltammetry is an adequate technique to characterise a correctly directed redox gradient. Besides, differential pulse voltammetry shall be used to check the degree of radicalisation, since this in general is not possible by means of NMR spectroscopy or mass spectrometry. Spectroelectrochemical measurements provide an insight into the spectral characteristics of the radical ions of the donor and acceptor moieties, which is important for an interpretation of the results obtained by transient absorption spectroscopy. The latter offer the opportunity to study the kinetics of the excited states down to the femtosecond time-regime.

4.2 Synthesis of Donor-Acceptor substituted Diketopyrrolopyrroles

One part of this work deals with the synthesis of donor-acceptor-substituted diketopyrrolopyrroles (DPPs). Since the accidental discovery of the DPP chromophore (Figure 4.2) by *Farnum et al*. in 1974[284] a great variety of the deeply coloured DPPs has been synthesised and investigated.

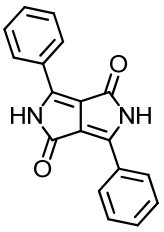

Figure 4.2: Structure of the DPP dye.

The outstanding thermal, photochemical and mechanical stability of the DPPs was the cornerstone for a class of commercially available high-performance pigments, which are widely used in paints, inks, and plastics.[285-287] The colour of the DPPs can easily be changed by variation of the substituents in *p*-position of the phenyl rings and ranges from orange-yellow to violet, which makes them an ideal candidate for application in OPVs. In addition, their excellent emission properties gave rise to investigate their performance in other optoelectronic devices.[288,289]

DPP-polymers show exceptional film-forming characteristics and film morphologies and are therefore firmly used in bulk-heterojunction (BHJ) solar cells. Copolymers with e.g. thiophene or fluorene moieties have been investigated as donor and acceptor materials, respectively. Albeit, research concerning solar cells is mainly centred on polymers, promising attempts with small DPPs attached to triarylamines have also been reported. DPPs are in the focus of interest in view of solid-state dye lasers,[290] two-photon absorbers,[291] and the application in OFETs.[292-294] Moreover, the DPP core showed excellent electron-transporting capabilities in small donor-acceptor compounds, with provided an application in dye-sensitised solar cells (DSSCs) with efficiencies up to 6 %.[289,295-303]

The main goal of this part of the work was the synthesis of a donor-acceptor substituted DPP. A triarylamine and a PCTM radical were chosen as a donor and an acceptor for the same reasons already discussed above (Chapter 4.1). To deal with the almost complete insolubility of the DPP core (Figure 4.2) it will be necessary to introduce alkyl-chains at the nitrogen atoms. The so-generated donor-acceptor compound (Figure 4.3) might serve as a monomer for a subsequent synthesised polymer. An investigation in view of the charge-transfer properties for both compounds would be of interest for a possible application of the polymer in optoelectronic devices.

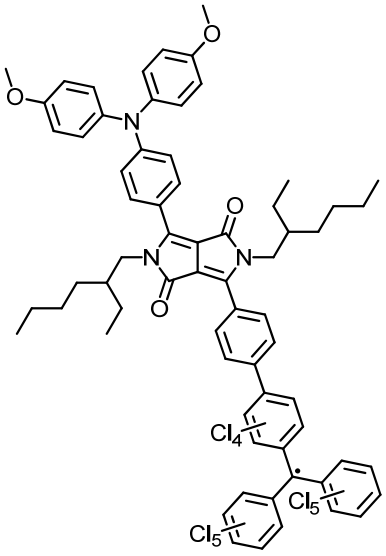

Figure 4.3: A donor-acceptor substituted DPP.

5 Results and Discussion

5.1 Synthesis

5.1.1 Synthesis of Cascades with Triazole Bridges

In this chapter, the synthesis of the reference compounds **1** and **4**, as well as the cascades **2**, **3**, **5**, and **6** will be discussed. In addition, synthesis of the required precursors will be presented. Chart 5.1 provides an overview of the herein synthesised compounds **1** – **6**.

Chart 5.1: Compounds 1 – 6.

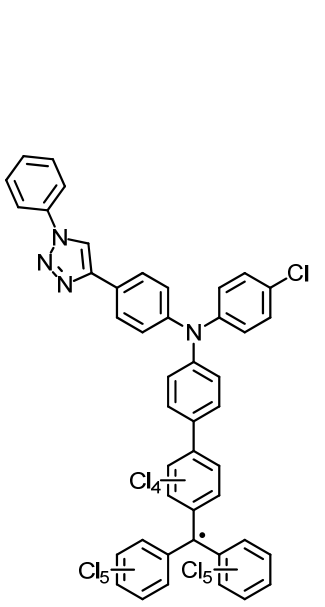

1

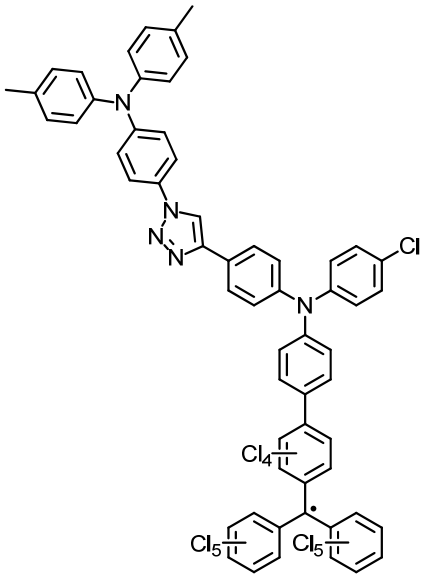

2

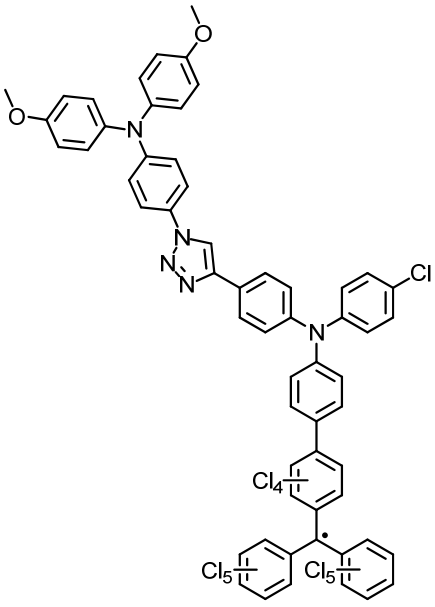

3

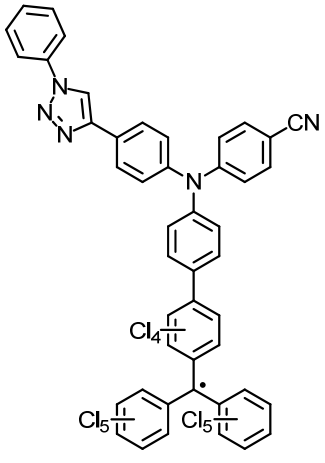

4

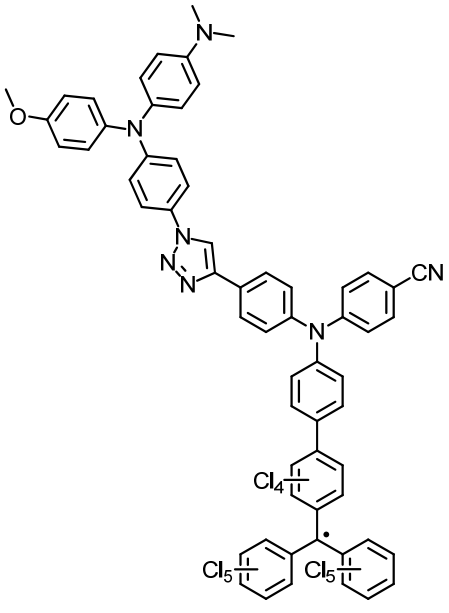

5

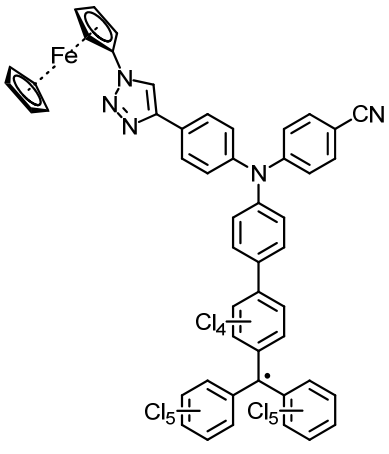

6

For a better understanding of the performed synthesis, a retrosynthetic approach is depicted in Scheme 5.1. All radicalised species shall in the following be generated from their corresponding *α*-H precursors. The triazole bridge, connecting the triarylamines D1 and D2, will be build up by click chemistry of an aromatic acetylene with an appropriate aromatic azide. The latter will be obtained from their corresponding bromo-analogues. A *Suzuki-Miyaura* coupling of the perchlorinated acceptor with a second triarylamine should provide access to the biphenyl spacer between D1 and A.

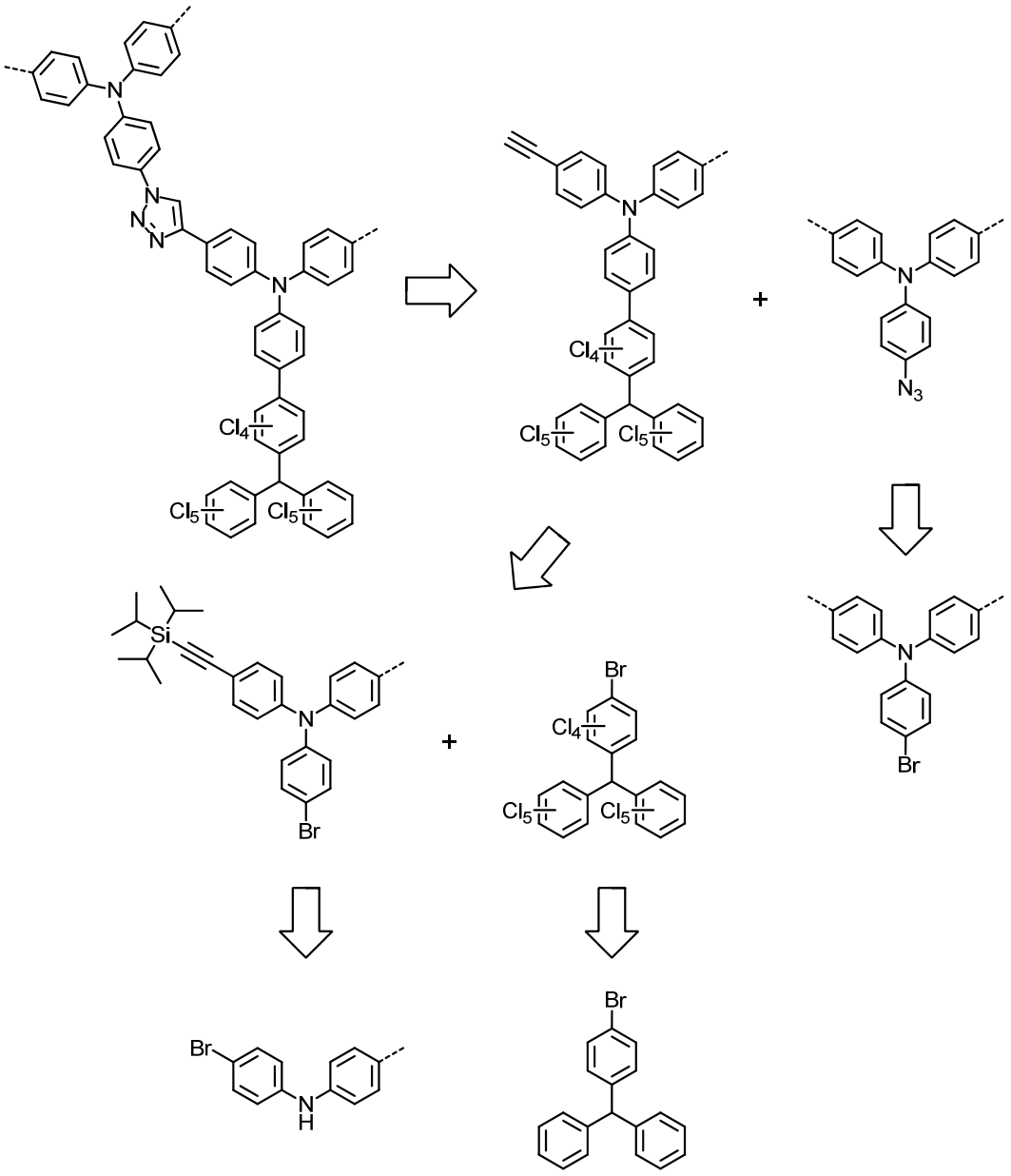

Scheme 5.1: Retrosynthetic route for the generation of compounds 1 – 6.

Synthesis of the chlorine-substituted reference compound **1** as well as the cascades **2** and **3** started with the generation of the diarylamine **7** by a Pd-catalysed *Buchwald-Hartwig* cross coupling[304,305] (Scheme 5.2). Compound **7** was subsequently brominated with $^{n}Bu_4NBr_3$ in $CHCl_3$[306] that is superior to Br_2 because it is much easier to handle and less toxic. Several

attempts were made to generate **9** directly in a one-step palladium or Cu-catalysed reaction from 4-chloroaniline and 4-bromoiodobenzene. Due to the electron poor character of both reactants, no reaction was observed. Therefore, 4-chloroaniline was first coupled with iodobenzene and subsequently brominated in a second step. First step in the synthesis of the cyano-substituted compounds **4 – 6** was the generation of **8** based on aniline and 4-bromobenzonitrile. Bromination of **8** was achieved in an analogueous way to **7** with tetra-*n*-butylammonium tribromide in $CHCl_3$.

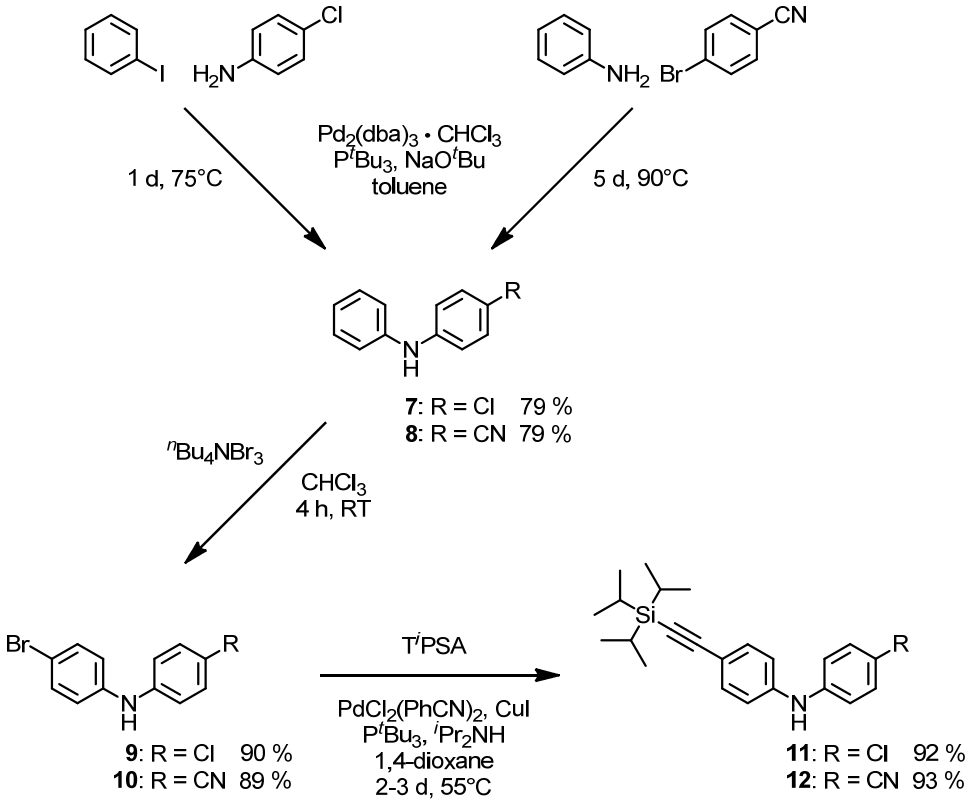

Scheme 5.2: Synthesis of the precursors 7 – 12.

In the following, an alkynyl moiety was introduced *via* Pd-catalysed *Sonogashira-Hagihara* coupling[307-309] with tri-*i*-propylsilylacetylene (T^{i}PSA) to generate **11** and **12**, respectively. The remarkable stability with respect to basic conditions played a decisive role in the choice of the tri-*i*-propyl protecting-group. Therefore, side reactions in subsequent coupling reactions should be minimised.

The triarylamines **13** and **14** were not accessible *via* standard *Buchwald-Hartwig* or *Ullmann*[310-312] reactions, due to the electron poor character of the reactants. Several transition-metal/phosphine ligand combinations were tested. Most of them led to very low yields (less than 5 %), the rest failed completely. Rather drastic conditions with activated Cu in *o*-dichlorobenzene at 180°C gave rise to the desired triarylamines **13** and **14** shown in Scheme 5.3. Further coupling with pinacolborane resulted in the pinacolesters **15** and **16**, which served as reagents for an aqueous *Suzuki-Miyaura* coupling[313,314] with the perchlorinated precursor **18** (Scheme 5.4).

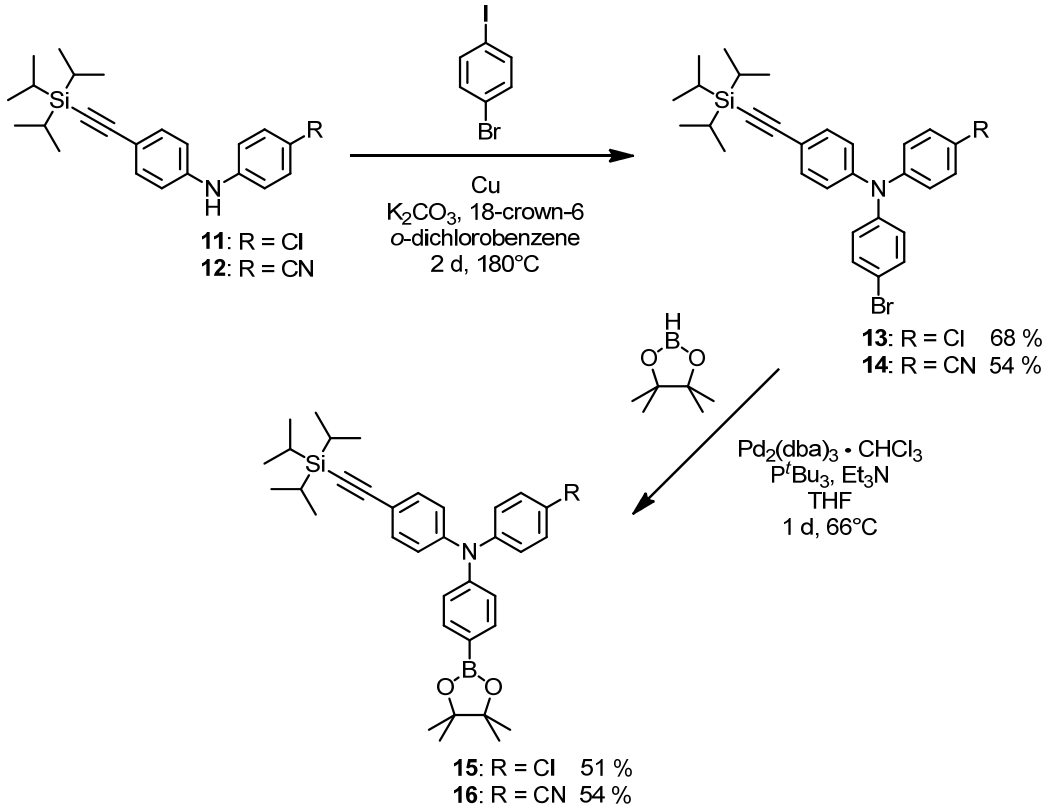

Scheme 5.3: Synthesis of the precursors 15 and 16.

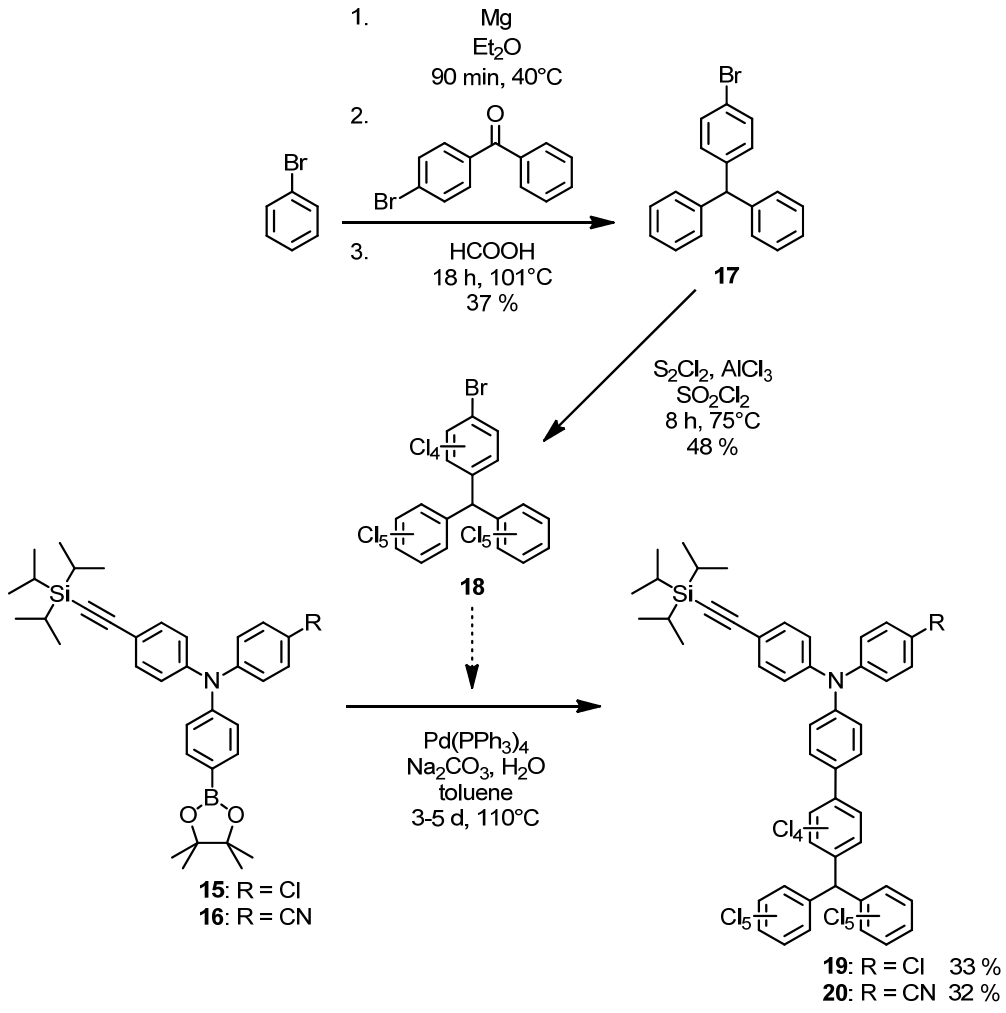

Scheme 5.4: Synthesis of the precursors 17 – 20.

In general, perchlorinated compounds are synthesised from their triphenylmethyl precursor, which in this case was obtained from 4-bromobenzophenone and bromobenzene in a *Grignard* reaction. The carbinole, resulting from the first step, was directly reduced to 1-bromo-4-(diphenylmethyl)-benzene **17** with formic acid. Compound **17** was then treated with a mixture of S_2Cl_2 and $AlCl_3$ in SO_2Cl_2 to achieve full chlorination by the so-called BMC (*Ballester*/*Molinet*/*Castañer*) method.[111,315] The *Suzuki-Miyaura* coupling of **18** with **15** and **16** to **19** and **20** was one of the crucial points in the synthesis, giving rather poor yields of around 30 %. No improvement of the yield was achieved in several attempts, which might be due to the high steric claim of the perchlorinated precursor originating from the chlorine substituents. Deprotection of the T^{i}PSA group was accomplished by tetra-*n*-butylammonium fluoride (^{n}Bu$_4$NF) in THF in the dark,[316] and resulted in the desired species **21** and **22**, featuring a free acetylene group (Scheme 5.5).

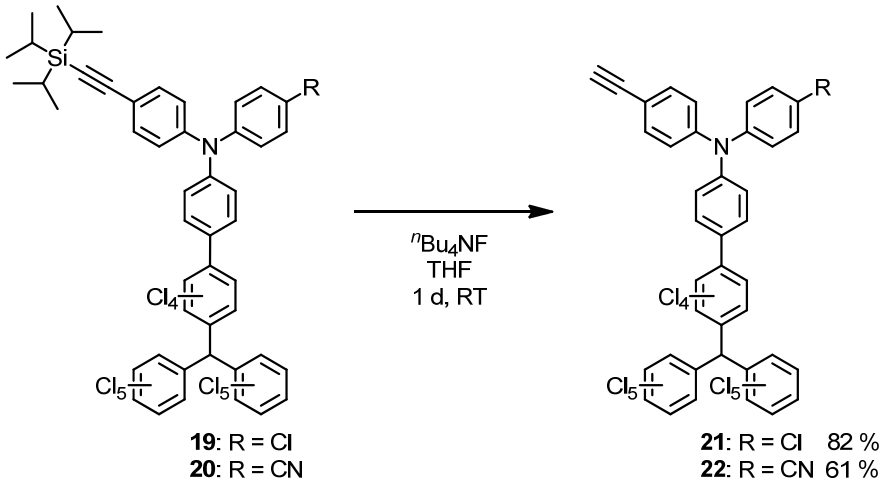

Scheme 5.5: Synthesis of the precursors 21 and 22.

Ullmann coupling of 4-bromoaniline with 4-iodotoluene and 4-iodoanisole led to the appropriate triarylamines **23** and **24**, respectively (Scheme 5.6). A different route had to be chosen to obtain the asymmetrical triarylamine **26**, which was synthesised by *Buchwald-Hartwig* cross coupling of 4-bromo-*N*,*N*-dimethylaniline and 4-methoxyaniline,[316] followed by an *Ullmann* coupling of **25** with 4-bromo-iodobenzene.

Conversion of the aryl bromides **23**, **24** and **26** into the corresponding aryl azides **27** – **29** was achieved *via* Cu(I)-catalysed reaction with NaN_3 (Scheme 5.7). CuI was chosen as the catalyst, supported by *N*,*N*'-dimethylethylenediamine (DMEDA) and L(+)-sodium ascorbate. L(+)-sodium ascorbate is used as a reducing agent to maintain the Cu(I) concentration at a high level during the reaction. This system provided reasonable reaction conditions, as well as good yields for several systems reported in the literature.[278,317,318]

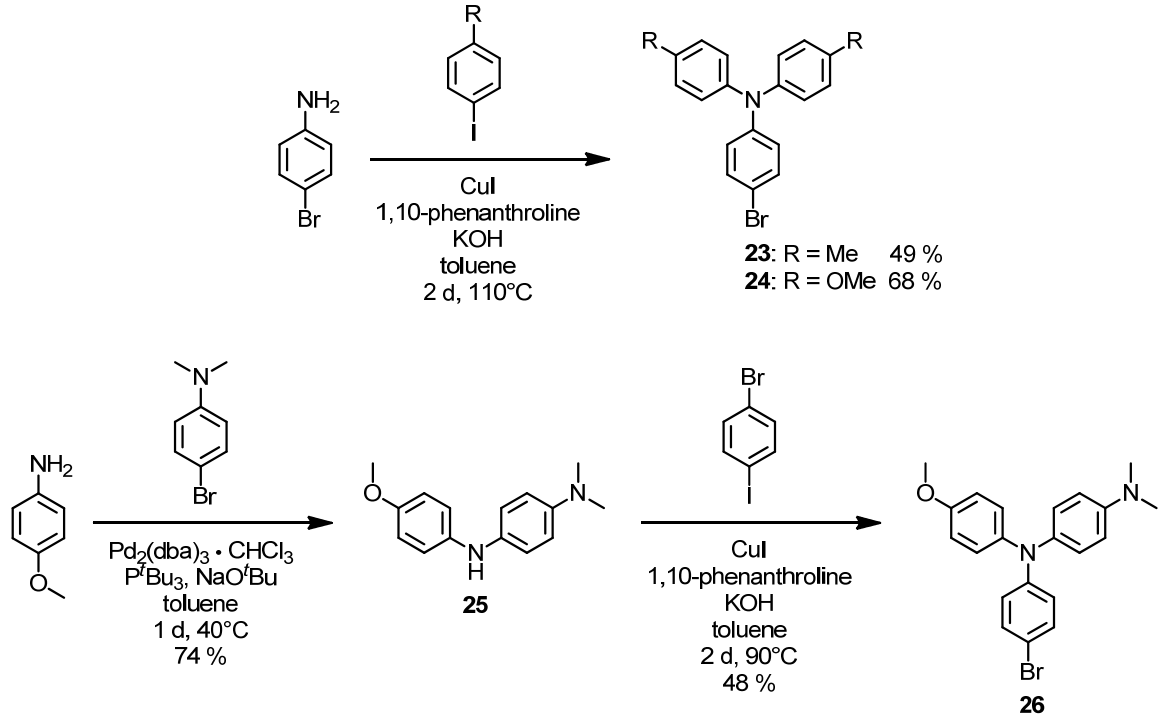

Scheme 5.6: Synthesis of the triarylamine precursors 23, 24 and 26.

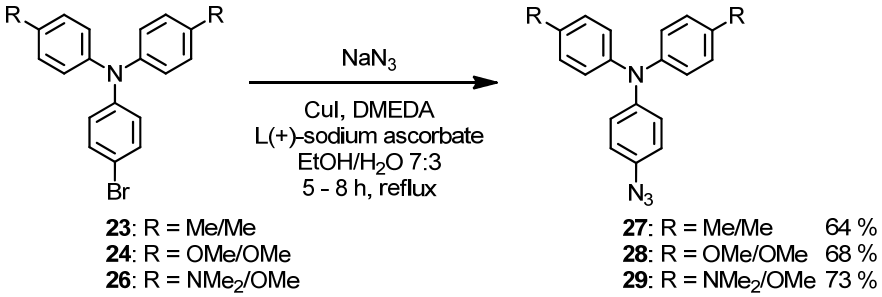

Scheme 5.7: Synthesis of the triarylamine azide precursors 27 – 29.

The solubility of triarylamine **26** was very low in the solvent recommended in the literature ($EtOH/H_2O$). Therefore, the received product **29** was contaminated with the precursor, which could not be removed by column chromatography. Purification by GPC was not performed, due to the instability and high toxicity of the aryl azides. Furthermore, using THF without stabiliser as the eluent, **29** may have been oxidised by peroxide impurities, due to its very low oxidation potential.

Ferrocenyl azide **30** was prepared in a similar way (Scheme 5.8, left) to the method described above.[319,320] Instead of CuI, CuCl was used by the authors, without the addition of additives. The product showed an impurity, which was identified as ferrocene. This impurity stems from the purchased bromoferrocene and was removed by column chromatography after generation of the triazole bridge.

Phenyl azide **31** was needed as a reactant in the synthesis of the reference compounds **1** and **4**. A different reaction pathway was chosen in this particular case (Scheme 5.8, right).[321]

Starting from aniline, reaction with $NaNO_2$ in aqueous HCl resulted in the appropriate diazonium salt. Subsequent treatment with NaN_3 at low temperatures gave the desired product. In contrast to the methods described above, no Cu(I) salt was necessary. In addition, the reaction time shortened clearly. A similar synthesis of **30** was not possible, since the required aminoferrocene was not commercially available. For the generation of compounds **27**, **28**, and **29**, synthesis of appropriate precursors (i.e. **23**, **24**, and **26** equipped with a free amine instead of the bromine atom) would be required. This synthesis might have included several steps, combined with possible problems during synthesis and purification. For this reason, the route starting from **23**, **24**, and **26** was chosen, according to a synthesis already established in our group.[278]

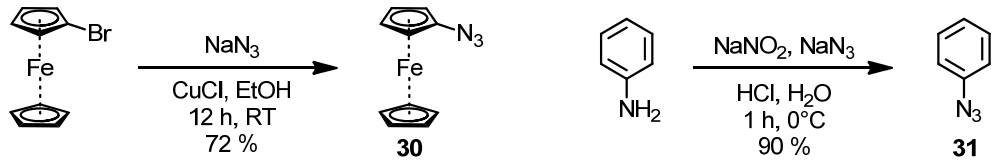

Scheme 5.8: Synthesis of ferrocenyl azide 30 (left) and phenyl azide 31 (right).

As described above, thermal generation of the bridging 1,4-substituted triazoles can in principle be achieved performing 1,3-dipolar *Huisgen* cycloadditions with azides and alkynes. As already mentioned in Chapter 3.4, these reactions often require elevated temperatures and produce mixtures of 1,4- and 1,5-substituted triazoles. Introducing a Cu(I) catalyst (click reaction) avoids formation of the 1,5-substituted regioisomer, which can be synthesised using specific Ru(II) catalysts (see Chapter 3.4 for details). Schemes 5.9 and 5.10 show the click reactions for the chlorine and cyano substituted compounds to compounds **32** – **37**, respectively.

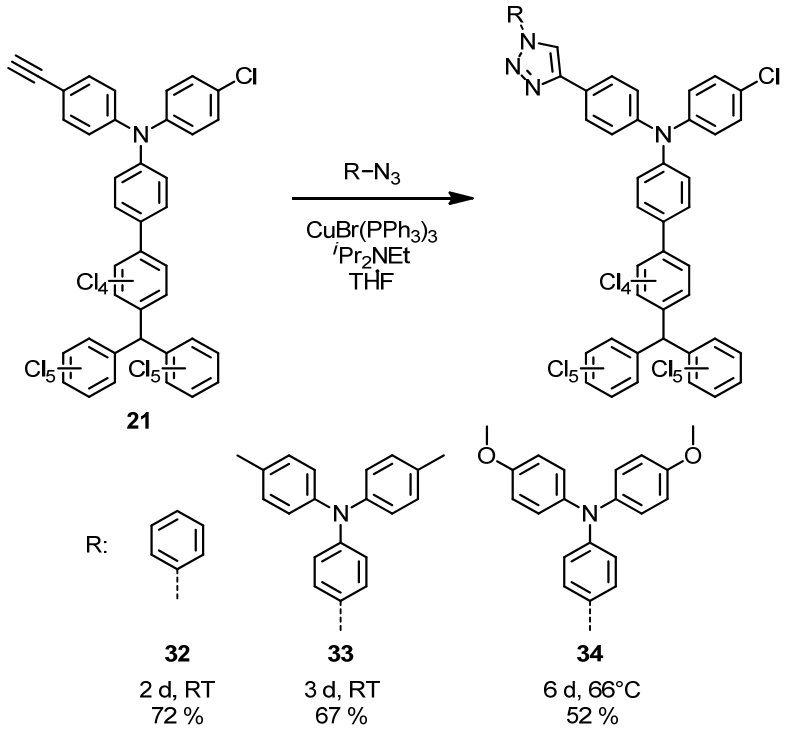

Scheme 5.9: Click reactions of 21 with azides 32 – 34.

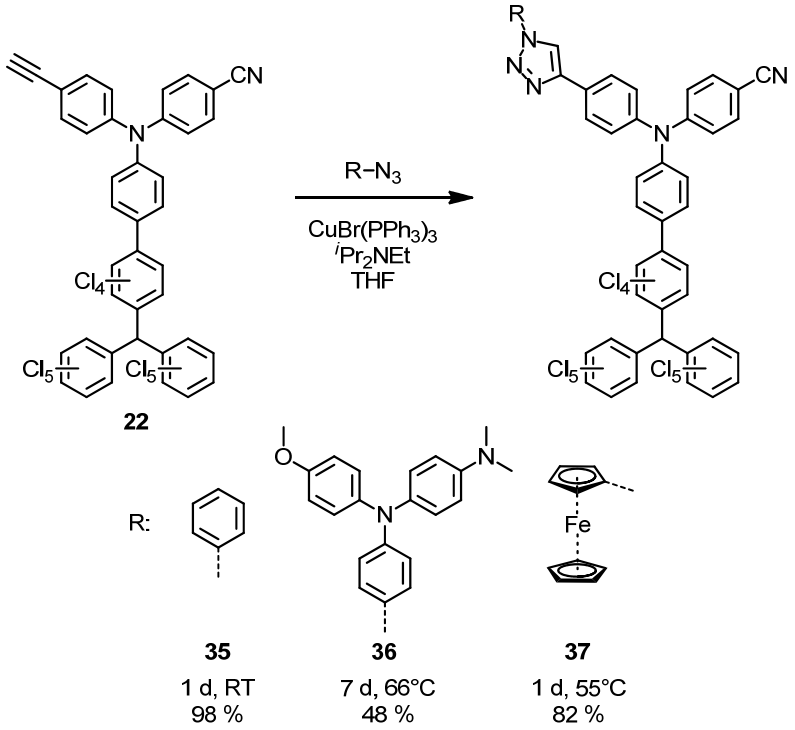

Scheme 5.10: Click reactions of 22 with azides 35 – 37.

All click reactions of aryl acetylenes and aryl azides were performed with $(Ph_3P)_3CuBr$ in THF in the dark with $^{i}Pr_2NEt$ as a base.[322] Reaction times and yields are directly related to the donor strength of the substituents of the aryl azides. Increasing donor strength led to a decrease in reaction conversion. In some cases, a prolongation of the reaction time and/or an increase of the reaction temperature were necessary to give acceptable yields.

The last step was the radicalisation of the PCTM moiety. For this purpose, the *α*-H compounds were first converted into their anions and subsequently oxidised to the corresponding radicals. The amount of the radicalised species in relation to the *α*-H precursor was determined by ^{1}H-NMR spectroscopy and DPV, respectively (see Chapter 5.1.4.2 and 5.3). In several reaction attempts, the degree of radicalisation was found to be insufficient for further spectroscopic investigations (< 90 %). This observation indicated problems in either the deprotonation and/or the subsequent oxidation process. For this reason, investigations concerning the bases and oxidation reagents, the stoichiometry of the reaction, and the reaction time were made. In most cases, only small amounts of the *α*-H precursors were available, which prevented a systematic study referring to one specific compound. Hence, no reactants were given in Table 5.1.

For the most part, reactions were performed with a solution of tetra-*n*-butylammonium hydroxid ($^{n}Bu_4NOH$) (40 % in H_2O) that served as a base. Subsequent oxidation was carried out with *p*-chloranil (PCA).[117] Scheme 5.11 shows the radicalisation process of the precursor **18** as an example.

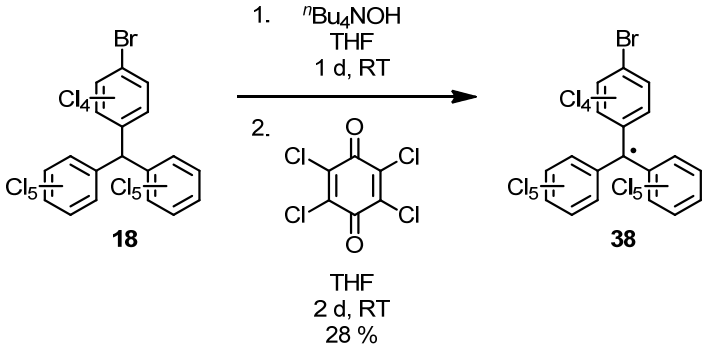

Scheme 5.11: Radicalisation of compound 18.

For this kind of radicalisation reaction many examples can be found in the literature. However, no statements concerning the degree of radicalisation, and consequently no reports of incomplete reactions were made in the literature. Application of this method on the herein synthesised compounds gave varying results (Table 5.1). The amount of radical after the reaction lay between 40 – 98 % in relation to the *α*-H precursor, as indicated by ^{1}H-NMR and DPV measurements. In some cases, increasing reaction time provided an enhancement of the amount of the radical of up to 98 %. In other cases, no improvement or even decomposition of the reactants was observed. No effect on the reaction yield was observed varying the stoichiometry of PCA and/or ^{n}Bu$_4$NOH, respectively.

Table 5.1: Radicalisation reactions with different bases and oxidation reagents in THF.

base	*t* / h	oxidation reagent	*t* / h	amount of radicalised species
^{n}Bu$_4$NOH	1	PCA	4	< 80 %
^{n}Bu$_4$NOH	1	PCA	8	< 90 %
^{n}Bu$_4$NOH	4	PCA	12	< 90 %
^{n}Bu$_4$NOH	8	PCA	36	< 98 % or decomposition
^{n}Bu$_4$NOH	8	AgNO$_3$[a]	2.5	98 % or decomposition
NaH	4	PCA	8	no reaction
NaH	8	DDQ	8	decomposition
LDA	3	PCA	8	no reaction
NaOEt	8	PCA	8	no reaction
KO^{t}Bu[b]	1	PCA[b]	8	decomposition

[a] Oxidation in CH_2Cl_2. [b] Reaction in DMSO.

Oxidation of the PCTM anion with $AgNO_3$ in CH_2Cl_2 seemed to be a promising option to improve the amount of radical in the reaction mixture. This method is well established in the literature for various compounds with PCTM moieties.[209] Since the oxidation potential of Ag^+ varies in different solvents, one has to be careful with respect to the oxidation of the triarylamines.[323] Therefore, reactions were performed with just a slight excess of $AgNO_3$. For some compounds, e.g. **6**, this method worked very well, but it failed completely for others (**1**). Variation of the base either led to decomposition or provided no reaction at all. Overall, no methodical behaviour was found, neither for the *α*-H reactants nor for the reagents used. Further radicalisation of the incomplete radicalised compounds in a second step after work up led to a deterioration of the degree of radicalisation in all cases.

For compounds **1** - **6**, the radicalisation was performed successfully (Scheme 5.12) with an amount of the radicalised species of > 95 %. In all cases, ^{n}Bu$_4$NOH was utilised as a base. For **1** - **5**, PCA served as the oxidation reagent, for **6**, $AgNO_3$ was implemented.

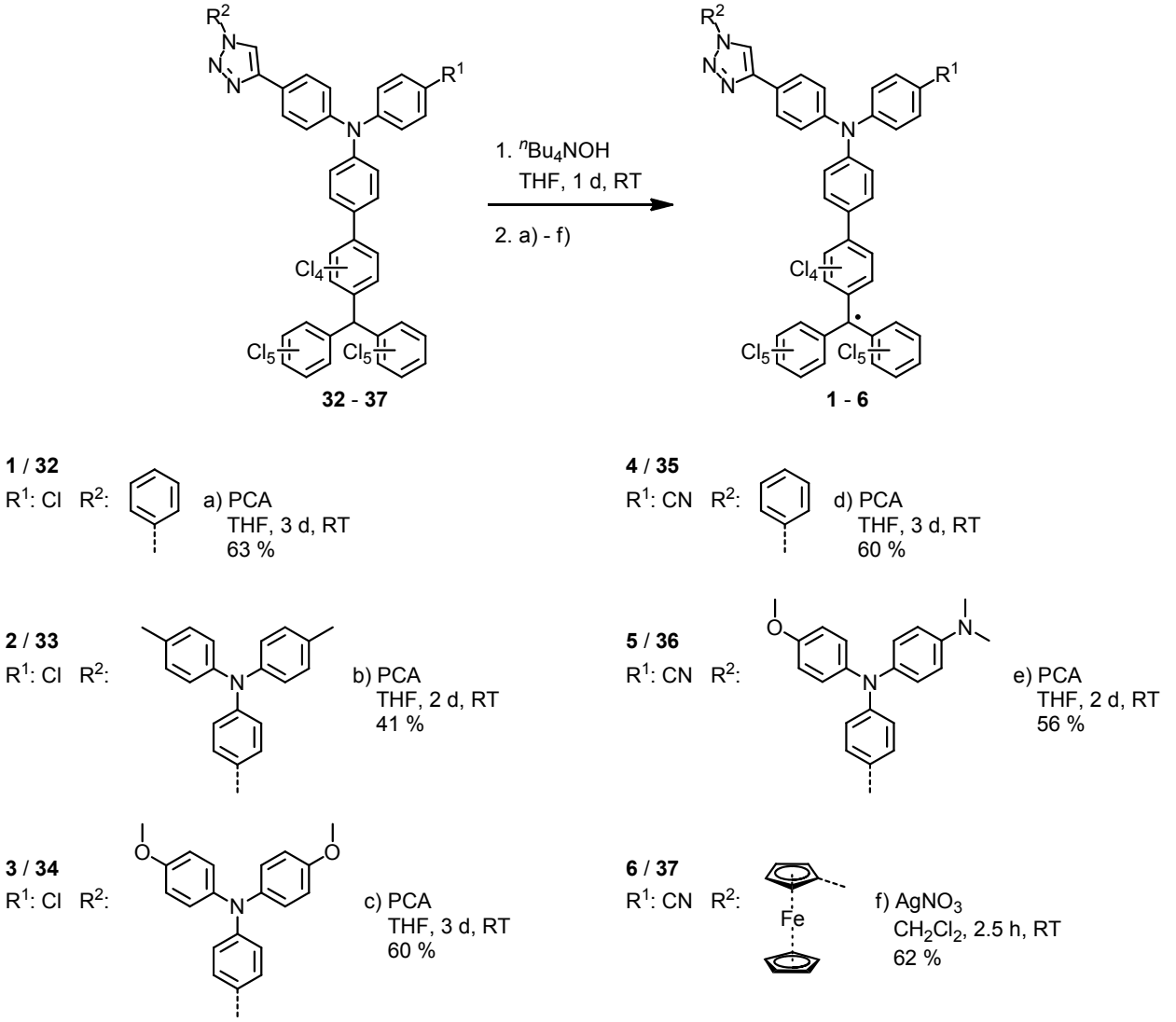

Scheme 5.12: Radicalisation reactions of the *α*-H precursors 32 – 37 to receive 1 – 6.

Purification was performed using flash column-chromatography and subsequent GPC (THF). Adsorption of a part of the product on the silica during flash column-chromatography caused the low isolated yields of 41 – 63 %.

As already mentioned in Chapter 3.3, one problem concerning this reaction might be the ability of HO^- ions to reduce the PCTM radical to its corresponding anion.[139] Removal of the base is commonly achieved by extracting the reaction mixture with H_2O before adding the oxidant. To investigate a possible decomposition or protonation during the extraction process, this was not performed in all cases. Apparently, better results were attained omitting the extraction.

For a better understanding of the results obtained by spectroelectrochemical measurements, reference compound **39** was synthesised (Scheme 5.13). The compounds obtained from the first two steps of the reaction sequence were not purified properly, due to the small amount of the starting material. For this reason, only ^{1}H-NMR measurements will be presented in the experimental section.[1] Starting from the asymmetrical triarylamine **39a**[2], reaction with TMSA[3] in a *Sonogashira* reaction provided a protected acetylene species **39b**, which was further treated with ^{n}Bu$_4$NF to receive the free acetylene **39c**. Click-chemistry with **31** in THF resulted in the desired triarylamine **39** in a yield of 15 %, referring to the last step. Due to various side-products, the purification of **39** was somewhat demanding, which explains the rather poor yield.

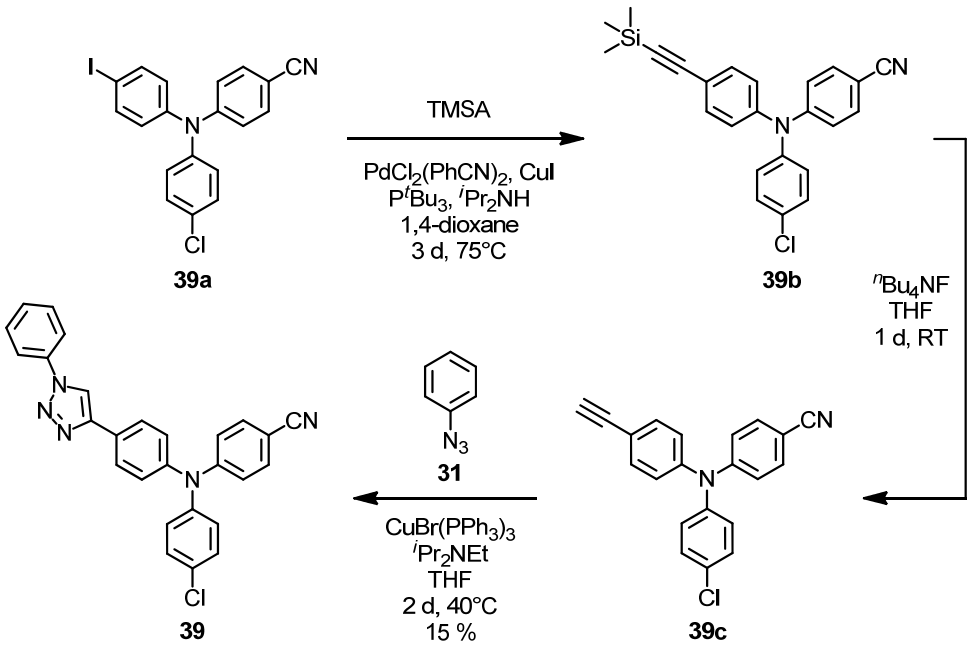

Scheme 5.13: Synthesis of 39.

[1] In the following, compounds that are not fully characterised will not be assigned to a separate number. They will be denoted referring to the product with a, b, c.
[2] Already available in our group.
[3] Trimethylsilylacetylene

5.1.2 Synthesis of Cascades with a Saturated Spacer

The aim of a second project was the synthesis of redox cascades containing saturated spacer units for the connection of the triarylamine donors D1 and D2 instead of using a 1,4-triazole bridge (Scheme 5.14). On the basis of a former study of our group, the combination of an ethylene and a methylene bridge was implemented, to guarantee a low flexibility of the donor chain.[272] The PCTM radical was again chosen as the electron acceptor A. As reported previously in the synthesis of compounds **1** – **6**, the radicalised species should be obtained from their corresponding *α*-H precursors. For the connection of A and D1, once more a biphenyl spacer should be build up by a *Suzuki-Miyaura* cross-coupling between an appropriate triarylamine and a perchlorinated *α*-H precursor. The commercial available dibenzosuberone should provide a suitable precursor for the synthesis of the saturated spacer unit.

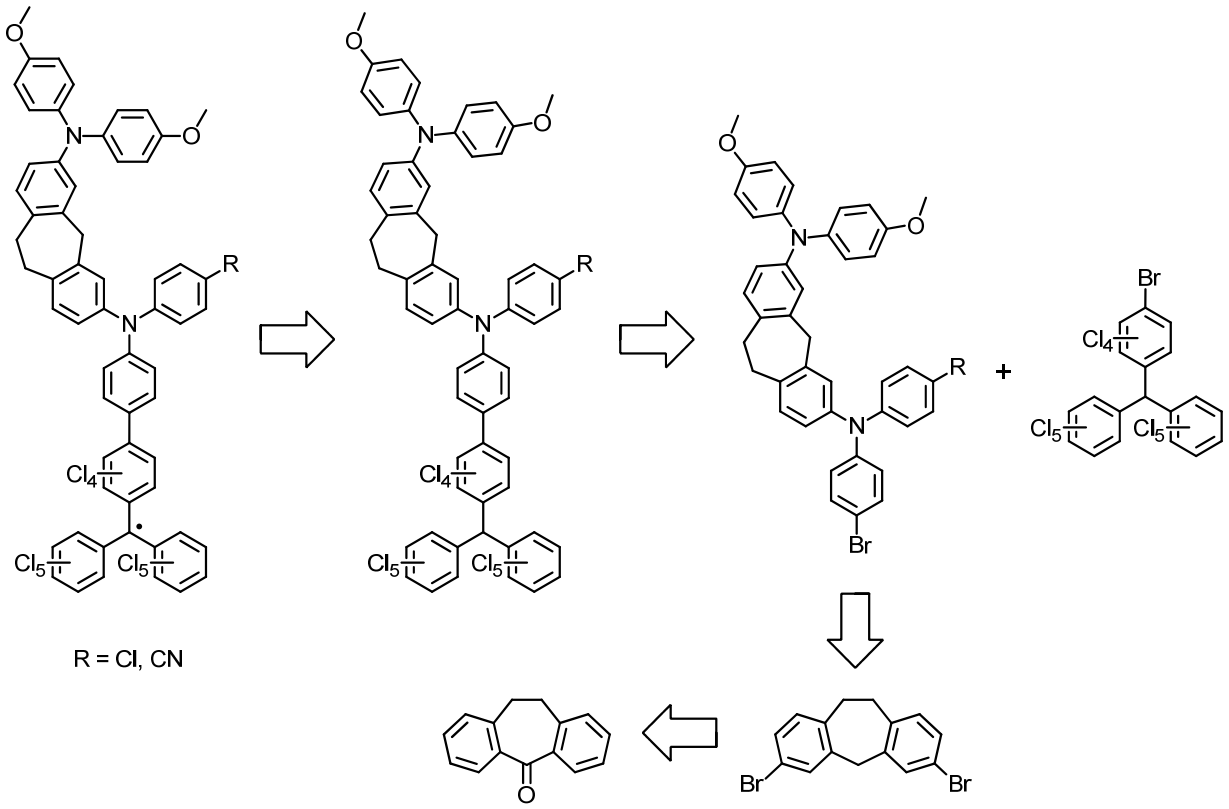

Scheme 5.14: Retrosynthetic approach for the synthesis of redox cascades with a saturated spacer unit.

Dibenzosuberone was originally converted into its dibromoanalogue in a three-step synthesis (reaction sequence shaded grey in Scheme 5.15), starting with a nitration using HNO_3 and H_2SO_4. The so obtained dinitrocompound was reduced with $SnCl_2$/HCl to the related amine, which was further submitted to a *Sandmeyer*-type reaction with $CuBr_2$. The overall yield of this reaction sequence was around 30 %.[316]

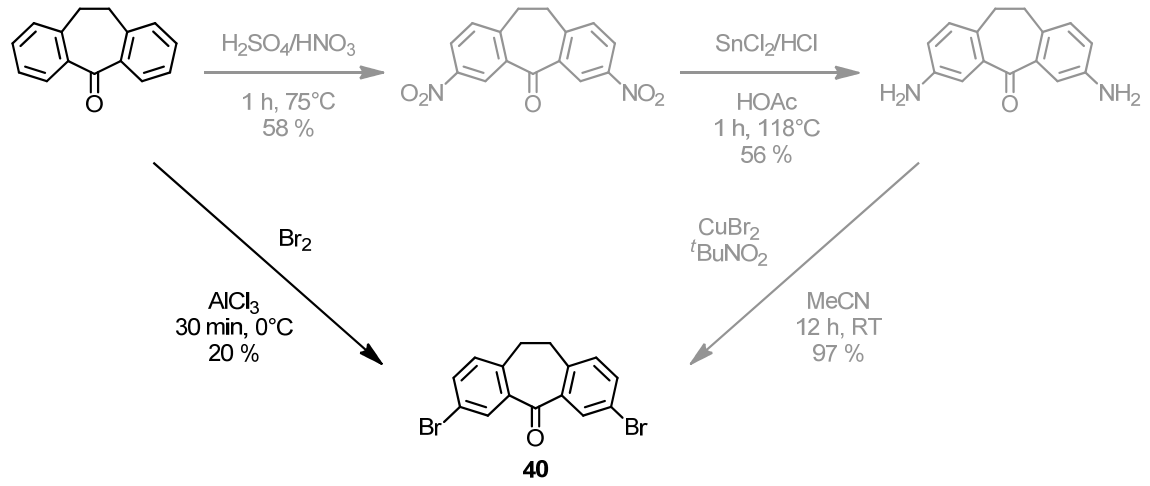

Scheme 5.15: Synthesis of 40.

To shorten this procedure, a direct bromination of the dibenzosuberone was accomplished with a mixture of Br_2 and $AlCl_3$ without using a solvent.[324] In this case, the yield of the desired product **40** was only around 20 %, but in consideration of the reduction of the number of steps, this route is preferred. Reduction of the ketone was accomplished by using a mixture of $NaBH_4$ and TFA (trifluoroacetic acid) in dry CH_2Cl_2.[316] The following *Buchwald-Hartwig* cross coupling with 4,4'-dimethoxydiphenylamine, using the Pd_2dba_3/P^tBu_3 catalyst system in toluene, resulted in a much higher yield of the twofold substituted species (grey in Scheme 5.16) than the desired onefold substituted product **42** (< 13 %).

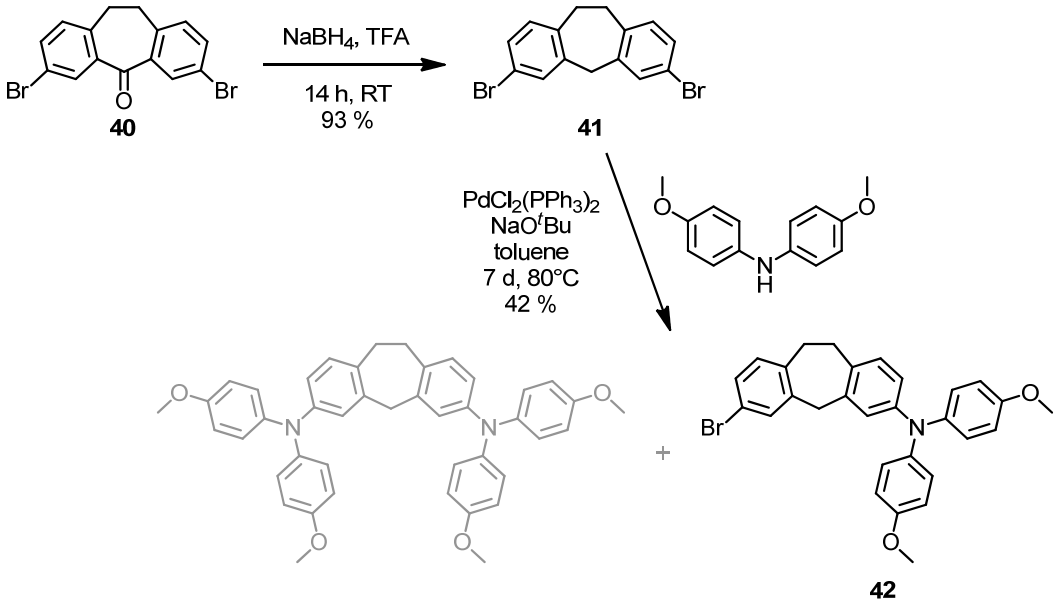

Scheme 5.16: Synthesis of 42.

Even using a great excess of **41** of up to ten equivalents brought nearly no improvement. Therefore, a great loss of the precursor was recorded for each reaction. Replacement of the catalyst system by $PdCl_2(PPh_3)_2$ led to an increase in the reaction time, but resulted in a drastic reduction of the twofold substituted species (only detectable in traces) and a higher yield of **42**

(42 %). Furthermore, it was possible to recover the precursor after the reaction. Application of other Pd-catalyst systems in combination with phosphino ligands, as well as *Ullman*-type reactions brought no improvements.

Purification of the compounds resulting from the following steps was not achieved during the scope of this work. For this reason, only ^{1}H-NMR measurements will be presented in the experimental section. Yields, if given, are just approximate values. In the next two steps, a second triarylamine was built up *via* different coupling reactions (**42a**, **42b** in Scheme 5.17).[1]

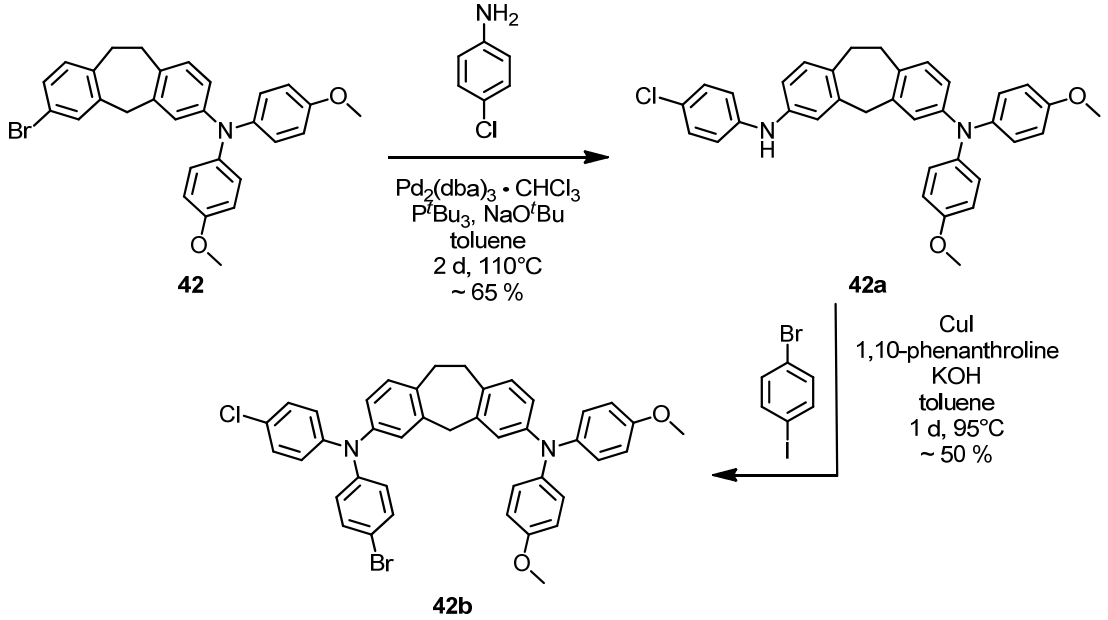

Scheme 5.17: Attempts of a subsequent synthesis of 42.

Conversion of the aryl bromide into the corresponding boronic ester **42c** was accomplished *via* Pd-catalysed reaction with pinacolborane. Further reaction of **42c** with **18** resulted in the desired product **43** and a second species (shaded grey in Scheme 5.18) with the boronic ester replaced by a hydrogen atom. Since this by-product could not be removed using column chromatography, **43** was purified by GPC in THF. This led to decomposition for the most part and to a small amount of not fully purified product. Radicalisation of the latter to receive compound **44** was incomplete in the first attempt (~80 %). Subsequent radicalisation of the same sample led to decomposition. For this reason, no spectroscopic investigations were made.

[1] In the following, compounds that are not fully characterised will not attain a separate number.They will be denoted referring to the reactant with a, b, c.

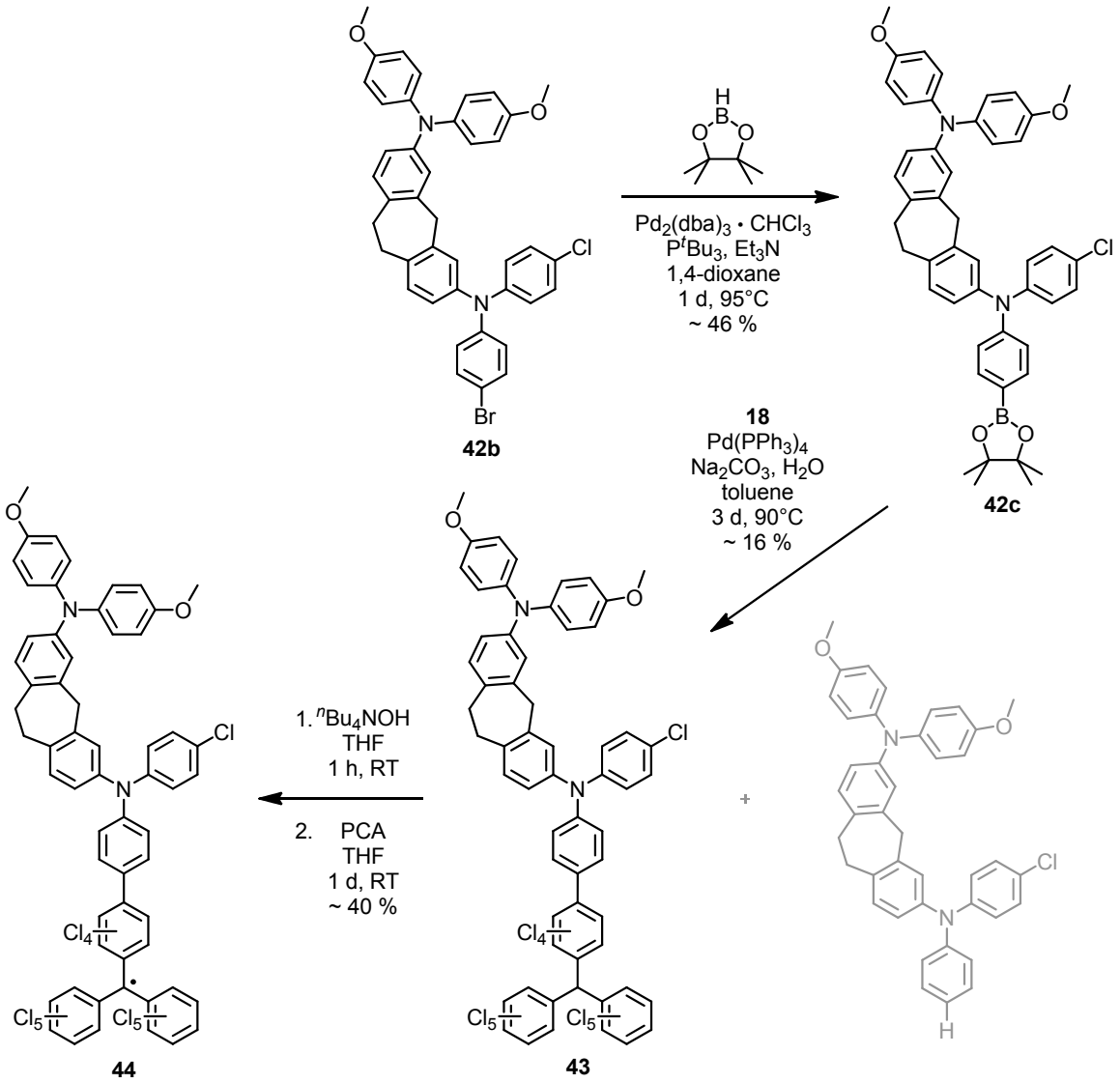

Scheme 5.18: Synthesis of 44.

To generate a higher potential difference between the triarylamines, the chlorine atom was exchanged by a cyano group. Trying to overcome the problems concerning the purification, a different route of synthesis was chosen (Scheme 5.19 and 5.20). In the first step, several amino protecting-groups were tested. The acetamide group gave the best results concerning synthesis, handling and removal. It was easily attained through reaction of the amine (4-iodoaniline) with acetic anhydride.[325] The resulting amide **45** was expected to be too electron poor to undergo reactions in the upcoming cross couplings. Introducing a boronic ester *via* Pd-catalysed coupling with pinacolborane, followed by an aqueous *Suzuki-Miyaura* coupling of **46** and **18** led to **47** (Scheme 5.19). Heating **47** in a mixture of EtOH and conc. HCl (2:1) resulted in the free amine **48**.[326] Compound **48** served as a precursor for different attempts generating cyano-substituted cascades containing the saturated spacer unit. The reaction of **48** with **42** was attained through Pd-catalysed *Buchwald-Hartwig* reaction with Pd_2dba_3/P^tBu_3 (Scheme 5.20). Synthesis of the cascade through a subsequent coupling with 4-iodobenzonitrile did not result in the desired product. Exchanging the order of the implemented coupling reactants was also not

successful, failing again in the second coupling step. This may either be due to the high steric claim, or the electron poor character of the diarylamine generated in the first step.

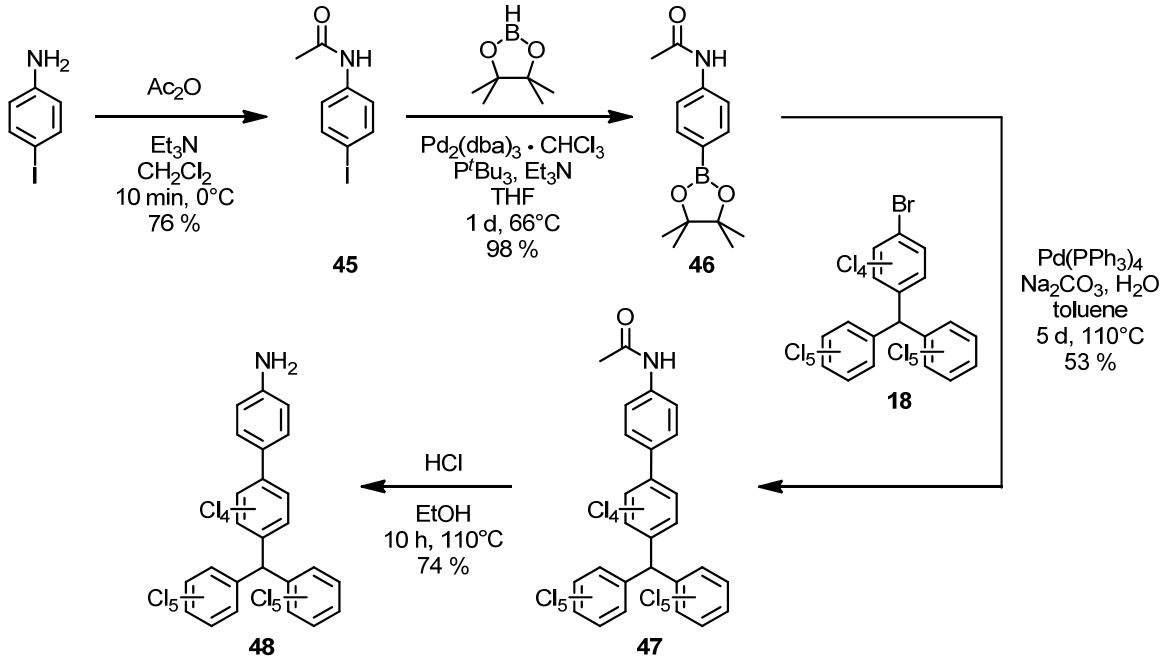

Scheme 5.19: Synthesis of 48.

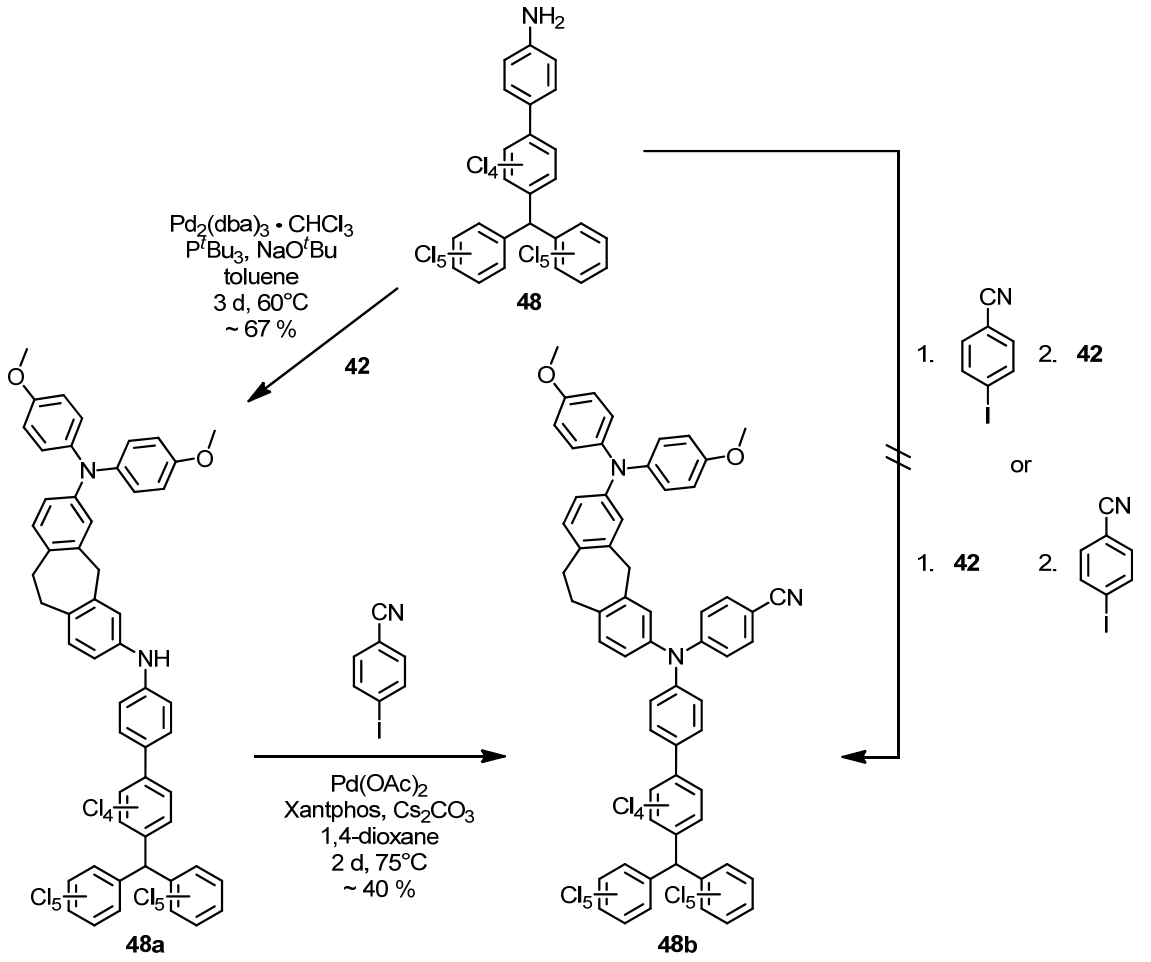

Scheme 5.20: Attempts generating cyano-substituted cascades containing the saturated spacer unit.

To overcome the latter problems, P^{t}Bu$_3$ was replaced by bidentate phosphino ligands. Reactions with dppf[1] and binap[2] did not result in successful reactions.[304] A study of *Buchwald et al.* showed Xantphos[3] to be an effective ligand for the Pd-catalysed reaction of inherently electron poor amides and aryl halides.[327] Furthermore, it has a large bite angle and is able to form *trans*-chelating structures in palladium complexes, which is useful for reactants with high steric claim. Coupling reactions implementing Xantphos, enabled an efficient reaction to **48b** with a yield of around 40 %. After purification of the cascade by means of flash column-chromatography, the NMR spectrum showed impurities that could not be identified. GPC in THF also brought no improvement and furthermore led to decomposition for the most part. Consequently, subsequent radicalisation reactions were not possible.

All above-mentioned compounds are built up with a biphenyl spacer, connecting the donor and acceptor units. Investigating spacers with varying properties might provide a better insight into the ET characteristics of such donor-acceptor compounds. Many examples using acetylene or tolane bridges can be found in the literature and initiated the following syntheses: starting from the phosphonium salt[4], reaction with paraformaldehyde resulted in an ethylene moiety, which was subsequently brominated (Scheme 5.21).[315]

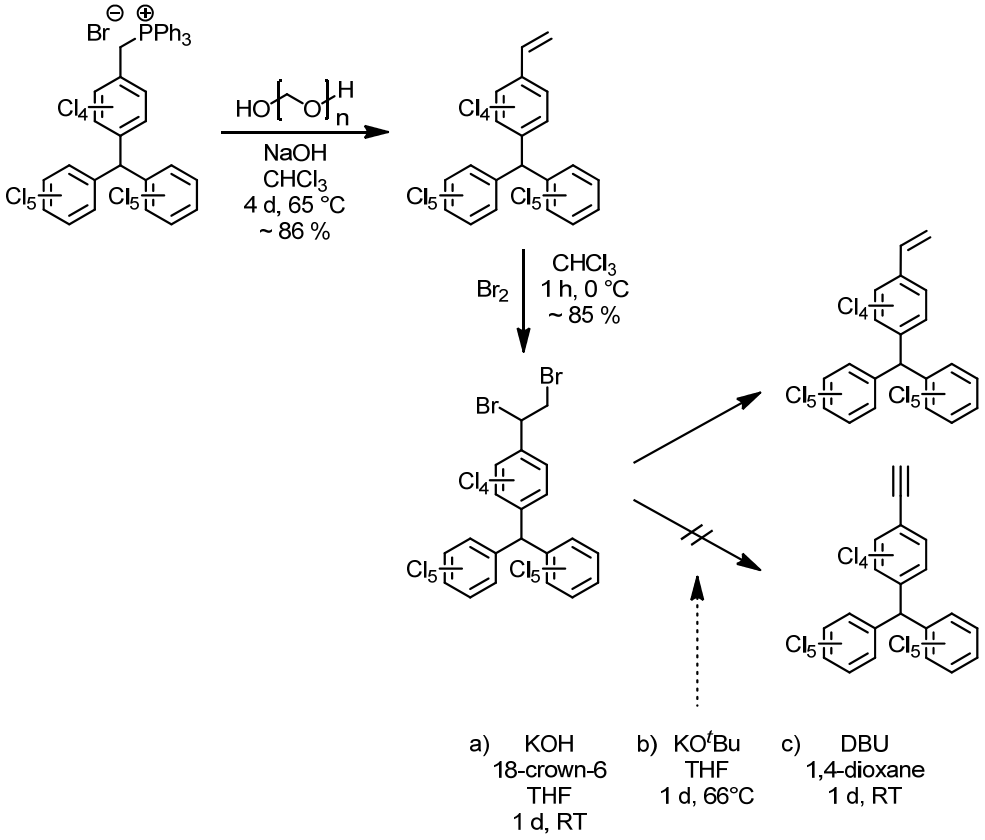

Scheme 5.21: Attempted syntheses of a perchlorinated precursor equipped with an acetylene moiety.

[1] 1,1'-bis(diphenylphosphino)ferrocene
[2] (±)-2,2'-bis(diphenylphosphino)-1,1'-binaphthalene
[3] 4,5-Bis(diphenylphosphino)-9,9-dimethylxanthene
[4] Already available in our group

Elimination of two equivalents of HBr was expected to give the desired product. Application of KOH in combination with 18-crown-6 in THF, however, resulted in the ethylene substituted precursor. Upon addition of KOH, the solution turned to a deep violet colour, indicating deprotonation of the *α*-H proton of the PCTM. As the elimination process might be influenced by this fact, non-nucleophilic bases (KO*t*Bu, DBU[1]) were used in the following. Both attempts were not successful, leading once again to the ethylene precursor. A problem might have been the inadequate work-up conditions. Addition of a small amount (<< 1 equiv.) of HCl (2N) resulted in a red solution as described in the literature. Upon addition of the full amount of HCl as demanded, the solution turned yellow, containing just the ethylene precursor. In all further attempts, HCl was replaced by sat. NH_4Cl solution, without any improvement.

As described before, *Suzuki-Miyaura* coupling of the bromo substituted PCTM **18** and an aryl boronic ester resulted in rather poor yields. Synthesis of a PCTM moiety, equipped with a boronic ester, was tried in order to carry out the reaction with exchanged reaction centres.

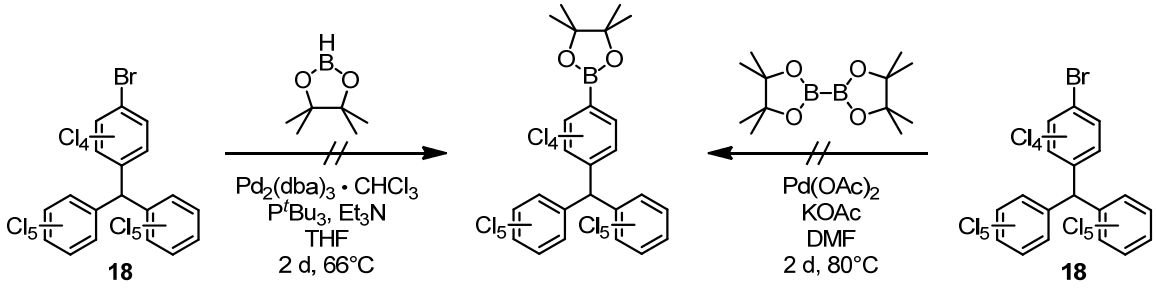

Scheme 5.22: Attempted syntheses of a perchlorinated precursor equipped with a boronic ester.

Neither the reaction with pinacolborane, nor with bis(pinacolato)diboron[328] gave the desired product. Since none of the preceding attempts resulted in a successful reaction the project was not further pursued.

5.1.3 Synthesis of Diketopyrrolopyrroles (DPPs)

Synthesis of the DPPs started with the generation of di-*i*-propyl succinate. In a first attempt, succinic acid was esterified with *i*-propanol in the presence of TosOH, providing the desired product **49** in a yield of 58 % (shaded grey in Scheme 5.23). As the reaction was not completed after several days, another procedure was tested. Esterification of succinyl chloride with *i*-propanol resulted in the successful isolation of **49** with a yield of 80 %. In the following step, **49** reacted with 4-bromobenzonitrile to form the deep red DPP **50**. The required sodium amylate was made from dry amyl alcohol and sodium in advance. Alkylation reactions of **50** with 2-ethylhexyl bromide to obtain **51** gave rise to many side products and provided rather poor

[1] 1,8-Diazabicyclo[5.4.0]undec-7-ene

yields of the bright yellow product of about 10 %.[329] A variation of the reaction conditions brought no improvement. NaOMe as well as KO^{t}Bu were used instead of K_2CO_3 without success. Reactions with different alkyl chains (3,7-dimethyloctyl, hexadecyl) did not increase the overall yield. Application of a better leaving group (tosylate) led to many more side products. The appearance of side products was probably due to alkylation of the oxygen atoms, which was also reported in the literature before.[330]

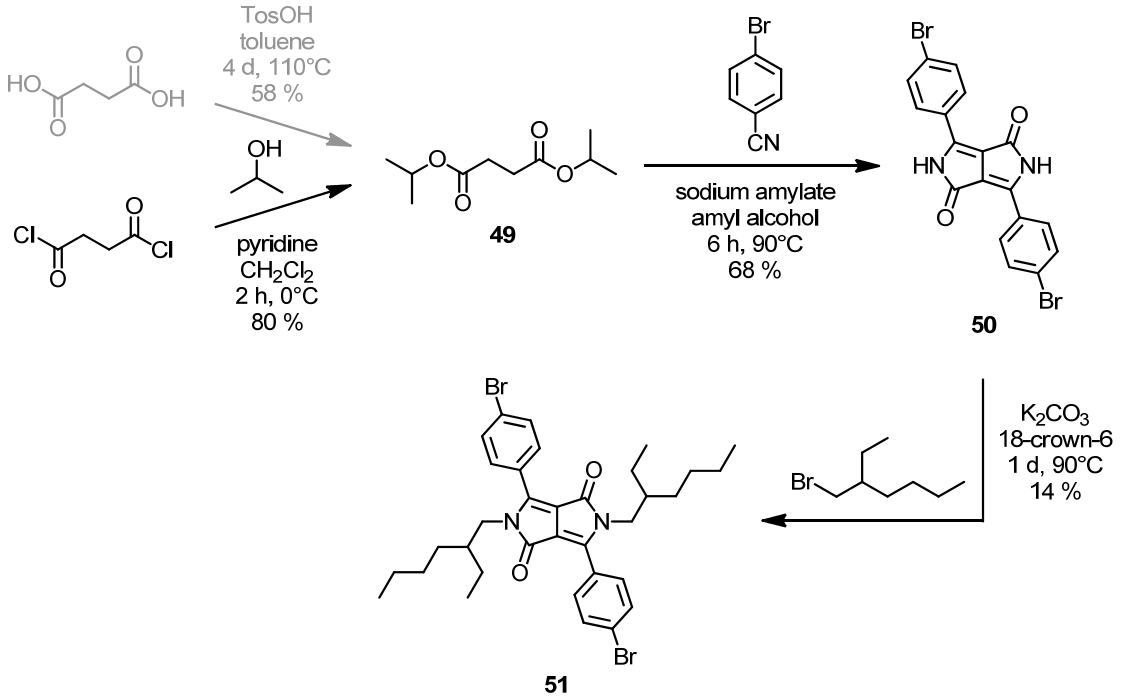

Scheme 5.23: Synthesis of 51.

As described in Chapter 4.2, the goal of this synthesis was building up an asymmetric DPP, equipped with an acceptor and a donor moiety. In case of the latter, once more a triarylamine was chosen. *Buchwald-Hartwig* coupling with 4,4'-dimethoxydiphenylamine using the Pd_2dba_3/P^tBu_3 catalyst system in toluene resulted in the two- (violet) and onefold (pink) substituted products (**52**/**53**) (Scheme 5.24) in rather poor yields of 8 % and 16 %, respectively. To avoid formation of the twofold substituted species, the catalyst system was replaced by $PdCl_2(PPh_3)_2$ as already described for the synthesis of **42**. This led to an increase of the yield up to 60 %, but also to a new side product, which could not be completely removed by column chromatography. The subsequent coupling reaction with pinacolborane to the boronic ester was not successful (Scheme 5.25).[331] Traces of the product were received from a reaction with bis(pinacolato)diboron,[330] but the sample consisted mostly of a species where the boronic ester was replaced by a hydrogen atom. Though KOAc and DMF were dried before, they may still have contained traces of water. Replacing $Pd(OAc)_2$ by $PdCl_2$(dppf) did not lead to the desired product. A further attempt with ^{n}BuLi, B(O^{i}Pr)$_3$ and pinacol also was not successful.

Though **52** was fully characterised during the scope of this work, no further spectroscopic or electrochemical measurements were performed due to a lack of time.

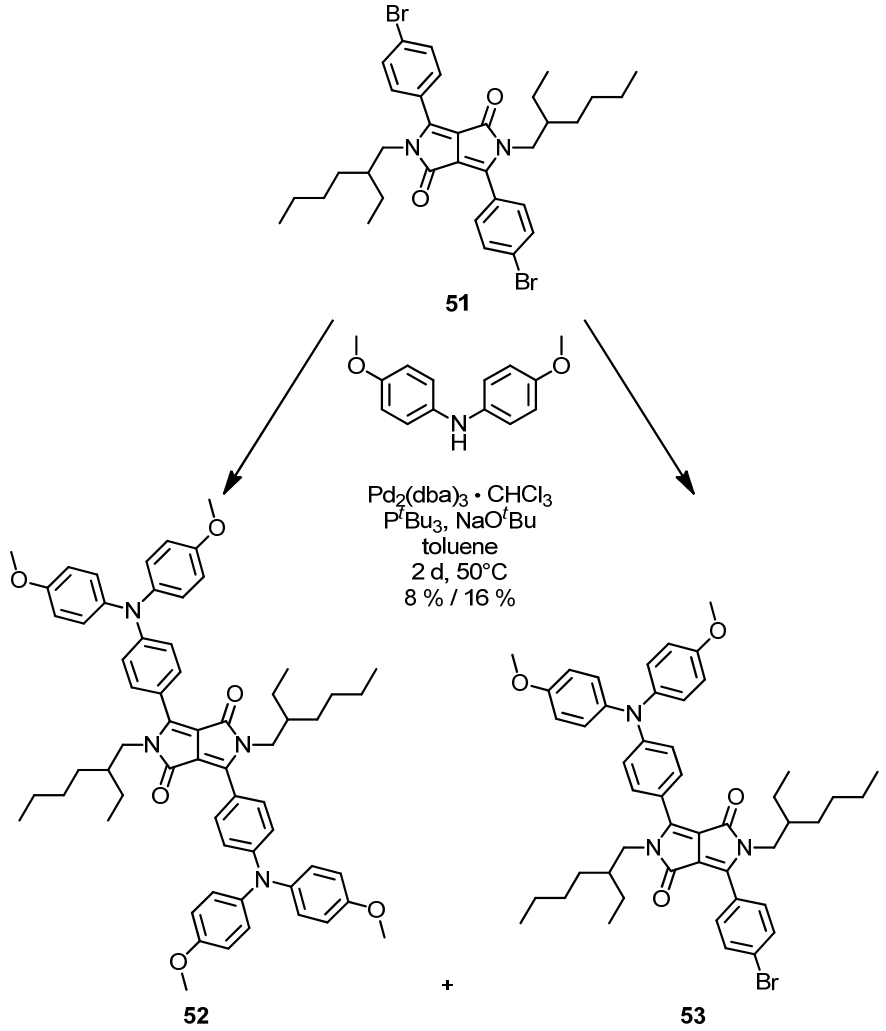

Scheme 5.24: Synthesis of 52 and 53.

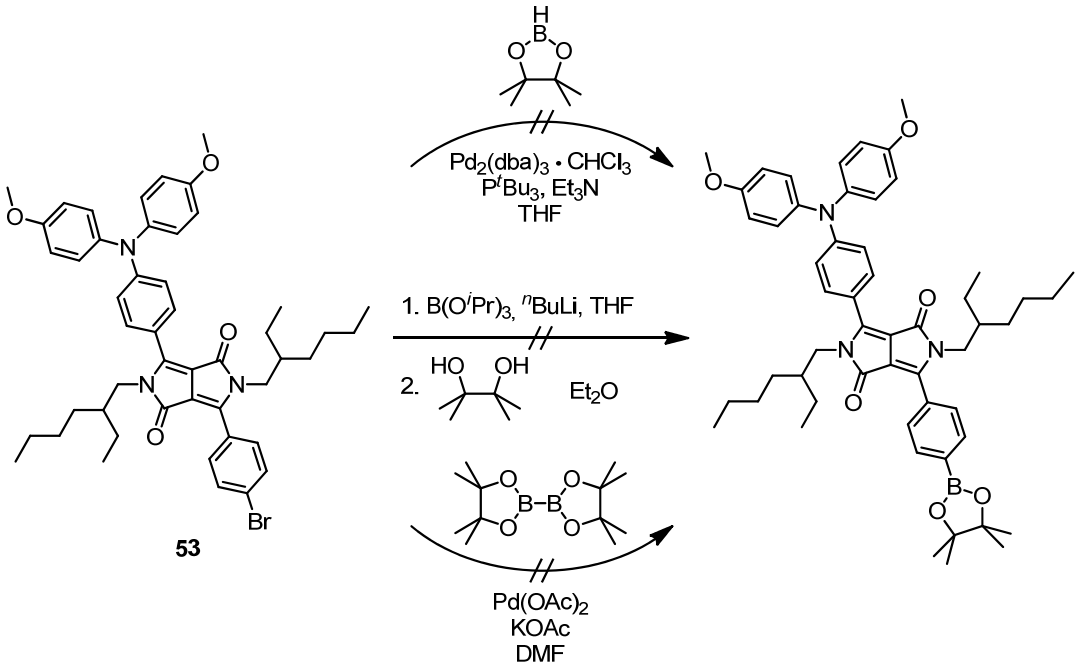

Scheme 5.25: Attempted syntheses of an asymmetrical DPP.

5.1.4 Analytical Methods

5.1.4.1 Mass Spectrometry

For a full characterisation of compounds **1** – **6** and their corresponding precursors, mass spectrometry experiments (ESI/APCI/MALDI) were performed in addition to NMR experiments. The mass spectra of all compounds including a PCTM unit and/or a triazole moiety showed several conspicuities, which shall be discussed in the following. Figure 5.1 shows the ESI mass spectrum of precursor **32** as a representative.

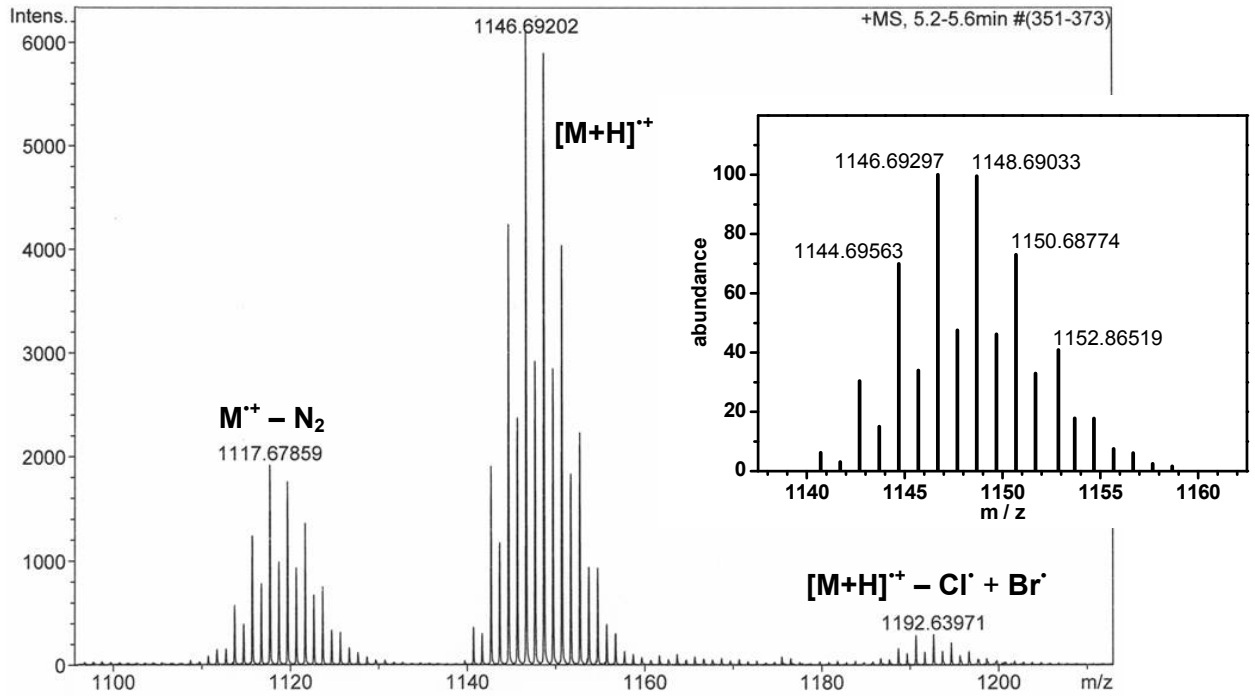

Figure 5.1: Experimental ESI mass spectrum of 32 an corresponding calculated spectrum[1] for $[M+H]^{\bullet+}$ (insertion).

In general, all compounds obtaining a PCTM moiety show a broad distribution over the m/z region, which is mainly caused by the isotopic effect of the chlorine atoms. Chlorine possesses two stable isotopes ^{35}Cl (I =3/2) and ^{37}Cl (I =3/2) with a natural abundance of about 76 % and 24 %. The splitting pattern of the signals obtained from the measurements match the calculated ones (insertion in Figure 5.1). The signals depicted in Figure 5.1 partially refer to the protonated species of **32** $[M + H]^{\bullet+}$.The signal on the right-hand side originates from a species with one chlorine atom replaced by a bromine atom (**$[M+H]^{\bullet+}$ – Cl$^{\bullet}$** + **Br$^{\bullet}$**). A comparable substitution was also observed in the mass spectra of compound **18**, and was therefore ascribed to take place during perchlorination.

[1] Bruker Daltonics IsotopePattern; Software Compass 1.1 from Bruker Daltonics GmbH, Bremen.

Since both compounds are not distinguishable by using NMR spectroscopy, no statement regarding their relative amount can be made. Assuming the electronic effect on the radical centre to be rather small, no further investigations were made concerning this phenomenon. However, the exchange of bromine by chlorine during the perchlorination reaction may lead to a multiple substitution of the PCTM moiety and therefore to a decrease in the amount of the radical compared to the triarylamines, which might distort the results obtained by DPV measurements (see Chapter 5.1.4.2 and 5.4).

Regarding the signal on the left-hand side of the spectrum, the received value is compatible with a species of **32**$^{\bullet+}$, in which two nitrogen atoms are absent. This phenomenon stems from thermal decomposition of the triazole moiety that may occur during mass spectrometry experiments and could be observed for nearly all compounds bearing a triazole spacer unit. Scheme 5.26 gives an overview of some of the thermal decomposition products, described in the literature.[332-336] Comparable results were reported for a photochemical process.[337] The loss of molecular nitrogen probably results first in a singlet iminocarbene. A hetero-*Wolff*-rearrangement (A) leads to an unstable ketenimine, which undergoes consecutive reactions, e.g. with H_2O. ^{13}C-labelling experiments by *Gilchrist et al.* proved the appearance of 1*H*-azirines (C) as reactive intermediates in more favourable pathways, like the formation of indoles (B).[332,333]

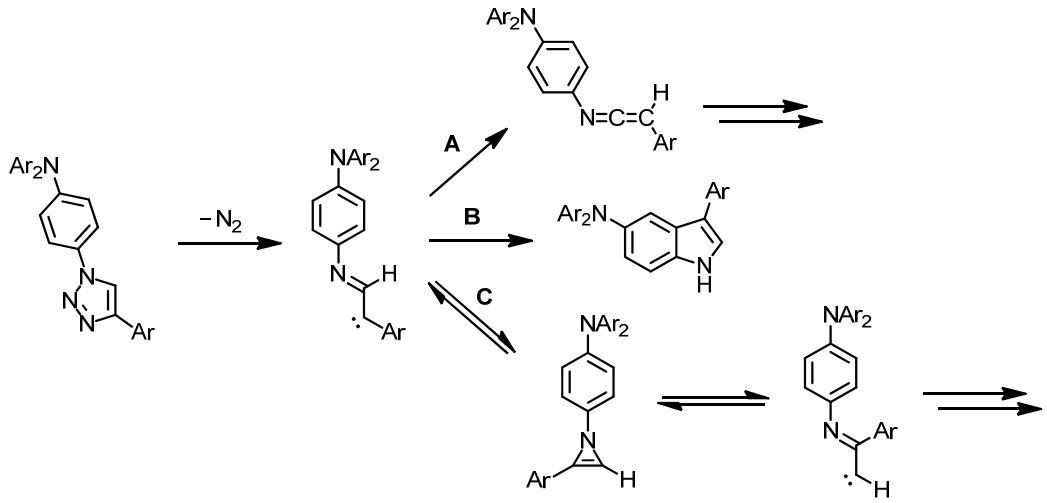

Scheme 5.26: Possible decomposition intermediates and products of the triazoles.

The signals found in the mass spectra cannot definitely be assigned to one of these species. Nevertheless, the decomposition pathways shown provide possible explanations for the above depicted additional mass peak.

5.1.4.2 NMR Spectroscopy

The ratio of radicalised species in comparison to the corresponding *α*-H precursor in a sample cannot be determined by mass spectrometry measurements, because mass spectrometry is not inherently quantitative. This may be ascribed to the fact that the mass spectrometric response of the investigated species depends on several properties such as size or charge. Voltammetric measurements, like DPV (differential pulse-voltammetry) or OSWV (*Osteryoung* square-wave-voltammetry) however, provide good results (details described in chapter 5.3), though they may be time-consuming, especially if inert gas conditions are recommended.

Looking for alternatives, NMR spectroscopy seems unsuitable, because the investigation of solutions containing paramagnetic substances is often demanding. Spin-lattice relaxation-times are much shorter in solutions with paramagnetic species, leading to a strong broadening of the recorded signals. This effect is known to be distance dependent, inversely correlated to the distance between the unpaired electron and the respective ^{1}H- or ^{13}C-nuclei. In addition, the signals of the radicalised species are clearly shifted compared to the signals of the *α*-H compounds. The shift depends on the concentration of the solution and is proportional to the hyperfine coupling constant *α*.[338-345]

However, in the PCTM radical, the propeller-like geometry (Chapter 3.3) leads to a strong shielding of the unpaired electron, which is enclosed by the bulky perchlorinated phenyl rings. The effect on the surrounding nuclei is therefore less pronounced and makes the NMR experiments feasible. Figure 5.2 shows the aromatic range of the ^{1}H-NMR spectra of the *α*-H precursor **32** (top) and its radicalised species **1** (bottom) as representatives. The left part of Figure 5.2 shows the triazole-proton signal of **1** in detail (green). Line broadening is observable for all signals and shows the expected distance dependence. In most cases, the signals are additionally shifted, except for the terminal phenyl ring. The signals stressed in pink stem from the protons located on the phenyl ring of the biphenyl spacer. These signals could not be recovered in the ^{1}H-spectrum of **1**, due to either the strong line broadening or the great shift. The characteristic singlet located at 7.16 ppm (blue), stemming from the *α*-H proton is absent in the spectrum of **1**, though small residues from the proton signals of the *α*-H species point to an incomplete radicalisation. The signal of the proton, located at the triazole ring, shows only little line broadening and is furthermore not superposed by signals of other ^{1}H-nuclei. Therefore, it is possible to estimate the amount of radical by integrating this and the residual signal of the precursor. For a better understanding, the signal of the triazole proton is enhanced on the left in Figure 5.2 (green). Integration indicates the amount of the precursor to be around 3 %, which was confirmed by DPV measurements (Figure 5.12 in Chapter 5.3). Altogether, ^{1}H-NMR measurements are a suitable and quick method to determine the amount of radicalised species, albeit they should be confirmed by DPV measurements.

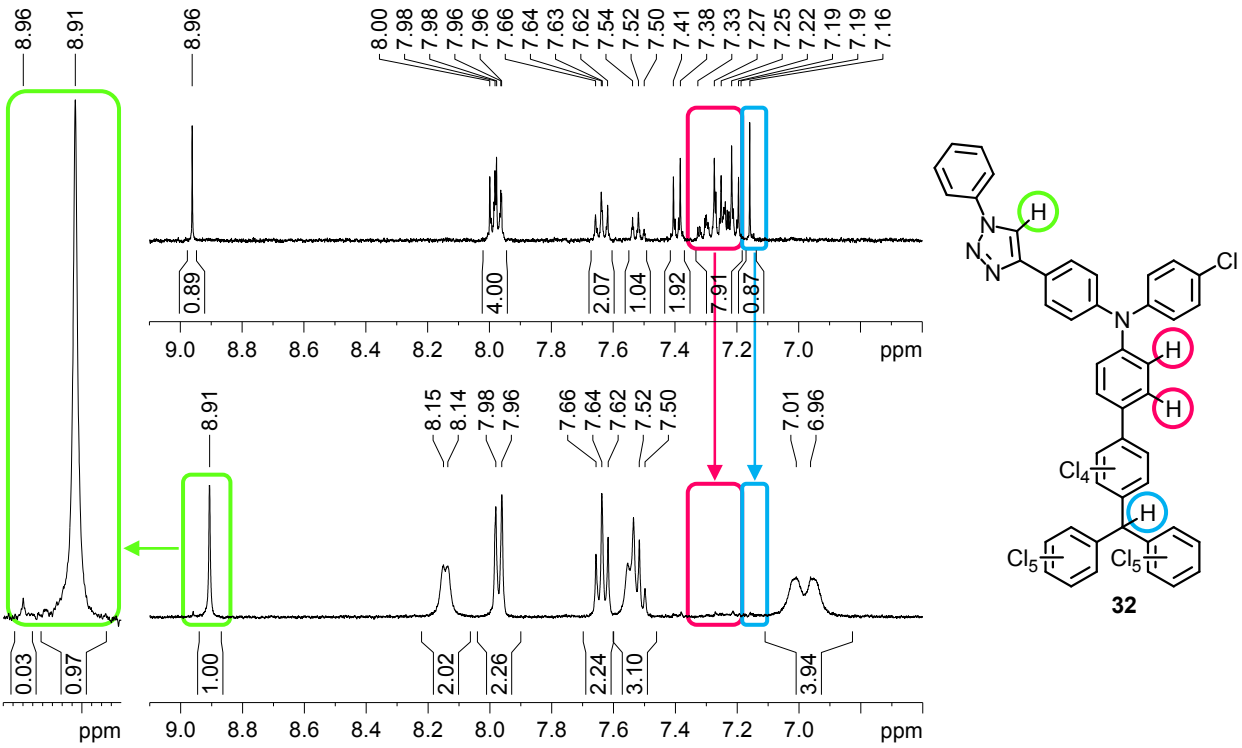

Figure 5.2: ^{1}H-NMR spectra of the *α*-H precursor 32 (top) and the corresponding radical 1 (bottom) in acetone-d_6. The blue box depicts the PCTM proton, which is absent in the spectrum of 1. The green box shows the signal of the triazole-proton and the corresponding enhancement (left). The pink box depicts the protons attached to the phenyl ring in the biphenyl spacer.

^{13}C-NMR spectra of the radicalised compounds show the same effects concerning width and shift of the recorded signals. The most part of the signals of the precursor **33** (Figure 5.3, top) was not recovered in the spectrum of the radicalised species **2** (Figure 5.3, bottom).

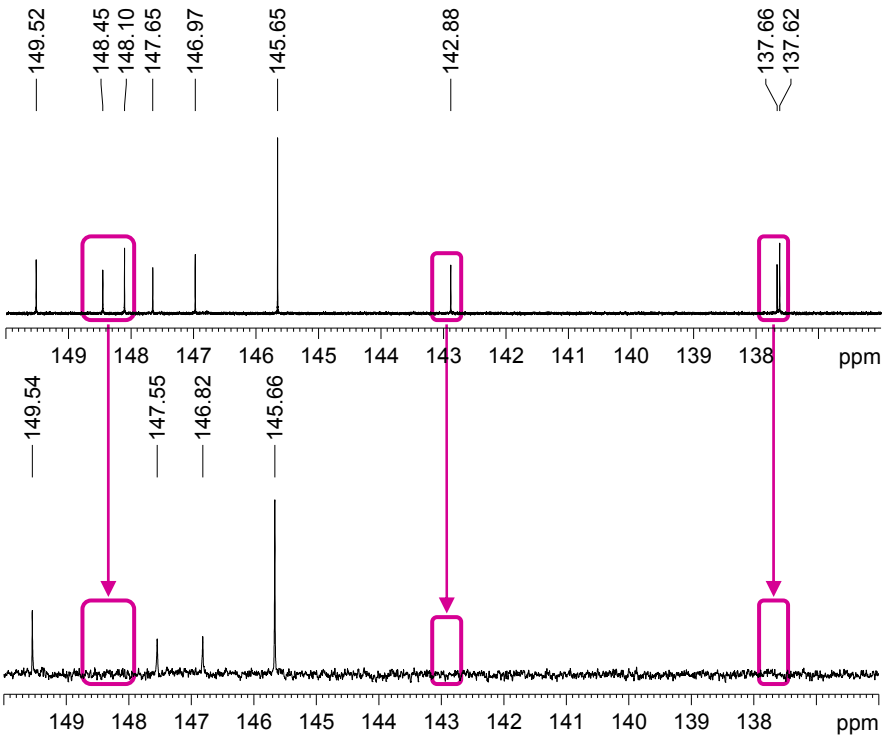

Figure 5.3: ^{13}C-NMR spectra of 33 (top) and 2 (bottom) in acetone-d_6.

This may either be due to strong line broadening, or to a great shift of the signals. For this reason, an exact assignment of the signals to certain C-atoms is rather difficult for the radical **2** and is therefore not discussed here. Since the reason for the lacking signals is not precisely known, ^{13}C-NMR spectroscopy was only performed for **2** and **3** during the scope of this work.

5.2 Absorption Spectroscopy

Absorption spectra were recorded at RT in solvents with different polarity. Solutions with varying concentrations (c = 1 × 10^{-5} – 0.125 × 10^{-5} M) were investigated to exclude aggregations.

All spectra display intensive bands located in the range of 29000 – 30000 cm^{-1}, originating from localised $\pi - \pi^*$ transitions within the triarylamines. In general, one intense HOMO → LUMO transition into a degenerate state can be observed for simple triarylamines with C_3 symmetry. Breaking this symmetry, for example by exchanging the substituents in *p*-position, leads to a splitting of the formerly degenerate LUMO orbitals.[224] For this reason, different transition pathways are conceivable for the herein investigated triarylamine moieties, which might sum up to the observed absorption bands.

The bands at 25900 cm^{-1} and 17600 – 19900 cm^{-1} are the so-called “radical bands”, which are typical of perchlorinated radical compounds.[109] They are absent in the nonradicalised precursor and originate from transitions involving the singly occupied molecular orbital (SOMO) within the PCTM radical moiety (HOMO → SOMO and SOMO → LUMO). These bands are present for all compounds and are almost unaffected by solvent polarity (Figure 5.4, Table 5.2).

To clarify the origin of the individual bands, Figure 5.4 depicts the spectra of the radicalised precursor **38** (blue), the triarylamine **39** (red) and the reference compound **1** (black) in CH_2Cl_2.

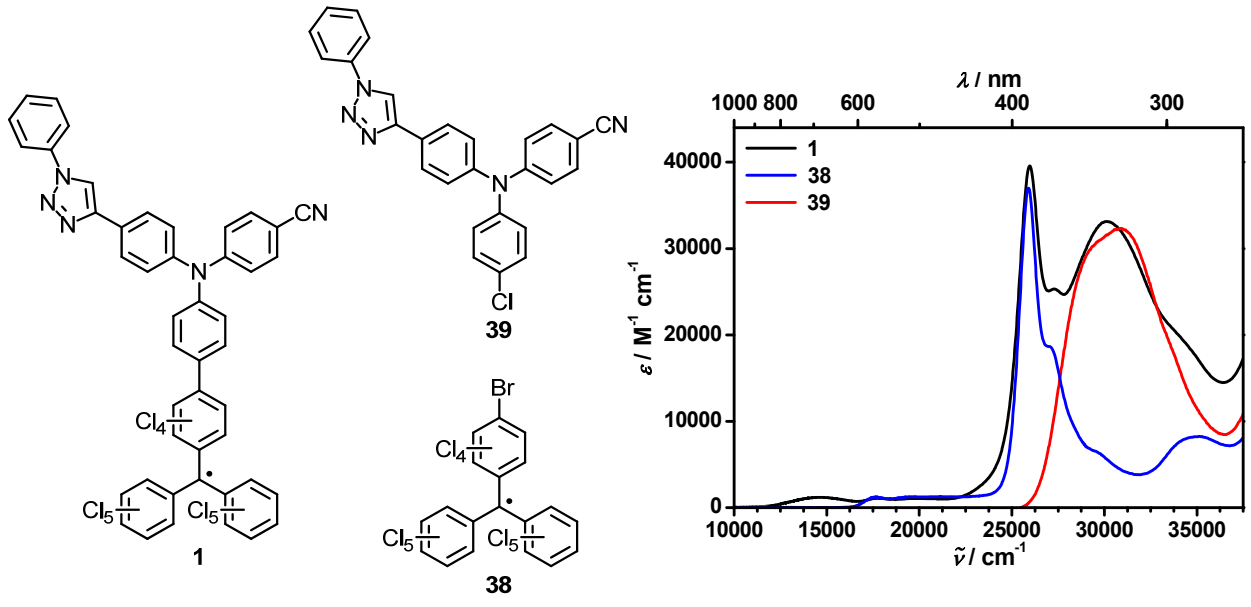

Figure 5.4: Absorption spectra of 1, 38 and 39 in CH_2Cl_2.

Comparison of the absorption spectra of reference compounds **1** and **4** (Figure 5.5) shows that the stronger electron withdrawing cyano group in **4** shifts the absorption maximum of the triarylamine at ~30000 cm^{-1} to lower energy, compared to the chlorine substituent in **1**. This indicates a more pronounced CT character of the transition within the triarylamine, which is

confirmed by the absorption spectrum of the triarylamine **39** (Figure 5.4). The absorption band of the triarylamine appears to be a superposition of both transitions.

The most interesting bands in the spectra are the so-called IVCT (inter-valence charge-transfer) bands, which originate from a CT from the triarylamine donor (D1) to the PCTM radical acceptor (A). As apparent from Figure 5.5 B, the IVCT band is more intense for **1** than for **4**. This indicates a more pronounced CT character for the chlorine-substituted compounds than for the cyano-substituted ones, as expected. An increase of the electron withdrawing character of the substituents attached to the triarylamine corresponds to a decrease in the donor strength. Therefore, a hypsochromic shift of the IVCT band was observed for **4** in contrast to **1**. A stronger acceptor on D1 destabilises the excited state, which results in an increase of ΔG^{00} (see Figure 2.3 D). This is only valid, if the other reorganisation parameters remain unaffected by the substituents.

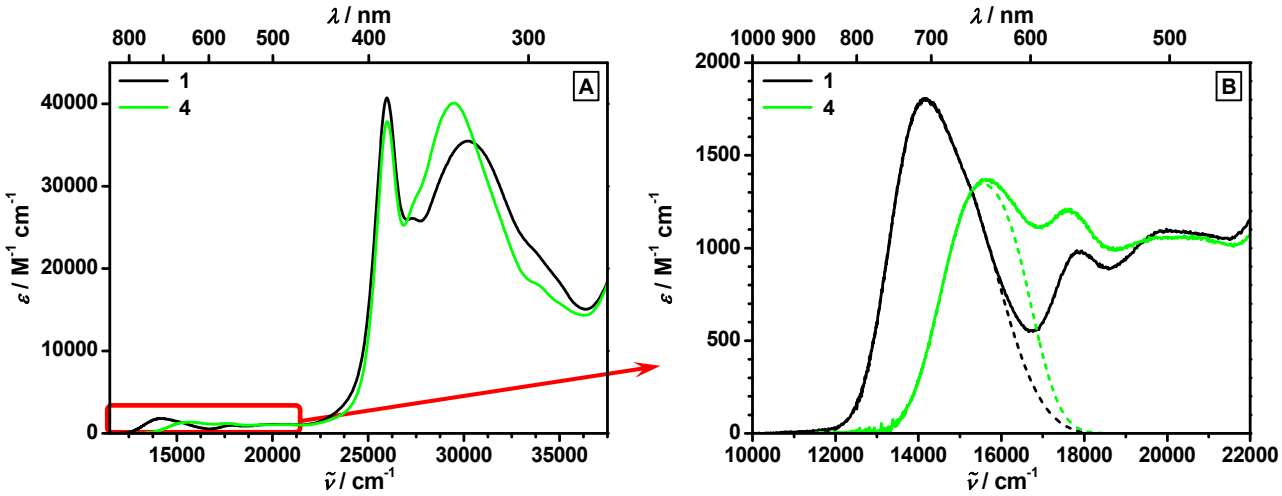

Figure 5.5: Absorption spectra of 1 and 4 in cyclohexane (A) and enlargement of the IVCT bands (B). Dotted lines show deconvolutions of the IVCT bands. Two *Gaussian* functions were used for the deconvolution of each band.

In order to analyse the photophysical properties of triads, it is helpful to compare them with suitable dyads as reference compounds. The absorption spectra of **1** and **4** are in good agreement with results for a series of comparable compounds already published by our group (see Chapter 3.3.3, Figure 3.33 for details).[225] As will be apparent from Chapter 5.3, the influence of the triazole unit on the oxidation potential of the triarylamine donor (D1) is similar to a methyl group. For this reason, compound **FI** was chosen as a reference for **1**. Since the corresponding reference for **4** was not available, **FJ** served as a substitute, due to its suitable redox potential difference between D1 and A. Absorption maxima and extinction coefficients for **FI** (14400 cm^{-1}, ε = 1900 M^{-1} cm^{-1}) and **FJ** (15500 cm^{-1}, ε = 1650 M^{-1} cm^{-1}) are nearly the same as for **1** (14200 cm^{-1}, ε = 1800 M^{-1} cm^{-1}) and **4** (15600 cm^{-1}, ε = 1500 M^{-1} cm^{-1}) (all measurements were performed in cyclohexane).

The band shape and the exact position of the band maxima are both influenced by solvent polarity (Figure 5.6). Increasing solvent polarity leads to a broadening of the bands. However, the shift of the maxima is unsystematic and much weaker as one would expect. In general, an increase of the solvent reorganisation energy λ_o with rising solvent polarity is observed. Concomitantly, ΔG^{00} should decrease, due to a stabilisation of the zwitterionic excited state. Combining the two contrary effects gives rise to the unsystematic behaviour of the absorption maxima.

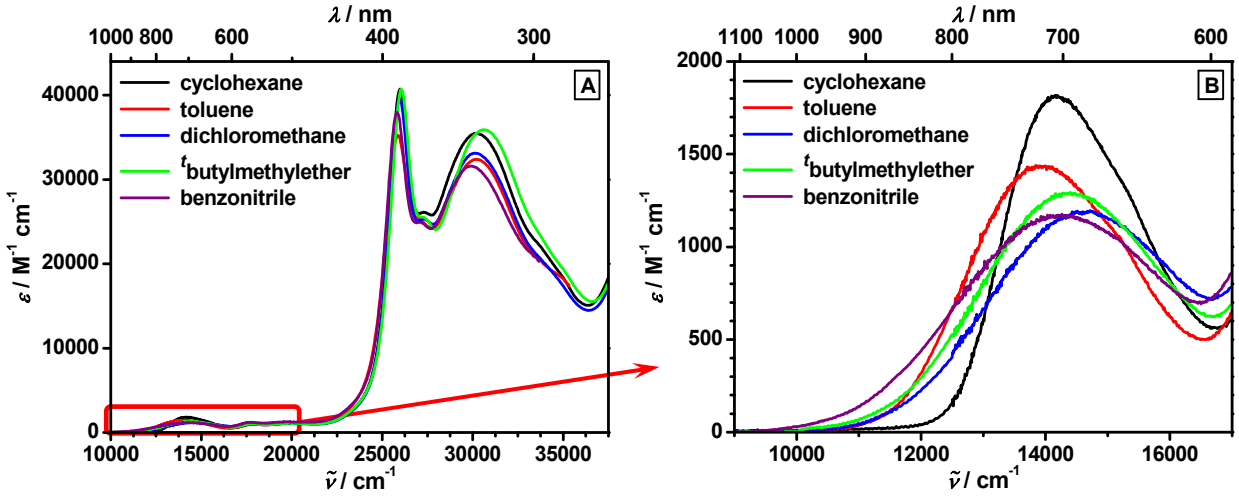

Figure 5.6: Absorption spectra of 1 in different solvents (A) and enlargement of the IVCT bands (B).

In general, the *Jortner*-model provides a possibility to gain insight into such phenomena. The IVCT bands of the herein synthesised compounds are partly superposed by the bands arising from localised transitions within the PCTM radical moiety. Furthermore, the observed bands are rather symmetric in shape, which is unfavourable for a *Jortner*-analysis as discussed in chapter 2.2. For this reasons, performing *Jortner*-fits of the absorption spectra was not possible. The rather poor solubility of some compounds hinders the proper determination of the extinction coefficients. Above all, compound **6** is almost insoluble in cyclohexane. Hence, no reliable values for **6** were observed and are therefore not listed in Table 5.2.

Table 5.2: Absorption maxima of compounds 1 – 6 in different solvents. Extinction coefficients are given in parentheses.

	$\tilde{\nu}$ / cm^{-1} (ε / M^{-1} cm^{-1})				
	cyclohexane				
1	30200 (35500)	26000 (40700)	19900 (1100)	17800 (1000)	14200 (1800)
2	28900 (56500)	26000 (43700)	19900 (1100)	17900 (1100)	14000 (1800)
3	29300 (50800)	26100 (42800)	19800 (1200)	17900 (1000)	14000 (1700)
4	29500 (40200)	26000 (37900)	19900 (1100)	17600 (1300)	15600 (1500)
5	28700 (37600)	26100 (30000)	19900 (900)	17700 (900)	15500 (900)
6	29100 (/)	26000 (/)	19700 (/)	17700 (/)	14700 (/)
	toluene				
1	30200 (32400)	25900 (35200)	19800 (1100)	17800 (1000)	13900 (1400)
2	28900 (51300)	25900 (38100)	19700 (1200)	17700 (1100)	13800 (1400)
3	29200 (54700)	26000 (44000)	19800 (1400)	17800 (1300)	13800 (1600)
4	29200 (39800)	25900 (36700)	19700 (900)	17600 (1100)	15200 (1100)
5	28500 (45700)	26100 (35200)	19900 (900)	17600 (900)	15100 (800)
6	29000 (30900)	25900 (27800)	19900 (1000)	17800 (800)	14200 (1000)
	benzonitrile				
1	29900 (31600)	25800 (38200)	19800 (1300)	17800 (1200)	14200 (1200)
2	28700 (49700)	25900 (42300)	19700 (1100)	17700 (1100)	14100 (1100)
3	29100 (49800)	25900 (45500)	19700 (1500)	17700 (1400)	14200 (1200)
4	29000 (35800)	25900 (39300)	19500 (1300)	17600 (1400)	15400 (1100)
5	28500 (43600)	26000 (38000)	19900 (1200)	17700 (1200)	15600 (800)
6	28700 (34100)	25900 (27800)	19800 (1100)	17700 (1000)	14500 (900)

5.3 Emission Spectroscopy

Steady state emission spectroscopy was carried out at RT in cyclohexane. All compounds showed weak to moderate fluorescence in the NIR range of the spectra (Figure 5.7, A). Measurements in more polar solvents, e.g. $^{n}Bu_2O$ were not possible with the herein used setup, due to the following reasons: In most cases, the emission intensity was too low, giving poor signal-to-noise ratios. Furthermore, fluorescence signals exceeded the range of the detector, due to a strong red shift of the emission maxima. The fact that the emission maxima strongly depend on the solvent polarity indicates emission from a highly polar excited state. For a better understanding of the results discussed in the following, Scheme 5.27 provides an overview over possible radiative and nonradiative processes in the cascades **2**, **3**, **5**, and **6**.

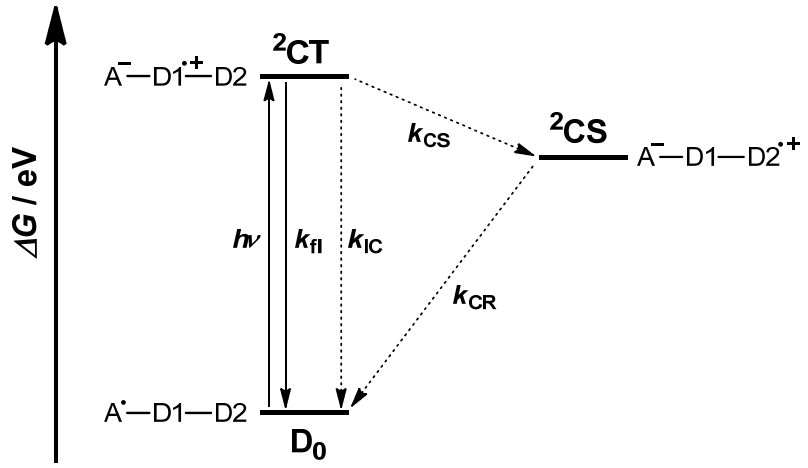

Scheme 5.27: Schematic state diagram for compounds 2, 3, 5, and 6.

In cyclohexane, excitation was performed at low energies, at the maxima of the IVCT absorption bands (14000 – 15600 cm^{-1}), which are depicted in Figure 5.7 B. Therefore, solely the local ^{2}CT state should be populated. Nevertheless, especially for **4** and **5**, a population of low-lying local states within the PCTM radical moiety can also not be excluded, because of the significant overlap of the IVCT band with the PCTM radical bands. No fluorescence was detectable for **6** upon excitation at 14500 cm^{-1}. For this reason, excitation at the energy of the absorption maximum of the PCTM radical (26000 cm^{-1}) was carried out instead. Investigations concerning excitations at different energies were made for some of the herein synthesised compounds, but brought no indication of a systematic behaviour, contrary to the results already published for the series of **FG** – **FM**.[225]

Emission maxima of compounds **1** – **6** are located in a range of 11900 – 13200 cm^{-1}. Compared to their references compounds **1** and **4**, cascades **2**, **3**, and **5** show small bathochromic shifts (~100 – 200 cm^{-1}), comparable to those found in the absorption spectra. According to this, attaching a second triarylamine donor (D2) to the triazole bridging unit (**2**, **3**, and **5**) has nearly no or only weak influence on the energy levels of both, ground and first

excited state. *Stokes*-shifts of 2100 – 2400 cm^{-1} were found for the chlorine- and for the cyano-substituted compounds, respectively. In case of **6**, the bathochromic shift of the emission (900 cm^{-1}) and absorption (1100 cm^{-1}) maxima was found to be more pronounced compared to **4**. This indicates a stronger influence of the ferrocene moiety on the energy levels of ground and excited state in **6**, although the electronic coupling *via* the triazole bridge was expected to be in a similar order of magnitude. The results obtained by cyclic voltammetry (Chapter 5.4) demonstrate that attachment of the triazole moiety to the ferrocene directly influences the redox potential of the ferrocene. Comparison of the emission maxima of compounds **1** and **4** with **FI** (12250 cm^{-1}) and **FJ** (13100 cm^{-1}) once more revealed almost identical results (see Table 5.3), which points to an emission from a similar CT state.

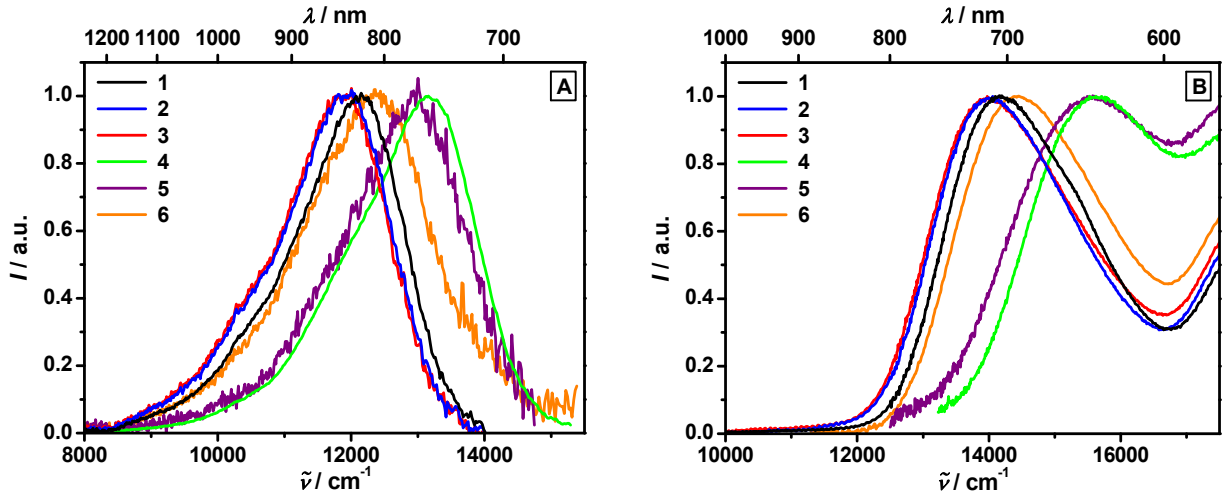

Figure 5.7: Normalised emission (A) and absorption (B) spectra of 1 – 6 in cyclohexane.

Fluorescence quantum yields were determined using Oxazine 1 in EtOH as a quantum yield standard (Φ = 0.15).[346-348] For the reference compounds **1** and **4**, quantum yields of 9 % and 29 %, respectively, similar to **FI** (15 %) and **FJ** (33 %) were determined. The quantum yields of the chlorine-substituted cascades are comparable to **1**. In case of their cyano-substituted analogues **5** and **6**, the obtained values (~1 %) are distinctly smaller than those of **4**. In contrast to **2** and **3**, additional non-radiative quenching processes reduce the fluorescence quantum yields in **5** and **6**. Hole transfer from D1 to D2 resulting in a CS state might provide an alternative deactivation pathway. Measurements of **5** and **6** exhibited a bad signal-to-noise ratio. Accordingly, the determined quantum yields might be erroneous.

Fluorescence lifetimes were obtained using a ns-laser diode excitation at 650 nm (15390 cm^{-1}). Measurements were performed under the same conditions as for steady-state emission experiments. Lifetimes were obtained assuming monoexponential decay kinetics.[1] The poor solubility and the low emission intensities hampered the measurements of **5** and **6** in cyclohexane.

[1] Decay curves are depicted in the Appendix (Figure A.1).

Table 5.3: Emission and absorption maxima $\tilde{\nu}_{max}$, *Stokes*-shift Δ, fluorescence quantum yield Φ_{fl}, fluorescence lifetime τ_{fl} and rate constants for the radiative k_{fl} and non-radiative k_{nr} processes of 1 – 6 in cyclohexane.

	$\tilde{\nu}_{max}$ abs / cm^{-1}	$\tilde{\nu}_{max}$ em / cm^{-1}	Δ / cm^{-1}	Φ_{fl} / %	τ_{fl}[a] / ns	k_{fl} / 10^7 s^{-1}	k_{nr} / 10^7 s^{-1}
1	14200	12100	2100	9	10	0.89	9.1
2	14000	11900	2100	8	5.9	1.4	16
3	14000	11900	2100	7	6.7	1.1	14
4	15600	13200	2400	29	19	1.5	3.7
5	15500	13000	2500	1	/[b]	/	/
6	14500	12300	2200	< 1	/[b]	/	/

[a]Measured in the emission range 11100 – 13200 cm^{-1}.
[b]Not measurable due to low fluorescence intensities.

The rate constants for the radiative k_{fl} and nonradiative processes k_{nr} were derived from equations (14) and (15).

$$k_{fl} = \frac{\Phi_{fl}}{\tau_{fl}} \tag{14}$$

$$k_{nr} = \frac{1-\Phi_{fl}}{\tau_{fl}} \tag{15}$$

In case of **2** and **3**, the values of k_{fl} and k_{nr} match those of **1**. This excludes an additional non-radiative hole transfer from D1 to D2, as already indicated by the similar quantum yields. The non-radiative processes in **1** – **3** are throughout faster than the radiative ones. A comparable, but less pronounced observation was made for **4**. Reference compounds **1** and **4** show similar values for k_{fl}. On the contrary, k_{nr} is clearly smaller for **4**, indicating non-radiative processes to play a minor role compared to **1**. The potential difference between A and D1 is more pronounced in **4** than in **1**. According to the gap rule, the greater energy difference between ground and excited state leads to a smaller value of k_{nr}, due to the decreasing *Franck-Condon* overlap-integral.

In contrast to the absorption spectra, *Jortner*-fits were viable for the emission bands of **1** – **6** (Figure 5.8). Since the obtained values are similar among the cascades and their corresponding reference compounds, only the data for **1** and **4** are presented in Table 5.4 and Figure 5.8.

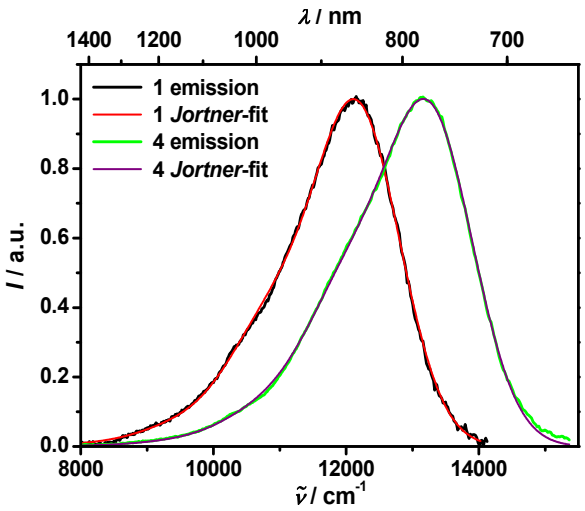

Figure 5.8: Normalised emission curves and corresponding *Jortner*-fits of 1 and 4 in cyclohexane.

Since back electron-transfer (BET) is assumed to be a non-radiative process within *Jortner*-theory, a concomitant decrease of the rate constant k_{nr} with increasing ΔG^{00} points to a process located in the *Marcus*-inverted region. With increasing oxidation potential of D1 (**1** → **4**), a significant increase in ΔG^{00} was observed (13200 cm^{-1} → 14300 cm^{-1}). Additionally, λ_i increases (450 cm^{-1} → 550 cm^{-1}), while the other parameters remain almost unaffected. Almost similar observations were made for **FI** and **FJ**, showing a simultaneous increase of the parameters λ_i (600 cm^{-1} → 800 cm^{-1}) and ΔG^{00} (13550 cm^{-1} → 14300 cm^{-1}).

Table 5.4: Electron transfer parameters λ_i, λ_o, ΔG^{00} and $\tilde{\nu}_v$, fitted to the emission spectra of 1 and 4 in cyclohexane.

	λ_o / cm^{-1}	λ_i / cm^{-1}	ΔG^{00} / cm^{-1}	$\tilde{\nu}_v$ / cm^{-1}
1	1000	450	13200	1350
FI[a]	1350	600	13550	1350
4	1050	550	14300	1250
FJ[a]	1100	800	14300	1250

[a]Values derived from lit [225].

In addition to the emission spectra, excitation spectra were recorded in cyclohexane. For this purpose, fluorescence probes were diluted by a factor of twenty. Figure 5.9 shows the excitation spectra of **1** and **5** as representatives. The measurements confirm complete energy transfer from higher excited states to the ^{2}CT.

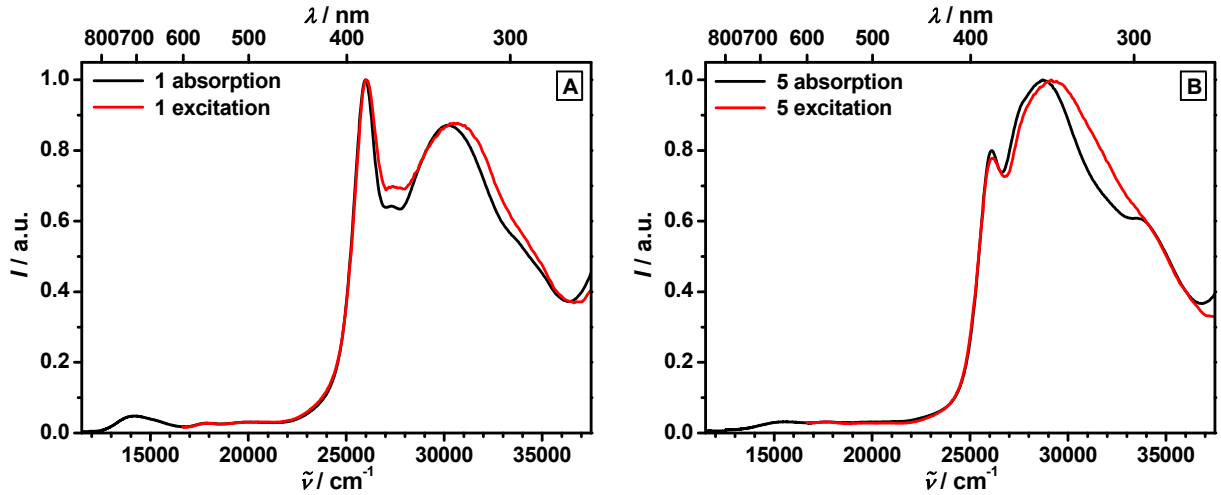

Figure 5.9: Absorption (black) and excitation spectra (red) of 1 (A) and 5 (B) in cyclohexane.

In conclusion, the results of the steady-state and time-resolved emission spectroscopy of **1** and **4** directly match those of **FI** and **FJ**, indicating the fluorescence to occur directly from the ^{2}CT state. In case of the chlorine-substituted cascades **2** and **3**, the obtained values resemble those of the reference compound **1**. Consequently, no additional non-radiative processes are present in this compounds. A different situation was found for **5** and **6** where a competing radiationless process leads to a decrease of the fluorescence quantum yields.

5.3 Cyclic Voltammetry

The preceding sections gave an overview of the absorption and emission characteristics of compounds **1** – **6**. For a better understanding of the photoinduced electron and hole transfer processes which take place, it is essential to determine the redox potentials of the donor and acceptor units. Therefore cyclic voltammograms were recorded in CH_2Cl_2 using $^{n}Bu_4NPF_6$ (0.2 M)[349] as a supporting electrolyte. The obtained results were referenced against the Fc/Fc^+ redox couple as an internal standard.[323]

Regarding the cyclic voltammogram of the chlorine-substituted reference compound **1** (Figure 5.10), a reversible wave is observable at –630 mV, which is ascribed to the reduction of the PCTM radical to the corresponding anion.

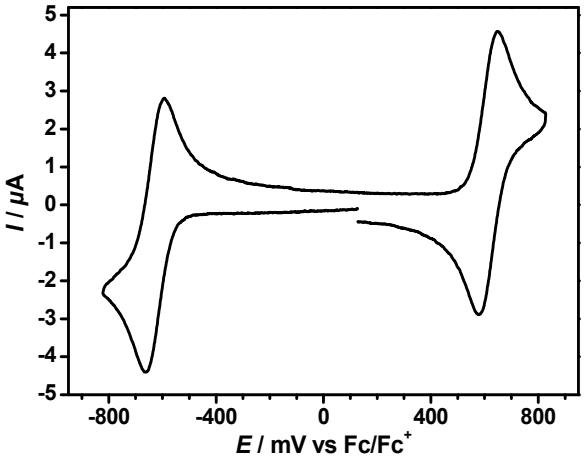

Figure 5.10: Cyclic voltammogram of 1 in CH_2Cl_2 (0.2 M $^{n}Bu_4NPF_6$).

For **1** – **6**, the reduction potential lies in a range between –620 mV to –650 mV, which is typical of PCTM radical acceptors. Reduction of the bromo-substituted PCTM radical **38** takes place at –580 mV. In general, reduction of the cyano-substituted compounds **4** – **6** occurs at more negative potentials than the reduction of **1** – **3**. This observation is rather unexpected, since the chlorine-substituted D1 is supposed to be a stronger donor to the PCTM radical moiety, but clearly indicates a small, non-negligible electronic coupling between A and D1. Since the reduction is nearly constant for all compounds, only oxidation processes will be discussed in the following.

It is well known, that the redox potential of triarylamines can easily be tuned by variation of the substituents in *p*-position. The PCTM radical moiety clearly acts as an electron acceptor on D1. Investigation of compound **39** (Figure 5.11) shows that the PCTM radical acceptor is comparable to a chlorine substituent, since **39** possesses a similar redox potential as **4**.

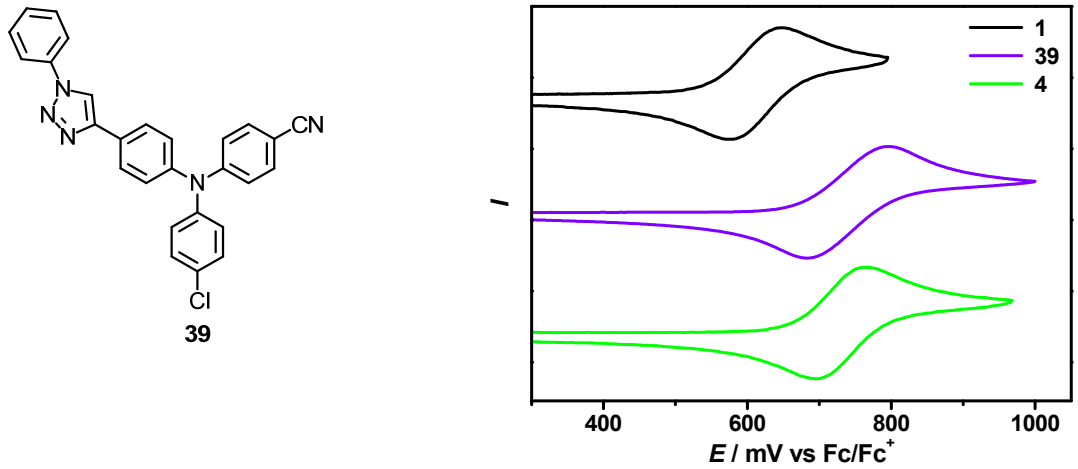

Figure 5.11: Cyclic voltammograms of 1, 4 and 39 in CH_2Cl_2 (0.2 M $^nBu_4NPF_6$).

To ensure the desired redox gradient, one position of the triarylamine donor D1 is substituted by an electron-withdrawing group. The chlorine-substituted reference compound **1** shows a reversible wave at 610 mV, corresponding to the first oxidation of D1. In compound **4**, the chlorine atom is replaced by a cyano group. Implementation of such a stronger electron-withdrawing group results in a shift of the oxidation potential of D1 to higher values (730 mV). This is also observable for cascades **5** and **6** in comparison with **2** and **3**.

In **2**, **3**, **5**, and **6**, D1 is connected to D2 by a triazole bridge. The triazole spacer-unit is attached to D1 *via* its carbon atom. The resulting influence on D1 is comparable to a methyl group.[350] Hence, it has an electron-donating character. On the contrary, connection of the triazole to D2 *via* the nitrogen atom showed an opposing effect. The electron lone pair of this nitrogen atom is part of the aromatic π-system of the triazole. Therefore, the nitrogen does not act as a donor (no +M-effect), but as an acceptor (–I-effect) because of its higher electronegativity compared to carbon.

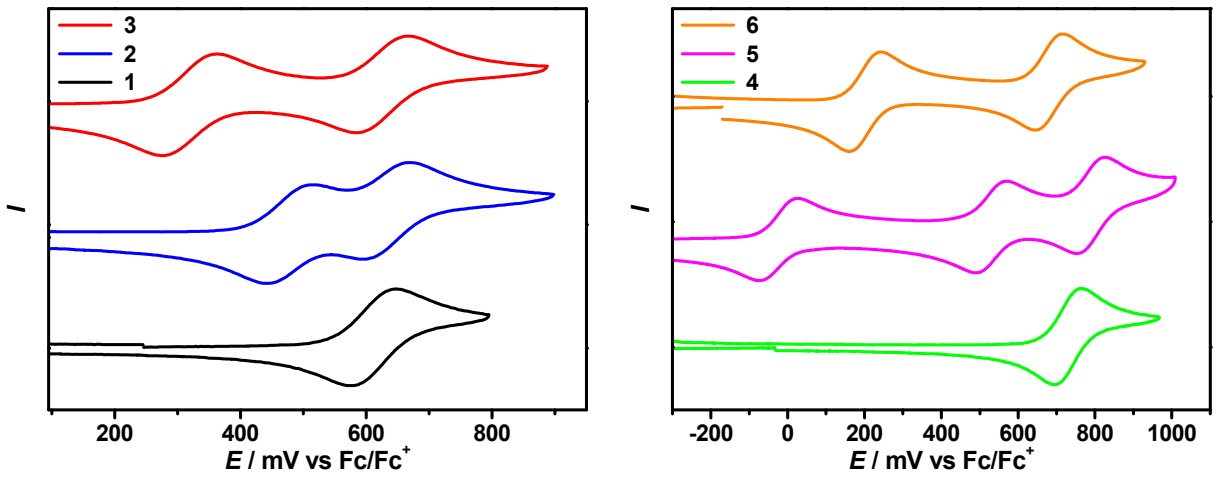

Figure 5.12: Cyclic voltammograms of 1 – 6 in CH_2Cl_2 (0.2 M $^nBu_4NPF_6$).

This is substantiated by comparison of **5** and **6**. Assuming the potential of the ferrocene moiety to be around 0 mV, synthesis of **6** was performed in order to generate a cascade with a similar

redox potential of D2 related to **5**. Albeit, the potential of the ferrocene moiety was shifted to higher values, compared to unsubstituted ferrocene. Actually, the oxidation potentials of D2 in both compounds differ by about 200 mV. Several similar results have already been published in the literature.[271,351] Comparing the oxidation potentials of D2 in **2**, **3**, and **5** with other compounds bearing similar donor units[316], a shift of about +100 mV is apparent. Table 5.5 provides an overview of the redox potentials obtained by cyclic voltammetry.

Table 5.5: Redox potentials obtained by cyclic voltammetry in CH_2Cl_2 (0.2 M $^nBu_4NPF_6$).

	$E_{1/2}^{red}$(A) / mV	$E_{1/2}^{ox}$ (D2) / mV	$E_{1/2}^{ox}$ (D1) / mV
1	–630	/	610
2	–630	470	630
3	–620	320 / 1060[a]	630
4	–650	/	730
5	–640	–20 / 540[a]	790
6	–640	200	680
38	–580	/	/
39	/	/	740

[a]Second oxidation of the same subunit

Apparently, the oxidation potential of the donor-substituted D2 (if present) is throughout lower than the one of the D1. For **3** and **5** a second oxidation of D2 was observed. All compounds show an additional oxidation process above 1200 mV (not shown in Table 5.5), which may be ascribed either to a further oxidation of D1 or to an oxidation of the PCTM radical. As both the radicalised precursor **38** ($E_{1/2}$ = 1200 mV), and the reference compound **39** ($E_{1/2}$ = 1280 mV) showed oxidations in this range of their voltammograms, no clear assignment can be made for this process.

In conclusion, the oxidation potentials of the triarylamines were tuned by variation of their substituents. Comparing the chlorine-substituted compounds **1**, **2**, and **3**, similar redox potentials were found for D1, which indicates a small influence of D2 on D1 *via* the triazole bridge. In case of the cyano-substituted compounds **4**, **5**, and **6**, somewhat different observations were made. Actually, the oxidation potentials of D1 differ by more than 100 mV. Regarding compound **5**, the higher potential of D1 might be explained by the fact that the first and second oxidation of D2 occur prior to the first oxidation of D1. Removal of a third electron is

supposed to be more difficult. Concerning **6**, the first oxidation already takes place at 200 mV at the iron atom of the ferrocene, which is attached directly to the triazole *via* one of the cyclopentadienyl rings. In **5**, oxidation occurs at the triarylamine nitrogen. The ferrocene cyclopentadienylring in **6** is a stronger donor compared to the D2-triarylamine in **5**, reducing the oxidation potential of D1 in **6**.

All in all, the measured values clearly demonstrate the successful generation of a suitable redox gradient for a hole transfer from D1 to D2 in the cascades **2**, **3**, **5**, and **6**.

Differential pulse-voltammetry (DPV) measurements as well as *Osteryoung* square-wave measurements (OSWV) were carried out to quantify the amount of the radicalised species in relation to the *α*-H precursor. For this reason, *Voigt*-fits of the oxidation and reduction signals were carried out. All measurements were performed under the same conditions as applied for cyclic voltammetry. The cyclic voltammogram of **1** (Figure 5.10) displays one oxidation as well as one reduction process. The same observation was made for the DPV (Figure 5.13) and OSWV (not shown) of **1**. In case of a complete radicalisation process, *Voigt*-fits of the oxidation and reduction curves were expected to give comparable results. Figure 5.12 shows the relative integral to be 1:1 in dyad **1**.

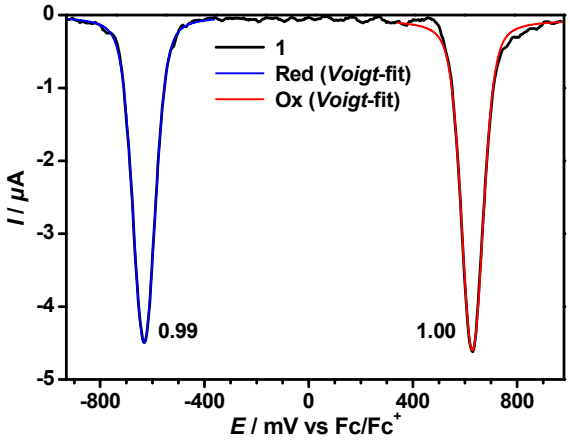

Figure 5.13: DPV of 1 in CH_2Cl_2 (0.2 M $^nBu_4NPF_6$) including *Voigt*-fits of oxidation and reduction. Fit curves are depicted in red (ox) and blue (red).

Voigt-fits of the DPV and OSWV measurements were performed for all compounds after the radicalisation reactions to confirm complete conversion.

5.4 Spectroelectrochemistry and Chemical Oxidation

The spectroscopic properties of the neutral compounds **1** – **6** were discussed in Chapter 5.1 and 5.2. To gain an insight into the spectroscopic properties of their ionic species, spectroelectrochemistry measurements were performed under the same conditions as for cyclic voltammetry (0.2 M $^{n}Bu_4NPF_6$ in CH_2Cl_2). Figure 5.13 A and B show the reduction and first oxidation of reference compound **4** as representatives.

During the reduction of **4** (Figure 5.14, A), the characteristic band of the PCTM radical at 26000 cm^{-1} vanished. An expected simultaneous decrease of the bands at 17600 – 19900 cm^{-1} was not observed due to superposition by the anion band, which arose at 19300 cm^{-1}. This band was found for all compounds upon reduction in the range of 19300 cm^{-1} to 19400 cm^{-1}. Simultaneously, the IVCT band at around 14500 cm^{-1} diminished. Since the reduction processes of the other compounds were found to be quite similar, only oxidation processes will be discussed in the following.

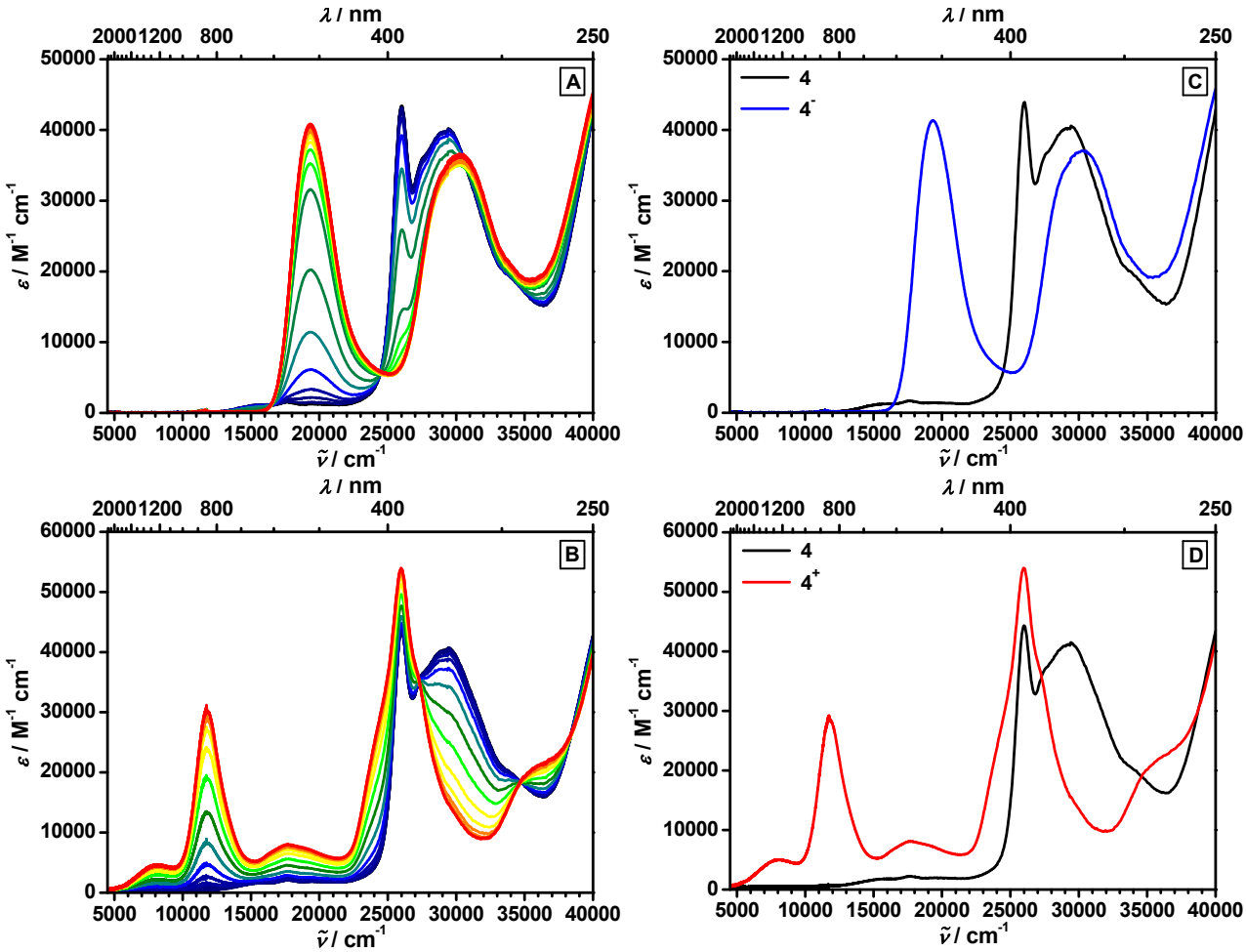

Figure 5.14: Left: Reduction of 4 (A). First oxidation of 4 (B). Early spectra are shown in blue/green, late ones in orange/red colours. Right: Spectra of 4 (black) and 4^- (blue) (C). Spectra of 4 (black) and 4^+ (red) (D). Spectra were recorded in CH_2Cl_2 (0.2 M $^{n}Bu_4NPF_6$).

As apparent from Figure 5.14, subsequent oxidation of **4** to **4**$^{+}$ (Figure 5.14, B) resulted in a decrease of the characteristic triarylamine band at 29300 cm^{-1}. Consequently, the radical cation bands of the triarylamine rose at 11800 cm^{-1} and 17700 cm^{-1}. In addition bands at 25000 cm^{-1} were observed, which are superposed by the absorption band of the PCTM radical. Investigations proving their origin will be discussed in the next paragraph (Figure 5.15). In the low energy range of the spectrum, a new IVCT band (8100 cm^{-1}) appeared. It may be assigned to a CT between the PCTM radical and the triarylamine cation, in which donor and acceptor exhibit exchanged redox properties. A CT between the triazole bridge and one of the triarylamines was excluded by spectroelectrochemical measurements of reference **39**.

Compound **39** (Figure 5.11) consists of a triarylamine, substituted by one chlorine atom and one cyano group in the *p*-positions of two of the phenyl rings. A phenyl substituted triazole is attached to the third ring. Since no PCTM radical acceptor is present in **39**, only oxidation processes were investigated.

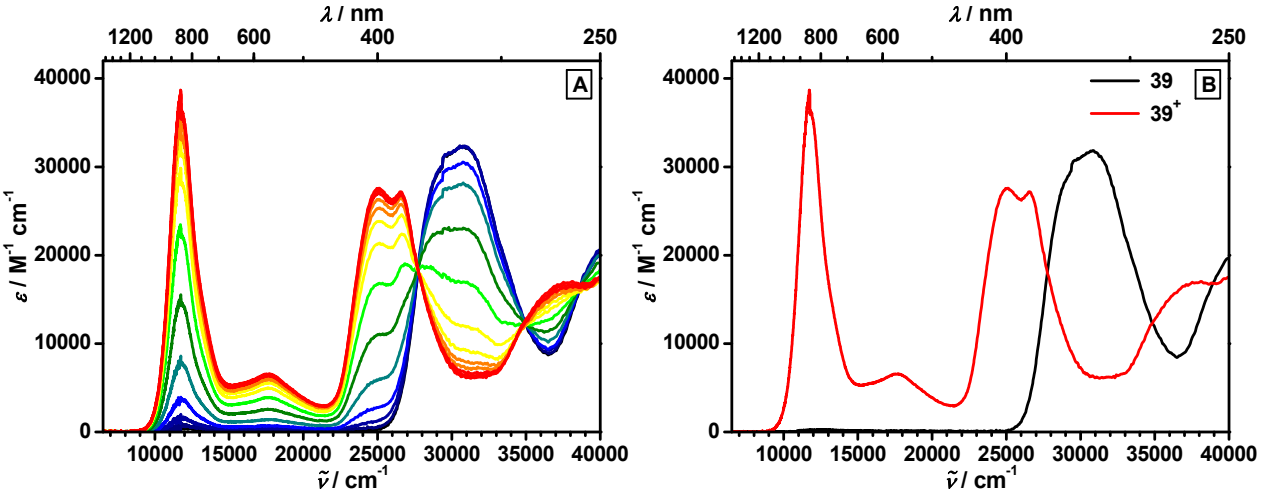

Figure 5.15: First oxidation of 39 (A). Early spectra are shown in blue/green, late ones in orange/red colours. Spectra of 39 (black) and 39^{+} (red) (B). Spectra were recorded in CH_2Cl_2 (0.2 M $^{n}Bu_4NPF_6$).

The cyclic voltammogram showed one reversible oxidation at 740 mV (Figure 5.11 in Chapter 5.3), which was comparable to the oxidation of D1 in **4** (730 mV). During oxidation (Figure 5.15), the radical cation band rises at 11800 cm^{-1}, as it was also found for compound **4**. Simultaneously, bands at 17700 cm^{-1} and 25000 cm^{-1} were observed. Due to the lack of a PCTM radical moiety in this compound, the bands at 25000 cm^{-1} can clearly be ascribed to the radical cation of the triarylamine. Several examples, showing additional bands of triarylamine radical cations at higher energies can be found in the literature. No explanations concerning their origin have been made so far. The IVCT band (8100 cm^{-1} for **4**) was absent in the spectrum of **39**. This observation excludes a possible CT between the triarylamine and the triazole bridge, and strengthens the interpretation of an IVCT between the PCTM radical and the triarylamine radical cation in **4**. Comparing the spectra of **4** with the ones of reference compound **1**, differences only were found in the position of the bands, as well as in their

extinction coefficients. Number and assignment of the bands are quite the same.

In case of the redox cascades **2**, **3**, **5**, and **6**, the spectra obtained by spectroelectrochemistry are more complex. Compounds **3** and **5** differ in their redox behaviour concerning D1 and D2, respectively. During oxidation, spectra of three different species were obtained for both compounds. Black lines in Figure 5.15 represent the spectra of the neutral compounds. Figure 5.16 A shows the absorption spectra of the radical cations of **3**. Subsequent increase of the applied voltage resulted in the first oxidation of D2 (blue), followed by the first oxidation of D1 (violet). The absorption maxima of both radical cations are at similar energies of 13100 cm^{-1} (1st ox. D2) and 12300 cm^{-1} (1st ox. D1). In addition, both radical cations showed bands with lower intensity at around 16000 cm^{-1}. Furthermore, a second oxidation process for D2 (red) was observed during the measurement. The corresponding triarylamine dication band is located at 18100 cm^{-1}.

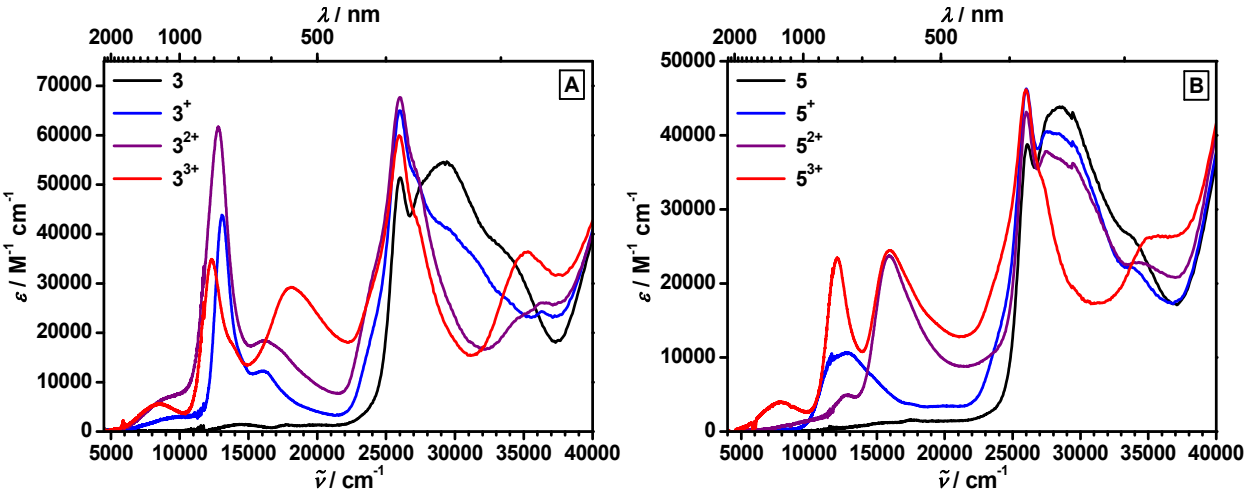

Figure 5.16: Oxidation of 3 (A) and 5 (B). Spectra of the neutral compound (black) and the oxidised species (blue/violet/red). Spectra were recorded in CH_2Cl_2 (0.2 M $^nBu_4NPF_6$).

Since the $-NMe_2$ group is a stronger donor than –OMe, it distinctly lowers the potential of D2 in **5** compared to **3**. Additionally, the cyano group in **5** shifts the potential of D1 to higher values than the chlorine substituent in **3**. For this reason, the blue and violet spectra of **5** (Figure 5.16, B) represent the first and second oxidation of D2. Further increase of the potential resulted in an oxidation of D1 (red). The characteristic bands of the radical cations are located at 12800 cm^{-1} (1st ox. D2), 15900 cm^{-1} (2nd ox. D2) and 12100 cm^{-1} (1st ox. D1). Obviously, no additional bands at ~16000 cm^{-1} were observed in the spectra of the radical cations of **5**. The band assigned to the first oxidised species of **5** is clearly broader and shows a lower intensity than any other band observed during the spectroelectrochemical investigation of **1** – **5**.This might be explained by a delocalisation of the charge within the phenylenediamine unit in D2.[352]

Regarding the low-energy range of the spectra, IVCT bands are present for nearly all cationic species of **3** and **5**. Scheme 5.28 provides an overview of conceivable hole-transfer (HT) processes that might give rise to the observed transitions. Solid arrows represent

processes, assignable to certain bands. Dashed arrows stand for other possible processes and will not be discussed further. The colours in Scheme 5.28 refer to the spectra of the corresponding cations of **3** and **5** depicted in Figure 5.16. The blue spectra in Figure 5.16 A and B refer to the singly oxidised species. In case of $\mathbf{3}^{+}$, the band at around 10000 cm^{-1} may be ascribed to an IVCT between $D2^{\bullet+}$ and D1. This band is not visible in the spectrum of $\mathbf{5}^{+}$ though the same transfer pathway is accessible. The corresponding redox potentials indicate a shift of the band maximum of about 4000 cm^{-1}. Thus, the band is probably superposed by the absorption bands of the radical cation at 12800 cm^{-1}.

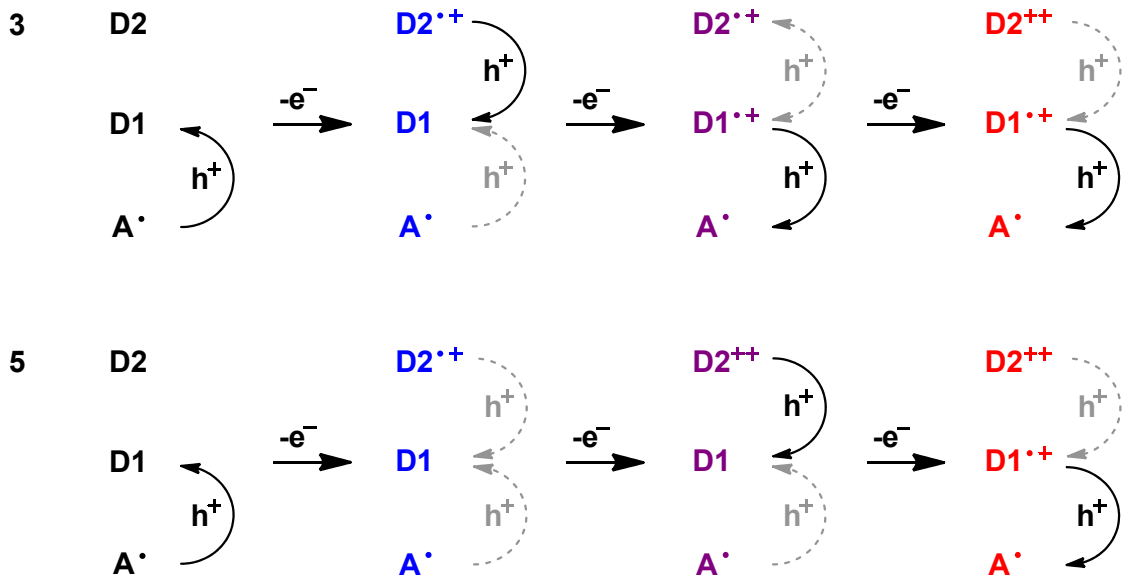

Scheme 5.28: Hole transfer in 3 (top) and 5 (bottom). Solid arrows represent processes visible in the spectra, dashed ones other transfer possibilities. Colours refer to the spectra of the corresponding species in Figure 5.16.

As apparent from Scheme 5.28, different processes have to be taken into account to explain the occurrence of the IVCT bands in the spectra of the doubly oxidised species $\mathbf{3}^{2+}$ and $\mathbf{5}^{2+}$ (violet). In case of $\mathbf{3}^{2+}$, a HT from $D1^{\bullet+}$ to $A^{\bullet}$ takes place, whereas for $\mathbf{5}^{2+}$, there is HT from $D2^{2+}$ to D1. For this reason, the IVCT bands in the violet spectra differ clearly in intensity and shape between $\mathbf{3}^{2+}$ and $\mathbf{5}^{2+}$. Removal of a third electron results in two nearly equivalent species $D2^{2+}$–$D1^{\bullet+}$–$A^{\bullet}$ for **3** and **5**. The IVCT bands in the corresponding spectra (red in Figure 5.16) at 8500 cm^{-1} (**3**) and 7900 cm^{-1} (**5**) are similar in shape and size, and can clearly be assigned to a HT from $D1^{\bullet+}$ to $A^{\bullet}$. This is confirmed by the fact that they also occur in the spectra of the reference compounds $\mathbf{1}^{+}$ (Figure 5.19) and $\mathbf{4}^{+}$ (Figure 5.14) where no D2 is present.

Overall, transitions between D1 and D2 show broader and less intense IVCT bands, than transitions between D1 and A. This observation can be explained by the throughout higher potential difference of D1 and A compared to D1 and D2. Comparing **1** and **4**, the IVCT band for **4** is more pronounced than for **1**, as expected. Spectroelectrochemical measurements of **2** gave quite similar results as of **3** and will therefore not be discussed in the following.

The results derived from cyclic voltammetry for **6** pointed to a deposition of this compound at the working electrode. For this reason, spectroelectrochemical measurements were not possible. Investigations of the oxidation processes were therefore performed by chemical oxidation with $SbCl_5$ (0.1 M in CH_2Cl_2) (Figure 5.17).

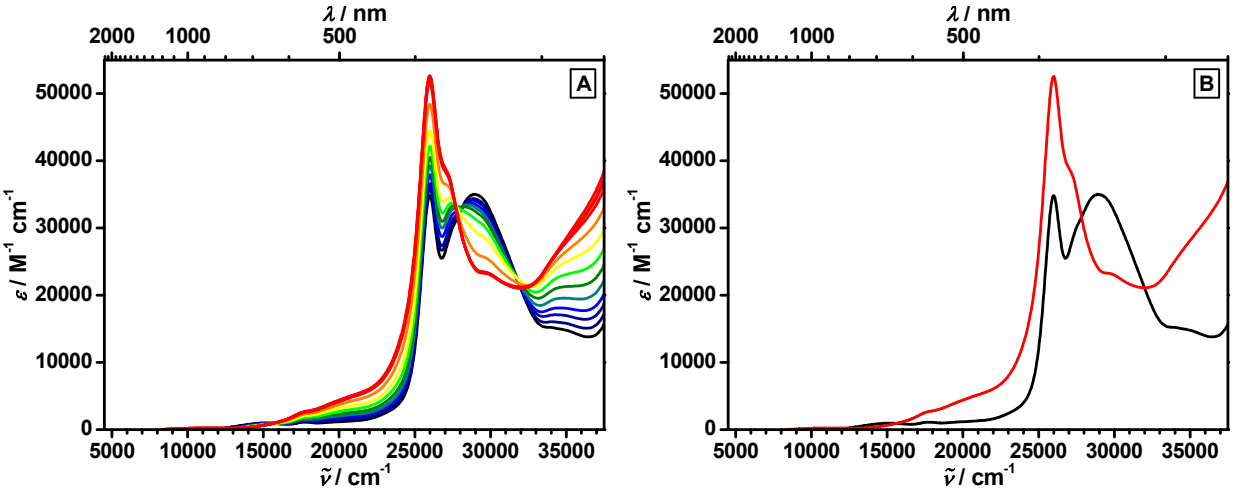

Figure 5.17: Chemical oxidation of 6 (A). Early spectra are shown in blue/green, late ones in orange/red colours. Spectra of the radical (black) and the oxidised species (red) (B). Chemical oxidation was performed with $SbCl_5$ (0.1 M in CH_2Cl_2).

The oxidation potential of $SbCl_5$ in CH_2Cl_2 is sufficiently high to oxidise the ferrocene (200 mV) as well as the triarylamine donor (680 mV).[1] The ferricenium cation shows a characteristic band in the absorption spectrum at 16200 cm^{-1} in CH_2Cl_2, which is assigned to a LMCT (ligand-to-metal charge-transfer) transition. Since the extinction coefficients of this bands are quite low[2], a superposition by absorption bands of the radical acceptor and the triarylamine donor, respectively, was assumed.[353-356]

During oxidation, the absorption bands of the triarylamine and the PCTM radical remained nearly constant at first. In the following, the absorption band of the triarylamine at 28900 cm^{-1} decreased. Furthermore an increase of the PCTM radical band at 26000 cm^{-1} occurred, as it was found before, e.g. for **3** and **5**. In the preceding section, this increase was ascribed to the superposition with absorption bands of the triarylamine cation. This explanation is not valid in case of **6**, because the expected absorption band of the triarylamine cation at ~12000 cm^{-1} was not observable. Simultaneously, the IVCT band decreased.

To exclude reaction of $SbCl_5$ with either the ferrocene moiety or the cyano group attached to the triarylamine, chemical oxidation was performed with the chlorine-substituted reference compound **1** under the same conditions. The experiments showed similar results, and thus gave no information to clarify the lack of the cation band. A possible explanation might be a decomposition of the triarylamine by reaction with $SbCl_5$ or $SbCl_3$ that is formed during the

[1] The triarylamine $N(C_6H_4Br)_3$ (700 mV vs. Fc/Fc^+) is oxidised by $SbCl_5$ in CH_2Cl_2.[323]
[2] Extinction coefficients are reported to be < 1000 M^{-1} cm^{-1}, e.g. ε = 420 M^{-1} cm^{-1} at 16200 cm^{-1} in H_2O.

oxidation process of the ferrocene in **6**. All in all, a clear assignment of the red spectra in Figure 5.17 B to a particular species (e.g. $\mathbf{6}^{+}$ or $\mathbf{6}^{2+}$) is therefore not possible.

5.5 Transient Absorption Spectroscopy

5.5.1 ns-Transient Absorption Spectroscopy

A detailed discussion of the emission properties of compounds **1** – **6** was presented in Chapter 5.3. Comparison of the fluorescence quantum yields of cascades **2**, **3**, **5**, and **6** with their corresponding reference compounds **1** and **4** pointed to an additional non-radiative deactivation pathway in case of the cyano-substituted cascades **5** and **6**. This deactivation process might be understood as a hole transfer from D1 to D2, generating a CS state. In order to elucidate the question about a possible CS state formation, ns-transient absorption measurements of compounds **1** – **6** were performed. Measurements were carried out in cyclohexane with an excitation wavelength of 18800 cm^{-1} (532 nm) to avoid ionisation of the triarylamine moieties. The poor solubility of **6** in cyclohexane required measurements in a more polar solvent (toluene). Additionally, a ns-transient absorption spectrum of **5** in benzonitrile was recorded. Spectra in solvents with medium or high polarity were not accessible for **1** – **4**, probably due to the fast kinetics of the processes. Time decays were fitted monoexponentially in the ns-regime. The corresponding lifetimes are given in Table 5.6. Figure 5.18 shows the ns-transient absorption spectrum of **5** in benzonitrile and the corresponding time decay at 19200 cm^{-1}.

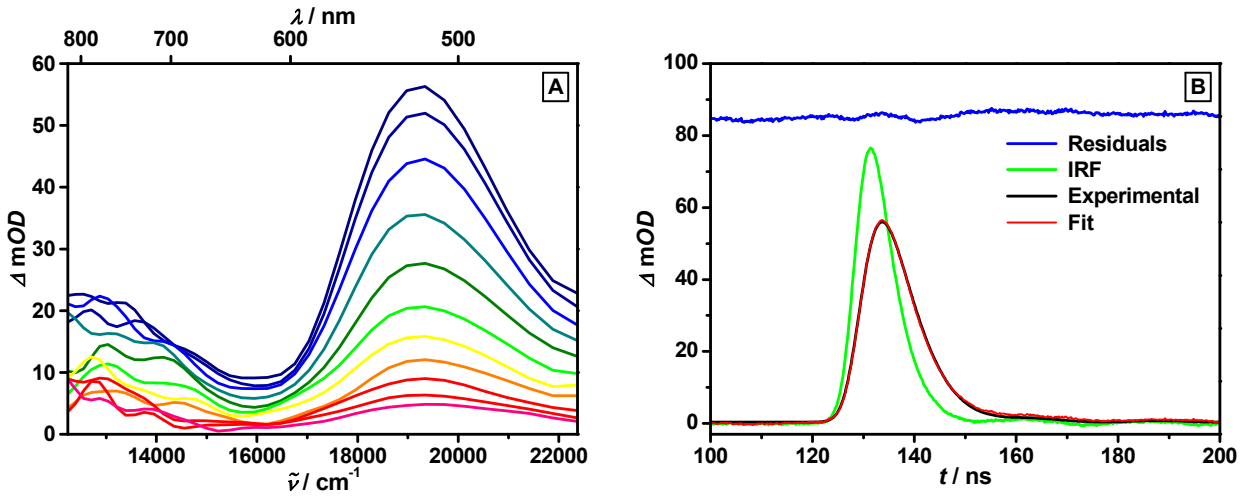

Figure 5.18: ns-transient absorption spectra of 5 in benzonitrile (excitation at 18800 cm^{-1}) (A). Early spectra are shown in blue/green, late ones in orange/red colours. Time decay at 19200 cm^{-1} (B).

For clarity, the results obtained from spectroelectrochemistry (CH_2Cl_2) will be displayed in Figure 5.19. Figure 5.19 A shows the first oxidation of D2 of **1** – **5**, as well as the first reduction of **1**. Figure 5.19 B, displays the superposition of the first oxidation and the corresponding reduction. Since the ns-transient absorption measurements only were performed for the visible range of the spectrum, Figure 5.19 C and D depict the visible range of the spectrum of **5** received from spectroelectrochemistry for a better comparison.

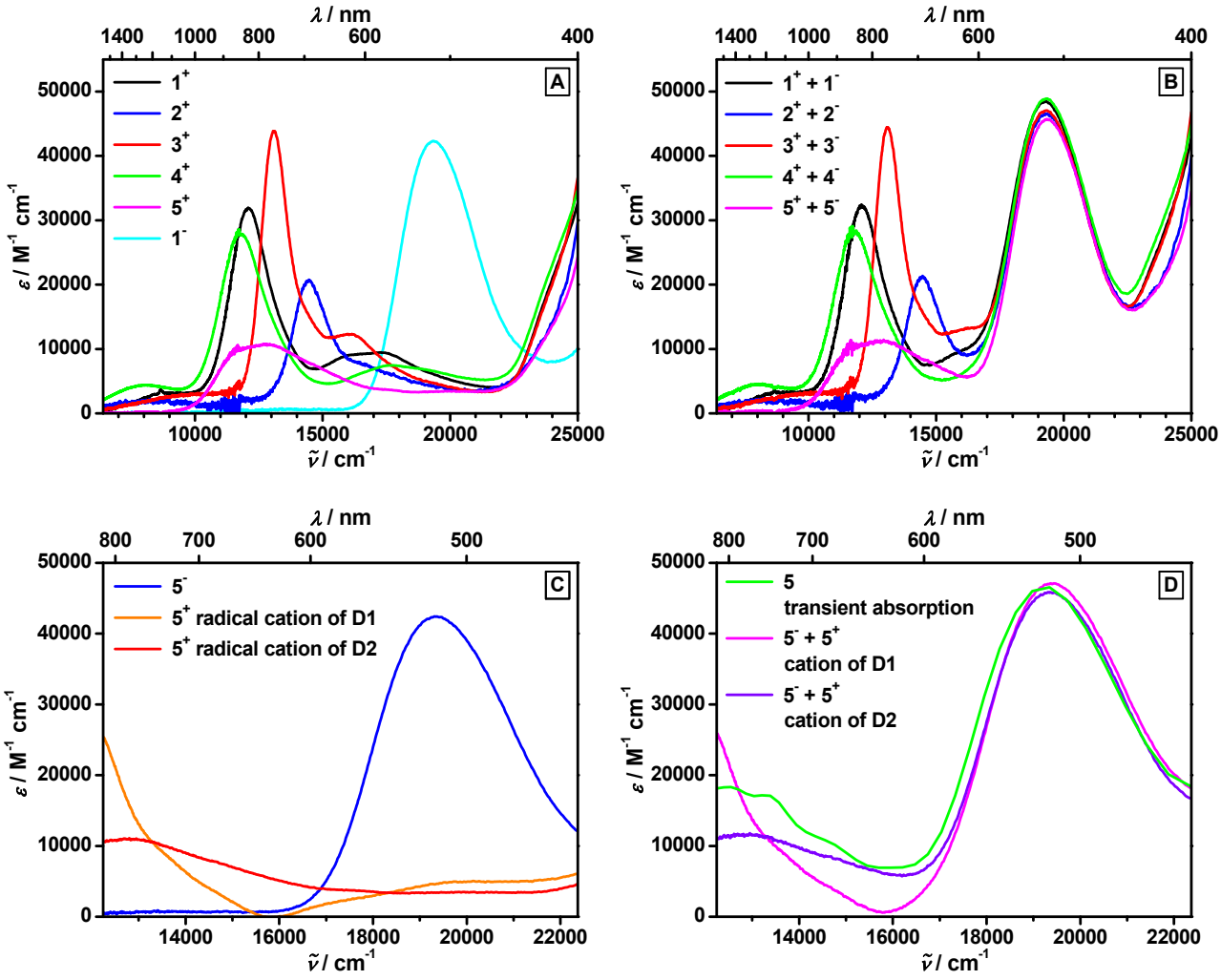

Figure 5.19: Spectra obtained by spectroelectrochemistry in CH_2Cl_2 (0.2 M $^nBu_4NPF_6$). First oxidation of 1 – 5 and reduction of 1 (A). Superposition of the first oxidation of 1 – 5 and the corresponding reduction (B). Spectra of 5^- (blue) and 5^+ in CH_2Cl_2, with the radical cation located either on D1 (orange) or D2 (red) (C).[1] Addition spectra of 5^- and 5^+ in CH_2Cl_2, with the radical cation located either on D1 (pink) or D2 (violet) as well as ns-transient absorption spectrum of 5 in benzonitrile (green) (D).

The ns-transient absorption spectrum shows one band at 19200 cm^{-1} and the high-energy tail of a second one at ~12500 cm^{-1}. Comparison with the data obtained by spectroelectrochemistry in CH_2Cl_2 allows an assignment of the band at 19200 cm^{-1} to the carbanion of the PCTM unit. The second band is expected to arise from a triarylamine cation located on either D1 or D2. The latter corresponds to the ^{2}CS state A^-–D1–D2$^{\bullet+}$ (see state diagram on p.73). In case of the ^{2}CT state, the cation is not entirely located on D1. For this reason, the exact signature of the ^{2}CT state is not known in detail. Hence, a comparison of the transient absorption spectra with the spectra of the radical cation located on D1 has to be regarded critically. The signal of the triarylamine radical cation exceeds the range of the detector, hindering a precise determination of the corresponding absorption maximum.

[1] The spectrum of **5^+**, where the radical cation is located on D1 was obtained by subtracting the spectra of **5^{2+}** from the spectra of **5^{3+}** (both spectra are depicted in Figure 5.15).

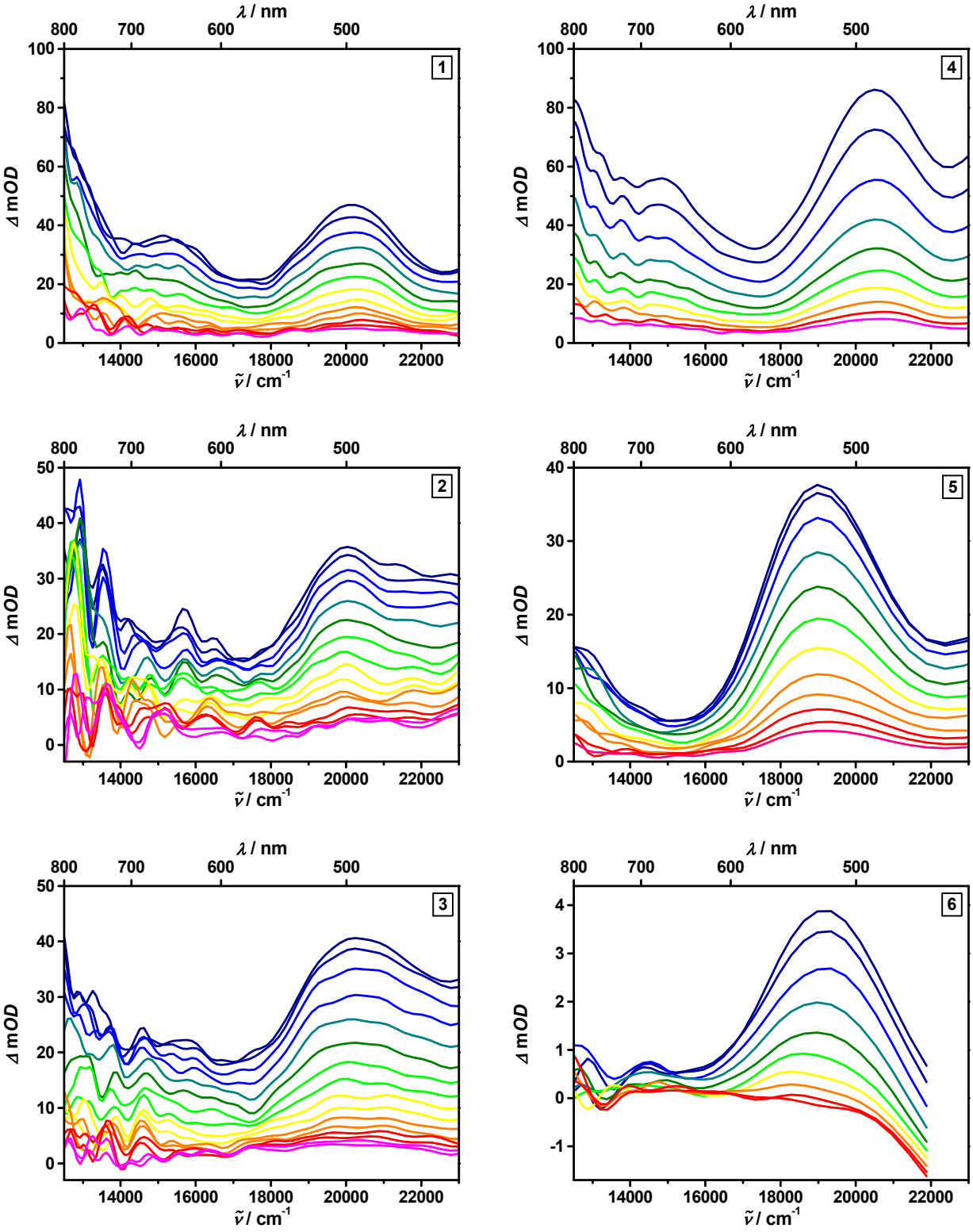

Figure 5.20: ns-transient absorption spectra of 1 – 6 (excitation at 18800 cm^{-1}). All measurements were performed in cyclohexane, except for 6 (toluene). Early spectra are shown in blue/green, late ones in orange/red colours.

For this reason, a clear allocation of the signal to one of the radical cations ($D1^{\bullet+}$ or $D2^{\bullet+}$) in **5** is impossible, since both show characteristic bands above 12500 cm^{-1}. Albeit, in Figure 5.18 D the transient absorption spectra (green) resembles the superposition of A^- and $D2^{\bullet+}$ (violet) instead of A^- and $D1^{\bullet+}$ (pink). This points to the formation of the ^{2}CS state, as already indicated by the results obtained from emission spectroscopy (see Chapter 5.3).

The results for compounds **1** – **5** obtained from the transient absorption spectroscopy measurements in cyclohexane are comparable to the results of **5** in benzonitrile. All spectra display the radical anion band of the PCTM moiety at 19000 cm^{-1} – 20500 cm^{-1}. The bands arising at ~12500 cm^{-1} exceed the range of the detector in all cases. As apparent from Figure 5.19, the results from spectroelectrochemistry and transient absorption in benzonitrile are in good agreement. This is not the case for the transient absorption spectroscopy in cyclohexane. The different polarity of cyclohexane and CH_2Cl_2[1] results in a shift of the absorption maxima, which further complicates a clear assignment of the triarylamine radical cation bands.

Measurements of **6** had to be performed in toluene (Figure 5.20), due to the poor solubility in cyclohexane. The transient absorption spectra show the PCTM anion band at 19200 cm^{-1}. The lack of any other band in the spectrum may be attributed to the following reasons. First, formation of the ^{2}CS state results in a cation where the charge is located on the ferrocene moiety. As already discussed in Chapter 5.4, the ferricenium cation possesses a small extinction coefficient and should therefore not exhibit any significant signature in the transient absorption spectrum. Second, as the chemical oxidation of **6** did not show distinct results, a shift of the cation band out of the detector range can also not be excluded.

Excited state lifetimes for compounds **1** – **6** were obtained by monoexponential fits of the decay kinetics at the maxima of the anion band of the PCTM unit. In case of the cation bands, decays were measured at ~12800 cm^{-1}.[2] The obtained values match those of the fits for the anion bands, which indicates that both signals belong to the same excited state. The excited state lifetimes of **1** – **4** resemble those derived from time-resolved emission spectroscopy. Furthermore, the results obtained for cascades **2** and **3** are alike those of reference **1**. Comparison of **1** and **4** with the reference compounds **FI** and **FJ** showed similar results of ~10 and ~20 ns, respectively. For these reasons, the signals observed in the ns-transient spectra of **1** – **4** can be attributed to the ^{2}CT state. In case of **5** and **6**, no reliable values were obtainable by deconvolution of the spectra, since the lifetimes were found to be to short (< 5 ns) compared to the instrument response. Albeit, the derived lifetimes are significantly smaller than the ones for **4**, which allows an exclusion of the ^{2}CT state for **5** and **6** in cyclohexane. In conclusion, this fact points to the presence of other nonradiative processes, such as the formation of the ^{2}CS state *via* hole transfer from D1 to D2.

[1] Addition of the supporting electrolyte $^n Bu_4NPF_6$ for spectroelectrochemical measurements further increases the polarity of CH_2Cl_2.
[2] Decay curves are depicted in the Appendix (Figure A.2).

Table 5.6: Fluorescence lifetime τ_{fl} and excited state lifetime τ of 1 – 4 in cyclohexane.

	τ_{fl}[a] / ns	τ[b] / ns			
1	10	11	(20000 cm^{-1})	11	(12500 cm^{-1})
2	5.9	8.1	(20000 cm^{-1})	7.2	(12800 cm^{-1})
3	6.7	8.0	(20800 cm^{-1})	8.4	(12800 cm^{-1})
4	19	20	(20400 cm^{-1})	22	(12800 cm^{-1})
FI[c]	13	11	(20400 cm^{-1})	9.5	(13500 cm^{-1})
FJ[c]	21	/		/	

[a] Derived from time-resolved emission spectroscopy (see Chapter 5.3)
[b] Derived from ns-transient absorption spectroscopy assuming monoexponential decay kinetics at the given wavenumber
[c] Results from [225] in cyclohexane

To reinforce this assumption, the overall free energy changes ΔG^0 of the intramolecular hole transfer processes in the cascades **2**, **3**, **5**, and **6** were estimated by means of equation (16).[41]

$$\Delta G^0_{(^2CT\rightarrow{}^2CS)} = \frac{N_A z e}{1000}\left(E_{ox}(D/D^+) - E_{red}(A/A^-)\right) - \frac{1}{1000}\frac{N_A e^2}{4\pi\varepsilon_0}\left[\left(\frac{1}{2r_D}+\frac{1}{2r_A}\right)\left(\frac{1}{\varepsilon_r}-\frac{1}{\varepsilon_s}\right)+\frac{1}{\varepsilon_s d_{DA}}\right] - \Delta G^{00}_{(S_1\leftarrow S_0)} \quad (16)$$

r_D[1], r_A[1] and d_{DA}[2] in meter are the radii of donor and acceptor and the centre-to-centre distance between them, respectively. N_A is Avogadro's constant, e the elementary charge, and z the transferred charge. The redox potentials in Volt of D and A were obtained from cyclic voltammetry (see Table 5.5 in Chapter 5.3). ΔG^{00} was determined from the onset of the absorption band in the corresponding solvent. ε_0 is the vacuum permittivity, ε_r is permittivity of the solvent used for cyclic voltammetry (CH_2Cl_2) and ε_s the permittivity of the solvent used for the transient absorption experiment. The calculated values for $\Delta G_{^2CT\rightarrow{}^2CS}$ (Table 5.7) clearly demonstrate that charge separation is an exergonic process for **2**, **3**, **5**, and **6** in benzonitrile. In case of **2**, the processes in the nonpolar solvents cyclohexane and toluene are endergonic and therefore unfavourable. Since the calculation of $\Delta G_{^2CT\rightarrow{}^2CS}$ using equation (16) is only a rough approximation, values derived for **3** and **6**, especially in toluene, lie in a range which makes it difficult to confirm or refute formation of the ^{2}CS state. A more detailed discussion about the

[1] Calculated from the corresponding *Connolly* molecular surfaces of the subunits from ChemBio3D 11.0.1, CambridgeSoft 2007.
[2] Derived from the geometry optimisation with the force field MM2 in ChemBio3D 11.0.1, CambridgeSoft 2007.

charge-separation process, including Marcus-behaviour and activation energies will be given in the following chapter (see p.98*ff*. and Table 5.8 on p.102)

Table 5.7: Free energy changes of the charge-separation process in cascades 2, 3, 5 and 6 derived from equation (16).

	$\Delta G_{^2CT \rightarrow ^2CS}$ / eV		
	cyclohexane	**toluene**	**benzonitrile**
2	0.30	0.25	–0.46
3	0.13	0.08	–0.65
5	–0.35	–0.37	–1.05
6	0.10	0.03	–0.82

5.5.2 fs-Transient Absorption Spectroscopy

In order to gain a better insight into the photophysical properties of compounds **1** – **6**, fs-transient absorption spectroscopy was performed. Measurements were carried out in the vis and NIR regime in toluene and benzonitrile. Excitation was accomplished at the maxima of the IVCT bands (13900 cm^{-1} – 15200 cm^{-1} in toluene and 14100 cm^{-1} – 15600 cm^{-1} in benzonitrile) to ensure population of the ^{2}CT state. Deconvolution of the transient absorption maps was attained by a global fitting routine to receive the evolution associated spectra (EAS) (see Chapter 7.1 for details), which are depicted in Figure 5.21 (toluene) and 5.22 (benzonitrile). For the measurements in toluene, global fitting routines were performed for the combination of the transient absorption maps in the vis and NIR range. Since this was not possible in case of **2**, **3**, and **6** in benzonitrile, the vis, and NIR range were fitted separately. Thus, the spectra will be depicted as separate figures. For the discussion, only lifetimes derived from the fitting of the vis range will be used.

All fs-transient absorption spectra of **1** – **6** in toluene and benzonitrile display the expected bands at 12000 cm^{-1} – 13000 cm^{-1} and 19000 cm^{-1} – 20000 cm^{-1}. The latter can be attributed to the PCTM anion, as already shown for the ns-transient absorption spectra, whereas the former belong to the triarylamine radical cations of either D1 or D2, respectively. This observation is in accordance with the results obtained by spectroelectrochemical measurements. Albeit, shifts of the absorption maxima may be ascribed to the fact, that the

measurements were performed in solvents with different polarity (CH_2Cl_2)[1], as already discussed in the preceding Chapter. In toluene, **1**, **2**, and **3** display additional bands at around 15000 cm^{-1}, which can also be ascribed to the radical cations of D1 or D2, respectively. A reliable assignment of the radical cation bands to the donors D1 or D2 is not possible, since the bands are located in the range of the fundamental wavenumber of the laser at 12500 cm^{-1}.

The EAS of the final state of reference compounds **1** (green) and **4** (blue) in toluene show the expected formation of the ^{2}CT state (see state diagram on p.73) (Figure 5.21). The fluorescence quantum yields for this compounds were found to be vanishingly low, thus, the radiative contribution to the deactivation process can be neglected according to equation (14). The non-radiative deactivation process for both compounds is located in the *Marcus*-inverted region ($-\Delta G^{00} > \lambda$, see Table 5.8 for details). Since ΔG^{00} was found to be larger in case of **4** (Table 5.8), the longer lifetime of **4** (840 ps) compared to **1** (310 ps) therefore is comprehensible. The first two species (black and red) of **1** and **4** show similar lifetimes. In case of **1**, an additional species (blue) is formed, resulting in a somewhat slower evolution of the ^{2}CT state.

Compared to **1**, compounds **2** and **3** show analogous EAS, with almost similar lifetimes. This observation substantiates the assumption from the emission and ns-transient absorption experiments that generation of the ^{2}CS state *via* hole transfer from D1 to D2 is not accessible in these compounds in toluene, which was also apparent from the values received from equation (16). The occurrence of several species during evolution of the ^{2}CT state possibly stems from the presence of different conformers. A somewhat different situation was found for compounds **5** and **6**. Regarding the PCTM anion band at ~20000 cm^{-1}, a bathochromic shift is observed for **5** and **6** in comparison to **4**. Furthermore, the maxima for this band are shifted among the spectra of the various species of **5** and **6**. The spectra of **5** display a broad radical cation band with medium intensity at ~12500 cm^{-1}, which can be attributed to the phenylene diamine cation in D2. No significant change in the size, shape, and position of this band is observable during evaluation of the final state.

In compound **6**, the triarylamine radical cation band ~12500 cm^{-1} vanishes during population of the final state, pointing to the formation of the ferricenium cation *via* hole transfer.[2] These observations confirm the presence of a ^{2}CS state in **5** and **6**, as already indicated by emission and ns-transient absorption spectroscopy. In the spectra of **6**, a stepwise population of the ^{2}CS can be observed, whereas the spectra of **5** do not show any signature of the ^{2}CT state. In addition, the lifetime of the ^{2}CS state (260 ps) in **5** and **6** (280 ps) are clearly shorter than the one of **4** (840 ps), which is rather unexpected, since both processes are located in the *Marcus*-inverted region. Further investigations are necessary to clear this observation.

[1] Addition of the supporting electrolyte $^n Bu_4NPF_6$ for spectroelectrochemical measurements further increases the polarity of CH_2Cl_2.

[2] As already mentioned in Chapter 5.4, the ferricenium cation has a low extinction coefficient and should therefore show almost no signature in the spectra.

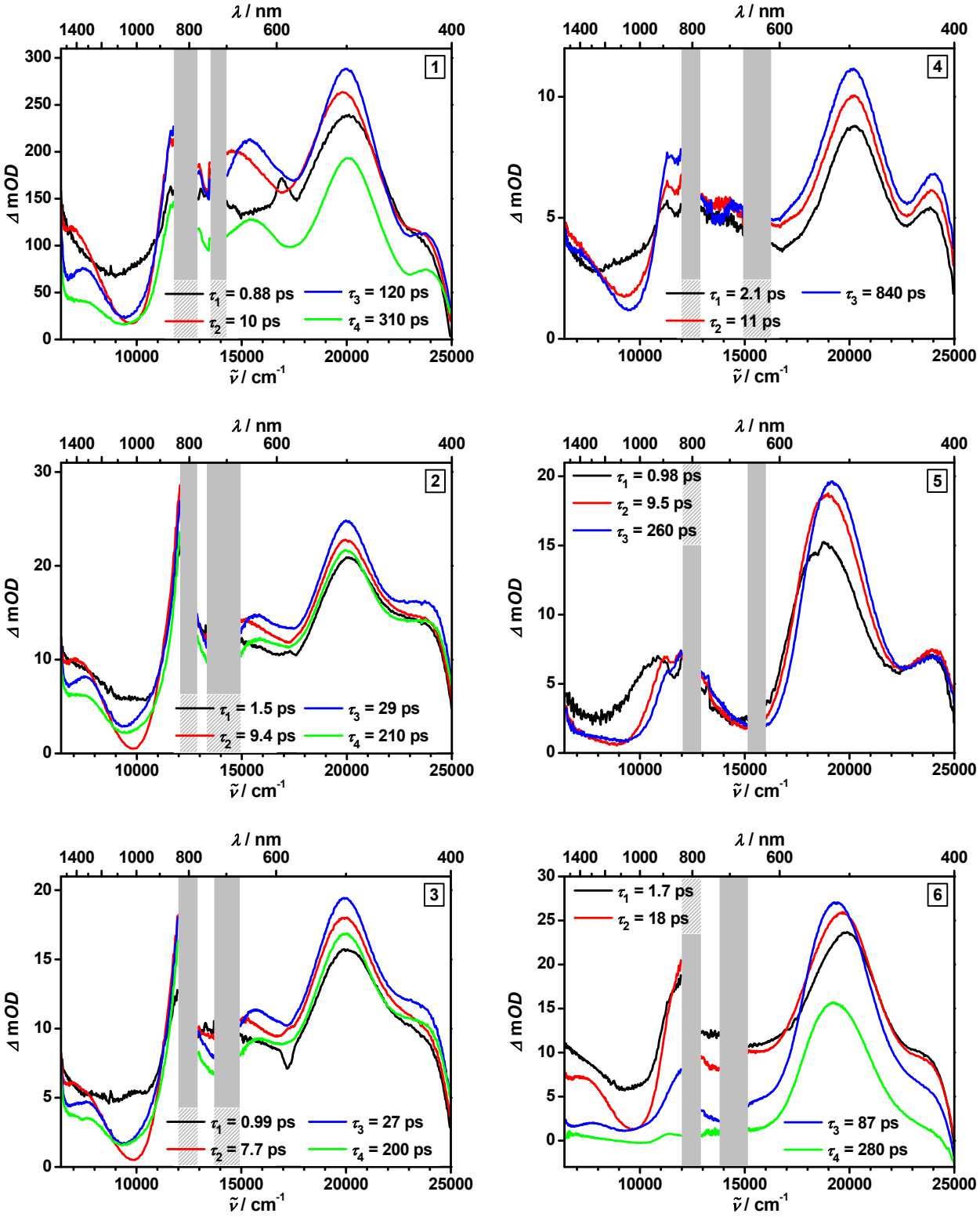

Figure 5.21: Evolution associated spectra of 1 – 6 in toluene.[1] Excitation was performed at the maxima of the IVCT bands in a range of 13900 cm^{-1} – 15200 cm^{-1}.

[1] The grey bars cover the sections of the central wavenumber of the laser at 12500 cm^{-1} and the corresponding excitation wavenumber.

One interesting feature in the EAS of compounds **1** – **4** is the occurrence of additional bands at 7000 – 8000 cm^{-1}. They are also present in the EAS of compound **6**, except for the final excited state (green). During population of the ^{2}CS state, these bands diminish simultaneously to the decrease of the radical cation band of the triarylamine. In the spectra of **5**, an appearance of these bands may only be visible in the first spectrum (black), but a clear statement is not possible in this case. For compounds **1** – **4**, a broadening of these bands and a shift to higher energies may be assumed. A possible explanation might be the fact, that during population of the ^{2}CT state, the dipole moment between A and D1 increases and simultaneously the geometry of the molecule changes. Assumption of a somehow stepwise process might give rise to different intermediate states and thus, to altering spectra. Comparable bands in the NIR range of the subpicosecond transient absorption spectra of compound **FA** (Figure 3.29) in CH_2Cl_2 were already reported by *Veciana et al.*.[216] The depicted spectra also show shifts of the absorption maxima in the vis and NIR range. The authors attributed the bands to the ^{2}CT state, but made no further statements concerning the different species that correspond to the single spectra.

The transient absorption spectra of **1** – **6** in benzonitrile are depicted in Figure 5.22. Compared to the measurements in toluene, the absorption maxima of the PCTM anion band of the final state in compounds **1** – **4** show a bathochromic shift. Additionally, the maxima for this band are again shifted among the spectra of the different species of **2**, **3**, **5**, and **6**. As already reported for the measurements in toluene, a clear assignment of the triarylamine radical cation bands to the donors D1 and D2 is once again not possible, for the same reasons already discussed above.

The final spectra of the reference compounds **1** and **4** (blue) can be attributed to the ^{2}CT state with lifetimes of 1.9 and 4.2 ps, respectively. Compared to toluene (310 and 840 ps), the lifetimes of the ^{2}CT of **1** and **4** are distinctly shorter, as expected for a process located in the *Marcus*-inverted region (Table 5.8). In case of **2** and **3**, the spectra of the first species (black and red) are associated with the ^{2}CT state with lifetimes similar to those of **1**. The final spectra (blue) of both compounds are allocated to the ^{2}CS state, with lifetimes of 9.2 and 6.8 ps, respectively. The free energy changes estimated from equation (16) (Table 5.7) show the charge-separation process to be exergonic for **2** and **3** in benzonitrile, thus substantiating the formation of the ^{2}CS state.

A population of the ^{2}CS state is also expected for compounds **5** and **6**. The red spectrum within the EAS of compound **5** shows a similar lifetime (4.3 ps) compared to the final state in **4** (4.2 ps) and may possibly represent the ^{2}CT state. The final ^{2}CS state of **5** shows a distinct prolongation of the lifetime from 260 ps in toluene up to 3.0 ns in benzonitrile. This can be explained by the fact, that the charge-recombination process in **5** in benzonitrile is located in the *Marcus*-normal region ($\Delta G^{00} < \lambda$) in contrast to toluene (Table 5.8).

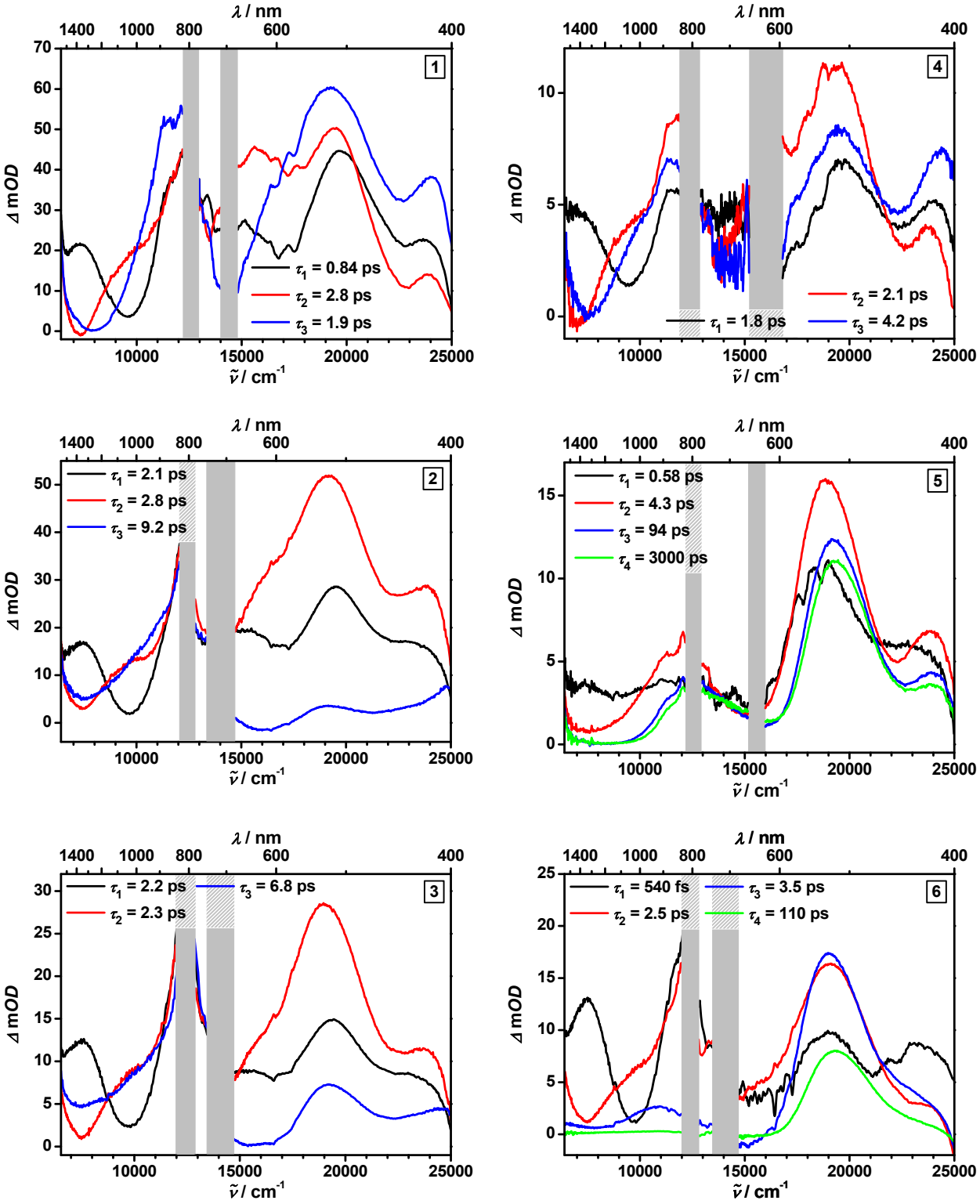

Figure 5.22: Evolution associated spectra of 1 – 6 in benzonitrile.[1] Excitation was performed at the maxima of the IVCT bands in a range of 14100 cm^{-1} – 15600 cm^{-1}.

[1] The grey bars cover the sections of the central wavenumber of the laser at 12500 cm^{-1} and the corresponding excitation wavenumber.

The EAS of **6** show a decay of the triarylamine cation band, as already observed for the spectra in toluene, which proves the formation of the ^{2}CS state. In toluene, the charge-recombination process is located in the *Marcus*-inverted region, whereas it was found to be in the *Marcus*-normal region in benzonitrile. Albeit, the lifetime of this state is shorter in benzonitrile (110 ps) than in toluene (280 ps). It points to the fact that the kinetics of this process may mainly be influenced by the electronic coupling V_{el}. The lifetime of the ^{2}CS in **5** (3.0 ns) exceeds the one in **6** (110 ps), as expected since both charge recombination processes are in the *Marcus*-normal region. The redox potential of D2 in **5** (–20 mV) is distinctly smaller than in **6** (200 mV). Hence, the smaller $\Delta G_{^2\mathrm{CT}\rightarrow{}^2\mathrm{CS}}$ for the charge recombination results in an increase of the corresponding lifetime.

The spectra of **1** – **6** all show additional bands in the NIR range (~7500 cm^{-1}), comparable to the experiments in toluene. The shift of this band to higher energies during evolution of the final state is distinctly stronger than in toluene. Albeit such bands are also present in the spectra obtained from spectroelectrochemical measurements a comparison with the results from the fs-transient absorption is difficult, due to the fact that the measurements were performed in a solvent with a different polarity (CH_2Cl_2). For this reason, the question about the origin of this bands cannot be settled at the moment.

The free energy of the charge transfer ΔG^{00} and the energy of the charge separated state $\Delta G_{^2\mathrm{CS}\rightarrow\mathrm{D}_0}$ as well as the activation barrier for the charge recombination ΔG^* are summarised in Table 5.8. ΔG^{00} was obtained from extrapolation of the low-energy flank of the IVCT band in the absorption spectra.[357] $\Delta G_{^2\mathrm{CS}\rightarrow\mathrm{D}_0}$ was estimated with equation (16) in Chapter 5.5.1. ΔG^* and the outer reorganisation energy λ_o were calculated with equation (2) and (5) in Chapter 2. The inner reorganisation energy λ_i for the charge-recombination process was estimated by the values of λ_i for the self-exchange of triphenylamine (0.12 eV)[358], ferrocene (0.03 eV)[359] and the PCTM radical (0.22 eV)[1]. In case of the reference compounds **1** and **4**, results for λ_i obtained from *Jortner*-fits of the emission bands were used. The results received for the activation barrier of the charge recombination ΔG^* are not directly related with the lifetimes obtained for compounds **1** – **6**.

Albeit the barrier is distinctly higher for **5** and **6** in toluene than in benzonitrile, the lifetimes are found to be shorter in both cases in toluene. Thus, the kinetics of this process may mainly be influenced by the electronic coupling V_{el}. To illustrate the results discussed above, free energy diagrams for **2**, **3**, **5**, and **6** are depicted in Scheme 5.29. In addition, Figure 5.23 shows the combined transient absorption spectra of **2**, **3**, **5**, and **6** obtained from the measurements in the ns-regime and the EAS from the measurements in the fs-regime.

[1] Calculated in our group with DFT using the UB3LYP functional and the 6-31+G* basis set.

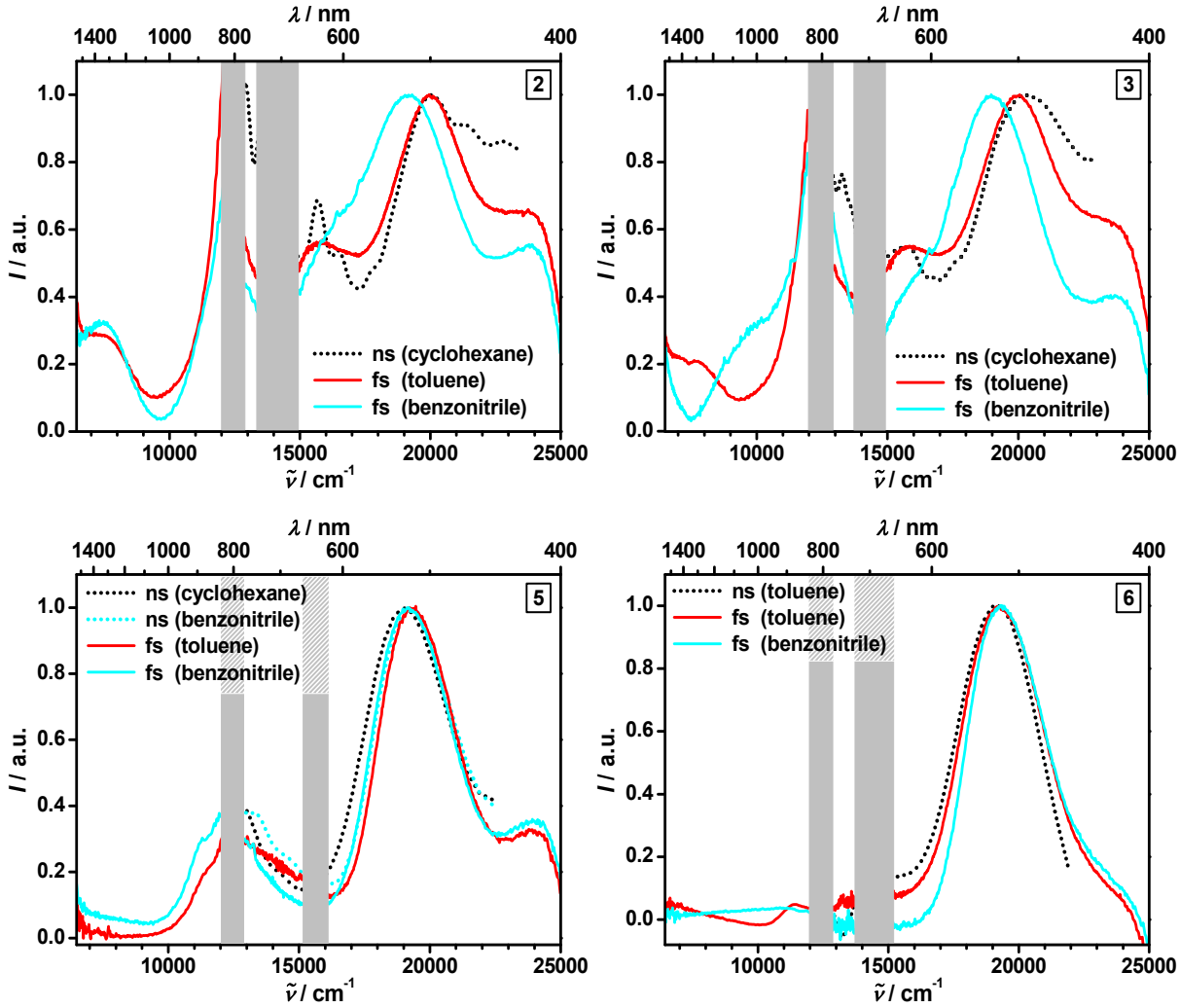

Figure 5.23: ns-transient absorption spectra and evolution associated spectra of 2, 3, 5, and 6 in different solvents.[1]

For compound **2** and **3**, the ns-spectrum in cyclohexane and the EAS in toluene are comparable, belonging both to the ^{2}CT state. A hole transfer from D1 to D2 in both solvents is improbable, because the charge-separation process is expected to be endergonic for both compounds. The EAS in benzonitrile clearly differ from the ones in cyclohexane/toluene, thus showing the signature of the ^{2}CS state. In case of compound **5** and **6** almost identical results were obtained in all solvents, indicating the spectra to represent the same state (^{2}CS). In case of **6**, the free energy changes obtained from equation (16) indicate a slightly endergonic charge-separation process in toluene. Nevertheless, formation of the ^{2}CS state was observed in both solvents used in the fs-transient absorption experiments. This fact clearly demonstrates that equation (16) only provides a rough approximation for the free energy changes.

[1] The grey bars cover the sections of the central wavenumber of the laser at 12500 cm^{-1} and the corresponding excitation wavenumber.

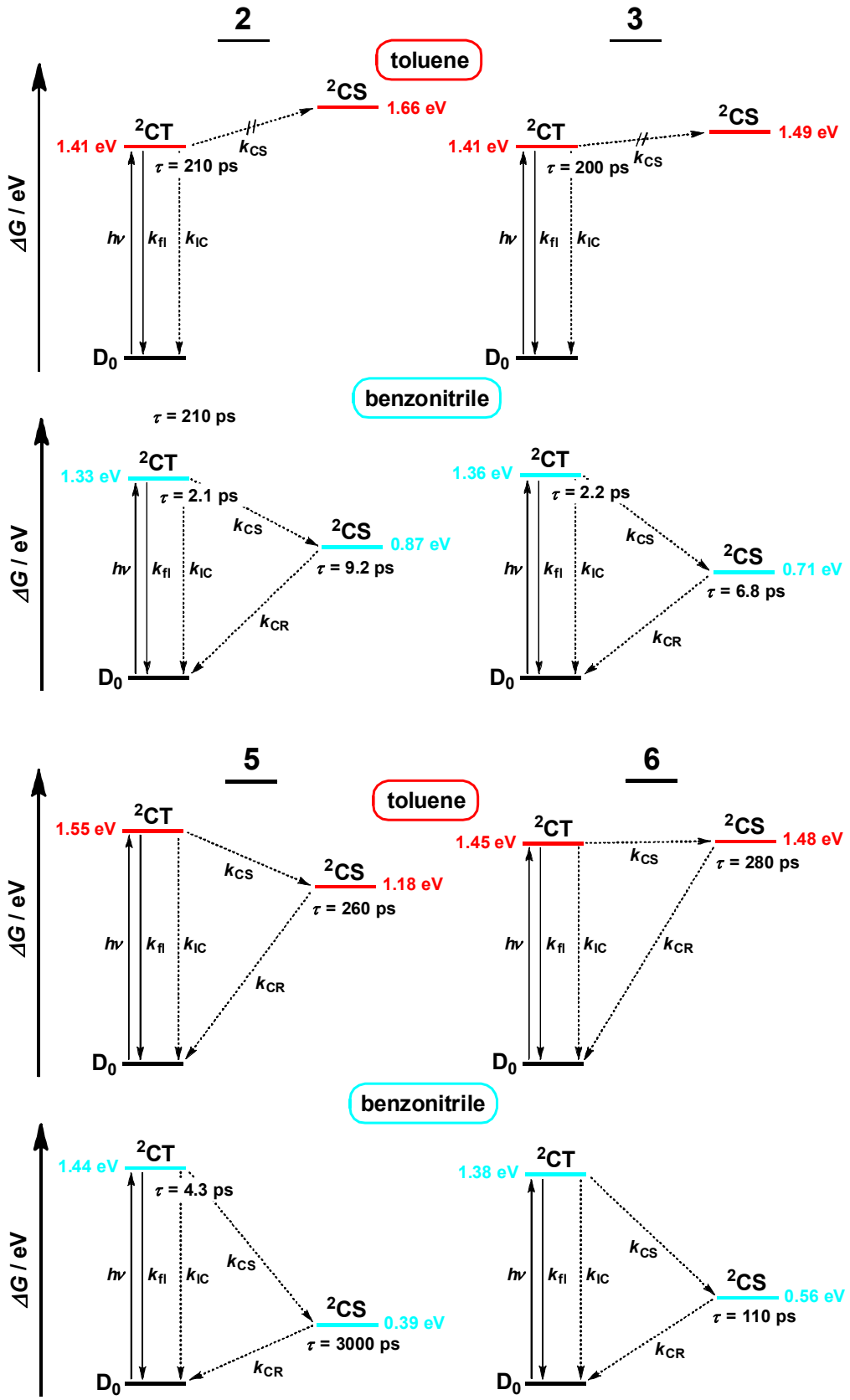

Scheme 5.29: State diagram for 3 (left) and 5 (right) in toluene (red) and benzonitrile (light blue) with the corresponding rate constants. fl: fluorescence IC: internal conversion CS: charge separation CR: charge recombination. The ^{2}CT states of 5 (toluene) and 6 (toluene and benzonitrile) is not assignable to certain spectra. Lifetimes are therefore not depicted.

To sum up, the desired charge-separation process was achieved for the cascades **2**, **3**, **5**, and **6** in benzonitrile and for **5** and **6** in toluene. Remarkably, in toluene, the ^{2}CS state in **5** and **6** shows a shorter lifetime than the ^{2}CT state of reference compound **4**. In general, charge-recombination processes were found to be located in the ps-time regime, except for **5**, which shows a lifetime of 3.0 ns in benzonitrile. An explanation for the high recombination rates was not attainable from the results received by transient absorption spectroscopy and the calculation of free energies and activation barriers. Albeit, it was shown that charge recombination is located in the *Marcus*-normal region for all cascades in benzonitrile and in the *Marcus*-inverted region in toluene. The fast recombination rates in both solvents point to the fact that *Marcus*-inverted region effects play a negligible role for the investigated compounds. The possible overestimation of those effects was already discussed by several authors,[20,22,28] which in some cases ascribe the existence of long-lived charge separation states to spin-correlation effects. Since all herein observed states are expected to be doublet states, an intersystem crossing between singlet and triplet states can be ruled out. Hence, charge recombination is not spin-forbidden in these cases, which might explain the fast rates for this process. Therefore, the charge-transfer dynamics may mainly be influenced by the electronic coupling V_{el}.

Table 5.8: Free energy of the charge transfer ΔG^{00} and charge separated states $\Delta G_{^2CS \rightarrow D_0}$, activation barrier for the charge recombination ΔG^* and reorganisation energies λ_i, λ_o and λ for cascades 1 – 6 in toluene and benzonitrile. All values are given in eV.

	λ_i / eV	λ_o[a] / eV	λ[b] / eV	ΔG^{00}[c] / eV	$\Delta G_{^2CS \rightarrow D_0}$[d] / eV	ΔG^*[e] / eV
			toluene			
1	0.06	0.04	0.10	1.44	/	/
2	0.17	0.07	0.24	1.41	1.66	2.10
3	0.17	0.07	0.24	1.41	1.49	1.63
4	0.07	0.04	0.11	1.59	/	/
5	0.17	0.07	0.24	1.55	1.18	0.92
6	0.13	0.08	0.21	1.45	1.48	1.92
			benzonitrile			
1	0.06	0.53	0.59	1.36	/	/
2	0.17	0.82	0.99	1.33	0.87	0.00
3	0.17	0.81	0.98	1.36	0.71	0.02
4	0.07	0.53	0.60	1.46	/	/
5	0.17	0.81	0.98	1.44	0.39	0.09
6	0.13	0.94	1.07	1.38	0.56	0.06

[a]Calculated from the *Born*-equation (5)
[b]$\lambda = \lambda_o + \lambda_i$
[c]Derived from extrapolation of the low-energy flank of the IVCT band in the absorption spectra
[d]Estimated from equation (16)
[e]Calculated from the *Marcus*-equation (2)

Table 5.9: Rate constants *k* and lifetimes *τ* derived from the EAS for 1 – 6 in toluene and benzonitrile.

	k / 10^{10} s^{-1} (τ / ps)			
	vis / NIR	**vis / NIR**	**vis**	**NIR**
	toluene		**benzonitrile**	
1	114 (0.88)	119 (0.84)		
	10 (10)	36 (2.8)		
	0.83 (120)	53 (1.9)		
	0.32 (310)			
2	67 (1.5)		48 (2.1)	135 (0.74)
	11 (9.4)		36 (2.8)	71 (1.4)
	3.4 (29)		11 (9.2)	29 (3.5)
	0.48 (210)			
3	101 (0.99)		46 (2.2)	128 (0.78)
	13 (7.7)		44 (2.3)	63 (1.6)
	3.7 (27)		15 (6.8)	37 (2.7)
	0.50 (200)			
4	48 (2.1)	56 (1.8)		
	9.1 (11)	48 (2.1)		
	0.12 (840)	24 (4.2)		
5	102 (0.98)	172 (0.58)		
	11 (9.5)	23 (4.3)		
	0.38 (260)	1.1 (94)		
		0.033 (3000)		
6	59 (1.7)		185 (0.54)	175 (0.57)
	5.6 (18)		40 (2.5)	39 (2.6)
	1.2 (87)		29 (3.5)	33 (3.0)
	0.36 (280)		0.91 (110)	1.0 (100)

5.6 Electron Spin Resonance Spectroscopy

X-band electron spin resonance (ESR) measurements of compounds **1**, **3**, and **6** were performed in toluene at RT. Figure 5.24 shows the experimental and simulated spectra of **1**.

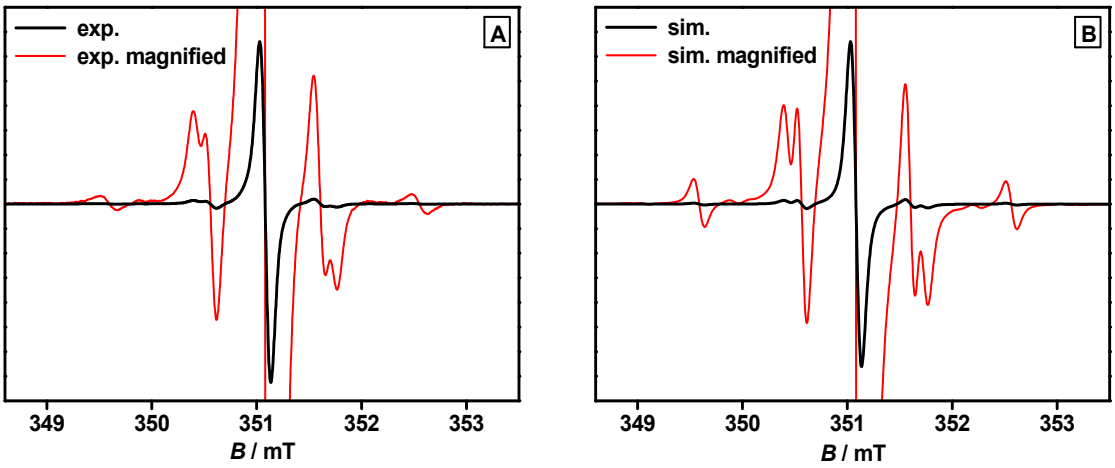

Figure 5.24: Experimental (A) and simulated (B) ESR spectra of 1 in toluene at RT. Red lines show the enlarged spectra.

All spectra showed one single main line as expected. Several weak satellite lines corresponding to hyperfine interactions of the unpaired electron with the ^{13}C (I = 1/2) nuclei also were observed. The three different line pairs can be ascribed to the *α*, *ipso* and *ortho* carbon atoms. Linebroadening probably results from unresolved couplings with the chlorine isotopes ^{35}Cl (I = 3/2) and ^{37}Cl (I = 3/2).[109] Table 5.10 provides an overview of the values of **1**, **3**, and **6**, which are representative for all other compounds.

Table 5.10: ESR data obtained for 1, 3, and 6 in toluene at RT.

	α_{C_α} / mT	α_{C_ipso} / mT	α_{C_ortho} / mT	g[a]
1	3.03	1.28	1.05	2.0066
3	2.99	1.31	1.03	2.0066
6	2.97	1.28	1.04	2.0066

[a]Not referenced.

The values of the obtained hyperfine coupling constants *α* are typical for this kind of perchlorotriphenylmethyl radicals.[360] In general, the *g*-factor is determined against DDPH[1] as a standard (*g*: 2.0030).[361] Based on the low information content of this property, reference

[1] 2,2-Diphenyl-1-picrylhydrazyl

measurements were not performed. *g*-factor values are only given for comparison of the results. The obtained results clearly prove that the desired radicals were successfully synthesised.

6 Summary

In this work, a series of redox cascades **2**, **3**, **5**, and **6** was synthesised and investigated in view of their photophysical and electrochemical properties. Most of the cascades are based on a perchlorinated triphenylmethyl radical acceptor (A) and two triarylamine donors (D1 and D2). Additionally, a cascade with one triarylamine (D1) and one ferrocene (D2) donor, as well as two reference compounds **1** and **4**, with the same PCTM acceptor and one triarylamine donor D1 were synthesised. The easily attainable tunability of the redox potentials of the triarylamines by changing the substituents in *p*-position of the phenyl rings provided the possibility to generate a directed redox gradient within the cascades. Connection of the PCTM acceptor A and the adjacent triarylamine donor D1 was achieved by implementation of a biphenyl spacer *via* Pd-catalysed cross coupling reaction. The almost perpendicular orientation of the biphenyl moiety guarantees a small electronic coupling between A and D1. In the cascades **2**, **3**, **5**, and **6** linkage of the donor moieties D1 and D2 was realised by a 1,2,3-triazole bridge, synthesised by means of click chemistry. The PCTM radical acceptor unit was generated in the last step of the synthesis *via* radicalisation of the corresponding *α*-H precursors. Since this step was not successful in the first attempts, the reaction was optimised in view of reactants, solvents, and reaction conditions, to result in a quantitative radicalisation process.

Absorption spectra of **1** – **6** showed the combined characteristic features of the triarylamines and the PCTM radical. Besides, the presence of IVCT bands in the NIR range of the spectra pointed to the population of a charge-transfer state (^{2}CT) between A and D1. The IVCT bands showed a weak and non-systematic dependence on the solvent polarity. A weak to moderate emission in the NIR range of the spectra was observable for all compounds in cyclohexane. Reliable measurements in more polar solvents were not possible, due to the much weaker and strongly red-shifted emission. In case of **5** and **6**, the fluorescence was quenched by an additional hole transfer process from D1 to D2, resulting in a charge separated state (^{2}CS). The correct direction of the redox gradient in the cascades **2**, **3**, **5**, and **6** was confirmed by cyclic voltammetry. Spectroelectrochemical measurements were used to investigate the characteristic spectral features of the oxidised and reduced species of all compounds.

The results obtained from spectroelectrochemistry were required for an interpretation of the transient absorption spectra, which were performed in the ns- and fs-time regime. Measurements in the ns-regime were performed in the visible range of the spectrum. In case of the fs-transient absorption spectra, measurements in the visible and NIR range were carried out. Evolution associated spectra were obtained by a global target analysis of the transient absorption maps. Albeit, an exact association of the particular EAS to specific states was not possible in any case. Nevertheless, the transient absorption spectra revealed that the desired hole transfer in the cascades from D1 to D2 strongly depends on the solvent polarity and the

size of redox gradient. In highly polar solvents (benzonitrile), formation of the ^{2}CS state was observable for all cascades **2**, **3**, **5**, and **6**. This is contrary to solvents with low polarity (cyclohexane, toluene), where population of the ^{2}CS state only was detected in case of cascades **5** and **6**, which possess a high redox gradient between D1 and D2 (> 480 mV). Charge-separation processes for compounds **1** – **6** were found to take place in the fs- to ps-time regime. Charge recombination occurred within picoseconds except for compound **5**, which showed a lifetime of 3.0 ns in benzonitrile. The fast recombination rates show that neither *Marcus*-inverted region effects nor spin correlation play an important role for the charge-transfer dynamics of the herein investigated compounds. For this reason, the dynamics are expected to depend mainly on the electronic coupling V_{el}.

7 Experimental Section

7.1 Analytical Methods

NMR Spectroscopy

- Bruker Avance 400 FT-Spectrometer (^{1}H: 400.1 MHz, ^{13}C: 100.6 MHz)
- Bruker Avance DMX 600 FT-Spectrometer (^{1}H: 600.1 MHz, ^{13}C: 150.9 MHz)

All ^{1}H- and ^{13}C-NMR spectra were recorded at 300 K. The signal of the respective solvent was used as the internal reference and the chemical shifts are given in ppm (δ-scale) *vs*. TMS. Multiplicities were denoted as: s (singlet), sb (broad singlet), d (doublet), dd (doublet of doublets), t (triplet), sept (septet), m (multiplet). Coupling constants are given in Hertz (Hz). NMR spectroscopy data is quoted as follows: chemical shift (multiplicity, coupling constant, number of protons). Solvents for ^{13}C-NMR spectra were degassed for at least 30 min with argon before each measurement.

In compounds including a PCTM moiety the rotation in the biphenyl spacer is inhibited. ^{1}H-NMR spectra therefore display no AA'/BB' pattern for the protons of the phenyl ring directly attached to the PCTM unit. For the same reason, ^{13}C-NMR spectra display separated signals for the tertiary carbon signals of the same phenyl ring. Signals in the ^{1}H-NMR spectra are often superposed with signals from other protons and are therefore not distinguishable in most cases. In case of the ^{13}C-NMR spectra the resulting signal splitting will be denoted in particular for the corresponding compounds.

For the radicals, only mass spectra will be given, except for compounds **2** and **3**.

Mass Spectroscopy

- Bruker Daltonics microTOF focus (ESI)
- Agilent ion source (G1947-60101) (APCI)
- Bruker Daltonics autoflex II (MALDI)

For ESI and APCI spectra, 10 μM solutions of the respective sample were prepared. MALDI spectra were measured in a DCTB matrix.[1] For calculation of the respective mass values of the isotopic distribution, the software module “Bruker Daltonics IsotopePattern” from the software Compass 1.1 from Bruker Daltonics GmbH, Bremen was used. Due to the isotopic

[1] 2-[(2E)-3-(4-tert-butylphenyl)-2-methylprop-2-enylidene]malononitrile

distribution over a broad m/z region caused by ^{35}Cl (I =3/2) and ^{37}Cl (I =3/2), the signal of monoisotopic signals was too small in intensity for an accurate measurement. In this case, typically the most intense signal (X+n) of the distribution was taken and compared with the respective calculated value.

Melting Points

- Reichert Thermovar HT1 B11

  All melting points are not corrected.

Electron Spin Resonance Spectroscopy

- Bruker ELEXSYS E580 CW/FT EPR spectrometer (software EasySpin v. 4.0.0, MATLAB® v.8.0)

ESR measurements at X-band (9.8 GHz) were carried out at RT in Wilmad® quartz (CFQ) ESR tubes (OD: 3.8 mm, L: 241 mm; SIGMA-ALDRICH). All measurements were performed in toluene, which was of spectroscopic grade and was used as received. The concentration of the solutions was about 10^{-4} – 10^{-3} M. All solutions were degassed with argon for at least 30 min before each measurement. Continuous wave (CW) ESR spectra were recorded using 1 mW microwave power and 0.1 G field modulation at 100 kHz.

Recycling Gel Permeation Chromatography

- Shimadzu Gel Permeation Chromatography System
  - card type system controller (CBM-20Alite)
  - high precision solvent delivery unit (LC-20AD)
  - 3-way online degassing unit (DGU-20A3)
  - high pressure flow channel selection valve (FCV-20AH2)
  - photodiode array detector 190 – 800 nm (SPD-M20A)
  - fraction collector (FRC-10A)
  - software LCsolution (v. 1.0.0.1)

- JASCO Gel Permeation Chromatography System
  - interface box (LC-NetII ADC)
  - intelligent HPLC pump (PU-2080 plus)
  - inline degasser (DG-2080-53)
  - solvent selection valve unit (LV-2080-03)
  - multi wavelength UV/vis detector 200 – 600 nm (UV-2077)
  - fraction collector (CHF122SC) with software FraColl (v. 3.0.2)
  - software Chrompass (v. 1.8)

All experiments were performed using three PSS columns (SVD / 10μ / 200 × 600 mm / 50 Å, 100 Å, 500 Å) with THF (Sigma Aldrich, HPLC grade) or $CHCl_3$ (Sigma Aldrich, HPLC grade) as eluent at 295 K with a flow rate of 4 ml/min.

Cyclic Voltammetry

- Electrochemical Workstation BAS CV-50W including corresponding software (v. 2.31)

Cyclic voltammograms were measured under an argon atmosphere (argon dried with Sicapent® from Merck, oxygen was removed by copper oxide catalyst R3-11 from BASF) in dry and oxygen free solvents with 0.2 M $^{n}Bu_4NPF_6$ as supporting electrolyte. The concentration of the solute was about 0.5 mM. A conventional three-electrode setup consisting of a platinum disc working-electrode (Ø 2 mm), a Ag/AgCl pseudoreference electrode and a platinum wire counter electrode was used. The redox potentials were referenced against the ferrocene/ferricenium redox couple as an internal standard. For measurements under thin-layer conditions, the working electrode was placed onto a mobile glass hemisphere.

UV/Vis/NIR Spectroscopy

- JASCO V-670 UV/Vis/NIR spectrometer (software SpectraManager v. 2.8.4.1)
- Agilent Technologies Cary UV-Vis-NIR spectrophotometer (software Agilent Cary WinUV Analysis and Bio v.4.2)

All solvents were of spectroscopic grade and were used without further purification. Absorption spectra were recorded in 1 cm quartz cuvettes (Helma) at RT. The concentration of the solution was about 10^{-5} M.

Spectroelectrochemistry

- JASCO V-670 UV/Vis/NIR spectrometer (software SpectraManager v. 2.8.4.1)
- Princeton Applied Research potentiostat/galvanostat model 283

All experiments were performed in reflection mode at a platinum disc electrode (Ø 6 mm) through a cylindrical quartz vessel. A Ag/AgCl electrode served as the pseudoreference electrode and a gold/nickel cover metal plate (V2A) as the counter electrode. The optical path length between the bottom of the quartz cell and the working electrode (100 μm) was adjusted by a micrometer screw. The potential was varied in steps of 20 – 100 mV. Solvents and electrolytes were the same as used for CV measurements and the experiments were performed under argon atmosphere.

Steady-State Fluorescence Spectroscopy / Time-Dependent Fluorescence-Decay / Excitation Spectroscopy

- Photon Technology International QuantaMaster™ model QM-2000-4 including a cooled photomultiplier (R928P), an InGaAs detector and a xenon short-arc lamp (75 W, Ushio UXL-75XE), (software FeliX32™ v. 1.2.0.56)
- Photon Technology International TimeMaster™ TM-200 LED strobe lifetime spectrofluorometer including a Photon Technology International nanosecond laser diode with a central emission wavelength of 650 nm and a pulse width of < 1.5 ns

All fluorescence spectra where recorded in 1 cm quartz cells (Starna) at RT. The concentration was ca. 10^{-5} – 10^{-6} M. All solvents were of spectroscopic grade and were used as received. All solutions were degassed with argon for at least 30 min before each measurement. Fluorescence quantum yields were determined by equation (17), where I_{fl}, OD and n denote the integral of the area below the emission band, the optical density of the solution at the excitation wavelength and the refractive index of the solvent, respectively. Oxazine 1 perchlorate (Acros) in EtOH was used as fluorescence standard (Φ_{ref}: 0.15)[346-348].

$$\Phi_{fl} = \Phi_{ref} \frac{\int I_{fl}(\tilde{\nu})\, OD_{ref}\, n^2}{\int I(\tilde{\nu})_{ref}\, OD\, n_{ref}^2} \qquad (17)$$

For time-dependent fluorescence decay measurements, Ludox® AS-30 colloidal silica in deionised water was used as a scatterer to determine the instrument response of the laser

diode. Deconvolution of the fluorescence decay curves was performed with the corresponding spectrometer software using the signal of the laser diode. The fluorescence decay curves were monoexponentially fitted in the ns-regime in order to obtain the relating fluorescence lifetimes.

ns-Transient Absorption Spectroscopy

- Edinburgh LP 920 laser flash spectrometer with a 450 W ozone-free Xe arc lamp including a photomultiplier (Hamamatsu R955), digital storage oscilloscope (Tektronix TD3012B) and software (L900 v. 6.5.6.3)
- Continuum Minilite II Nd:YAG laser operating at 10 Hz, 3-5 ns pulse duration, pulse energy 25 mJ at 532 nm

All measurements were carried out in 1 cm quartz cells (Starna) at RT with an optical density between 0.2 – 0.4 at the excitation energy. All solvents were of spectroscopic grade and used as received. All solutions were degassed with argon for at least 30 min before each measurement. Samples were excited at 18800 cm^{-1} (532 nm).

fs-Transient Absorption Spectroscopy

- Newport-Spectra-Physics Solstice one box ultrafast Ti:Sapphire amplifier with a central wavenumber of 12500 cm^{-1} (800 nm), a pulse length of 100 fs and a repetition rate of 1 kHz
- Newport-Spectra-Physics TOPAS-C optical parametric amplifier as the source for the pump pulse with a pulse length of 140 fs
- Ultrafast Systems Helios transient absorption spectrometer with a CMOS sensor (1.5 nm intrinsic resolution, 350 – 800 nm sensitivity range) and an InGaAs sensor (3.5 nm intrinsic resolution, 800 – 1600 nm sensitivity range)

All pump-probe experiments were performed in 2 mm quartz cells (Spectrocell Inc.) equipped with a magnetic stirrer. Solvents were of spectroscopic grade and used as received. All solutions were degassed with argon for at least 30 min before each measurement. Measurements were carried out with an optical density between 0.06 – 0.12 at the excitation energy at RT.

The output beam received from the Solstice was split into two parts, of which one was used to pump the optical parametric amplifier (TOPAS-C) as the source for the pump pulse with a pulse length of 140 fs, a wavenumber of 15400 cm^{-1} (650 nm) as well as 14300 cm^{-1} (700 nm) and an attenuated energy of 250 nJ. The second, rather small fraction of the output

beam was focused on a moving CaF_2-plate to produce a white light continuum between 12050 cm^{-1} (830 nm) and 28570 cm^{-1} (350 nm) which acted as the probe pulse. The depolarised excitation pulse was collimated to a spot, which was at least two times larger than the diameter of the spatially overlapping linear polarised probe pulse.

Detection of the probe pulses was accomplished with a CMOS sensor for UV/Vis-, respectively an InGaAs sensor for NIR-measurements. A mechanical chopper, working at 500 Hz, blocked every second pulse, in order to measure I and I_0, thus enabling low noise-to-shot-measurements. The photoinduced change in optical density can directly be recorded by comparing the transmitted spectral intensity of consecutive pulses [$I(\lambda, \tau)$, $I_0(\lambda)$]:

$$\Delta OD = -\log\left[\frac{I(\lambda,\tau)}{I_0(\lambda)}\right] \tag{18}$$

The relative temporal delay between pump and probe pulses was varied over a maximum range of 8 ns with a motorised, computer-controlled linear stage. For small delay times, the delay interval between two consecutive data points was 20 fs and was increased up to 200 ps for very large delay times.

The time resolved spectra were analyzed by global fitting with GLOTARAN (v. 1.2). For this purpose a sequential model (i. e. unbranched unidirectional model) was applied to model the white light dispersion (chirp), a gaussian type IRF and the coherent artefact at the time zero to yield the evolution associated spectra (EAS) and their corresponding time constants. The white light dispersion (chirp) was corrected by fitting a third order polynomial to the crossphase modulation signal of the pure solvent under otherwise identical experimental conditions. Singular value decomposition was used to estimate the number components and the quality of the fits.

For the dual probe alignment (sample/reference), each pair of laser pulses was normalised to the linear absorption spectra, after acquiring a certain number of transient spectra:

$$\Delta A = \log\left[\left(\frac{I_{ex}(\text{sample})}{I_0(\text{sample})}\right)\left(\frac{I_{ex}(\text{reference})}{I_0(\text{reference})}\right)\right] \tag{19}$$

I_{ex} (sample): intensity of the probe light after the sample when the excitation light was incident on the sample

I_{ex} (reference): intensity of light in the reference channel when the excitation light was incident on the sample

I_0 (sample): intensity of probe light after the sample when the excitation light was blocked by optical chopper

I_0 (reference): intensity of light in the reference channel when the excitation light was blocked by optical chopper

Assuming the splitting ratio between the sample and the reference probe beam to be constant, reflection of the fluctuations in the sample beam by the corresponding fluctuations in the reference beam are not related to the excitation pulse. This method is used mainly with less stable white light.

7.2 Synthesis

7.2.1 General Experimental Procedures

All reactions were performed under inert gas conditions (nitrogen, dried with Sicapent® from Merck, oxygen was removed by the cupric oxide catalyst PuriStar® R3-11 from BASF) in flame-dried Schlenk tubes. If necessary, the solvents were purified and dried by standard procedures and kept under inert gas atmosphere. All chemicals were of standard quality and were used without further purification; exceptions are described below. If not quoted otherwise flash column-chromatography was carried out using silica gel (40 – 63 *µ*m) from Macherey-Nagel. In some cases neutral aluminium oxide (AlO_x) from Macherey-Nagel (50 – 200 *µ*m, activity grade V) was used.

General Procedure for the Pd-catalysed *Buchwald-Hartwig* Coupling (GP1)

The aryl halide (1 equiv.), the aryl amine (1 equiv.), NaO^tBu (1.5 equiv.), P^tBu_3 (1 M in toluene, 0.06 equiv.) and $Pd_2(dba)_3 \cdot CHCl_3$ (0.04 equiv.) were dissolved in the given solvent under a nitrogen atmosphere and stirred at the given temperature for the given time. Afterwards the mixture was diluted with EtOAc and washed with H_2O. The organic phase was dried with Na_2SO_4 and the solvent was removed under reduced pressure. The crude product was purified by flash column-chromatography.

General Procedure for the Pd-Catalysed Borylation of Aryl Halides with Pinacolborane (GP2)

A solution of the aryl halide (1 equiv.), pinacolborane (1.2 equiv.), NEt_3 (1.02 equiv.), P^tBu_3 (1 M in toluene, 0.06 equiv.) and $Pd_2(dba)_3 \cdot CHCl_3$ (1 equiv.) was stirred in the given solvent under a nitrogen atmosphere at the given temperature for the given time. The mixture was diluted with EtOAc and washed with H_2O. The organic phase was dried with Na_2SO_4 and the solvent was removed under reduced pressure. The crude product was purified by flash column-chromatography.

General Procedure for the Pd-Catalysed *Suzuki-Miyaura* Coupling (GP3)

The aryl halide (1 equiv.), the boronic ester (1 equiv.), Na_2CO_3 (1 M solution in H_2O, 2.8 equiv.) and $Pd(PPh_3)_4$ (0.02 equiv.) were dissolved in the given solvent under a nitrogen atmosphere and stirred for the given time at the given temperature. The mixture was diluted with EtOAc and

washed with H_2O. The organic phase was dried with Na_2SO_4 and the solvent was removed under reduced pressure. The crude product was purified by flash column-chromatography.

General Procedure for the Cu-Catalysed *Huisgen* Cycloaddition (GP4)

The aryl alkyne (1 equiv.), the aryl azide (1.2 equiv.) and $CuBr(PPh_3)_3$ (0.07 equiv.) were dissolved in the given solvent under a nitrogen atmosphere. $^{i}Pr_2NEt$ (1 equiv.) was added and the mixture was stirred for the given time at the given temperature. The mixture was diluted with EtOAc and washed with H_2O. The organic phase was dried with Na_2SO_4 and the solvent was removed under reduced pressure. The crude product was purified by flash column-chromatography.

General Procedure for the Cu-Catalysed *Ullmann* Coupling (GP5)

The aryl amine (1 equiv.), the aryl iodide (2.2 equiv.), 1,10-phenanthroline (0.04 equiv.), powdered KOH (8 equiv.) and CuI (0.04 equiv.) were dissolved in the given solvent and were stirred for the given time at the given temperature. EtOAc was added and the suspension was washed with H_2O. The organic phase was dried with Na_2SO_4 and the solvent was removed under reduced pressure. The crude product was purified by flash column-chromatography.

General Procedure for the Cu-Catalysed Formation of Aromatic Azides (GP6)

The aryl bromide (1 equiv.) was dissolved in an EtOH/H_2O-mixture (7:3). (+)-Sodium-L-ascorbate (0.05 equiv.), *N*,*N*'-dimethylethylenediamine (0.15 equiv.), NaN_3 (2 equiv.) and CuI (0.1 equiv.) were added and the mixture was stirred for the given time at the given temperature. After cooling down to RT the mixture was diluted with ^{t}BME and washed thoroughly with H_2O to remove unreacted NaN_3. The solvent was removed under reduced pressure and the crude product was purified by flash column-chromatography.

Activation of Cu Powder[362]

Copper powder (2.00 g) together with I_2 (40.0 mg) was stirred in acetone (20 ml) for 10 min, filtered and stirred for 5 min in conc. HCl/acetone (1:1, 20 ml). The activated copper was filtered, washed with acetone until neutral, dried *in vacuo* and stored under inert gas.

Purification of 18-Crown-6[363]

18-crown-6 (20.0 g) was dissolved in MeCN (50 ml) and the suspension was cooled to –45°C whereupon a white solid precipitated. After filtration of the resulting 18-crown-6 acetonitrile complex, it was distilled under reduced pressure to receive pure 18-crown-6. The colourless solid was stored under inert gas.

7.2.2 Redox Cascades with Triazole-Spacer Units

7.2.2.1 Precursors and Redox Cascades with Chlorine-Substituents

Compound 7

CA: [1205-71-6]

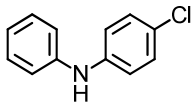

Synthesis according to GP1:
Iodobenzene (600 mg, 2.94 mmol), 4-chloroaniline (375 mg, 2.94 mmol), NaO^{t}Bu (424 mg, 4.41 mmol), P^{t}Bu$_3$ (35.7 mg, 176 *µ*mol, 1 M in toluene), $Pd_2(dba)_3 \cdot CHCl_3$ (122 mg, 118 *µ*mol), toluene (5 ml); 1 d at 75°C; flash column-chromatography (PE/EtOAc 40:1).

Formula: $C_{12}H_{10}ClN$ [203.67].
Yield: 474 mg (2.32 mmol; 79 %) brown solid.
^{1}H-NMR (400.1 MHz, acetone-d_6): δ (ppm) = 7.48 (sb, 1H, N*H*), 7.29 – 7.21 (-, 4H), 7.14 – 7.09 (-, 4H), 6.90 (m, 1H).

Compound 9

CA: [13676-98-7]

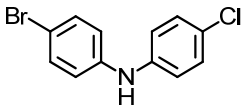

Synthesis according to literature[306]

Compound **7** (474 mg, 2.33 mmol) was dissolved in $CHCl_3$ (3 ml) and was cooled to 0°C. A solution of $^{n}Bu_4NBr_3$ (1.12 g, 2.33 mmol) in $CHCl_3$ (10 ml) was added dropwise over 4 h. After stirring for additional 30 min at RT sat. $Na_2S_2O_3$ solution (15 ml) was added. The organic layer was extracted with sat. $NaHCO_3$ solution (2 × 10 ml), washed with H_2O (2 × 10 ml) and dried over Na_2SO_4. The solvent was removed under reduced pressure and the residue was purified by flash column-chromatography (PE/EtOAc 60:1).

Formula: $C_{12}H_9BrClN$ [282.56].
Yield: 593 mg (2.10 mmol; 90 %) beige solid.
^{1}H-NMR (400.1 MHz, acetone-d_6): δ (ppm) = 7.62 (sb, 1H, N*H*), 7.38 (AA', 2H), 7.25 (AA', 2H), 7.12 (BB', 2H), 7.06 (BB', 2H).

Compound 11

CA: [/]

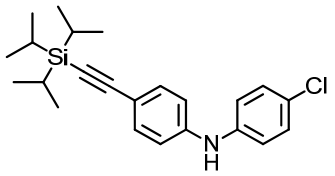

Compound **9** (349 mg, 1.24 mmol), T^{i}PSA (293 mg, 1.61 mmol, 357 µl), $PdCl_2(PhCN)_2$ (14.2 mg, 37.0 µmol) and CuI (4.70 mg, 25.0 µmol) were suspended in 1,4-dioxane (4 ml). After degassing the mixture for 10 min, P$^{t}Bu_3$ (15.0 mg, 74.0 µmol, 1 M in toluene) and $^{i}Pr_2NH$ (137 mg, 1.36 mmol, 192 µl) were added. The reaction mixture was heated to 55°C for 3 d. The solvent was removed *in vacuo* and the residue was purified by flash column-chromatography (PE/EtOAc 99:1). Subsequently the brown residue was recrystallised three times from *n*-hexane.

Formula: $C_{23}H_{30}ClNSi$ [384.03].
Yield: 293 mg (843 µmol; 68 %) white needles.
^{1}H-NMR (400.1 MHz, acetone-d_6): δ (ppm) = 7.77 (sb, 1H, N*H*), 7.37 (AA', 2H), 7.28 (AA', 2H), 7.17 (BB', 2H), 7.08 (BB', 2H) 1.14 (-, 21H).
^{13}C-NMR (100.6 MHz, acetone-d_6): δ (ppm) = 144.9 (quart.), 142.5 (quart.), 134.0 (tert.), 130.0 (tert.), 126.0 (quart.), 120.5 (tert.), 117.1 (tert.), 115.3 (quart.), 109.0 (quart.), 88.4 (quart.), 19.1 (prim.), 12.1 (tert.).
ESI pos. (high resolution): $[M^+]$ = $C_{23}H_{30}ClNSi^+$; calcd: 383.18306; found: 383.18270 (Δ = 0.94 ppm).

Compound 13

CA: [/]

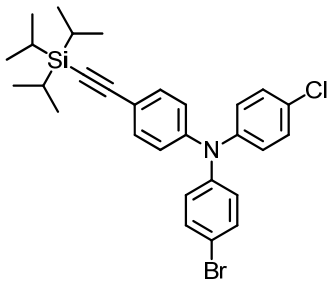

Compound **11** (720 mg, 1.88 mmol), 4-bromo-iodobenzene (796 mg, 2.81 mmol), 18-crown-6 (61.9 mg, 234 *µ*mol) and K_2CO_3 (1.30 g, 9.37 mmol) were suspended in 1,2-dichlorobenzene (20 ml). After degassing the mixture for 10 min, activated Cu (298 mg, 4.69 mmol) was added. The reaction mixture was heated to 240°C for 2 d. Afterwards the unreacted Cu was removed by filtration and the residue was washed with CH_2Cl_2. The so obtained organic mixture was washed with brine (2 × 10 ml) and H_2O (3 × 10 ml) and dried over Na_2SO_4. After removing the solvent *in vacuo* the yellow residue was purified by flash column-chromatography (PE) and GPC (THF).

Formula: $C_{29}H_{33}BrClNSi$ [539.02].
Yield: 537 mg (996 *µ*mol; 68 %) colourless oil.
^{1}H-NMR (400.1 MHz, acetone-d_6): δ (ppm) = 7.48 (AA', 2H), 7.41 (AA', 2H), 7.35 (AA', 2H), 7.10 (BB', 2H), 7.04 (BB', 2H), 7.01 (BB', 2H), 1.14 (-, 21H).
^{13}C-NMR (100.6 MHz, acetone-d_6): δ (ppm) = 148.3 (quart.), 147.2 (quart.), 146.6 (quart.), 134.1 (tert.), 133.5 (tert.), 130.5 (tert.), 129.4 (quart.), 127.2 (tert.), 127.1 (tert.), 123.9 (tert.), 118.3 (quart.), 116.8 (quart.), 108.3 (quart.), 90.1 (quart.), 19.0 (prim.), 12.1 (tert.).
ESI pos. (high resolution): $[M^+]$ = $C_{29}H_{33}BrClNSi^+$; calcd: 537.12487; found: 537.12500 (Δ = 0.24 ppm).

Compound 15

CA: [/]

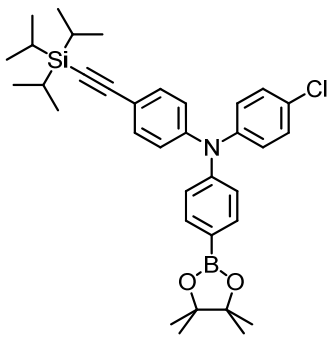

Synthesis according to GP2:

13 (200 mg, 371 *µ*mol), pinacolborane (57.0 mg, 445 *µ*mol, 64.6 *µ*l), Et_3N (38.3 mg, 378 *µ*mol, 53.2 *µ*l), P^tBu_3 (4.50 mg, 22.0 *µ*mol, 1 M in toluene), $Pd_2(dba)_3 \cdot CHCl_3$ (15.4 mg, 15.0 *µ*mol), 1,4-dioxane (5 ml); 2 d at 100°C; flash column-chromatography (PE). The so received yellow oil was dissolved in *n*-hexane and kept at –18°C overnight. The white solid was filtered and dried *in vacuo*.

Formula: $C_{35}H_{45}BClNO_2Si$ [586.09].

Yield: 110 mg (187 *µ*mol; 51 %) white solid.

^{1}H-NMR (400.1 MHz, acetone-d_6): *δ* (ppm) = 7.68 (AA', 2H), 7.42 (AA', 2H), 7.35 (AA', 2H), 7.10 (BB', 2H), 7.05 (BB', 2H), 7.03 (BB', 2H) 1.33 (s, 12H), 1.15 (-, 21H).

^{13}C-NMR (100.6 MHz, acetone-d_6): *δ* (ppm) = 150.5 (quart.), 148.3 (quart.), 146.7 (quart.), 136.9 (tert.), 134.0 (tert.), 130.5 (tert.), 129.4 (quart.), 127.4 (tert.), 124.4 (tert.), 123.7 (tert.), 118.5 (quart.), 108.3 (quart.), 90.1 (quart.), 84.4 (2 × quart.), 25.0 (prim.), 18.8 (prim.), 11.8 (tert.).

ESI pos. (high resolution): $[M+H^+]$ = $C_{35}H_{46}BClNO_2Si^+$; calcd: 585.31102; found: 585.31123 (*Δ* = 0.36 ppm).

Compound 19

CA: [/]

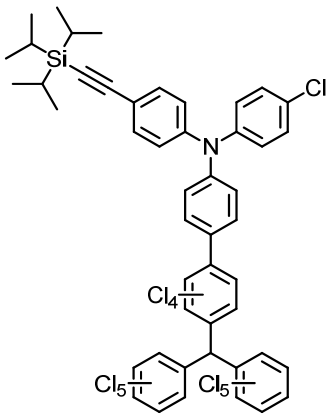

Synthesis according to GP3:

15 (110 mg, 188 *µ*mol), **18** (151 mg, 188 *µ*mol), Na_2CO_3 (55.7 mg, 526 *µ*mol, 1 M in H_2O), $Pd(PPh_3)_4$ (4.34 mg, 3.75 *µ*mol), toluene (3 ml); 3 d at 75°C; flash column-chromatography (PE/EtOAc 100:1). The so received grey solid was purified by GPC (THF).

Formula: $C_{48}H_{34}Cl_{15}NSi$ [1184.67].

Yield: 71.3 mg (56.4 *µ*mol; 32 %) white solid.

^{1}H-NMR (600.1 MHz, acetone-d_6): δ (ppm) = 7.45 (AA', 2H), 7.39 (AA', 2H), 7.32 – 7.27 (-, 2H), 7.23 – 7.20 (-, 2H), 7.18 (BB', 2H), 7.14 (s, 1H), 7.09 (BB', 2H), 1.14 (-, 21H).
^{13}C-NMR (150.9 MHz, acetone-d_6): δ (ppm) = 148.3 (quart.), 148.0 (quart.), 146.6 (quart.), 142.8 (quart.), 137.68 (quart.), 137.65 (quart.), 137.61 (quart.), 135.91 (quart.), 135.90 (quart.), 135.3 (quart.), 135.2 (quart.), 134.89 (quart.), 134.85 (quart.), 134.325 (quart.), 134.322 (quart.), 134.319 (quart.), 134.29 (quart.), 134.27 (quart.), 134.1 (tert.), 134.0 (quart.), 133.18 (quart.), 133.17 (quart.), 133.1 (quart.), 131.22 (tert.)[1], 131.16 (tert.)[1], 130.6 (tert.), 129.5 (quart.), 127.5 (tert.), 124.4 (tert.), 124.2 (tert.), 118.5 (quart.), 108.2 (quart.), 90.1 (quart.), 57.6 (tert.), 19.0 (prim.), 12.0 (tert.).
ESI pos. (high resolution): $[M+H^+]$ = $C_{48}H_{35}Cl_{15}NSi^+$; calcd for X+6: 1183.77822; found: 1183.77892 (Δ = 0.59 ppm).

Compound 21

CA: [/]

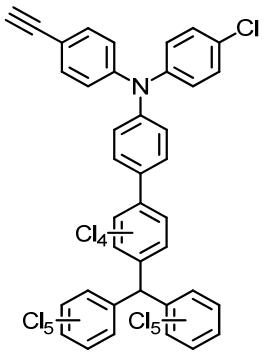

To a solution of **19** (70.0 mg, 59.0 μmol) in THF (3 ml) $^{n}Bu_4NF$ (17.0 mg, 65.0 μmol, 1 M in THF) was added dropwise at RT. The violet solution was stirred overnight and the solvent was removed *in vacuo*. ^{t}BME (5 ml) was added, the solution was washed with brine (1 × 5 ml) and H_2O (4 × 5 ml) and dried over Na_2SO_4. The solvent was removed under reduced pressure and the crude product was purified by flash column-chromatography (PE).

Formula: $C_{39}H_{14}Cl_{15}N$ [1028.33].
Yield: 49.7 mg (48.4 μmol; 82 %) grey solid.
^{1}H-NMR (600.1 MHz, acetone-d_6): δ (ppm) = 7.44 (AA', 2H), 7.39 (AA', 2H), 7.33 – 7.27 (m, 2H), 7.23 – 7.14 (-, 5H), 7.09 (BB', 2H), 3.60 (s, 1H).
^{13}C-NMR (150.9 MHz, acetone-d_6): δ (ppm) = 148.4 (quart.), 148.0 (quart.), 146.6 (quart.), 142.8 (quart.), 137.7 (quart.), 137.63 (quart.), 137.59 (quart.), 135.90 (quart.), 135.89 (quart.), 135.3 (quart.), 135.2 (quart.), 134.9 (quart.), 134.8 (quart.), 134.32 (3 × quart.), 134.30 (quart.), 134.27

[1] See Chapter 7.1 for explanation.

(quart.), 134.1 (tert.), 134.0 (quart.), 133.18 (quart.), 133.17 (quart.), 133.1 (quart.), 131.23 (tert.)[1], 131.16 (tert.)[46], 130.6 (tert.), 129.6 (quart.), 127.6 (tert.), 124.3 (tert.), 124.2 (tert.), 117.5 (quart.), 84.1 (quart.), 78.8 (tert.), 57.6 (tert.).

ESI pos. (high resolution): $[M+H^+]$ = $C_{39}H_{15}Cl_{15}N^+$; calcd for X+6: 1027.64443; found: 1027.64534 (Δ = 0.89 ppm).

Compound 32

CA: [/]

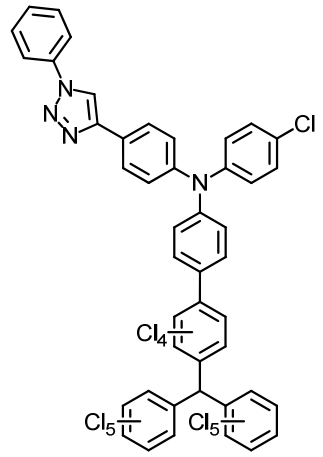

Synthesis according to GP4:

21 (190 mg, 185 μmol), **31** (26.4 mg, 222 μmol), $CuBr(PPh_3)_3$ (34.4 mg, 37.0 μmol, $^iPr_2NEt$ (23.9 mg, 185 μmol, 33.0 μl), THF (10 ml); 2 d at RT; flash column-chromatography (PE/EtOAc 50:1 → 5:1). The resulting yellow solid was purified by GPC (THF).

Formula: $C_{45}H_{19}Cl_{15}N_4$ [1147.45].

Yield: 160 mg (97.0 μmol; 72 %) white solid.

^{1}H-NMR (600.1 MHz, acetone-d_6): δ (ppm) = 8.99 (s, 1H), 8.00 – 7.96 (-, 4H), 7.66 – 7.62 (-, 2H), 7.52 (m, 1H), 7.40 (AA', 2H), 7.32 – 7.19 (-, 8H), 7.15 (s, 1H).

^{13}C-NMR (150.9 MHz, acetone-d_6): δ (ppm) = 148.5 (quart.), 148.4 (quart.), 147.8 (quart.), 147.0 (quart.), 142.9 (quart.), 138.2 (quart.), 137.7 (quart.), 137.641 (quart.), 137.637 (quart.), 135.91 (quart.), 135.90 (quart.), 135.3 (quart.), 135.2 (quart.), 134.90 (quart.), 134.85 (quart.), 134.33 (quart.), 134.32 (2 × quart.), 134.29 (quart.), 134.28 (quart.), 134.1 (quart.), 133.18 (quart.), 133.17 (quart.), 132.6 (quart.), 131.16 (tert.)[2], 131.09 (tert.)[46], 130.7 (tert.), 130.5 (tert.), 129.4 (tert.), 129.0 (quart.), 127.8 (tert.), 127.3 (quart.), 127.0 (tert.), 125.9 (tert.), 123.6 (tert.), 120.9 (tert.), 119.2 (tert.), 57.6 (tert.).

[1] See Chapter 7.1 for explanation.
[2] See Chapter 7.1 for explanation.

ESI pos. (high resolution): $[M+H^+]$ = $C_{45}H_{20}Cl_{15}N_4^+$; calcd for X+6: 1146.69297; found: 1146.69202 (Δ = 0.83 ppm).

Compound 1

CA: [/]

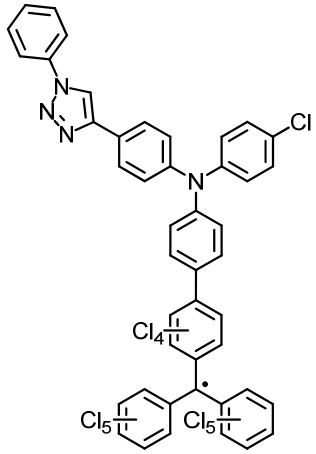

To a solution of **32** (80.0 mg, 70.0 μmol) in THF (5 ml), ^{n}Bu$_4$NOH (54.3 mg, 209 μmol, 1.5 M in H_2O) was added in the dark. After stirring the violet solution for 1 d at RT, PCA (60.0 mg, 244 μmol) was added and the mixture was stirred for 3 d. The solvent was removed *in vacuo* and the residue was purified by flash column-chromatography (CH_2Cl_2). The received dark brown solid was purified by GPC (THF).

Formula: $C_{45}H_{18}Cl_{15}N_4$ [1146.45].
Yield: 50.0 mg (43.8 μmol; 63 %) black solid.
ESI pos. (high resolution): $[M+H^+]$ = $C_{45}H_{19}Cl_{15}N_4^+$; calcd for X+6: 1145.68514; found: 1145.68530 (Δ = 0.14 ppm).
Smp.: 202 °C (MeOH).

Compound 33

CA: [/]

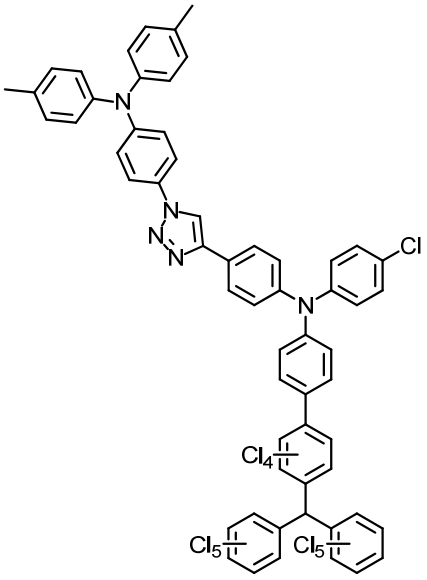

Synthesis according to GP4:
21 (50.0 mg, 49.0 *µ*mol), **27** (20.2 mg, 58.0 *µ*mol), $CuBr(PPh_3)_3$ (3.10 mg, 3.33 *µ*mol), $^{i}Pr_2NEt$ (6.28 mg, 49.0 *µ*mol, 8.27 *µ*l), THF (3.5 ml); 3 d at RT; flash column-chromatography (PE/EtOAc 60:1 → 40:1). The so received brown solid was purified by GPC (THF) and precipitated from MeOH.

Formula: $C_{59}H_{32}Cl_{15}N_5$ [1342.71].
Yield: 45.0 mg (33.5 *µ*mol; 67 %) brown solid.
^{1}H-NMR (600.1 MHz, acetone-d_6): *δ* (ppm) = 8.86 (s, 1H), 7.96 (AA', 2H), 7.77 (AA', 2H), 7.38 (AA', 2H), 7.31 – 7.17 (-, 12H), 7.14 (s, 1H), 7.10 (BB', 2H), 7.04 (BB', 4H), 2.32 (s, 6H, CH_3).
^{13}C-NMR (150.9 MHz, acetone-d_6): *δ* (ppm) = 149.5 (quart.), 148.5 (quart.), 148.1 (quart.), 147.7 (quart.), 147.0 (quart.), 145.7 (quart.), 142.9 (quart.), 137.7 (quart.), 137.6 (quart.), 135.90 (quart.), 135.89 (quart.), 135.3 (quart.), 135.2 (quart.), 134.9 (quart.), 134.8 (quart.), 134.33 (quart.), 134.32 (quart.), 134.31 (2 × quart.), 134.29 (quart.), 134.27 (quart.), 134.1 (quart.), 133.18 (quart.), 133.17 (quart.), 132.5 (quart.), 131.5 (quart.), 131.14 (tert.)[1], 131.07 (tert.)[46], 131.0 (tert.), 130.5 (tert.), 129.0 (quart.), 127.7 (tert.), 127.5 (quart.), 127.0 (tert.), 126.0 (tert.), 125.9 (tert.), 125.7 (quart.), 123.5 (tert.), 122.6 (tert.), 122.0 (tert.), 118.9 (tert.), 57.6 (tert.), 20.8 (prim.).

ESI pos. (high resolution): $[M+H^+]$ = $C_{59}H_{33}Cl_{15}N_5^+$; calcd for X+6: 1341.79826; found: 1341.79876 (*Δ* = 0.37 ppm).

[1] See Chapter 7.1 for explanation.

Compound 2

CA: [/]

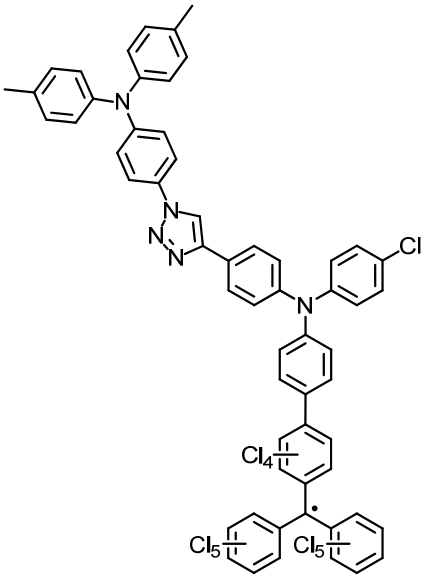

To a solution of **33** (30.0 mg, 22.0 *µ*mol) in THF (5 ml) $^{n}Bu_4NOH$ (12.8 mg, 49.0 *µ*mol, 1.5 M in H_2O) was added in the dark. After stirring the violet solution for 1 d, PCA (14.3 mg, 58.0 mmol) was added and the mixture was stirred for 2 d. The solvent was removed *in vacuo* and the residue was dissolved in CH_2Cl_2 (3 ml). The solution was washed with H_2O (4 × 3 ml) and dried over Na_2SO_4. After removing the solvent under reduced pressure the residue was purified by flash column-chromatography (PE/EtOAc 60:1 → 40:1). In addition the received brown solid was purified by GPC (THF) and precipitated from MeOH.

Formula: $C_{59}H_{31}Cl_{15}N_5$ [1341.71].
Yield: 12.0 mg (8.94 *µ*mol; 41 %) brown solid.
^{1}H-NMR (600.1 MHz, acetone-d_6): *δ* (ppm) = 8.79 (sb, 1H), 8.13 (-b, 2H), 7.77 (AA', 2H), 7.54 (-b, 2H), 7.18 (AA', 4H), 7.11 (BB', 2H), 7.02 – 6.84 (BB', 4H, -b, 8H), 2.32 (s, 6H, C*H*$_3$).[1]
^{13}C-NMR (150.9 MHz, acetone-d_6): *δ* (ppm) = 149.5 (quart.), 147.6 (quart.), 146.8 (quart.), 145.7 (quart.), 134.4 (quart.), 131.5 (quart.), 131.1 (tert.), 130.6 (quart.), 126.0 (tert.), 122.6 (tert.), 122.0 (tert.), 119.3 (tert.), 20.8 (prim.).[1]
ESI pos. (high resolution): $[M+H^+]$ = $C_{59}H_{32}Cl_{15}N_5^+$; calcd for X+6: 1340.79045; found: 1341.78952 (*Δ* = 0.69 ppm).
Smp.: 208 °C (MeOH).

[1] An explanation for the lacking of signals is given in Chapter 5.1.4.

Compound 34

CA: [/]

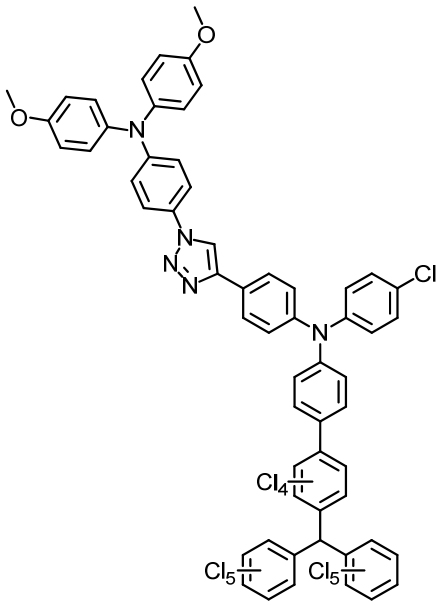

Synthesis according to GP4:

21 (130 mg, 126 *µ*mol), **28** (52.5 mg, 152 *µ*mol), $CuBr(PPh_3)_3$ (23.5 mg, 25.0 *µ*mol), $^{i}Pr_2NEt$ (16.3 mg, 126 *µ*mol, 21.3 *µ*l), THF (2 ml); 6 d at 70°C; flash column-chromatography (PE/EtOAc 40:1 → 20:1). The so received brown solid was purified by GPC (THF) and precipitated from MeOH.

Formula: $C_{59}H_{32}Cl_{15}N_5O_2$ [1374.71].

Yield: 90.0 mg (62.2 *µ*mol; 52 %) white solid.

^{1}H-NMR (600.1 MHz, acetone-d_6): *δ* (ppm) = 8.82 (s, 1H), 7.96 (AA', 2H), 7.71 (AA', 2H), 7.38 (AA', 2H), 7.31 – 7.18 (-, 8H), 7.15 – 7.13 (-, 5H), 6.99 – 6.94 (-, 6H), 3.81 (s, 6H, OCH_3).

^{13}C-NMR (150.9 MHz, acetone-d_6): *δ* (ppm) = 157.7 (quart.), 150.2 (quart.), 148.5 (quart.), 148.0 (quart.), 147.6 (quart.), 147.0 (quart.), 142.9 (quart.), 140.9 (quart.), 137.7 (quart.), 137.625 (quart.), 137.621 (quart.), 135.91 (quart.), 135.90 (quart.), 135.3 (quart.), 135.2 (quart.), 134.89 (quart.), 134.85 (quart.), 134.33 (quart.), 134.319 (quart.), 134.316 (quart.), 134.29 (quart.), 134.27 (quart.), 134.1 (quart.), 133.18 (quart.), 133.17 (quart.), 132.5 (quart.), 131.14 (tert.)[1], 131.07 (tert.)[46], 130.5 (tert.), 130.4 (quart.), 128.9 (quart.), 128.2 (tert.), 127.7 (tert.), 127.6 (quart.), 127.0 (tert.), 126.0 (tert.), 123.5 (tert.), 122.0 (tert.), 120.2 (tert.), 118.9 (tert.), 115.8 (tert.), 57.6 (tert.), 55.7 (prim.).

ESI pos. (high resolution): $[M^+]$ = $C_{59}H_{32}Cl_{15}N_5O_2^+$; calcd: 1366.78784; found: 1366.78831 (*Δ* = 0.21 ppm).

[1] See Chapter 7.1 for explanation.

Compound 3

CA: [/]

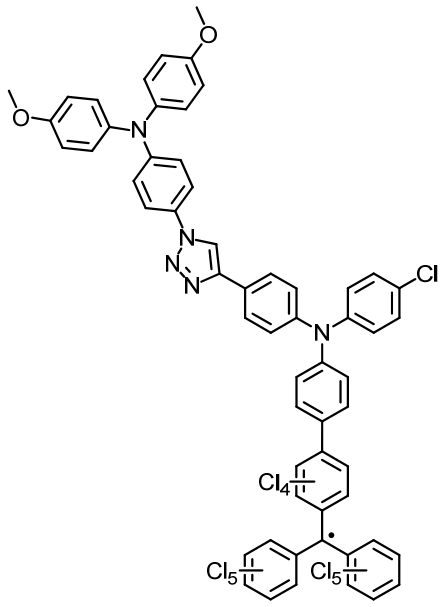

To a solution of **34** (47.0 mg, 34.0 *µ*mol) in THF (2 ml) $^{n}Bu_4NOH$ (19.5 mg, 75.0 *µ*mol, 1.5 M in H_2O) was added in the dark. After stirring the violet solution for 1 d at RT, PCA (21.9 mg, 89.0 mmol) was added and the mixture was stirred for 2 d. The solvent was removed *in vacuo* and the residue was dissolved in EtOAc (8 ml). The solution was washed with H_2O (5 × 5 ml) and dried over Na_2SO_4. After removing the solvent under reduced pressure the residue was purified by flash column-chromatography (PE/EtOAc 60:1). In addition the received brown solid was purified by GPC (THF) and precipitated from MeOH.

Formula: $C_{59}H_{31}Cl_{15}N_5O_2$ [1373.70].
Yield: 40.0 mg (28.9 *µ*mol; 85 %) brown solid.
^{1}H-NMR (600.1 MHz, acetone-d_6): *δ* (ppm) = 9.23 (sb, 1H), 8.20 (-b, 2H), 7.84 (AA', 2H), 7.54 (-b, 2H), 7.13 (AA', 4H), 6.98 – 6.94 (-, 14H), 3.81 (s, 6H, OCH_3).[1]
^{13}C-NMR (150.9 MHz, acetone-d_6): *δ* (ppm) = 157.8 (quart.), 141.0 (quart.), 128.2 (tert.), 122.1 (tert.), 120.3 (tert.), 115.9 (tert.), 55.8 (prim.).[1]
ESI pos. (high resolution): $[M+H^+]$ = $C_{59}H_{31}Cl_{15}N_5O_2^+$; calcd for X+8: 1373.77243; found: 1373.77003 (*Δ* = 1.75 ppm).
Smp.: 215 °C (MeOH).

[1] An explanation for the lacking of signals is given in Chapter 5.1.4.

7.2.2.2 Precursors and Redox Cascades with Cyano-Substituents

Compound 8

CA: [36602-01-4]

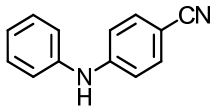

Synthesis according to GP1:
Aniline (500 mg, 5.37 mmol), 4-bromobenzonitrile (977 mg, 5.37 mmol), NaO^{t}Bu (774 mg, 8.05 mmol), P^{t}Bu$_3$ (65.2 mg, 322 *µ*mol, 1 M in toluene), $Pd_2(dba)_3 \cdot CHCl_3$ (222 mg, 215 *µ*mol), toluene (5 ml); 2 d at 75°C, 3 d at 90°C; flash column-chromatography (PE/EtOAc 20:1 → 10:1 → 5:1).

Formula: $C_{13}H_{10}N_2$ [194.23].
Yield: 821 mg (4.32 mmol; 79 %) yellow solid.
^{1}H-NMR (400.1 MHz, acetone-d_6): *δ* (ppm) = 8.06 (sb, 1H, N*H*), 7.54 (AA', 2H), 7.38 – 7.33 (m, 2H), 7.26 – 7.24 (m, 2H), 7.15 (BB', 2H), 7.07 – 7.04 (m, 1H).

Compound 10

CA: [1019601-02-5]

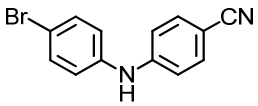

Synthesis according to literature[306]
Compound **8** (821 mg, 4.23 mmol) was dissolved in $CHCl_3$ (5 ml) and was cooled to 0°C. A solution of ^{n}Bu$_4$NBr$_3$ (2.04 g, 4.23 mmol) in $CHCl_3$ (18 ml) was added dropwise over 4 h. After stirring for additional 30 min at RT sat. $Na_2S_2O_3$ solution (20 ml) was added. The organic layer was extracted with sat. $NaHCO_3$ solution (2 × 15 ml), washed with H_2O (2 × 15 ml) and dried over Na_2SO_4. The solvent was removed under reduced pressure and the residue was purified by flash column-chromatography (PE/EtOAc 10:1).

Formula: $C_{13}H_9BrN_2$ [273.13].
Yield: 996 mg (3.65 mmol; 86 %) light yellow solid.
^{1}H-NMR (600.1 MHz, acetone-d_6): *δ* (ppm) = 8.14 (sb, 1H, N*H*), 7.57 (AA', 2H), 7.48 (AA', 2H), 7.20 (BB', 2H), 7.17 (BB', 2H).

^{13}C-NMR (150.9 MHz, acetone-d_6): δ (ppm) = 148.8 (quart.), 141.4 (quart.), 134.5 (tert.), 133.2 (tert.), 122.7 (tert.), 120.1 (quart.), 116.2 (tert.), 115.2 (quart.), 102.4 (quart.).
ESI pos. (high resolution): [M+H$^+$] = $C_{13}H_{10}BrN_2^+$; calcd: 273.00219; found: 273.00230 (Δ = 0.40 ppm).

Compound 12

CA: [/]

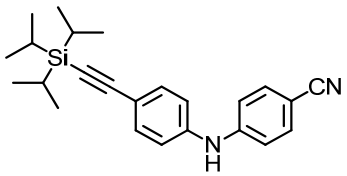

Compound **10** (966 mg, 3.54 mmol), T^{i}PSA (839 mg, 4.60 mmol, 1.02 ml), $PdCl_2(PhCN)_2$ (40.7 mg, 106 μmol) and CuI (13.5 mg, 71.0 μmol) were suspended in 1,4-dioxane (20 ml). After degassing the mixture for 10 min, P^{t}Bu$_3$ (42.9 mg, 212 μmol, 1 M in toluene) and ^{i}Pr$_2$NH (394 mg, 3.89 mmol, 550 μl) were added. The reaction mixture was heated to 55°C for 3 d. The solvent was removed *in vacuo* and the residue was purified by flash column-chromatography (PE/EtOAc 20:1 → 10:1).

Formula: $C_{24}H_{30}N_2Si$ [374.59].
Yield: 1.32 mg (3.92 mmol; 93 %) light brown solid.
^{1}H-NMR (400.1 MHz, acetone-d_6): δ (ppm) = 8.28 (sb, 1H, N*H*), 7.60 (AA', 2H), 7.46 (AA', 2H), 7.26 – 7.22 (-, 4H), 1.15 (-, 21H).
^{13}C-NMR (100.6 MHz, acetone-d_6): δ (ppm) = 148.3 (quart.), 148.2 (quart.), 134.5 (tert.), 134.0 (tert.), 120.1 (quart.), 119.8 (tert.), 177.6 (quart.), 116.8 (tert.), 108.4 (quart.), 102.8 (quart.), 89.4 (quart.), 19.0 (prim.), 12.1 (tert.).
ESI pos. (high resolution): [M+H$^+$] = $C_{24}H_{31}N_2Si^+$; calcd: 375.22510; found: 375.22490 (Δ = 0.53 ppm).

Compound 14

CA: [/]

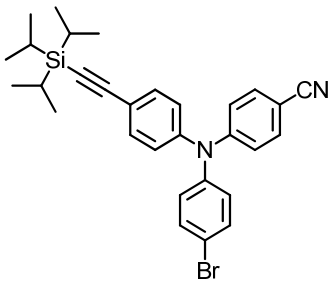

Compound **12** (1.15 g, 3.07 mmol), 4-bromo-iodobenzene (1.30 mg, 4.60 mmol), 18-crown-6 (101 mg, 384 *µ*mol) and K_2CO_3 (1.30 mg, 2.12 mmol) were suspended in 1,2-dichlorobenzene (33 ml). After degassing the mixture for 10 min, activated Cu (488 mg, 7.67 mmol) was added. The reaction mixture was heated to 240°C for 2 d. Afterwards the unreacted Cu was removed by filtration and the residue was washed with CH_2Cl_2. The so obtained organic mixture was washed with brine (2 × 20 ml) and H_2O (3 × 20 ml) and dried over Na_2SO_4. After removing the solvent *in vacuo* the residue was purified by flash column-chromatography (PE/EtOAc 100:1 → 20:1 → 5:1). The received solid was identified as a mixture of the desired product and a species iodine in the *p*-position instead of bromine. Based on the assumption that both species serve as a reagent for the Pd-catalysed coupling with pinacolborane, the mixture was used directly for the next step without further characterisation.

Formula: $C_{30}H_{33}BrN_2Si$ [529.59]; $C_{30}H_{33}IN_2Si$ [576.59].
Yield: 880 mg (1.66 mmol; 54 %) light yellow solid.
^{1}H-NMR (400.1 MHz, acetone-d_6):
$C_{30}H_{33}BrN_2Si$: *δ* (ppm) = 7.62 (AA', 2H), 7.59 (AA', 2H), 7.50 (AA', 2H), 7.04 – 6.96 (-, 6H), 1.15 (-, 21H).
$C_{30}H_{33}IN_2Si$: *δ* (ppm) = 7.75 (AA', 2H), 7.62 (AA', 2H), 7.50 (AA', 2H), 7.15 (BB', 2H), 7.11 (BB', 2H), 7.01 (BB', 2H), 1.15 (-, 21H).
ESI pos. (high resolution):
$[M^+] = C_{30}H_{33}BrN_2Si^+$; calcd: 528.15909; found: 528.14522 (*Δ* = 0.70 ppm);
$[M^+] = C_{30}H_{33}IN_2Si^+$; calcd: 576.14522; found: 576.14685 (*Δ* = 2.83 ppm).

Compound 16

CA: [/]

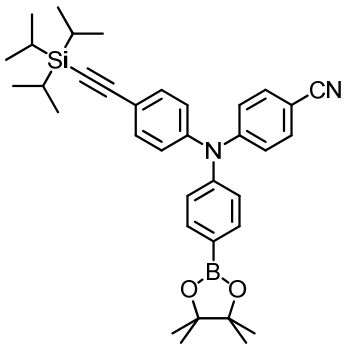

Synthesis according to GP2:

14 (540 mg, 1.02 mmol), pinacolborane (196 mg, 1.53 mmol, 222 µl), Et_3N (105 mg, 1.04 mmol, 146 µl), P^tBu_3 (12.4 mg, 61.0 µmol, 1 M in toluene), $Pd_2(dba)_3 \cdot CHCl_3$ (42.2 mg, 41.0 µmol), 1,4-dioxane (5 ml); 2 d at 75°C; flash column-chromatography (PE/EtOAc 60:1 → 20:1). The so received yellow solid was purified by GPC (THF), which resulted in a white solid. The residue was dissolved in 1 ml of ^{t}BME and precipitated from *n*-hexane. The ^{1}H- as well as the ^{13}C-NMR showed 5 % of an impurity which could not be further characterised.

Formula: $C_{36}H_{45}BN_2O_2Si$ [576.65].

Yield: 318 mg (551 µmol; 54 %) white solid.

^{1}H-NMR (400.1 MHz, acetone-d_6): δ (ppm) = 7.76 (AA', 2H), 7.62 (AA', 2H), 7.49 (AA', 2H), 7.17 – 7.11 (-, 6H), 1.34 (s, 12H), 1.15 (-, 21H).

^{13}C-NMR (100.6 MHz, acetone-d_6): δ (ppm) = 151.8 (quart.), 149.5 (quart.), 147.3 (quart.), 137.2 (tert.), 134.3 (2 × tert.), 126.3 (tert.), 125.5 (tert.), 122.9 (tert.), 120.4 (quart.), 119.6 (quart.), 107.9 (quart.), 105.4 (quart.), 90.9 (quart.), 84.6 (2 × quart.), 25.2 (prim.), 19.0 (prim.), 12.1 (tert.).

MALDI-MS: calcd for $C_{35}H_{45}BN_2O_2Si^+$: 575.337; found: 575.292.

Compound 20

CA: [/]

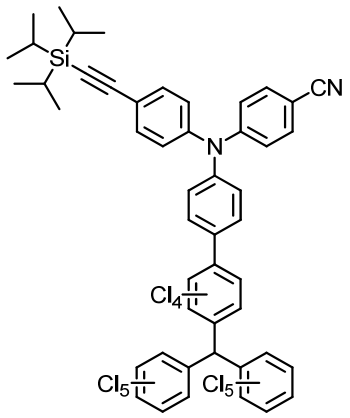

Synthesis according to GP3:

16 (470 mg, 815 *µ*mol), **18** (656 mg, 815 *µ*mol), Na_2CO_3 (242 mg, 2.28 mmol, 1 M in H_2O), $Pd(PPh_3)_4$ (18.8 mg, 16.0 *µ*mol), toluene (8 ml); 2 d at 110°C; flash column-chromatography (PE/EtOAc 500:1→ 60:1). The so received grey solid was purified by GPC (THF).

Formula: $C_{49}H_{34}Cl_{14}N_2Si$ [1175.24].

Yield: 320 mg (272 *µ*mol; 33 %) light grey solid.

^{1}H-NMR (600.1 MHz, dichloromethane-d_2): *δ* (ppm) = 7.51 (AA', 2H), 7.46 (AA', 2H), 7.24 – 7.19 (-, 4H), 7.13 (BB', 2H), 7.11 (BB', 2H), 7.07 (s, 1H), 1.13 (-, 21H).

^{13}C-NMR (150.9 MHz, dichloromethane-d_2): *δ* (ppm) = 151.1 (quart.), 146.4 (quart.), 146.3 (quart.), 141.6 (quart.), 137.4 (quart.), 136.93 (quart.), 136.92 (quart.), 135.50 (quart.), 135.46 (quart.), 135.1 (quart.), 134.5 (quart.), 134.45 (quart.), 134.43 (quart.), 134.14 (quart.), 134.07 (quart.), 133.98 (quart.), 133.96 (quart.), 133.88 (quart.), 133.87 (quart.), 133.82 (tert.), 133.76 (tert.), 133.49 (quart.), 132.9 (quart.), 132.8 (quart.), 130.9 (tert.)[1], 130.8 (tert.)[46], 125.8 (tert.), 125.6 (tert.), 122.0 (tert.), 120.2 (quart.), 119.6 (quart.), 106.8 (quart.), 104.7 (quart.), 91.4 (quart.), 57.0 (tert.), 18.8 (prim.), 11.8 (tert.).

MALDI-MS: calcd for $C_{49}H_{34}Cl_{14}N_2Si^+$: 1173.805; found: 1173.810.

[1] See Chapter 7.1 for explanation.

Compound 22

CA: [/]

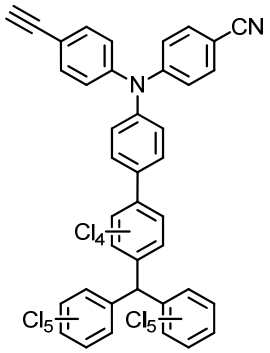

To a solution of **20** (320 mg, 272 *µ*mol) in THF (3 ml) $^{n}Bu_4NF$ (78.0 mg, 300 *µ*mol, 1 M in THF) was added dropwise at RT. The violet solution was stirred overnight and the solvent was removed *in vacuo*. ^{t}BME (5 ml) was added, the solution was washed with brine (1 × 5 ml) and H_2O (4 × 5 ml) and dried over Na_2SO_4. The solvent was removed under reduced pressure and the crude product was purified by flash column-chromatography (PE/EtOAc 50:1) and GPC (THF).

Formula: $C_{40}H_{14}Cl_{14}N_2$ [1018.89].
Yield: 170 mg (166 *µ*mol; 61 %) grey solid.
^{1}H-NMR (600.1 MHz, THF-d_8): δ (ppm) = 7.56 (AA', 2H), 7.45 (AA', 2H), 7.28 – 7.24 (-, 4H), 7.16 – 7.13 (-, 5H), 3.55 (s, 1H).
^{13}C-NMR (150.9 MHz, THF-d_8): δ (ppm) = 151.7 (quart.), 147.4 (quart.), 147.3 (quart.), 142.7 (quart.), 137.9 (quart.), 137.7 (quart.), 137.6 (quart.), 136.08 (quart.), 136.05 (quart.), 135.6 (quart.), 135.2 (quart.), 135.00 (quart.), 134.96 (quart.), 134.6 (quart.), 134.52 (quart.), 134.50 (quart.), 134.47 (2 × quart.), 134.46 (quart.), 134.4 (tert.), 134.2 (tert.), 134.0 (quart.), 133.4 (quart.), 133.3 (quart.), 131.5 (tert.)[1], 131.3 (tert.)[46], 126.3 (tert.), 125.81 (tert.)[46], 125.79 (tert.)[46], 123.1 (tert.), 119.8 (quart.), 119.2 (quart.), 106.2 (quart.), 83.7 (quart.), 79.1 (tert.), 57.7 (tert.).
MALDI-MS: calcd for $C_{40}H_{14}Cl_{14}N_2^{+}$: 1117.671; found: 1117.680.

[1] See Chapter 7.1 for explanation.

Compound 35

CA: [/]

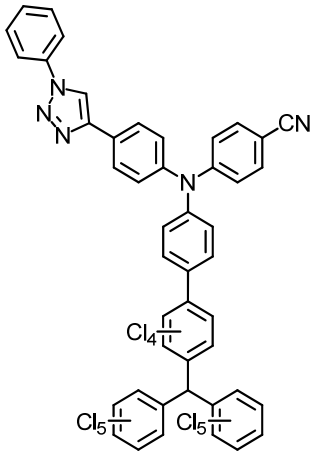

Synthesis according to GP4:

22 (100 mg, 98.0 *µ*mol), **31** (14.0 mg, 118 *µ*mol), $CuBr(PPh_3)_3$ (18.3 mg, 20.0 *µ*mol), $^{i}Pr_2NEt$ (12.7 mg, 98.0 *µ*mol, 17.0 *µ*l), THF (6 ml); 3 d at RT; flash column-chromatography (PE/EtOAc 10:1).

Formula: $C_{46}H_{19}Cl_{14}N_5$ [1138.02].

Yield: 110 mg (97.0 *µ*mol; 98 %) light brown solid.

^{1}H-NMR (400.1 MHz, acetone-d_6): *δ* (ppm) = 9.02 (s, 1H), 8.07 (AA', 2H), 7.98 (m, 2H), 7.66 – 7.62 (-, 4H), 7.55 – 7.50 (m, 1H), 7.41 – 7.36 (-, 6H), 7.18 (BB', 2H), 7.16 (s, 1H).

^{13}C-NMR (150.9 MHz, acetone-d_6): *δ* (ppm) = 152.1 (quart.), 148.1 (quart.), 147.2 (quart.), 146.6 (quart.), 142.6 (quart.), 138.2 (quart.), 137.8 (quart.), 137.64 (quart.), 137.60 (quart.), 135.91 (quart.), 135.90 (quart.), 135.3 (quart.), 135.1 (quart.), 134.90 (quart.), 134.85 (quart.), 134.6 (quart.), 134.4 (quart.), 134.34 (quart.), 134.33 (quart.), 134.32 (tert.), 134.31 (quart.), 134.29 (quart.), 133.9 (quart.), 133.2 (2 × quart.), 131.54 (tert.)[1], 131.48 (tert.)[46], 130.8 (tert.), 129.5 (tert.), 129.0 (quart.), 128.1 (tert.), 127.7 (tert.), 126.2 (tert.), 121.8 (tert.), 121.0 (tert.), 119.8 (quart.), 119.5 (tert.), 104.6 (quart.), 57.6 (tert.).

ESI pos. (high resolution): $[M+H^+]$ = $C_{46}H_{20}Cl_{14}N_5^+$; calcd for X+6: 1137.72729; found: 1137.72608 (*Δ* = 1.06 ppm).

[1] See Chapter 7.1 for explanation.

Compound 4

CA: [/]

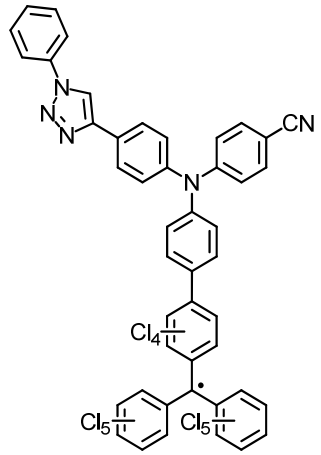

To a solution of **35** (50.0 mg, 44.0 *µ*mol) in THF (2 ml) $^{n}Bu_4NOH$ (34.2 mg, 132 *µ*mol, 1.5 M in H_2O) was added in the dark. After stirring the violet solution for 1 d at RT, PCA (37.8 mg, 154 *µ*mol) was added and the mixture was stirred for 3 d. The solvent was removed *in vacuo* and the residue was purified by flash column-chromatography (CH_2Cl_2 → CH_2Cl_2/EtOAc 2:1).

Formula: $C_{46}H_{18}Cl_{14}N_5$ [1137.01].
Yield: 30.0 mg (26.4 *µ*mol; 60 %) black solid.
ESI pos. (high resolution): $[M+H^+]$ = $C_{46}H_{19}Cl_{14}N_5^+$; calcd for X+6: 1136.71946; found: 1136.71940 (*Δ* = 0.05 ppm).
Smp.: 210 °C (MeOH).

Compound 36

CA: [/]

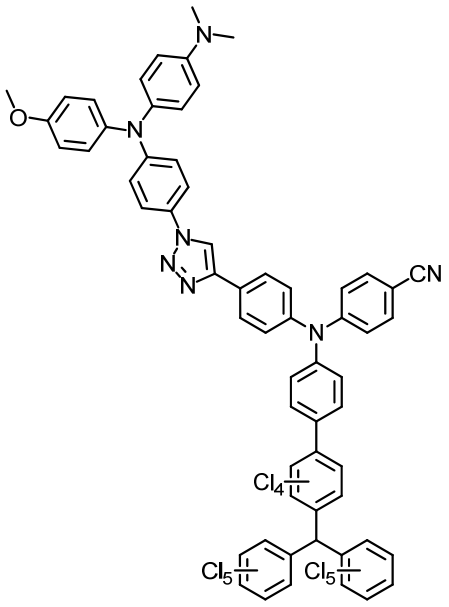

Synthesis according to GP4:

22 (100 mg, 98.0 *µ*mol), **29** (42.3 mg, 118 *µ*mol), $CuBr(PPh_3)_3$ (18.3 mg, 20.0 *µ*mol), $^{i}Pr_2NEt$ (12.7 mg, 98.0 *µ*mol, 17.0 *µ*l), THF (6 ml); 2 d at RT; 7 d at 70°C; flash column-chromatography (PE/EtOAc 10:1 → 5:1 → 2:1). The so received yellow solid was purified by GPC (THF) and precipitated from MeOH.[1]

Formula: $C_{61}H_{35}Cl_{14}N_7O$ [1378.32].

Yield: 65.0 mg (47.2 *µ*mol; 48 %) light yellow solid.

^{1}H-NMR (400.1 MHz, acetone-d_6): *δ* (ppm) = 8.84 (s, 1H), 8.04 (AA', 2H), 7.68 (AA', 2H), 7.64 (AA', 2H), 7.42 – 7.34 (-, 7H), 7.19 – 7.13 (-, 6H), 7.08 (AA', 2H), 6.95 (BB', 2H), 6.79 (BB', 2H), 3.81 (s, 3H, OCH_3), 2.95 (s, 6H, N(CH_3)$_2$).

ESI pos. (high resolution): [M^+] = $C_{61}H_{35}Cl_{14}N_7O^+$; calcd: 1376.84633; found: 1376.84779 (*Δ* = 1.06 ppm).

[1] No ^{13}C-NMR spectra was accessible, due to decomposition processes, even in degassed solutions.

Compound 5

CA: [/]

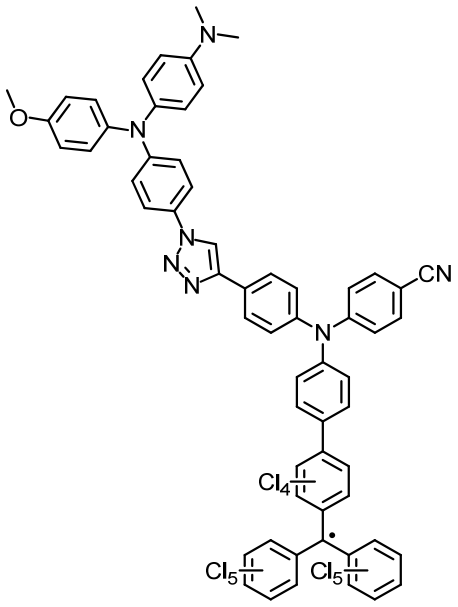

To a solution of **36** (80.0 mg, 58.0 *µ*mol) in THF (3 ml) $^{n}Bu_4NOH$ (45.2 mg, 174 *µ*mol, 1.5 M in H_2O) was added in the dark. After stirring the violet solution for 1 d at RT, PCA (49.9 mg, 203 mmol) was added and the mixture was stirred for 2 d. The solvent was removed *in vacuo* and the residue was purified by flash column-chromatography (CH_2Cl_2 → CH_2Cl_2/EtOAc 10:1 → 1:1). The so received dark brown solid was purified by GPC (THF) and precipitated from MeOH.

Formula: $C_{61}H_{34}Cl_{14}N_7O$ [1377.31].
Yield: 45.0 mg (33.0 *µ*mol; 56 %) dark brown solid.
ESI pos. (high resolution): $[M^+]$ = $C_{61}H_{34}Cl_{14}N_7O^+$; calcd for X+6: 1375.83851; found: 1375.83704 (Δ = 1.07 ppm).
Smp.: >305 °C (MeOH).

Compound 37

CA: [/]

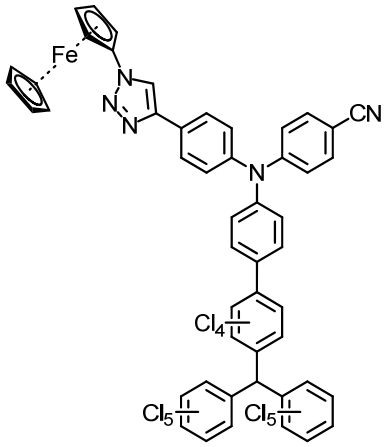

Synthesis according to GP4:

22 (100 mg, 98.0 *µ*mol), **30** (22.3 mg, 98.0 *µ*mol), $CuBr(PPh_3)_3$ (18.3 mg, 20.0 *µ*mol), $^{i}Pr_2NEt$ (12.7 mg, 98.0 *µ*mol, 17.0 *µ*l), THF (6 ml); 1 d at 55°C; flash column-chromatography (PE/EtOAc 20:1 → 10:1 → 5:1).

Formula: $C_{50}H_{23}Cl_{14}FeN_5$ [1245.94].

Yield: 100 mg (98.0 *µ*mol; 82 %) brown solid.

^{1}H-NMR (400.1 MHz, acetone-d_6): *δ* (ppm) = 8.78 (s, 1H), 8.02 (AA', 2H), 7.65 (AA', 2H), 7.43 – 7.34 (-, 6H), 7.19 – 7.15 (-, 3H), 5.05 (-, 2H), 4.37 (-, 2H), 4.27 (s, 5H).

^{13}C-NMR (150.9 MHz, acetone-d_6): *δ* (ppm) = 152.2 (quart.), 147.5 (quart.), 147.3 (quart.), 146.5 (quart.), 142.7 (quart.), 137.9 (quart.), 137.69 (quart.), 137.65 (quart.), 136.0 (2 × quart.), 135.4 (quart.), 135.2 (quart.), 135.0 (quart.), 134.9 (quart.), 134.6 (quart.), 134.44 (quart.), 134.39 – 134.32 (5 × quart., 1 × tert.), 134.0 (quart.), 133.2 (quart.), 131.6 (tert.)[1], 131.5 (tert.)[46], 129.3 (quart.), 128.1 (tert.), 127.8 (tert.), 126.1 (tert.), 121.8 (tert.), 120.8 (tert.), 119.8 (quart.), 104.6 (quart.), 94.9 (quart.), 70.9 (tert.), 67.6 (tert.), 62.7 (tert.), 57.7 (tert.).

ESI pos. (high resolution): $[M+H^+]$ = $C_{50}H_{24}Cl_{14}FeN_5^+$; calcd for X+6: 1245.69385; found: 1245.69297 (*Δ* = 0.71 ppm).

[1] See Chapter 7.1 for explanation.

Compound 6

CA: [/]

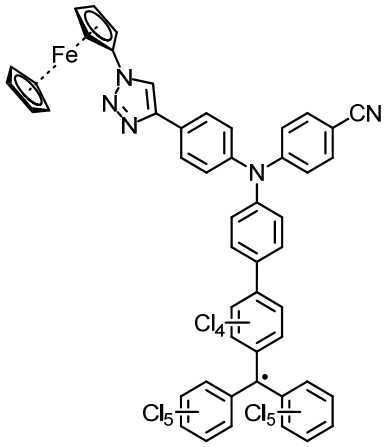

To a solution of **37** (50.0 mg, 40.0 *µ*mol) in THF (2 ml) $^{n}Bu_4NOH$ (15.6 mg, 60.0 *µ*mol, 1.5 M in H_2O) was added in the dark. After stirring the violet solution for 1 d at RT, the solvent was removed under reduced pressure. The dark violet residue was redissolved in CH_2Cl_2 (2 ml) and $AgNO_3$ (7.16 mg, 42.0 *µ*mol) was added and the mixture was stirred for 2.5 h at RT. The precipitated Ag was filtered off, and the solvent was removed under reduced pressure. The brown residue was purified by flash column-chromatography (CH_2Cl_2) and GPC (THF).

Formula: $C_{50}H_{22}Cl_{14}FeN_5$ [1244.93].
Yield: 31.0 mg (25.0 *µ*mol; 62 %) brown solid.
ESI pos. (high resolution): $[M+H_3O^+]$ = $C_{50}H_{25}Cl_{14}FeN_5O^+$; calcd for X+6: 1262.69660; found: 1262.69688 (*Δ* = 0.22 ppm).
Smp.: >305 °C (MeOH).

7.2.3 Redox Cascades with Saturated Spacer Units

Compound 40

CA: [226946-20-9]

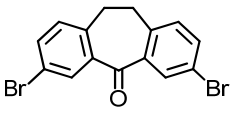

Synthesis according to literature[324]

$AlCl_3$ (8.80 g, 66.0 mmol) was added to Br_2 (28.8 g, 180.0 mmol) at 0°C. The suspension was stirred for 15 min and dibenzosuberone (6.25 g, 30.0 mmol) was added dropwise. The mixture was stirred for 30 min at 0°C and gradually warmed to RT. H_2O (30 ml) and sat. $Na_2S_2O_3$ solution (40 ml) was added carefully. After extraction with EtOAc (3 × 30 ml) the combined organic layers were dried over $MgSO_4$. The obtained yellow oil was purified by flash column-chromatography (PE/EtOAc 12.5:1).

Formula: $C_{15}H_{10}Br_2O$ [366.05].
Yield: 1.95 g (5.33 mmol; 18 %) white solid.
^{1}H-NMR (400.1 MHz, acetone-d_6): δ (ppm) = 8.05 (d, 2H, ^4J = 2.2 Hz), 7.68 (dd, 2H, ^3J = 8.1 Hz, ^4J = 2.2 Hz), 7.34 (d, 2H, ^3J = 8.2 Hz), 3.22 (s, 4H, CH_2).

Compound 41

CA: [1001909-72-3]

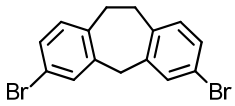

Synthesis according to literature[316]
$NaBH_4$ (1.68 g, 44.4 mmol) was suspended cautiously in TFA (60.7 g, 533 mmol, 41.0 ml) at 0°C. A solution of **40** (1.95 g; 5.33 mmol) in CH_2Cl_2 (50 ml) was added slowly at RT and the mixture was stirred for 12 h. An additional amount of $NaBH_4$ (840 mg; 22.2 mmol) was added and the solution was stirred for further 2 h. It was hydrolysed with water (100 ml) and extracted with CH_2Cl_2 (3 x 20 ml). The combined organic layers were washed with H_2O (2 x 40 ml) and dried over $MgSO_4$. The crude product was purified by flash column-chromatography (PE).
Formula: $C_{15}H_{12}Br_2$ [352.06].
Yield: 1.75 g (4.96 mmol; 93 %) white solid.
^{1}H-NMR (400.1 MHz, acetone-d_6): δ (ppm) = 7.44 (d, 2H, ^4J = 2.0 Hz), 7.30 (dd, 2H, ^3J = 8.1 Hz, ^4J = 2.2 Hz), 7.09 (d, 2H, ^3J = 8.1 Hz), 4.15 (s, 2H, CH_2), 3.14 (s, 4H, CH_2).

Compound 42

CA: [1001909-76-7]

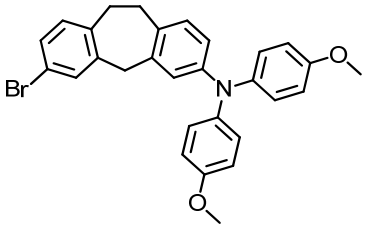

Synthesis according to literature[316]

41 (1.00 g, 2.84 mmol), 4,4'-dimethoxydiphenylamine (651 mg, 2.84 mmol), NaO^{t}Bu (409 mg, 4.26 mmol), $PdCl_2(PPh_3)_2$ (100 mg, 142 μmol), toluene (5 ml); 3 d at 95°C; flash column-chromatography (PE/EtOAc 40:1).

Formula: $C_{29}H_{26}BrNO_2$ [500.43].

Yield: 597 mg (1.19 mmol; 42 %) white solid.

^{1}H-NMR (400.1 MHz, acetone-d_6): δ (ppm) = 7.38 (d, 1H, ^4J = 2.2 Hz), 7.28 (dd, 1H, ^3J = 8.1 Hz, ^4J = 2.2 Hz), 7.09 (d, 1H, ^3J = 8.1 Hz), 6.98 – 6.94 (-, 5H), 6.86 (BB', 4H), 6.80 (d, 2H, ^4J = 2.3 Hz), 6.66 (dd, 1H, ^3J = 8.2 Hz, ^4J = 2.4 Hz), 4.00 (s, 2H, CH_2), 3.77 (s, 6H, OCH_3), 3.10 (-, 4H, CH_2).

Compound 42a

CA: [/]

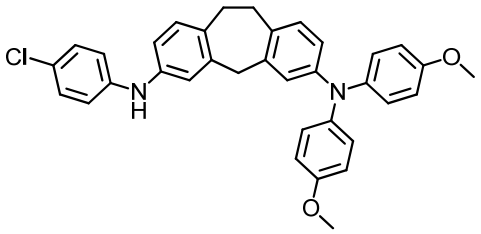

Synthesis according to GP1:

42 (70.0 mg, 140 μmol), 4-chloroaniline (17.8 mg, 140 μmol), NaO^{t}Bu (20.2 mg, 210 μmol), P^{t}Bu$_3$ (1.70 mg, 8.39 μmol, 1 M in toluene), $Pd_2(dba)_3 \cdot CHCl_3$ (5.79 mg, 5.60 μmol), toluene (3 ml); 4 d at 110°C; flash column-chromatography (PE/EtOAc 10:1).

Formula: $C_{35}H_{31}ClN_2O_2$ [547.09].

Yield: 32.9 mg (60.2 μmol; 43 %) light yellow solid.[1]

^{1}H-NMR (400.1 MHz, acetone-d_6): δ (ppm) = 7.35 (sb, 1H, NH), 7.17 (AA', 2H), 7.05 – 7.01 (-, 3H), 6.97 – 6.90 (-, 7H), 6.84 (BB', 4H), 6.77 (d, 1H, ^4J = 2.4 Hz), 6.66 (dd, 1H, ^3J = 8.2 Hz, ^4J = 2.5 Hz), 3.91 (s, 2H, CH_2), 3.76 (s, 6H, OCH_3), 3.07 (-, 4H, CH_2).

ESI pos. (high resolution): $[M^+] = C_{35}H_{31}ClN_2O_2^+$; calcd: 546.20686; found: 546.20687 (Δ = 0.02 ppm).

[1] The resulting solid still showed impurities in the ^{1}H-NMR spectrum. It was directly used for the next step without further purification.

Compound 42b

CA: [/]

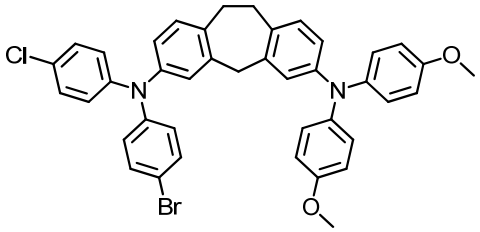

Synthesis according to GP5:

42a (390 mg, 713 *µ*mol), 4-bromoiodobenzene (1.61 mg, 5.70 mmol), KOH (320 mg, 5.70 mmol), 1,10-phenanthroline (5.14 mg, 29.0 *µ*mol), CuI (5.43 mg, 29.0 *µ*mol), toluene (4 ml); 1 d at 95°C; flash column-chromatography (PE/EtOAc 30:1 → 20:1).

Formula: $C_{41}H_{34}BrClN_2O_2$ [702.08].

Yield: 245 mg (349 *µ*mol; 49 %) light yellow solid.[1]

^{1}H-NMR (400.1 MHz, acetone-d_6): δ (ppm) = 7.38 (AA', 2H), 7.26 (AA', 2H), 7.10 (d, 1H, ^3J = 8.1 Hz), 7.01 – 6.90 (-, 10H), 6.86 – 6.82 (-, 5H), 6.74 (d, 1H, ^4J = 2.4 Hz), 6.66 (dd, 1H, ^3J = 8.2 Hz, ^4J = 2.5 Hz), 3.90 (s, 2H, CH_2), 3.77 (s, 6H, OCH_3), 3.11 (-, 4H, CH_2).

Compound 42c

CA: [/]

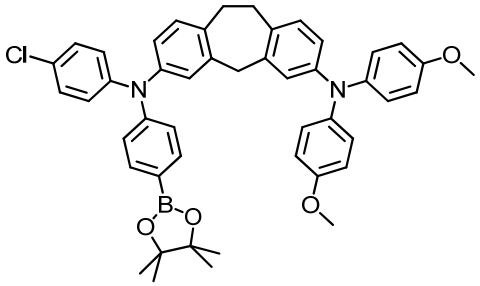

Synthesis according to GP2:

42b (215 mg, 306 *µ*mol), pinacolborane (40.0 mg, 312 *µ*mol, 45.3 *µ*l), Et_3N (31.6 mg, 312 *µ*mol, 43.9 *µ*l), P^tBu_3 (3.72 mg, 18.0 *µ*mol, 1 M in toluene), $Pd_2(dba)_3 \cdot CHCl_3$ (12.7 mg, 12.0 *µ*mol), 1,4-dioxane (5 ml); 1 d at 95°C; flash column-chromatography (PE/EtOAc 30:1).

Formula: $C_{47}H_{46}BClN_2O_4$ [749.14].

Yield: 105 mg (140 mmol; 46 %) yellow solid.[1]

[1] The resulting solid still showed impurities in the ^{1}H-NMR spectrum. It was directly used for the next step without further purification.

^{1}H-NMR (400.1 MHz, acetone-d_6): δ (ppm) = 7.60 (AA', 2H), 7.27 (AA', 2H), 7.10 (d, 1H, ^3J = 8.2 Hz), 7.01 (BB', 2H), 6.98 – 6.93 (-, 8H), 6.87 – 6.82 (-, 5H), 6.75 (d, 1H, ^4J = 2.4 Hz), 6.67 (dd, 1H, ^3J = 8.2 Hz, ^4J = 2.4 Hz), 3.90 (s, 2H, CH_2), 3.76 (s, 6H, OCH_3), 3.11 (-, 4H, CH_2), 1.32 (s, 12H, CCH_3)

Compound 43

CA: [/]

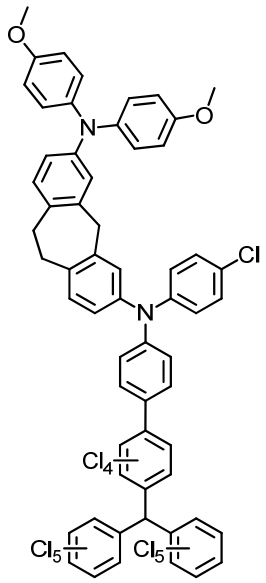

Synthesis according to GP3:
43c (100 mg, 133 μmol), **18** (108 mg, 133 μmol), Na_2CO_3 (39.6 mg, 374 μmol, 1 M in H_2O), $Pd(PPh_3)_4$ (3.09 mg, 2.67 μmol), toluene (3 ml); 2 d at 90°C; flash column-chromatography (PE/EtOAc 60:1). The so received brown solid was purified by GPC (THF).

Formula: $C_{60}H_{35}Cl_{15}N_2O_2$ [1347.72].
Yield: 29.0 mg (46.5 μmol; 16 %) light yellow solid.
^{1}H-NMR (600.1 MHz, THF-d_8): δ (ppm) = 7.23 (AA', 2H), 7.12 (s, 1H), 7.10 – 7.04 (-, 7H), 6.97 (d, 1H, ^4J = 2.3 Hz), 6.94 – 6.89 (-, 6H), 6.77 – 6.74 (-, 5H), 6.67 (dd, 1H, ^3J = 8.4 Hz, ^4J = 2.4 Hz), 3.89 (s, 2H), 3.71 (s, 6H, OCH_3), 3.09 (-, 4H).
^{13}C-NMR (150.9 MHz, THF-d_8): δ (ppm) = 156.8 (quart.), 148.9 (quart.), 147.9 (quart.), 147.3 (quart.), 145.6.0 (quart.), 143.2 (quart.), 142.3 (quart.), 141.7 (quart.), 140.4 (quart.), 137.8 (quart.), 137.7 (quart.), 137.6 (quart.), 136.8 (quart.), 136.11 (quart.), 136.10 (quart.), 135.5 (2 × quart.), 134.998 (quart.), 134.991 (quart.), 134.47 (2 × quart.), 134.45 (quart.), 134.435 (quart.), 134.426 (quart.), 134.28 (quart.), 133.34 (quart.), 133.33 (quart.), 132.7 (quart.), 131.7 (tert.)[1], 131.4 (quart.), 130.8 (tert.), 130.7 (tert.)[46], 130.6 (tert.), 130.2 (tert.), 128.7 (quart.), 127.2 (tert.),

[1] See Chapter 7.1 for explanation.

126.8 (tert.), 126.7 (tert.), 124.7 (tert.), 122.7 (tert.), 122.21 (tert.), 122.18 (tert.), 120.5 (tert.), 115.3 (tert.), 57.7 (tert.), 55.5 (prim.), 41.3 (sec.), 33.3 (sec.), 32.7 (sec.).

ESI pos. (high resolution): $[M^+]$ = $C_{60}H_{35}Cl_{15}N_2O_2^+$; calcd for X+8: 1347.79215; found: 1347.79169 (Δ = 0.34 ppm).

Compound 44

CA: [/]

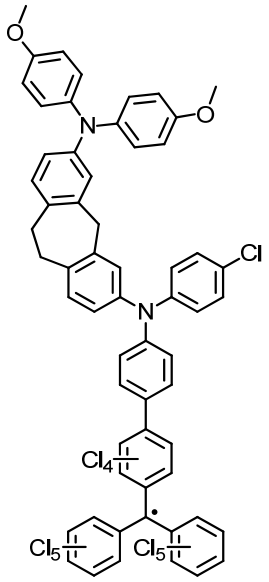

To a solution of **43** (29.0 mg, 22.0 μmol) in THF (2 ml) ^{n}Bu$_4$NOH (12.3 mg, 47.0 μmol, 1.5 M in H_2O) was added in the dark. After stirring the violet solution for 1 h, PCA (13.8 mg, 56.0) was added and the mixture was stirred overnight. The solvent was removed *in vacuo* and the residue was dissolved in ^{t}BME (3 ml). The solution was washed with H_2O (4 × 3 ml) and dried over Na_2SO_4. After removing the solvent under reduced pressure the residue was purified by flash column-chromatography (PE/EtOAc 35:1).

Formula: $C_{60}H_{34}Cl_{15}N_2O_2$ [1346.72].
Yield: 12.0 mg (8.91 μmol; 30 %) dark brown solid.
ESI pos. (high resolution): $[M^+]$ = $C_{60}H_{34}Cl_{15}N_2O_2^+$; calcd for X+8: 1346.78432; found: 1346.78492 (Δ = 0.45 ppm).

Compound 45

CA: [622-50-4]

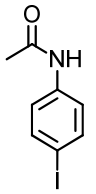

Synthesis according to literature[325]:
To a solution of 4-iodoaniline (1.50 g, 6.85 mmol) and Et_3N (2.08 g, 20.6 mmol) in CH_2Cl_2 (10 ml), acetic anhydride (2.10 g, 20.6 mmol) was added dropwise at 0°C. The mixture was stirred for 10 min at 0°C and 2 h at RT. The volatile materials were removed under reduced pressure and the obtained white residue was dissolved in hot CH_2Cl_2 (5 ml) and filtered. The so received solid was recrystallised from acetone.

Formula: C_8H_8NO [261.06].
Yield: 1.35 g (5.17 mmol; 76 %) colourless solid.
^{1}H-NMR (400.1 MHz, dimethylsulfoxide-d_6): δ (ppm) = 10.01 (sb, 1H, N*H*), 7.62 (AA', 2H), 7.42 (BB', 2H), 2.04 (s, 3H, CH_3).

Compound 46

CA: [214360-60-8]

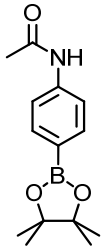

Synthesis according to GP2:
45 (600 mg, 2.30 mmol), pinacolborane (300 mg, 2.34 mmol), Et_3N (237 mg, 2.34 mmol), P^{t}Bu$_3$ (27.9 mg, 138 μmol, 1 M in toluene), $Pd_2(dba)_3 \cdot CHCl_3$ (95.2 mg, 91.9 μmol), 1,4-dioxane (5 ml); 2 d at 75°C; flash column-chromatography (AlO_x) (PE → PE/CH_2Cl_2 1:1 → CH_2Cl_2).

Formula: $C_{14}H_{20}BNO_3$ [261.12].
Yield: 250 mg (957 μmol; 42 %) light yellow solid.
^{1}H-NMR (400.1 MHz, chloroform-d_3): δ (ppm) = 7.76 (AA', 2H), 7.62 (BB', 2H), 7.18 (sb, 1H), 2.18 (s, 3H), 1.33 (s, 12H).

Compound 47

CA: [/]

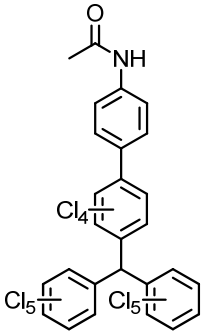

Synthesis according to GP3:
46 (675 mg, 2.58 mmol), **18** (2.08 g, 2.58 mmol), Na_2CO_3 (766 mg, 7.22 mmol, 1 M in H_2O), $Pd(PPh_3)_4$ (59.7 mg, 52.0 *µ*mol), toluene (40 ml); 3 d at 110°C; flash column-chromatography (AlO_x) (PE → PE/EtOAc 5:1). The so received white solid was purified by GPC (THF).

Formula: $C_{27}H_9Cl_{14}NO$ [859.71].
Yield: 500 mg (582 *µ*mol; 23 %) white solid.
^{1}H-NMR (400.1 MHz, dichloromethane-d_2): *δ* (ppm) = 7.66 – 7.64 (m, 2H), 7.39 (sb, 1H, N*H*), 7.22 – 7.20 (m, 2H), 7.08 (s, 1H), 2.17 (s, 3H, CH_3).
^{13}C-NMR (100.6 MHz, dichloromethane-d_2): *δ* (ppm) = 168.7 (quart.), 141.8 (quart.), 139.1 (quart.), 137.4 (quart.), 137.1 (2 × quart.), 135.6 (quart.), 135.5 (quart.), 135.1 (quart.), 134.7 (quart.), 134.5 (2 × quart.), 134.1 (quart.), 134.04 (quart.), 134.02 (quart.), 133.97 (quart.), 133.9 (quart.), 133.7 (quart.), 133.5 (quart.), 132.9 (2 × quart.), 130.2 (tert.), 130.0 (tert.), 119.9 (2 × tert.), 57.1 (tert.), 24.8 (prim.).
MALDI-MS: calcd for $C_{27}H_8Cl_{14}NO^+$: 857.616; found: 857.602.

Compound 48

CA: [/]

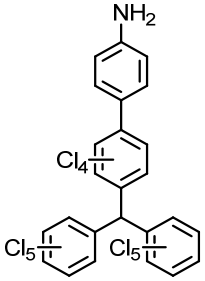

Synthesis according to literature[326]:

Compound **47** (408 mg, 499 mmol) was dissolved in EtOH (158 g, 3.43 mol, 200 ml) and HCl conc. (118 g, 3.27 mol, 100 ml) was added carefully. The mixture was heated to 105°C for 5 h. After cooling to RT the solution was neutralised with NaOH and dissolved with EtOAc. Subsequently the phases were separated, the organic phase was washed with H_2O (3 × 100 ml) and dried over Na_2SO_4. The solvent was removed under reduced pressure and the so received white solid was purified by GPC (THF).

Formula: $C_{25}H_7Cl_{14}N$ [817.67].
Yield: 408 mg (499 mol; 95 %) white solid.
^{1}H-NMR (400.1 MHz, dichloromethane-d_2): δ (ppm) = 7.07 (s, 1H), 7.03 – 6.70 (m, 2H), 6.77 (m, 2H), 3.91 (sb, 2H, NH_2).
^{13}C-NMR (100.6 MHz, dichloromethane-d_2): δ (ppm) = 147.6 (quart.), 142.6 (quart.), 137.18 (quart.), 137.16 (quart.), 136.8 (quart.), 135.6 (quart.), 135.5 (quart.), 135.1 (quart.), 134.9 (quart.), 134.54 (quart.), 134.52 (quart.), 134.1 (quart.), 133.97 (quart.), 133.96 (quart.), 133.95 (quart.), 133.94 (quart.), 133.9 (quart.), 132.89 (quart.), 132.87 (quart.), 130.5 (tert.), 130.4 (tert.), 127.7 (quart.), 114.86 (tert.), 114.84 (tert.), 57.1 (tert.).
MALDI-MS: calcd for $C_{25}H_7Cl_{14}N^+$: 816.613; found: 816.663.

Compound 48a

CA: [/]

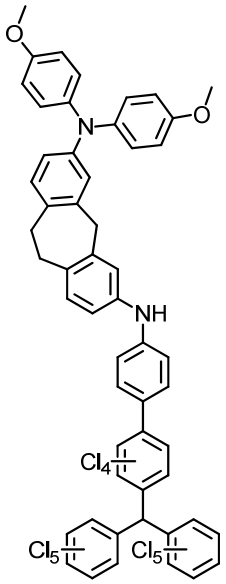

Synthesis according to GP1:
48 (310 mg, 380 mmol), **42** (190 mg, 380 mmol), NaO^{t}Bu (54.7 mg, 570 mmol), P^{t}Bu$_3$ (4.61 mg, 23.0 μmol, 1 M in toluene), $Pd_2(dba)_3 \cdot CHCl_3$ (15.7 mg, 15.0 μmol), toluene (7 ml); 3 d at 60°C; flash column-chromatography (PE/EtOAc 25:1 → 15:1).

Formula: $C_{54}H_{32}Cl_{14}N_2O_2$ [1237.19].

Yield: 316 mg (255 mmol; 67 %) yellow solid.[1]

^{1}H-NMR (400.1 MHz, acetone-d_6): δ (ppm) = 7.50 (sb, 1H, N*H*), 7.18 – 6.94 (-, 13H), 6.85 (BB', 4H), 6.79 (d, 1H, ^4J = 2.5 Hz), 6.67 (dd, 1H, ^3J = 8.2 Hz, ^4J = 2.6 Hz), 3.96 (s, 2H), 3.76 (s, 6H, OCH_3), 3.10 (-, 4H).

Compound 48b

CA: [/]

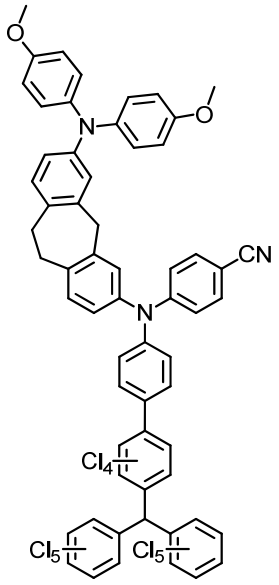

Compound **48a** (215 mg, 174 mmol), 4-iodobenzonitrile (59.7 mg, 261 mmol), Cs_2CO_3 (50.3 mg, 261 μmol) and Xantphos (1.51 mg, 2.61 μmol) were suspended in 1,4-dioxane (4 ml). After degassing the mixture for 10 min, $Pd(OAc)_2$ (390 μg, 1.74 μmol) was added. The reaction mixture was heated to 75°C for 2 d. The solvent was removed *in vacuo* and the residue was purified by flash column-chromatography (PE/CH_2Cl_2 2:1 → CH_2Cl_2) and subsequently by GPC (THF). The resulting white solid was still impure as indicated by ^{1}H-NMR spectroscopy. Therefore only ^{1}H-NMR data will be given.

Formula: $C_{61}H_{35}Cl_{15}N_3O_2$ [1338.29].

Yield: 65.0 mg (49.0 μmol; 40 %) white solid.

^{1}H-NMR (400.1 MHz, acetone-d_6): δ (ppm) = 7.56 (AA', 2H), 7.36 – 7.27 (-, 4H), 7.22 (d, 1H, ^3J = 8.2 Hz), 7.15 (s, 1H), 7.13 (d, 1H, ^4J = 2.1 Hz), 7.05 – 6.93 (-, 8H), 6.84 (BB', 4H), 6.76 (d, 1H, ^4J = 2.5 Hz), 6.68 (dd, 1H, ^3J = 8.2 Hz, ^4J = 2.4 Hz), 3.97 (s, 2H), 3.76 (s, 6H, OCH_3), 3.16 (-, 4H).

[1] The resulting solid still showed impurities in the ^{1}H-NMR spectrum. It was directly used for the next step without further purification.

7.2.4 Precursors and Reference Compounds

Compound 23

CA: [58047-42-0]

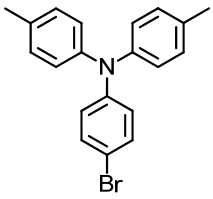

Synthesis according to GP5:
4-Iodotoluene (5.58 g, 25.6 mmol), 4-bromoaniline (2.00 g, 11.6 mmol), 1,10-phenanthroline (84.0 mg, 465 *µ*mol), KOH (5.22 g, 93.0 mmol), CuI (89.0 mg, 465 *µ*mol); toluene (30 ml), 2 d at 110°C; flash column-chromatography (PE → PE/EtOAc 500:1).

Formula: $C_{20}H_{18}BrN$ [352.27].
Yield: 1.99 g (5.65 mmol; 49 %) white solid.
^{1}H-NMR (400.1 MHz, acetone-d_6): δ (ppm) = 7.35 (AA', 2H), 7.13 (AA', 4H), 6.96 (BB', 4H), 6.86 (BB', 2H), 2.30 (s, 6H).

Compound 24

CA: [194416-45-0]

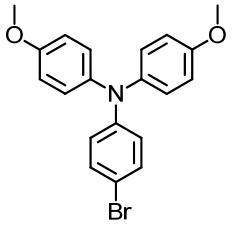

Synthesis according to GP5:
4-Iodoanisole (14.3 g, 61.0 mmol), 4-bromoaniline (5.00 g, 29.1 mmol), 1,10-phenanthroline (209 mg, 1.16 mmol), KOH (12.7 g, 227 mmol), CuI (160 mg, 1.16 mmol); toluene (30 ml), 2 d at 110°C; flash column-chromatography (PE/CH_2Cl_2 2:1).

Formula: $C_{20}H_{18}BrNO_2$ [484.27].
Yield: 9.58 g (19.8 mmol; 68 %) beige solid.
^{1}H-NMR (400.1 MHz, acetone-d_6): δ (ppm) = 7.29 (AA', 2H), 7.06 (AA', 4H), 6.92 (BB', 4H), 6.75 (BB', 2H), 3.79 (s, 6H).

Compound 25

CA: [54480-44-3]

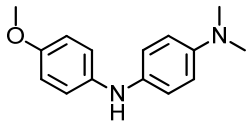

Synthesis according to GP1:
4-Bromo-*N*,*N*-dimethylamine (1.63 g, 8.12 mmol), 4-methoxyaniline (1.00 g, 8.12 mmol), NaO^{t}Bu (1.17 g, 12.2 mmol), P^{t}Bu$_3$ (99.0 mg, 487 µmol, 1 M in toluene), $Pd_2(dba)_3 \cdot CHCl_3$ (336 mg, 325 µmol), toluene (20 ml); 1 d at 40°C; flash column-chromatography (PE/EtOAc 10:1).

Formula: $C_{15}H_{18}N_2O$ [242.32].
Yield: 1.46 g (6.01 mmol; 74 %) beige solid.
^{1}H-NMR (400.1 MHz, acetone-d_6): δ (ppm) = 6.96 (AA', 2H), 6.91 (AA', 2H), 6.78 (BB', 2H), 6.72 (BB', 2H), 7.55 (sb, 1H, N*H*), 3.72 (s, 3H), 2.85 (s, 6H).

Compound 26

CA: [/]

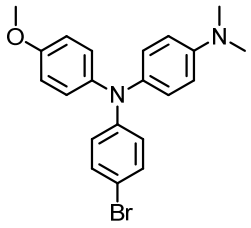

Synthesis according to GP5:
25 (800 mg, 3.30 mmol), 4-bromo-1-iodobenzene (934 mg, 3.30 mmol), 1,10-phenanthroline (23.8 mg, 132 µmol), KOH (1.48 g, 26.4 mmol), CuI (25.2 mg, 132 µmol); toluene (10 ml); 2 d at 90°C; flash column-chromatography (PE/EtOAc 60:1 → 40:1 → 20:1).

Formula: $C_{21}H_{21}BrN_2O$ [397.31].
Yield: 630 mg (1.58 mmol; 48 %) yellow solid.
^{1}H-NMR (400.1 MHz, benzene-d_6): δ (ppm) = 7.19 (AA', 2H), 7.07 (AA', 2H), 7.04 (AA', 2H), 6.84 (BB', 2H), 6.71 (BB', 2H), 6.52 (BB', 2H), 3.30 (s, 3H), 2.49 (s, 6H).

Compound 27

CA: [/]

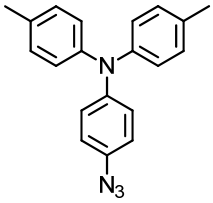

Synthesis according to GP6:

23 (1.00 g, 2.84 mmol), NaN_3 (369 mg, 5.68 mmol), *N*,*N'*-dimethylethylenediamine (38.0 mg, 426 *µ*mol), (+)-sodium-L-ascorbate (28.0 mg, 142 *µ*mol), CuI (54.0 mg, 284 *µ*mol), EtOH/H_2O (7:3, 50 ml); 5 h at 105°C, 12 h at RT; flash column-chromatography (PE).

Formula: $C_{20}H_{18}N_4$ [314.38].

Yield: 615 mg (2.07 mmol; 73 %) orange solid.

^{1}H-NMR (400.1 MHz, chloroform-d_1): *δ* (ppm) = 7.05 (AA', 4H), 7.02 (AA', 2H), 6.95 (BB', 4H), 6.87 (BB', 2H), 2.31 (s, 6H).

Compound 28

CA: [/]

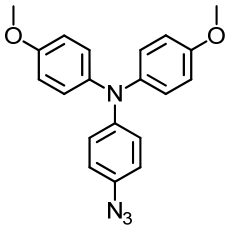

Synthesis according to GP6:

24 (1.00 g, 2.60 mmol), NaN_3 (338 mg, 5.20 mmol), *N*,*N'*-dimethylethylenediamine (34.0 mg, 390 *µ*mol), (+)-sodium-L-ascorbate (26.0 mg, 130 *µ*mol), CuI (50.0 mg, 260 *µ*mol), EtOH/H_2O (7:3, 50 ml); 5 h at 105°C, 12 h at RT; flash column-chromatography (PE/EtOAc 30:1 → 20:1).

Formula: $C_{20}H_{18}N_4O_2$ [346.38].

Yield: 537 mg (996 *µ*mol; 68 %) orange oil.

^{1}H-NMR (400.1 MHz, chloroform-d_1): *δ* (ppm) = 7.01 (AA', 4H), 6.93 (AA', 2H), 6.86 – 6.80 (-, 6H), 3.79 (s, 6H).

Compound 29

CA: [/]

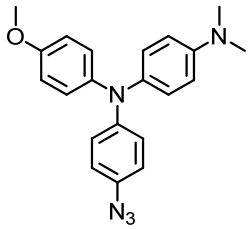

Synthesis according to GP6:
26 (630 mg, 1.59 mmol), NaN_3 (206 mg, 3.17 mmol), *N*,*N'*-dimethylethylenediamine (21.0 mg, 238 *µ*mol), (+)-sodium-L-ascorbate (15.7 mg, 79.0 *µ*mol), CuI (30.2 mg, 159 *µ*mol), EtOH/H_2O (7:3, 30 ml); 5 h at 105°C, 1 h at RT; flash column-chromatography (PE/EtOAc 10:1). The ^{1}H-NMR spectrum shows **26** as an impurity in a quantity of about 10 %. Despite several attempts **26** could not be removed, hence the brown solid was used as received for the next step.

Formula: $C_{21}H_{21}N_5O$ [359.42].
Yield: 366 mg (1.02 mmol; 64 %) brown solid.
^{1}H-NMR (400.1 MHz, benzene-d_6): δ (ppm) = 7.11 (AA', 2H), 7.09 (AA', 2H), 6.98 (AA', 2H), 6.74 (BB', 2H), 6.69 (BB', 2H), 6.56 (BB', 2H), 3.31 (s, 3H), 2.51 (s, 6H).

Compound 30

CA: [1273-77-4]

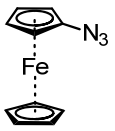

Synthesis according to literature[319,320]:
To a mixture of bromoferrocene (500 mg, 1.89 mmol) and CuCl (218 mg, 1.17 mmol) in EtOH (12 ml) was added a solution of NaN_3 (241 mg, 1.97 mmol) in H_2O (1.2 ml). The light green suspension was stirred for 48 h in the dark meanwhile it turned dark brown. Afterwards the mixture was extracted with Et_2O (3 × 10 ml) and the combined organic fractions were washed with water (3 × 15 ml) and dried over Na_2SO_4. The solvent was removed *in vacuo* to afford an orange solid, which was stored in *n*-hexane (10 ml) in the fridge.

Formula: $C_{10}H_9FeN_3$ [227.04].

Yield: 310 mg (1.37 mmol; 72 %) orange solid.
^{1}H-NMR (400.1 MHz, benzene-d_6): δ (ppm) = 4.02 (s, 5H), 4.00 (-, 2H, ^3J = 1.9 Hz), 3.67 (-, 2H, ^3J = 1.9 Hz).

Compound 31

CA: [622-37-7]

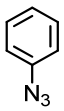

HCl conc. (820 mg, 22.6 mmol) was slowly added to a suspension of aniline (1.00 g, 10.7 mmol) in H_2O (12 ml) at 0°C. Afterwards a cooled solution of $NaNO_2$ (740 mg, 10.7 mmol) in H_2O (3 ml) and a solution of NaN_3 (700 mg, 10.7 mmol) in H_2O (4 ml) were added carefully. During addition the temperature was kept between 0 – 5°C. The light orange suspension was stirred for 1 h at 0°C and 3 h at RT. The mixture was diluted with *n*-hexane (10 ml), washed with H_2O (3 × 15 ml) and dried over Na_2SO_4. The solvent was removed *in vacuo* and the residue was dissolved in *n*-hexane (10 ml) and stored in the fridge.

Formula: $C_6H_5N_3$ [119.12].
Yield: 1.15 g (9.63 mmol; 90 %) yellow oil.
^{1}H-NMR (400.1 MHz, acetone-d_6): δ (ppm) = 7.44 – 7.39 (m, 2H), 7.21 – 7.17 (m, 1H), 7.11 – 7.08 (m, 2H).

Compound 39a

CA: [/]

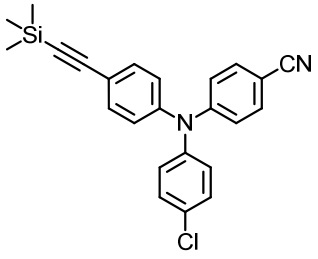

Compound **39a** (90.0 mg, 209 μmol), TMSA (20.5 mg, 209 μmol, 29.0 μl), $PdCl_2(PhCN)_2$ (2.41 mg, 6.27 μmol) and CuI (796 μg, 4.18 μmol) were suspended in 1,4-dioxane (3 ml). After degassing the mixture for 5 min, P^tBu_3 (2.54 mg, 13.0 μmol, 1 M in toluene) and $^iPr_2NH$ (23.3 mg, 230 μmol, 32.0 μl) were added. The reaction mixture was heated to 75°C for 1 d. The

solvent was removed *in vacuo* and the residue was purified by flash column-chromatography (PE/EtOAc 300:1 → 200:1).

Formula: $C_{24}H_{21}ClN_2Si$ [400.98].

Yield: 70.0 mg (175 *µ*mol; 84 %) yellow solid.[1]

^{1}H-NMR (400.1 MHz, acetone-d_6): *δ* (ppm) = 7.62 (AA', 2H), 7.47 – 7.41 (2 × AA', 4H), 7.21 (BB', 2H), 7.14 (BB', 2H), 7.10 (BB', 2H), 0.23 (s, 9H).

Compound 39b

CA: [/]

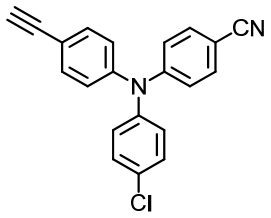

To a solution of **39b** (70.0 mg, 175 *µ*mol) in THF (3 ml) ^{n}Bu$_4$NF (60.0 mg, 192 *µ*mol, 1 M in THF) was added dropwise at RT. The violet solution was stirred overnight and the solvent was removed *in vacuo*. ^{t}BME (5 ml) was added, the solution was washed with brine (1 × 3 ml) and H_2O (4 × 3 ml) and dried over Na_2SO_4. The solvent was removed under reduced pressure.

Formula: $C_{21}H_{13}ClN_2$ [328.79].

Yield: 50.0 mg (152 *µ*mol; 87 %) yellow solid.[1]

^{1}H-NMR (400.1 MHz, acetone-d_6): *δ* (ppm) = 7.63 (AA', 2H), 7.49 (AA', 2H), 7.44 (AA', 2H), 7.21 (BB', 2H), 7.16 (BB', 2H), 7.10 (BB', 2H), 3.65 (s, 1H).

Compound 39

CA: [/]

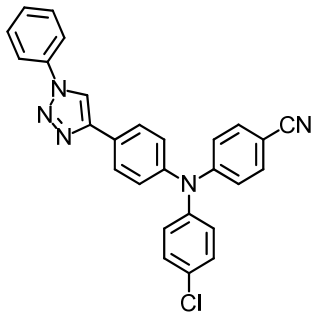

Synthesis according to GP4:

[1] The resulting solid still showed impurities in the 1H-NMR spectrum. It was directly used for the next step without further purification.

39c (50.0 mg, 152 *µ*mol), **31** (18.1 mg, 152 *µ*mol), $CuBr(PPh_3)_3$ (28.3 mg, 30.0 *µ*mol), $^iPr_2NEt$ (19.7 mg, 152 *µ*mol, 26.0 *µ*l), THF (2 ml); 3 d at 40°C; flash column-chromatography (PE/EtOAc 50:1 → 20:1 → 10:1 → 5:1). The resulting yellow solid was purified by GPC (THF) and recrystallised from *n*-hexane/EtOAc 1:1.

Formula: $C_{27}H_{18}ClN_5$ [447.92].
Yield: 10.0 mg (22.3 *µ*mol; 15 %) colourless solid.
^{1}H-NMR (400.1 MHz, acetone-d_6): δ (ppm) = 9.00 (s, 1H), 8.03 (AA', 2H), 7.99 – 7.96 (m, 2H), 7.66 – 7.60 (-, 4H), 7.52 (m, 1H), 7.44 (AA', 2H), 7.31 (BB', 2H), 7.26 (BB', 2H), 7.10 (BB', 2H).
^{13}C-NMR (100.6 MHz, acetone-d_6): δ (ppm) = 152.1 (quart.), 148.2 (quart.), 146.6 (quart.), 145.8 (quart.), 138.2 (quart.), 134.3 (tert.), 130.9 (tert.), 130.8 (tert.), 130.7 (quart.), 129.5 (tert.), 128.8 (quart.), 128.5 (tert.), 128.1 (tert.), 127.3 (tert.), 121.4 (tert.), 121.0 (tert.), 119.8 (quart.), 119.5 (tert.), 104.5 (quart.).
ESI pos. (high resolution): $[M+H^+]$ = $C_{27}H_{19}ClN_5^+$; calcd: 448.13235; found: 448.13262 (Δ = 0.60 ppm).

Compound 17

CA: [5410-05-9]

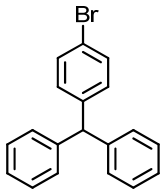

Synthesis according to literature[315]:
A solution of bromobenzene (23.4 g, 149 mmol) in Et_2O (150 ml) was added dropwise to magnesium fillings (4.00 g, 165 mmol). The mixture was stirred 30 min at RT and 90 min under reflux. After cooling to RT, 4-bromobenzophenone (24.7 g, 94.6 mmol) in Et_2O (200 ml) was added over a period of 45 min. The reaction mixture was heated under reflux for another 60 min. The resulting reddish suspension was cooled down to RT and mixed with crushed ice (30 g). Afterwards HCl (7 M) was added until a pH of 3 was reached. The aqueous phase was extracted with Et_2O (3 × 100 ml) and the combined organic phases were subsequently washed with sat. $NaHCO_3$ solution (80 ml) and H_2O (80 ml). After drying the solution over $MgSO_4$ the solvent was removed under reduced pressure. Formic acid (60 ml) was added to the resulting yellow oil and the mixture was heated under reflux for 18 h. The solution was cooled to RT, H_2O (200 ml) and Et_2O (50 ml) were added and the phases were separated. The aqueous phase was extracted with Et_2O (2 × 50 ml) and the combined organic phases were washed with NaOH (2 M) until a slight basic reaction of the aqueous phase occurred. Subsequently the organic

phase was washed with H_2O (2 × 40 ml). The solvent was removed under reduced pressure and the resulting brown solid was recrystallised twice from EtOAc.

Formula: $C_{19}H_{15}Br$ [323.23].

Yield: 11.4 g (35.3 mmol; 37 %) light brown solid.

^{1}H-NMR (400.1 MHz, acetone-d_6): δ (ppm) = 7.49 (AA', 2H), 7.34 – 7.30 (-, 4H), 7.26 – 7.21 (-, 2H), 7.16 – 7.13 (-, 4H), 7.10 (BB', 2H), 5.64 (s, 1H).

Compound 18

CA: [937739-64-5]

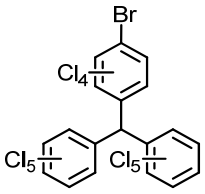

Synthesis according to literature[315]:

A mixture of $AlCl_3$ (2.38 g, 17.8 mmol) and S_2Cl_2 (4.69 g, 34.7 mmol) in SO_2Cl_2 (450 ml) was heated to 70°C, followed by the dropwise addition of a solution of **17** (14.8 g, 45.7 mmol) in SO_2Cl_2 (250 ml) over a period of 1 h. The colour of the reaction mixture changed from cloudy orange to red to clear dark brown. After the reaction was heated for 8 h, the solvent was removed by distillation; first at atmospheric pressure, then *in vacuo*. The resulting dark brown solid was suspended in H_2O (700 ml) and $NaHCO_3$ was added until no gas evolved. The mixture was heated under reflux for 1 h and cooled to RT, whereupon conc. HCl was added until a pH of 1 was reached. The resulting grey solid was filtered off and was washed thoroughly with water to removed traces of acid. The crude product was repeatedly heated in *n*-hexane and filtered off, until the *n*-hexane remained colourless. The resulting grey solid was washed with acetone (600 ml), ^{t}BME (300 ml) and with boiling *n*-hexane (300 ml). The ^{1}H-NMR data showed that the received grey solid was not fully chlorinated, so the reaction was accomplished for a second time the way it was described above.

Formula: $C_{19}HCl_{14}Br$ [805.46].

Yield: 17.7 g (21.9 mmol; 48 %) light grey solid.

^{1}H-NMR (400.1 MHz, acetone-d_6): δ (ppm) = 6.98 (s, 1H).

APCI neg. (high resolution): $[M^-]$ = $C_{19}Cl_{14}Br^-$; calcd for X+8: 804.47168; found: 804.47293 (Δ = 1.55 ppm).

Compound 38

CA: [79855-16-6]

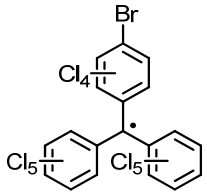

To a solution of **18** (200 mg, 248 *µ*mol) in THF (12 ml) $^{n}Bu_4NOH$ (193 mg, 745 *µ*mol, 1.5 M in H_2O) was added in the dark. After stirring the violet solution for 1 d at RT, PCA (214 mg, 869 *µ*mol) was added and the mixture was stirred for 2 d. The solvent was removed *in vacuo* and the residue was purified by flash column-chromatography (*n*-hexane → CH_2Cl_2) and GPC ($CHCl_3$).

Formula: $C_{19}Cl_{14}Br$ [804.45].
Yield: 56.0 mg (69.6 mmol; 28 %) dark red solid.
APCI neg. (high resolution): $[M^-]$ = $C_{19}Cl_{14}Br^-$; calcd for X+8: 804.47168; found: 804.47100 (Δ = 0.85 ppm).

7.2.5 Synthesis of Diketopyrrolopyrroles

Compound 49

CA: [924-88-9]

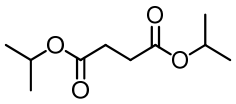

A mixture of $^{i}PrOH$ (36.8 g, 613 mmol) and pyridine (36.4 g, 460 mmol) in CH_2Cl_2 (40 ml) was cooled to –10°C. Succinyl chloride was slowly added dropwise, whereas the temperature was kept at –10°C. After warming up to RT, the solution was stirred overnight. H_2O (50 ml) was carefully added and the layers were separated. The aqueous layer was extracted with CH_2Cl_2 (3 × 40 ml). After removing the solvent *in vacuo*, the colourless solid was distilled under reduced pressure.
Formula: $C_{10}H_{18}O_4$ [202.25].
Yield: 24.7 g (122 mmol; 80 %) colourless liquid.
^{1}H-NMR (400.1 MHz, acetone-d_6): δ (ppm) = 4.95 (sept, 2H, C*H*), 2.60 – 2.51 (-, 4H, CH_2), 1.20 (d, 12H, CH_3).

Compound 50

CA: [84632-54-2]

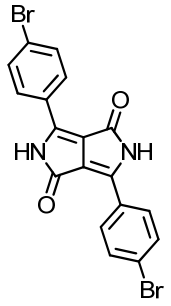

Synthesis according to literature[329]:
Sodium (632 mg, 27.5 mol) was carefully dissolved in ^{t}pentyl alcohol (20 ml). After addition of $FeCl_3$ (27.0 mg, 165 *µ*mol), the mixture was heated to 90°C until the sodium was completely dissolved. Subsequently, the solution was cooled to 50°C and 4-bromobenzonitrile (2.50 g, 13.7 mmol) was added in one portion. **49** (1.11 g, 5.49 mmol) was dissolved in ^{t}pentyl alcohol (20 ml) and slowly added (~1.5 h) at 90°C. After 3 h at 90°C the mixture was cooled to RT and stirred overnight. The deep red precipitate was filtered of, washed thoroughly with MeOH and H_2O to remove residual reactants and dried in air. Since the solid is insoluble in common solvents, a characterisation *via* NMR spectroscopy was not viable.

Formula: $C_{18}H_{10}Br_2N_2O_2$ [446.09].
Yield: 2.10 g (4.71 mmol; 86 %) red solid.
MALDI-MS: calcd for $C_{10}H_{18}Br_2N_2O_2^+$: 445.908; found: 445.906.

Compound 51

CA: [852434-82-3]

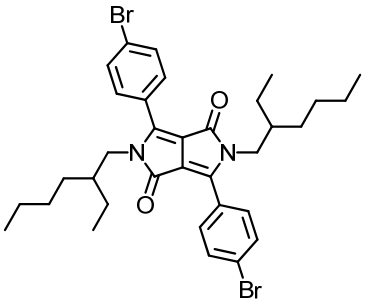

Synthesis according to literature[329]:
Compound **50** (800 mg, 1.79 mmol) was suspended in DMF (10 ml). 18-crown-6 (4.74 mg, 18.0 *µ*mol) and K_2CO_3 (867 mg, 6.28 mmol) were added and the mixture was heated to 120°C. After

dropwise addition of 2-ethylhexyl bromide (1.21 g, 6.28 mmol), the mixture was stirred for 3 d at 90°C. Unreacted **50** was filtered off and the orange solution was washed with H_2O (3 × 10 ml). The solvent was removed *in vacuo* and the brown residue was purified by flash column-chromatography (PE/CH_2Cl_2 8:1 → 2:1 → CH_2Cl_2).

Formula: $C_{34}H_{42}Br_2N_2O_2$ [670.52].
Yield: 170 g (254 *µ*mol; 14 %) bright yellow solid.
^{1}H-NMR (400.1 MHz, acetone-d_6): *δ* (ppm) = 7.87 (AA', 4H), 7.80 (BB', 4H), 3.79 (-, 4H, NC*H*$_2$), 1.41 (-, 2H, C*H*), 1.23 – 1.08 (-, 16H), 0.80 (t, 6H, C*H*$_3$), 0.72 (t, 6H, C*H*$_3$).

Compound 52

CA: [/]

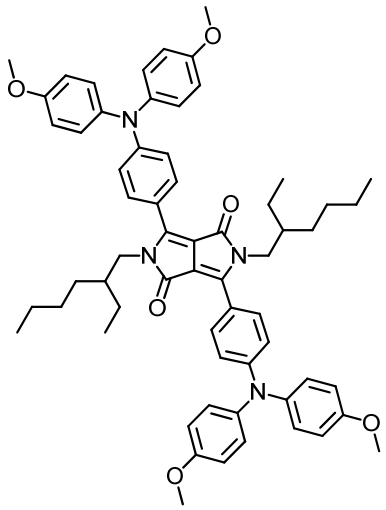

Synthesis according to GP1:
51 (150 mg, 224 *µ*mol), 4,4'-dimethoxydiphenylamine (51.3 mg, 224 *µ*mol), NaO^{t}Bu (32.2 mg, 336 *µ*mol), P^{t}Bu$_3$ (2.72 mg, 13.0 *µ*mol, 1 M in toluene), $Pd_2(dba)_3 \cdot CHCl_3$ (9.26 mg, 8.95 *µ*mol), toluene (7 ml); 2 d at 50°C; flash column-chromatography (PE/EtOAc 7:1 → 5:1).

Formula: $C_{62}H_{70}N_4O_6$ [967.23].
Yield: 23.0 mg (23.8 *µ*mol; 8 %) violet solid.
^{1}H-NMR (400.1 MHz, acetone-d_6): *δ* (ppm) = 7.81 (AA', 4H), 7.19 (AA', 8H), 6.99 (BB', 8H), 6.86 (BB', 4H), 3.85 – 3.78 (-, 16H, NC*H*$_2$, OC*H*$_3$), 1.56 (-, 2H, C*H*), 1.25 – 1.13 (-, 16H), 0.84 (t, 6H, C*H*$_3$), 0.76 (t, 6H, C*H*$_3$).
^{13}C-NMR (150.9 MHz, acetone-d_6): *δ* (ppm) = 163.4 (quart.), 158.3 (quart.), 151.9 (quart.), 147.6 (quart.), 140.2 (quart.), 130.9 (tert.), 128.8 (tert.), 120.1 (quart.), 117.8 (tert.), 115.9 (tert.), 109.3

(quart.), 55.8 (prim., O*C*H$_3$), 45.4 (sec., N*C*H$_2$), 39.3 (tert.), 31.2 (sec.), 29.1 (sec.), 24.6 (sec.), 23.5 (sec.), 14.3 (prim., C*C*H$_3$), 10.9 (prim., C*C*H$_3$).

ESI pos. (high resolution): [M$^+$] = $C_{62}H_{70}N_4O_6^+$; calcd: 966.52899; found: 966.53016 (Δ = 1.21 ppm).

Compound 53

CA: [/]

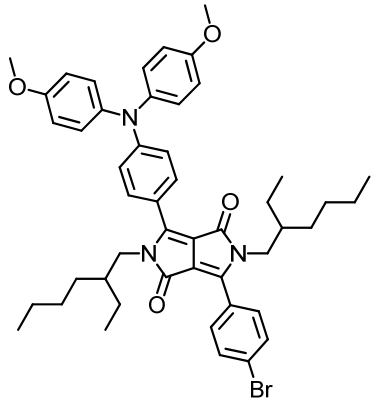

Synthesis according to GP1:

51 (150 mg, 224 μmol), 4,4'-dimethoxydiphenylamine (51.3 mg, 224 μmol), NaO^{t}Bu (32.2 mg, 336 μmol), P^{t}Bu$_3$ (2.72 mg, 13.0 μmol, 1 M in toluene), $Pd_2(dba)_3 \cdot CHCl_3$ (9.26 mg, 8.95 μmol), toluene (7 ml); 2 d at 50°C; flash column-chromatography (PE/EtOAc 7:1 → 5:1).

Formula: $C_{48}H_{56}BrN_3O_4$ [818.88].

Yield: 30.0 mg (37.0 μmol; 16 %) pink solid.

^{1}H-NMR (400.1 MHz, acetone-d_6): δ (ppm) = 7.87 (AA', 2H), 7.84 (AA', 2H), 7.76 (BB', 2H), 7.22 (AA', 4H), 7.00 (BB', 4H), 6.87 (BB', 2H), 3.86 – 3.76 (-, 10H, NC*H*$_2$, OC*H*$_3$), 1.57 (-, 1H, C*H*), 1.43 (-, 1H, C*H*), 1.25 – 1.04 (-, 16H), 0.92 – 0.67 (-, 12H, C*H*$_3$).

8 Literature

(1) Gust, D.; Moore, T. A.; Moore, A. L. *Acc. Chem. Res.* **1993**, *26*, 198-205.
(2) Kurreck, H.; Huber, M. *Angew. Chem., Int. Ed. Engl.* **1995**, *34*, 849-866.
(3) Kurreck, J.; Niethammer, D.; Kurreck, H. *Chem. unserer Zeit* **1999**, *33*, 72-83.
(4) Adams, D. M.; Brus, L.; Chidsey, C. E. D.; Creager, S.; Creutz, C.; Kagan, C. R.; Kamat, P. V.; Lieberman, M.; Lindsay, S.; Marcus, R. A.; Metzger, R. M.; Michel-Beyerle, M. E.; Miller, J. R.; Newton, M. D.; Rolison, D. R.; Sankey, O.; Schanze, K. S.; Yardley, J.; Zhu, X. Y. *J. Phys. Chem. B* **2003**, *107*, 6668-6697.
(5) Fukuzumi, S. *Bull. Chem. Soc. Jpn.* **2006**, *79*, 177-195.
(6) Wasielewski, M. R. *J. Org. Chem.* **2006**, *71*, 5051-5066.
(7) Balzani, V.; Credi, A.; Venturi, M. *Chemsuschem* **2008**, *1*, 26-58.
(8) Rosspeintner, A.; Lang, B.; Vauthey, E. *Annu. Rev. Phys. Chem.* **2013**, *64*, 247-271.
(9) Hertel, D.; Muller, C. D.; Meerholz, K. *Chem. unserer Zeit* **2005**, *39*, 336-347.
(10) Grätzel, M. *Acc. Chem. Res.* **2009**, *42*, 1788-1798.
(11) Allard, S.; Forster, M.; Souharce, B.; Thiem, H.; Scherf, U. *Angew. Chem., Int. Ed.* **2008**, *47*, 4070-4098.
(12) Heath, J. R.; Ratner, M. A. *Physics Today* **2003**, *56*, 43-49.
(13) Bredas, J. L.; Beljonne, D.; Coropceanu, V.; Cornil, J. *Chem. Rev.* **2004**, *104*, 4971-5003.
(14) Bendikov, M.; Wudl, F.; Perepichka, D. F. *Chem. Rev.* **2004**, *104*, 4891-4945.
(15) Forrest, S. R.; Thompson, M. E. *Chem. Rev.* **2007**, *107*, 923-925.
(16) Shirota, Y.; Kageyama, H. *Chem. Rev.* **2007**, *107*, 953-1010.
(17) O'Neill, M.; Kelly, S. M. *Adv. Mater.* **2011**, *23*, 566-584.
(18) Figueira-Duarte, T. M.; Müllen, K. *Chem. Rev.* **2011**, *111*, 7260-7314.
(19) Balzani, V.; Scandola, F. *Supramolecular Chemistry* **1991**, Ellis Horwood Limited.
(20) Paddon-Row, M. N. *Aust. J. Chem.* **2003**, *56*, 729-748.
(21) Harriman, A. *Angew. Chem., Int. Ed.* **2004**, *43*, 4985-4987.
(22) Verhoeven, J. W.; van Ramesdonk, H. J.; Groeneveld, M. M.; Benniston, A. C.; Harriman, A. *ChemPhysChem* **2005**, *6*, 2251-2260.
(23) Benniston, A. C.; Harriman, A. *Chem. Soc. Rev.* **2006**, *35*, 169-179.
(24) Klumpp, T.; Linsenmann, M.; Larson, S. L.; Limoges, B. R.; Burssner, D.; Krissinel, E. B.; Elliott, C. M.; Steiner, U. E. *J. Am. Chem. Soc.* **1999**, *121*, 4092-4092.
(25) Larson, S. L.; Elliott, C. M.; Kelley, D. F. *J. Phys. Chem.* **1995**, *99*, 6530-6539.
(26) Verhoeven, J. W.; Paddon-Row, M. N. *Int. J. Photoen.* **2001**, *3*, 79-87.
(27) Benniston, A. C.; Harriman, A.; Li, P. Y.; Rostron, J. P.; van Ramesdonk, H. J.; Groeneveld, M. M.; Zhang, H.; Verhoeven, J. W. *J. Am. Chem. Soc.* **2005**, *127*, 16054-16064.
(28) Verhoeven, J. W. *J. Photochem. Photobiol. C* **2006**, *7*, 40-60.
(29) Lefler, K. M.; Co, D. T.; Wasielewski, M. R. *J. Phys. Chem. Lett.* **2012**, *3*, 3798-3805.
(30) Conron, S. M. M.; Shoer, L. E.; Smeigh, A. L.; Ricks, A. B.; Wasielewski, M. R. *J. Phys. Chem. B* **2013**, *117*, 2195-2204.
(31) Marcus, R. A.; Sutin, N. *Biochim. Biophys. Acta* **1985**, *811*, 265-322.
(32) Sumi, H.; Marcus, R. A. *J. Chem. Phys.* **1986**, *84*, 4894-4914.
(33) Sutin, N. *J. Phys. Chem.* **1986**, *90*, 3465-3466.
(34) Marcus, R. A. *J. Phys. Chem.* **1989**, *93*, 3078-3086.
(35) Marcus, R. A. *Pure Appl. Chem.* **1997**, *69*, 13-29.
(36) Weaver, M. J. *Chem. Rev.* **1992**, *92*, 463-480.
(37) Heitele, H. *Angew. Chem., Int. Ed. Engl.* **1993**, *32*, 359-377.
(38) Zener, C. *Current Contents/Physical Chemical & Earth Sciences* **1983**, 24-24.
(39) Bolton, J. R.; Archer, M. D. *Advances in Chemistry Series* **1991**, 7-23.
(40) Vauthey, E.; Suppan, P.; Haselbach, E. *Helv. Chim. Acta* **1988**, *71*, 93-99.
(41) Kavarnos, G. J. *Fundamentals of Photoinduced Electron Transfer* **1993**, VCH Publishers, Inc.
(42) Closs, G. L.; Miller, J. R. *Science* **1988**, *240*, 440-447.
(43) Ulstrup, J.; Jortner, J. *J. Chem. Phys.* **1975**, *63*, 4358-4368.

(44) Jortner, J.; Bixon, M. *J. Chem. Phys.* **1988**, *88*, 167-170.
(45) Jortner, J.; Rips, I. *Perspectives in Photosynthesis* **1990**, Kluwer Academic Publishers, 293-299.
(46) Kommandeur, J.; Meerts, W. L. *Isr. J. Chem.* **1990**, *30*, 131-134.
(47) Bixon, M.; Jortner, J. *Chem. Phys.* **1993**, *176*, 467-481.
(48) Cortes, J.; Heitele, H.; Jortner, J. *J. Phys. Chem.* **1994**, *98*, 2527-2536.
(49) Nelsen, S. F.; Ramm, M. T.; Wolff, J. J.; Powell, D. R. *J. Am. Chem. Soc.* **1997**, *119*, 6863-6872.
(50) Strickler, S. J.; Berg, R. A. *J. Chem. Phys.* **1962**, *37*, 814-822.
(51) Weiss, E. A.; Wasielewski, M. R.; Ratner, M. A. *Topp. Curr. Chem.* **2005**, *257*, 103-133.
(52) Kiefer, A. M.; Kast, S. M.; Wasielewski, M. R.; Laukenmann, K.; Kothe, G. *J. Am. Chem. Soc.* **1999**, *121*, 188-198.
(53) Gust, D.; Moore, T. A.; Moore, A. L. *Chem. Commun.* **2006**, 1169-1178.
(54) Megiatto, J. D.; Antoniuk-Pablant, A.; Sherman, B. D.; Kodis, G.; Gervaldo, M.; Moore, T. A.; Moore, A. L.; Gust, D. *Proc. Natl. Acad. Sci. U. S. A.* **2012**, *109*, 15578-15583.
(55) Urbani, M.; Ohkubo, K.; Islam, D. M. S.; Fukuzumi, S.; Langa, F. *Chem.–Eur. J.* **2012**, *18*, 7473-7485.
(56) Suneesh, C. V.; Gopidas, K. R. *J. Phys. Chem. C* **2009**, *113*, 1606-1614.
(57) Suneesh, C. V.; Vinayak, M. V.; Gopidas, K. R. *J. Phys. Chem. C* **2010**, *114*, 18735-18744.
(58) Morisue, M.; Kalita, D.; Haruta, N.; Kobuke, Y. *Chem. Commun.* **2007**, 2348-2350.
(59) Shetti, V. S.; Ravikanth, M. *Eur. J. Org. Chem.* **2010**, 494-508.
(60) Romero, T.; Orenes, R. A.; Espinosa, A.; Tárraga, A.; Molina, P. *Inorg. Chem.* **2011**, *50*, 8214-8224.
(61) Liddell, P. A.; Kodis, G.; de la Garza, L.; Bahr, J. L.; Moore, A. L.; Moore, T. A.; Gust, D. *Helv. Chim. Acta* **2001**, *84*, 2765-2783.
(62) Kodis, G.; Liddell, P. A.; de la Garza, L.; Moore, A. L.; Moore, T. A.; Gust, D. *J. Mater. Chem.* **2002**, *12*, 2100-2108.
(63) Li, H. C.; Lambert, C. *Chem.–Eur. J.* **2006**, *12*, 1144-1155.
(64) Takahashi, S.; Nozaki, K.; Kozaki, M.; Suzuki, S.; Keyaki, K.; Ichimura, A.; Matsushita, T.; Okada, K. *J. Phys. Chem. A* **2008**, *112*, 2533-2542.
(65) Voloshchuk, R.; Gryko, D. T.; Chotkowski, M.; Ciuciu, A. I.; Flamigni, L. *Chem.–Eur. J.* **2012**, *18*, 14845-14859.
(66) Hankache, J.; Wenger, O. S. *Chem. Commun.* **2011**, *47*, 10145-10147.
(67) Hankache, J.; Niemi, M.; Lemmetyinen, H.; Wenger, O. S. *Inorg. Chem.* **2012**, *51*, 6333-6344.
(68) Hankache, J.; Niemi, M.; Lemmetyinen, H.; Wenger, O. S. *J. Phys. Chem. A* **2012**, *116*, 8159-8168.
(69) Kaiser, C.; Schmiedel, A.; Holzapfel, M.; Lambert, C. *J. Phys. Chem. C* **2012**, *116*, 15265-15280.
(70) Yamanaka, K. I.; Fujitsuka, M.; Araki, Y.; Ito, O.; Aoshima, T.; Fukushima, T.; Miyashi, T. *J. Phys. Chem. A* **2004**, *108*, 250-256.
(71) Martin-Gomis, L.; Ohkubo, K.; Fernandez-Lazaro, F.; Fukuzumi, S.; Sastre-Santos, A. *Chem. Commun.* **2010**, *46*, 3944-3946.
(72) Garg, V.; Kodis, G.; Chachisvilis, M.; Hambourger, M.; Moore, A. L.; Moore, T. A.; Gust, D. *J. Am. Chem. Soc.* **2011**, *133*, 2944-2954.
(73) Wasielewski, M. R.; Gaines, G. L.; Oneil, M. P.; Svec, W. A.; Niemczyk, M. P. *J. Am. Chem. Soc.* **1990**, *112*, 4559-4560.
(74) Laukenmann, K.; Weber, S.; Kothe, G.; Oesterle, C.; Angerhofer, A.; Wasielewski, M. R.; Svec, W. A.; Norris, J. R. *J. Phys. Chem.* **1995**, *99*, 4324-4329.
(75) D'Souza, F.; Wijesinghe, C. A.; El-Khouly, M. E.; Hudson, J.; Niemi, M.; Lemmetyinen, H.; Tkachenko, N. V.; Zandler, M. E.; Fukuzumi, S. *Phys. Chem. Chem. Phys.* **2011**, *13*, 18168-18178.
(76) Nöll, G.; Daub, J.; Lutz, M.; Rurack, K. *J. Org. Chem.* **2011**, *76*, 4859-4873.
(77) Eggenspiller, A.; Takai, A.; El-Khouly, M. E.; Ohkubo, K.; Gros, C. P.; Bernhard, C.; Goze, C.; Denat, F.; Barbe, J. M.; Fukuzumi, S. *J. Phys. Chem. A* **2012**, *116*, 3889-3898.

(78) Bai, D.; Benniston, A. C.; Hagon, J.; Lemmetyinen, H.; Tkachenko, N. V.; Clegg, W.; Harrington, R. W. *Phys. Chem. Chem. Phys.* **2012**, *14*, 4447-4456.
(79) Leonardi, M. J.; Topka, M. R.; Dinolfo, P. H. *Inorg. Chem.* **2012**, *51*, 13114-13122.
(80) Benniston, A. C.; Copley, G.; Lemmetyinen, H.; Tkachenko, N. V. *Eur. J. Org. Chem.* **2010**, 2867-2877.
(81) Supur, M.; El-Khouly, M. E.; Seok, J. H.; Kay, K. Y.; Fukuzumi, S. *J. Phys. Chem. A* **2011**, *115*, 14430-14437.
(82) Ricks, A. B.; Brown, K. E.; Wenninger, M.; Karlen, S. D.; Berlin, Y. A.; Co, D. T.; Wasielewski, M. R. *J. Am. Chem. Soc.* **2012**, *134*, 4581-4588.
(83) Kobr, L.; Gardner, D. M.; Smeigh, A. L.; Dyar, S. M.; Karlen, S. D.; Carmieli, R.; Wasielewski, M. R. *J. Am. Chem. Soc.* **2012**, *134*, 12430-12433.
(84) Werner, U.; Sakaguchi, Y.; Hayashi, H.; Nohya, G.; Yoneshima, R.; Nakajima, S.; Osuka, A. *J. Phys. Chem.* **1995**, *99*, 13930-13937.
(85) Gunderson, V. L.; Smeigh, A. L.; Kim, C. H.; Co, D. T.; Wasielewski, M. R. *J. Am. Chem. Soc.* **2012**, *134*, 4363-4372.
(86) Zeng, Y.; Zimmt, M. B. *J. Am. Chem. Soc.* **1991**, *113*, 5107-5109.
(87) Zeng, Y.; Zimmt, M. B. *J. Phys. Chem.* **1992**, *96*, 8395-8403.
(88) Lawson, J. M.; Paddon-Row, M. N.; Schuddeboom, W.; Warman, J. M.; Clayton, A. H. A.; Ghiggino, K. P. *J. Phys. Chem.* **1993**, *97*, 13099-13106.
(89) Roest, M. R.; Lawson, J. M.; Paddon-Row, M. N.; Verhoeven, J. W. *Chem. Phys. Lett.* **1994**, *230*, 536-542.
(90) Roest, M. R.; Verhoeven, J. W.; Schuddeboom, W.; Warman, J. M.; Lawson, J. M.; Paddon-Row, M. N. *J. Am. Chem. Soc.* **1996**, *118*, 1762-1768.
(91) Shephard, M. J.; Paddon-Row, M. N. *J. Phys. Chem. A* **1999**, *103*, 3347-3350.
(92) Seischab, M.; Lodenkemper, T.; Stockmann, A.; Schneider, S.; Koeberg, M.; Roest, M. R.; Verhoeven, J. W.; Lawson, J. M.; Paddon-Row, M. N. *Phys. Chem. Chem. Phys.* **2000**, *2*, 1889-1897.
(93) Imahori, H.; Guldi, D. M.; Tamaki, K.; Yoshida, Y.; Luo, C. P.; Sakata, Y.; Fukuzumi, S. *J. Am. Chem. Soc.* **2001**, *123*, 6617-6628.
(94) Imahori, H.; Tamaki, K.; Araki, Y.; Sekiguchi, Y.; Ito, O.; Sakata, Y.; Fukuzumi, S. *J. Am. Chem. Soc.* **2002**, *124*, 5165-5174.
(95) Guldi, D. M.; Imahori, H.; Tamaki, K.; Kashiwagi, Y.; Yamada, H.; Sakata, Y.; Fukuzumi, S. *J. Phys. Chem. A* **2004**, *108*, 541-548.
(96) Hasharoni, K.; Levanon, H.; Greenfield, S. R.; Gosztola, D. J.; Svec, W. A.; Wasielewski, M. R. *J. Am. Chem. Soc.* **1995**, *117*, 8055-8056.
(97) Greenfield, S. R.; Svec, W. A.; Gosztola, D.; Wasielewski, M. R. *J. Am. Chem. Soc.* **1996**, *118*, 6767-6777.
(98) Smirnov, S. N.; Braun, C. L.; Greenfield, S. R.; Svec, W. A.; Wasielewski, M. R. *J. Phys. Chem.* **1996**, *100*, 12329-12336.
(99) Lukas, A. S.; Bushard, P. J.; Weiss, E. A.; Wasielewski, M. R. *J. Am. Chem. Soc.* **2003**, *125*, 3921-3930.
(100) Weiss, E. A.; Ratner, M. A.; Wasielewski, M. R. *J. Phys. Chem. A* **2003**, *107*, 3639-3647.
(101) Weiss, E. A.; Tauber, M. J.; Ratner, M. A.; Wasielewski, M. R. *J. Am. Chem. Soc.* **2005**, *127*, 6052-6061.
(102) Mi, Q. X.; Ratner, M. A.; Wasielewski, M. R. *J. Phys. Chem. A* **2010**, *114*, 162-171.
(103) Di Valentin, M.; Bisol, A.; Agostini, G.; Liddell, P. A.; Kodis, G.; Moore, A. L.; Moore, T. A.; Gust, D.; Carbonera, D. *J. Phys. Chem. B* **2005**, *109*, 14401-14409.
(104) Kuciauskas, D.; Liddell, P. A.; Lin, S.; Johnson, T. E.; Weghorn, S. J.; Lindsey, J. S.; Moore, A. L.; Moore, T. A.; Gust, D. *J. Am. Chem. Soc.* **1999**, *121*, 8604-8614.
(105) Kodis, G.; Liddell, P. A.; de la Garza, L.; Clausen, P. C.; Lindsey, J. S.; Moore, A. L.; Moore, T. A.; Gust, D. *J. Phys. Chem. A* **2002**, *106*, 2036-2048.
(106) Gomberg, M.; Cone, L. H. *Berichte* **1904**, *37*, 2033-2051.
(107) Hicks, R. G. *Org. Biomol. Chem.* **2007**, *5*, 1321-1338.
(108) Ballester, M. *Acc. Chem. Res.* **1985**, *18*, 380-387.
(109) Ballester, M. *Adv. Phys. Org. Chem.* **1989**, *25*, 267-445.
(110) Veciana, J.; Ratera, I. *Stable Radicals: Fundamentals and Applied Aspects of Odd-Electron Compounds* **2010**, *John Wiley & Sohns, Ltd.*, 33-80.

(111) Ballester, M.; Molinet, C.; Castañer, J. *J. Am. Chem. Soc.* **1960**, *82*, 4254-4258.
(112) Ballester, M.; Castañer, J. *J. Am. Chem. Soc.* **1960**, *82*, 4259-4261.
(113) Silberrad, O. *J. Chem. Soc., Trans.* **1921**, *119*, 2029-2036.
(114) Silberrad, O. *J. Chem. Soc., Trans.* **1922**, *121*, 1015-1022.
(115) Ruff, O.; Golla, H. *Z. Anorg. Allg. Chem.* **1924**, *138*, 33-42.
(116) Ballester, M.; Riera, J.; Castañer, J.; Badià, C.; Monsò, J. M. *J. Am. Chem. Soc.* **1971**, *93*, 2215-2225.
(117) Rovira, C.; Ruiz-Molina, D.; Elsner, O.; Vidal-Gancedo, J.; Bonvoisin, J.; Launay, J. P.; Veciana, J. *Chem.–Eur. J.* **2001**, *7*, 240-250.
(118) Armet, O.; Veciana, J.; Rovira, C.; Riera, J.; Castañer, J.; Molins, E.; Rius, J.; Miravitlles, C.; Olivella, S.; Brichfeus, J. *J. Phys. Chem.* **1987**, *91*, 5608-5616.
(119) Veciana, J.; Carilla, J.; Miravitlles, C.; Molins, E. *J. Chem. Soc., Chem. Commun.* **1987**, 812-814.
(120) Rius, J.; Miravitlles, C.; Molins, E.; Crespo, M.; Veciana, J. *Mol. Cryst. Liq. Cryst.* **1990**, *187*, 155-163.
(121) Guasch, J.; Fontrodona, X.; Ratera, I.; Rovira, C.; Veciana, J. *Acta Crystallogr., Sec. C: Cryst. Struct. Commun.* **2013**, *69*, 255-U141.
(122) Ballester, M.; Castañer, J.; Riera, J.; Ibanez, A.; Pujadas, J. *J. Org. Chem.* **1982**, *47*, 259-264.
(123) Ruberu, S. R.; Fox, M. A. *J. Phys. Chem.* **1993**, *97*, 143-149.
(124) Ratera, I.; Marcen, S.; Montant, S.; Ruiz-Molina, D.; Rovira, C.; Veciana, J.; Letard, J. F.; Freysz, E. *Chem. Phys. Lett.* **2002**, *363*, 245-251.
(125) Ratera, I.; Ruiz-Molina, D.; Sporer, C.; Marcen, S.; Montant, S.; Letard, J. F.; Freysz, E.; Rovira, C.; Veciana, J. *Polyhedron* **2003**, *22*, 1851-1856.
(126) Ballester, M.; Castañer, J.; Pujadas, J. *Tetrahedron Lett.* **1971**, 1699-1702.
(127) Luckhurst, G. R.; Ockwell, J. N. *Tetrahedron Lett.* **1968**, 4123-4126.
(128) Fox, M. A.; Gaillard, E.; Chen, C. C. *J. Am. Chem. Soc.* **1987**, *109*, 7088-7094.
(129) Breslin, D. T.; Fox, M. A. *J. Org. Chem.* **1994**, *59*, 7557-7561.
(130) Breslin, D. T.; Fox, M. A. *J. Phys. Chem.* **1994**, *98*, 408-411.
(131) Ballester, M.; Riera-Figueraz, J.; Rodríguez-Síurana, A. *Tetrahedron Lett.* **1970**, 3615-1618.
(132) Ballester, M.; Miravitlles, C.; Molins, E.; Carreras, C. *J. Org. Chem.* **2003**, *68*, 2748-2751.
(133) Molins, E.; Mas, M.; Maniukiewicz, W.; Ballester, M.; Castañer, J. *Acta Crystallogr., Sec. C: Cryst. Struct. Commun.* **1996**, *52*, 2412-2414.
(134) Ballester, M.; Riera, J.; Castañer, J.; Rodriguez, A.; Rovira, C.; Veciana, J. *J. Org. Chem.* **1982**, *47*, 4498-4505.
(135) Ballester, M.; de la Fuente, G. D. *Tetrahedron Lett.* **1970**, 4509-4510.
(136) Miravitlles, C.; Molins, E.; Solans, X.; Germain, G.; Declercq, J. P. *Journal of Inclusion Phenomena* **1985**, *3*, 27-34.
(137) Ballester, M.; Riera, J.; Castañer, J.; Casulleras, M. *Tetrahedron Lett.* **1978**, 643-644.
(138) Ballester, M.; Pascual, I. *Tetrahedron Lett.* **1985**, *26*, 5589-5592.
(139) Ballester, M.; Pascual, I. *J. Org. Chem.* **1991**, *56*, 841-844.
(140) Umemoto, K. *Chem. Lett.* **1985**, 1415-1418.
(141) Umemoto, K.; Okamura, N. *Bull. Chem. Soc. Jpn.* **1986**, *59*, 3047-3052.
(142) Domingo, V. M.; Castañer, J.; Riera, J.; Labarta, A. *J. Org. Chem.* **1994**, *59*, 2604-2607.
(143) Ballester, M.; Riera, J.; Castañer, J.; Rovira, C.; Veciana, J.; Onrubia, C. *J. Org. Chem.* **1983**, *48*, 3716-3720.
(144) Ballester, M.; Veciana, J.; Riera, J.; Castañer, J.; Rovira, C.; Armet, O. *J. Org. Chem.* **1986**, *51*, 2472-2480.
(145) Ballester, M.; Veciana, J.; Riera, J.; Castañer, J.; Rovira, C.; Armet, O. *Tetrahedron Lett.* **1982**, *23*, 5075-5078.
(146) Ballester, M.; Veciana, J.; Riera, J.; Castañer, J.; Armet, O.; Rovira, C. *J. Chem. Soc., Chem. Commun.* **1983**, 982-983.
(147) Ballester, M.; Pascual, I. *J. Org. Chem.* **1991**, *56*, 4314-4317.
(148) Ballester, M.; Castañer, J.; Riera, J.; Pascual, I. *J. Am. Chem. Soc.* **1984**, *106*, 3365-3366.

(149) Pedersen, B. F. *Acta Crystallogr., Sec. B: Struct. Sci.* **1975**, *31*, 2931-2933.
(150) Ballester, M.; Pascual, I.; Torres, J. *J. Org. Chem.* **1990**, *55*, 3035-3044.
(151) Ballester, M.; Castañer, J.; Riera, J. *J. Am. Chem. Soc.* **1966**, *88*, 957-963.
(152) Ballester, M.; Pascual, I.; Riera, J.; Castañer, J. *J. Org. Chem.* **1991**, *56*, 217-225.
(153) Ballester, M.; Pascual, I.; Carreras, C.; Vidal-Gancedo, J. *J. Am. Chem. Soc.* **1994**, *116*, 4205-4210.
(154) Domingo, V. M.; Castañer, J.; Riera, J. *J. Chem. Soc., Chem. Commun.* **1994**, 2521-2522.
(155) Domingo, V. M.; Castañer, J.; Riera, J.; Brillas, E.; Molins, E.; Martinez, B.; Knight, B. *Chem. Mater.* **1997**, *9*, 1620-1629.
(156) Bonvoisin, J.; Launay, J. P.; Rovira, C.; Veciana, J. *Angew. Chem., Int. Ed. Engl.* **1994**, *33*, 2106-2109.
(157) Elsner, O.; Ruiz-Molina, D.; Vidal-Gancedo, J.; Rovira, C.; Veciana, J. *Nano Lett.* **2001**, *1*, 117-120.
(158) Lloveras, V.; Vidal-Gancedo, J.; Ruiz-Molina, D.; Figueira-Duarte, T. M.; Nierengarten, J. F.; Veciana, J.; Rovira, C. *Faraday Discuss.* **2006**, *131*, 291-305.
(159) Lloveras, V.; Vidal-Gancedo, J.; Figueira-Duarte, T. M.; Nierengarten, J. F.; Novoa, J. J.; Mota, F.; Ventosa, N.; Rovira, C.; Veciana, J. *J. Am. Chem. Soc.* **2011**, *133*, 5818-5833.
(160) Veciana, J.; Rovira, C.; Armet, O.; Domingo, V. M.; Crespo, M. I.; Palacio, F. *Mol. Cryst. Liq. Cryst.* **1989**, *176*, 77-84.
(161) Veciana, J.; Rovira, C.; Crespo, M. I.; Armet, O.; Domingo, V. M.; Palacio, F. *J. Am. Chem. Soc.* **1991**, *113*, 2552-2561.
(162) Veciana, J.; Crespo, M. I. *Angew. Chem., Int. Ed. Engl.* **1991**, *30*, 74-76.
(163) Veciana, J.; Rovira, C.; Ventosa, N.; Crespo, M. I.; Palacio, F. *J. Am. Chem. Soc.* **1993**, *115*, 57-64.
(164) Ventosa, N.; Ruiz, D.; Rovira, C.; Veciana, J. *Mol. Cryst. Liq. Cryst.* **1993**, *232*, 333-342.
(165) Sedo, J.; Ruiz, D.; Vidal-Gancedo, J.; Rovira, C.; Bonvoisin, J.; Launay, J. P.; Veciana, J. *Adv. Mater.* **1996**, *8*, 748-752.
(166) Sato, K.; Shiomi, D.; Takui, T.; Itoh, K.; Veciana, J.; Rovira, C. *Mol. Cryst. Liq. Cryst.* **1996**, *278*, 295-300.
(167) Takui, T.; Sato, K.; Shiomi, D.; Itoh, K.; Veciana, J.; Rovira, C. *Bull. Magn. Reson.* **1996**, *18*, 165-166.
(168) Sedo, J.; Ruiz, D.; Vidal-Gancedo, J.; Rovira, C.; Bonvoisin, J.; Launay, J. P.; Veciana, J. *Synth. Met.* **1997**, *85*, 1651-1654.
(169) Ruiz-Molina, D.; Veciana, J.; Palacio, F.; Rovira, C. *J. Org. Chem.* **1997**, *62*, 9009-9017.
(170) Ruiz, D.; Veciana, J.; Rovira, C. *Synlett* **1997**, 1205-1207.
(171) Mesa, J. A.; Velazquez-Palenzuela, A.; Brillas, E.; Coll, J.; Torres, J. L.; Julià, L. *J. Org. Chem.* **2012**, *77*, 1081-1086.
(172) Castillo, M.; Brillas, E.; Rillo, C.; Kuzmin, M. D.; Julià, L. *Tetrahedron* **2007**, *63*, 708-716.
(173) Elsner, O.; Ruiz-Molina, D.; Vidal-Gancedo, J.; Rovira, C.; Veciana, J. *Chem. Commun.* **1999**, 579-580.
(174) Elsner, O.; Ruiz-Molina, D.; Ratera, I.; Vidal-Gancedo, J.; Rovira, C.; Veciana, J. *J. Organomet. Chem.* **2001**, *637*, 251-257.
(175) Ruiz-Molina, D.; Ratera, I.; Vidal-Gancedo, J.; Daro, N.; Letard, J. F.; Rovira, C.; Veciana, J. *Synth. Met.* **2001**, *121*, 1804-1805.
(176) Ratera, I.; Ruiz-Molina, D.; Sanchez, C.; Alcala, R.; Rovira, C.; Veciana, J. *Synth. Met.* **2001**, *121*, 1834-1835.
(177) Ratera, I.; Ruiz-Molina, D.; Vidal-Gancedo, J.; Wurst, K.; Daro, N.; Letard, J. F.; Rovira, C.; Veciana, J. *Angew. Chem., Int. Ed.* **2001**, *40*, 919-922.
(178) Ratera, I.; Ruiz-Molina, D.; Vidal-Gancedo, J.; Novoa, J. J.; Wurst, K.; Letard, J. F.; Rovira, C.; Veciana, J. *Chem.–Eur. J.* **2004**, *10*, 603-616.
(179) Maspoch, D.; Catala, L.; Gerbier, P.; Ruiz-Molina, D.; Vidal-Gancedo, J.; Wurst, K.; Rovira, C.; Veciana, J. *Chem.–Eur. J.* **2002**, *8*, 3635-3645.
(180) Maspoch, D.; Domingo, N.; Ruiz-Molina, D.; Wurst, K.; Tejada, J.; Rovira, C.; Veciana, J. *J. Am. Chem. Soc.* **2004**, *126*, 730-731.
(181) Maspoch, D.; Domingo, N.; Ruiz-Molina, D.; Wurst, K.; Vaughan, G.; Tejada, J.; Rovira, C.; Veciana, J. *Angew. Chem., Int. Ed.* **2004**, *43*, 1828-1832.

(182) Maspoch, D.; Domingo, N.; Ruiz-Molina, D.; Warst, K.; Tejada, J.; Rovira, C.; Veciana, J. *C. R. Chim.* **2005**, *8*, 1213-1225.
(183) Roques, N.; Maspoch, D.; Wurst, K.; Ruiz-Molina, D.; Rovira, C.; Veciana, J. *Chem.–Eur. J.* **2006**, *12*, 9238-9253.
(184) Roques, N.; Maspoch, D.; Datcu, A.; Wurst, K.; Ruiz-Molina, D.; Rovira, C.; Veciana, J. *Polyhedron* **2007**, *26*, 1934-1948.
(185) Maspoch, D.; Ruiz-Molina, D.; Wurst, K.; Rovira, C.; Veciana, J. *Chem. Commun.* **2002**, 2958-2959.
(186) Maspoch, D.; Ruiz-Molina, D.; Wurst, K.; Rovira, C.; Veciana, J. *Polyhedron* **2003**, *22*, 1929-1934.
(187) Maspoch, D.; Ruiz-Molina, D.; Wurst, K.; Vidal-Gancedo, J.; Rovira, C.; Veciana, J. *J. Chem. Soc., Dalton Trans.* **2004**, 1073-1082.
(188) Maspoch, D.; Domingo, N.; Ruiz-Molina, D.; Wurst, K.; Hernandez, J. M.; Lloret, F.; Tejada, J.; Rovira, C.; Veciana, J. *Inorg. Chem.* **2007**, *46*, 1627-1633.
(189) Roques, N.; Perruchas, S.; Maspoch, D.; Datcu, A.; Wurst, K.; Sutter, J. P.; Rovira, C.; Veciana, J. *Inorg. Chim. Acta* **2007**, *360*, 3861-3869.
(190) Ribas, X.; Maspoch, D.; Wurst, K.; Veciana, J.; Rovira, C. *Inorg. Chem.* **2006**, *45*, 5383-5392.
(191) Roques, N.; Domingo, N.; Maspoch, D.; Wurst, K.; Rovira, C.; Tejada, J.; Ruiz-Molina, D.; Veciana, J. *Inorg. Chem.* **2010**, *49*, 3482-3488.
(192) Maspoch, D.; Ruiz-Molina, D.; Wurst, K.; Domingo, N.; Cavallini, M.; Biscarini, F.; Tejada, J.; Rovira, C.; Veciana, J. *Nat. Mater.* **2003**, *2*, 190-195.
(193) Maspoch, D.; Domingo, N.; Roques, N.; Wurst, K.; Tejada, J.; Rovira, C.; Ruiz-Molina, D.; Veciana, J. *Chem.–Eur. J.* **2007**, *13*, 8153-8163.
(194) Roques, N.; Maspoch, D.; Luis, F.; Camón, A.; Wurst, K.; Datcu, A.; Rovira, C.; Ruiz-Molina, D.; Veciana, J. *J. Mater. Chem.* **2008**, *18*, 98-108.
(195) Maspoch, D.; Domingo, N.; Molina, D. R.; Wurst, K.; Hernandez, J. M.; Vaughan, G.; Rovira, C.; Lloret, F.; Tejada, J.; Veciana, J. *Chem. Commun.* **2005**, 5035-5037.
(196) Maspoch, D.; Ruiz-Molina, D.; Wurst, K.; Rovira, C.; Veciana, J. *Chem. Commun.* **2004**, 1164-1165.
(197) Datcu, A.; Roques, N.; Jubera, V.; Maspoch, D.; Fontrodona, X.; Wurst, K.; Imaz, I.; Mouchaham, G.; Sutter, J. P.; Rovira, C.; Veciana, J. *Chem.–Eur. J.* **2012**, *18*, 152-162.
(198) Datcu, A.; Roques, N.; Jubera, V.; Imaz, I.; Maspoch, D.; Sutter, J. P.; Rovira, C.; Veciana, J. *Chem.–Eur. J.* **2011**, *17*, 3644-3656.
(199) Roques, N.; Maspoch, D.; Imaz, I.; Datcu, A.; Sutter, J. P.; Rovira, C.; Veciana, J. *Chem. Commun.* **2008**, 3160-3162.
(200) Grillo, F.; Mugnaini, V.; Oliveros, M.; Francis, S. M.; Choi, D. J.; Rastei, M. V.; Limot, L.; Cepek, C.; Pedio, M.; Bromley, S. T.; Richardson, N. V.; Bucher, J. P.; Veciana, J. *J. Phys. Chem. Lett.* **2012**, *3*, 1559-1564.
(201) Crivillers, N.; Furukawa, S.; Minoia, A.; Heyen, A. V.; Mas-Torrent, M.; Sporer, C.; Linares, M.; Volodin, A.; Van Haesendonck, C.; Van der Auweraer, M.; Lazzaroni, R.; De Feyter, S.; Veciana, J.; Rovira, C. *J. Am. Chem. Soc.* **2009**, *131*, 6246-6252.
(202) Vera, F.; Mas-Torrent, M.; Esquena, J.; Rovira, C.; Shen, Y. F.; Nakanishi, T.; Veciana, J. *Chem. Sci.* **2012**, *3*, 1958-1962.
(203) Mas-Torrent, M.; Crivillers, N.; Mugnaini, V.; Ratera, I.; Rovira, C.; Veciana, J. *J. Mater. Chem.* **2009**, *19*, 1691-1695.
(204) Crivillers, N.; Mas-Torrent, M.; Perruchas, S.; Roques, N.; Vidal-Gancedo, J.; Veciana, J.; Rovira, C.; Basabe-Desmonts, L.; Ravoo, B. J.; Crego-Calama, M.; Reinhoudt, D. N. *Angew. Chem., Int. Ed.* **2007**, *46*, 2215-2219.
(205) Crivillers, N.; Mas-Torrent, M.; Rovira, C.; Veciana, J. *J. Mater. Chem.* **2012**, *22*, 13883-13890.
(206) Simao, C.; Mas-Torrent, M.; Veciana, J.; Rovira, C. *Nano Lett.* **2011**, *11*, 4382-4385.
(207) Crivillers, N.; Paradinas, M.; Mas-Torrent, M.; Bromley, S. T.; Rovira, C.; Ocal, C.; Veciana, J. *Chem. Commun.* **2011**, *47*, 4664-4666.
(208) Crivillers, N.; Munuera, C.; Mas-Torrent, M.; Simao, C.; Bromley, S. T.; Ocal, C.; Rovira, C.; Veciana, J. *Adv. Mater.* **2009**, *21*, 1177-1181.

(209) Crivillers, N.; Mas-Torrent, M.; Vidal-Gancedo, J.; Veciana, J.; Rovira, C. *J. Am. Chem. Soc.* **2008**, *130*, 5499-5506.
(210) Simão, C.; Mas-Torrent, M.; Crivillers, N.; Lloveras, V.; Artes, J. M.; Gorostiza, P.; Veciana, J.; Rovira, C. *Nature Chemistry* **2011**, *3*, 359-364.
(211) Mugnaini, V.; Paradinas, M.; Shekhah, O.; Roques, N.; Ocal, C.; Woll, C.; Veciana, J. *J. Mater. Chem. C* **2013**, *1*, 793-800.
(212) Shekhah, O.; Roques, N.; Mugnaini, V.; Munuera, C.; Ocal, C.; Veciana, J.; Woll, C. *Langmuir* **2008**, *24*, 6640-6648.
(213) Guasch, J.; Grisanti, L.; Jung, S.; Morales, D.; D'Avino, G.; Souto, M.; Fontrodona, X.; Painelli, A.; Renz, F.; Ratera, I.; Veciana, J. *Chem. Mater.* **2013**, *25*, 808-814.
(214) Grisanti, L.; D'Avino, G.; Painelli, A.; Guasch, J.; Ratera, I.; Veciana, J. *J. Phys. Chem. B* **2009**, *113*, 4718-4725.
(215) D'Avino, G.; Grisanti, L.; Guasch, J.; Ratera, I.; Veciana, J.; Painelli, A. *J. Am. Chem. Soc.* **2008**, *130*, 12064-12072.
(216) Ratera, I.; Sporer, C.; Ruiz-Molina, D.; Ventosa, N.; Baggerman, J.; Brouwer, A. M.; Rovira, C.; Veciana, J. *J. Am. Chem. Soc.* **2007**, *129*, 6117-6129.
(217) Sporer, C.; Ratera, I.; Ruiz-Molina, D.; Gancedo, J. V.; Wurst, K.; Jaitner, P.; Rovira, C.; Veciana, J. *J. Phys. Chem. Solids* **2004**, *65*, 753-758.
(218) Sporer, C.; Ratera, I.; Ruiz-Molina, D.; Zhao, Y. X.; Vidal-Gancedo, J.; Wurst, K.; Jaitner, P.; Clays, K.; Persoons, A.; Rovira, C.; Veciana, J. *Angew. Chem., Int. Ed.* **2004**, *43*, 5266-5268.
(219) Ratera, I.; Ruiz-Molina, D.; Renz, F.; Ensling, J.; Wurst, K.; Rovira, C.; Gutlich, P.; Veciana, J. *J. Am. Chem. Soc.* **2003**, *125*, 1462-1463.
(220) Sporer, C.; Ratera, I.; Ruiz-Molina, D.; Gancedo, J. V.; Ventosa, N.; Wurst, K.; Jaitner, P.; Rovira, C.; Veciana, J. *Solid State Sci.* **2009**, *11*, 786-792.
(221) Guasch, J.; Grisanti, L.; Souto, M.; Lloveras, V.; Vidal-Gancedo, J.; Ratera, I.; Painelli, A.; Rovira, C.; Veciana, J. *J. Am. Chem. Soc.* **2013**, *135*, 6958-6967.
(222) Guasch, J.; Grisanti, L.; Lloveras, V.; Vidal-Gancedo, J.; Souto, M.; Morales, D. C.; Vilaseca, M.; Sissa, C.; Painelli, A.; Ratera, I.; Rovira, C.; Veciana, J. *Angew. Chem., Int. Ed.* **2012**, *51*, 11024-11028.
(223) Chopin, S.; Cousseau, J.; Levillain, E.; Rovira, C.; Veciana, J.; Sandanayaka, A. S. D.; Araki, Y.; Ito, O. *J. Mater. Chem.* **2006**, *16*, 112-121.
(224) Amthor, S.; Noller, B.; Lambert, C. *Chem. Phys.* **2005**, *316*, 141-152.
(225) Heckmann, A.; Dümmler, S.; Pauli, J.; Margraf, M.; Kohler, J.; Stich, D.; Lambert, C.; Fischer, I.; Resch-Genger, U. *J. Phys. Chem. C* **2009**, *113*, 20958-20966.
(226) Maksimenka, R.; Margraf, M.; Kohler, J.; Heckmann, A.; Lambert, C.; Fischer, I. *Chem. Phys.* **2008**, *347*, 436-445.
(227) Heckmann, A.; Lambert, C. *J. Am. Chem. Soc.* **2007**, *129*, 5515-5527.
(228) Heckmann, A.; Lambert, C. *Angew. Chem., Int. Ed.* **2012**, *51*, 326-392.
(229) Heckmann, A.; Lambert, C.; Goebel, M.; Wortmann, R. *Angew. Chem., Int. Ed.* **2004**, *43*, 5851-5856.
(230) Dümmler, S.; Roth, W.; Fischer, I.; Heckmann, A.; Lambert, C. *Chem. Phys. Lett.* **2005**, *408*, 264-268.
(231) Reitzenstein, D.; Quast, T.; Kanal, F.; Kullmann, M.; Ruetzel, S.; Hammer, M. S.; Deibel, C.; Dyakonov, V.; Brixner, T.; Lambert, C. *Chem. Mater.* **2010**, *22*, 6641-6655.
(232) Mesa, J. A.; Torres, J. L.; Julià, L. *Talanta* **2012**, *101*, 141-147.
(233) Castellanos, S.; Velasco, D.; López-Calahorra, F.; Brillas, E.; Julià, L. *J. Org. Chem.* **2008**, *73*, 3759-3767.
(234) Velasco, D.; Castellanos, S.; López, M.; López-Calahorra, F.; Brillas, E.; Julià, L. *J. Org. Chem.* **2007**, *72*, 7523-7532.
(235) Gamero, V.; Velasco, D.; Latorre, S.; López-Calahorra, F.; Brillas, E.; Julià, L. *Tetrahedron Lett.* **2006**, *47*, 2305-2309.
(236) Castellanos, S.; Gaidelis, V.; Jankauskas, V.; Grazulevicius, J. V.; Brillas, E.; López-Calahorra, F.; Julià, L.; Velasco, D. *Chem. Commun.* **2010**, *46*, 5130-5132.
(237) López, M.; Velasco, D.; López-Calahorra, F.; Julià, L. *Tetrahedron Lett.* **2008**, *49*, 5196-5199.
(238) Huisgen, R. *Pure Appl. Chem.* **1989**, *61*, 613-628.

(239) Huisgen, R.; Szeimies, G.; Mobius, L. *Chem. Ber. Recl.* **1967**, *100*, 2494-2507.
(240) Rostovtsev, V. V.; Green, L. G.; Fokin, V. V.; Sharpless, K. B. *Angew. Chem., Int. Ed.* **2002**, *41*, 2596-2599.
(241) Tornoe, C. W.; Christensen, C.; Meldal, M. *J. Org. Chem.* **2002**, *67*, 3057-3064.
(242) Zhang, L.; Chen, X.; Xue, P.; Sun, H. H. Y.; Williams, I. D.; Sharpless, K. B.; Fokin, V. V.; Jia, G. *J. Am. Chem. Soc.* **2005**, *127*, 15998-15999.
(243) Juricek, M.; Kouwer, P. H. J.; Rowan, A. E. *Chem. Commun.* **2011**, *47*, 8740-8749.
(244) Hein, J. E.; Fokin, V. V. *Chem. Soc. Rev.* **2010**, *39*, 1302-1315.
(245) Fabbrizzi, P.; Cicchi, S.; Brandi, A.; Sperotto, E.; van Koten, G. *Eur. J. Org. Chem.* **2009**, 5423-5430.
(246) Meldal, M.; Tornoe, C. W. *Chem. Rev.* **2008**, *108*, 2952-3015.
(247) Wu, P.; Fokin, V. V. *Aldrichimica Acta* **2007**, *40*, 7-17.
(248) Meudtner, R. M.; Ostermeier, M.; Goddard, R.; Limberg, C.; Hecht, S. *Chem.–Eur. J.* **2007**, *13*, 9834-9840.
(249) Tanaka, K.; Kageyama, C.; Fukase, K. *Tetrahedron Lett.* **2007**, *48*, 6475-6479.
(250) Rodionov, V. O.; Presolski, S. I.; Gardinier, S.; Lim, Y. H.; Finn, M. G. *J. Am. Chem. Soc.* **2007**, *129*, 12696-12704.
(251) Rodionov, V. O.; Presolski, S. I.; Diaz, D. D.; Fokin, V. V.; Finn, M. G. *J. Am. Chem. Soc.* **2007**, *129*, 12705-12712.
(252) Bräse, S.; Gil, C.; Knepper, K.; Zimmermann, V. *Angew. Chem., Int. Ed.* **2005**, *44*, 5188-5240.
(253) Feldman, A. K.; Colasson, B.; Fokin, V. V. *Org. Lett.* **2004**, *6*, 3897-3899.
(254) Kolb, H. C.; Finn, M. G.; Sharpless, K. B. *Angew. Chem., Int. Ed.* **2001**, *40*, 2004-2021.
(255) Worrell, B. T.; Malik, J. A.; Fokin, V. V. *Science* **2013**, *340*, 457-460.
(256) Himo, F.; Lovell, T.; Hilgraf, R.; Rostovtsev, V. V.; Noodleman, L.; Sharpless, K. B.; Fokin, V. V. *J. Am. Chem. Soc.* **2005**, *127*, 210-216.
(257) Jarowski, P. D.; Wu, Y. L.; Schweizer, W. B.; Diederich, F. *Org. Lett.* **2008**, *10*, 3347-3350.
(258) Zhang, Q.; Ning, Z. J.; Tian, H. *Dyes Pigm.* **2009**, *81*, 80-84.
(259) de Miguel, G.; Wielopolski, M.; Schuster, D. I.; Fazio, M. A.; Lee, O. P.; Haley, C. K.; Ortiz, A. L.; Echegoyen, L.; Clark, T.; Guldi, D. M. *J. Am. Chem. Soc.* **2011**, *133*, 13036-13054.
(260) Astruc, D.; Liang, L. Y.; Rapakousiou, A.; Ruiz, J. *Acc. Chem. Res.* **2012**, *45*, 630-640.
(261) Duan, T. N.; Fan, K.; Fu, Y.; Zhong, C.; Chen, X. G.; Peng, T. Y.; Qin, J. G. *Dyes Pigm.* **2012**, *94*, 28-33.
(262) Zoon, P. D.; van Stokkum, I. H. M.; Parent, M.; Mongin, O.; Blanchard-Desce, M.; Brouwer, A. M. *Phys. Chem. Chem. Phys.* **2010**, *12*, 2706-2715.
(263) Oton, F.; Gonzalez, M. D.; Espinosa, A.; de Arellano, C. R.; Tárraga, A.; Molina, P. *J. Org. Chem.* **2012**, *77*, 10083-10092.
(264) Oton, F.; Gonzalez, M. D.; Espinosa, A.; Tárraga, A.; Molina, P. *Organometallics* **2012**, *31*, 2085-2096.
(265) Plazuk, D.; Rychlik, B.; Blauz, A.; Domagala, S. *J. Organomet. Chem.* **2012**, *715*, 102-112.
(266) Kilpin, K. J.; Gavey, E. L.; McAdam, C. J.; Anderson, C. B.; Lind, S. J.; Keep, C. C.; Gordon, K. C.; Crowley, J. D. *Inorg. Chem.* **2011**, *50*, 6334-6346.
(267) Kolb, H. C.; Sharpless, K. B. *Drug Discovery Today* **2003**, *8*, 1128-1137.
(268) Parent, M.; Mongin, O.; Kamada, K.; Katan, C.; Blanchard-Desce, M. *Chem. Commun.* **2005**, 2029-2031.
(269) Bakbak, S.; Leech, P. J.; Carson, B. E.; Saxena, S.; King, W. P.; Bunz, U. H. F. *Macromolecules* **2006**, *39*, 6793-6795.
(270) Juricek, M.; Felici, M.; Contreras-Carballada, P.; Lauko, J.; Bou, S. R.; Kouwer, P. H. J.; Brouwer, A. M.; Rowan, A. E. *J. Mater. Chem.* **2011**, *21*, 2104-2111.
(271) Romero, T.; Caballero, A.; Tárraga, A.; Molina, P. *Org. Lett.* **2009**, *11*, 3466-3469.
(272) Holzapfel, M.; Lambert, C. *J. Phys. Chem. C* **2008**, *112*, 1227-1243.
(273) Lambert, C.; Schelter, J.; Fiebig, T.; Mank, D.; Trifonov, A. *J. Am. Chem. Soc.* **2005**, *127*, 10600-10610.
(274) Lambert, C.; Nöll, G. *J. Chem. Soc., Perkin Trans. 2* **2002**, 2039-2043.

(275) Dapperheld, S.; Steckhan, E.; Brinkhaus, K. H. G.; Esch, T. *Chem. Ber.* **1991**, *124*, 2557-2567.
(276) Schmidt, W.; Steckhan, E. *Chem. Ber. Recl.* **1980**, *113*, 577-585.
(277) Yurchenko, O.; Freytag, D.; Borg, L. Z.; Zentel, R.; Heinze, J.; Ludwigs, S. *J. Phys. Chem. B* **2012**, *116*, 30-39.
(278) Zieschang, F. *Diploma Thesis* **2009**, *University of Würzburg*.
(279) Weiss, E. A.; Chernick, E. T.; Wasielewski, M. R. *J. Am. Chem. Soc.* **2004**, *126*, 2326-2327.
(280) Rozenshtein, V.; Berg, A.; Stavitski, E.; Levanon, H.; Franco, L.; Corvaja, C. *J. Phys. Chem. A* **2005**, *109*, 11144-11154.
(281) Chernick, E. T.; Mi, Q. X.; Kelley, R. F.; Weiss, E. A.; Jones, B. A.; Marks, T. J.; Ratner, M. A.; Wasielewski, M. R. *J. Am. Chem. Soc.* **2006**, *128*, 4356-4364.
(282) Colvin, M. T.; Smeigh, A. L.; Giacobbe, E. M.; Conron, S. M. M.; Ricks, A. B.; Wasielewski, M. R. *J. Phys. Chem. A* **2011**, *115*, 7538-7549.
(283) Colvin, M. T.; Carmieli, R.; Miura, T.; Richert, S.; Gardner, D. M.; Smeigh, A. L.; Dyar, S. M.; Conron, S. M.; Ratner, M. A.; Wasielewski, M. R. *J. Phys. Chem. A* **2013**, *117*, 5314-5325.
(284) Farnum, D. G.; Mehta, G.; Moore, G. G. I.; Siegal, F. P. *Tetrahedron Lett.* **1974**, 2549-2552.
(285) Hao, Z. M.; Iqbal, A. *Chem. Soc. Rev.* **1997**, *26*, 203-213.
(286) Lenz, R.; Wallquist, O. *Surface Coatings International Part B: Coatings Transactions* **2002**, *85*, 19-26.
(287) Wallquist, O.; Lenz, R. *Macromol. Symp.* **2002**, *187*, 617-629.
(288) M. A. Naik, S. P. *J. Polym. Sci.* **2013**.
(289) Qu, S. Y.; Tian, H. *Chem. Commun.* **2012**, *48*, 3039-3051.
(290) Fukuda, M.; Kodama, K.; Yamamoto, H.; Mito, K. *Dyes Pigm.* **2004**, *63*, 115-125.
(291) Guo, E. Q.; Ren, P. H.; Zhang, Y. L.; Zhang, H. C.; Yang, W. J. *Chem. Commun.* **2009**, 5859-5861.
(292) Bijleveld, J. C.; Zoombelt, A. P.; Mathijssen, S. G. J.; Wienk, M. M.; Turbiez, M.; de Leeuw, D. M.; Janssen, R. A. J. *J. Am. Chem. Soc.* **2009**, *131*, 16616-16617.
(293) Bronstein, H.; Chen, Z. Y.; Ashraf, R. S.; Zhang, W. M.; Du, J. P.; Durrant, J. R.; Tuladhar, P. S.; Song, K.; Watkins, S. E.; Geerts, Y.; Wienk, M. M.; Janssen, R. A. J.; Anthopoulos, T.; Sirringhaus, H.; Heeney, M.; McCulloch, I. *J. Am. Chem. Soc.* **2011**, *133*, 3272-3275.
(294) Ashraf, R. S.; Chen, Z. Y.; Leem, D. S.; Bronstein, H.; Zhang, W. M.; Schroeder, B.; Geerts, Y.; Smith, J.; Watkins, S.; Anthopoulos, T. D.; Sirringhaus, H.; de Mello, J. C.; Heeney, M.; McCulloch, I. *Chem. Mater.* **2011**, *23*, 768-770.
(295) Beyerlein, T.; Tieke, B. *Macromol. Rapid Commun.* **2000**, *21*, 182-189.
(296) Tamayo, A. B.; Walker, B.; Nguyen, T. Q. *J. Phys. Chem. C* **2008**, *112*, 11545-11551.
(297) Zhou, E. J.; Yamakawa, S. P.; Tajima, K.; Yang, C. H.; Hashimoto, K. *Chem. Mater.* **2009**, *21*, 4055-4061.
(298) Kanimozhi, C.; Balraju, P.; Sharma, G. D.; Patil, S. *J. Phys. Chem. B* **2010**, *114*, 3095-3103.
(299) Qu, S. Y.; Wu, W. J.; Hua, J. L.; Kong, C.; Long, Y. T.; Tian, H. *J. Phys. Chem. C* **2010**, *114*, 1343-1349.
(300) Karsten, B. P.; Bouwer, R. K. M.; Hummelen, J. C.; Williams, R. M.; Janssen, R. A. J. *Photochem. Photobiol. Sci.* **2010**, *9*, 1055-1065.
(301) Welterlich, I.; Charov, O.; Tieke, B. *Macromolecules* **2012**, *45*, 4511-4519.
(302) Qu, S. Y.; Qin, C. J.; Islam, A.; Wu, Y. Z.; Zhu, W. H.; Hua, J. L.; Tian, H.; Han, L. Y. *Chem. Commun.* **2012**, *48*, 6972-6974.
(303) Qu, S. Y.; Wang, B.; Guo, F. L.; Li, J.; Wu, W. J.; Kong, C.; Long, Y. T.; Hua, J. L. *Dyes Pigm.* **2012**, *92*, 1384-1393.
(304) Muci, A. R.; Buchwald, S. L. *Topp. Curr. Chem.* **2002**, *219*, 131-209.
(305) Surry, D. S.; Buchwald, S. L. *Chem. Sci.* **2011**, *2*, 27-50.
(306) Hirao, Y.; Ino, H.; Ito, A.; Tanaka, K.; Kato, T. *J. Phys. Chem. A* **2006**, *110*, 4866-4872.
(307) Nicolaou, K. C.; Bulger, P. G.; Sarlah, D. *Angew. Chem., Int. Ed.* **2005**, *44*, 4442-4489.
(308) Yin; Liebscher, J. *Chem. Rev.* **2006**, *107*, 133-173.

(309) Chinchilla, R.; Nájera, C. *Chem. Rev.* **2007**, *107*, 874-922.
(310) Hassan, J.; Sévignon, M.; Gozzi, C.; Schulz, E.; Lemaire, M. *Chem. Rev.* **2002**, *102*, 1359-1470.
(311) Beletskaya, I. P.; Cheprakov, A. V. *Coord. Chem. Rev.* **2004**, *248*, 2337-2364.
(312) Monnier, F.; Taillefer, M. *Angew. Chem., Int. Ed.* **2009**, *48*, 6954-6971.
(313) Miyaura, N.; Suzuki, A. *J. Chem. Soc., Chem. Commun.* **1979**, *0*, 866-867.
(314) Miyaura, N.; Suzuki, A. *Chem. Rev.* **1995**, *95*, 2457-2483.
(315) Heckmann, A. *Diploma Thesis* **2004**, *University of Würzburg*.
(316) Holzapfel, M. *Dissertation* **2007**, *University of Würzburg*.
(317) Andersen, J.; Bolvig, S.; Liang, X. *Synlett* **2005**, *19*, 2941-2947.
(318) Andersen, J.; Madsen, U.; Björkling, F.; Liang, X. *Synlett* **2005**, *14*, 2209-2213.
(319) Shafir, A.; Power, M. P.; Whitener, G. D.; Arnold, J. *Organometallics* **2000**, *19*, 3978-3982.
(320) Tennyson, A. G.; Khramov, D. M.; Varnado, C. D.; Creswell, P. T.; Kamplain, J. W.; Lynch, V. M.; Bielawski, C. W. *Organometallics* **2009**, *28*, 5142-5147.
(321) McNulty, J.; Keskar, K. *Eur. J. Org. Chem.* **2012**, *2012*, 5462-5470.
(322) Andersen, J.; Bolvig, S.; Liang, X. F. *Synlett* **2005**, 2941-2947.
(323) Connelly, N. G.; Geiger, W. E. *Chem. Rev.* **1996**, *96*, 877-910.
(324) Wei, Y.; Chen, C. T. *J. Am. Chem. Soc.* **2007**, *129*, 7478-7479.
(325) Björnestedt, R.; Zhong, G. F.; Lerner, R. A.; Barbas, C. F. *J. Am. Chem. Soc.* **1996**, *118*, 11720-11724.
(326) Kizuka, H.; Hanson, R. N. *J. Med. Chem.* **1987**, *30*, 722-726.
(327) Yin, J. J.; Buchwald, S. L. *J. Am. Chem. Soc.* **2002**, *124*, 6043-6048.
(328) Ishiyama, T.; Murata, M.; Miyaura, N. *J. Org. Chem.* **1995**, *60*, 7508-7510.
(329) Cao, D. R.; Liu, Q. L.; Zeng, W. J.; Han, S. H.; Peng, J. B.; Liu, S. P. *J. Polym. Sci.* **2006**, *44*, 2395-2405.
(330) Rabindranath, A. R.; Zhu, Y.; Heim, I.; Tieke, B. *Macromolecules* **2006**, *39*, 8250-8256.
(331) Zhu, Y.; Rabindranath, A. R.; Beyerlein, T.; Tieke, B. *Macromolecules* **2007**, *40*, 6981-6989.
(332) Gilchrist, T. L.; Gymer, G. E.; Rees, C. W. *J. Chem. Soc., Perkin Trans. 1* **1975**, 1-8.
(333) Gilchrist, T. L.; Rees, C. W.; Thomas, C. *J. Chem. Soc., Perkin Trans. 1* **1975**, 8-11.
(334) Winnewisser, M.; Vogt, J.; Ahlbrecht, H. *J. Chem. Res., Synop.* **1978**, 298-299.
(335) Tyrkov, A. G.; Solov'ev, N. A.; Ladyzhnikova, T. D.; Altukhov, K. V. *Russ. J. Org. Chem.* **2004**, *40*, 1151-1155.
(336) da Silva, G.; Bozzelli, J. W. *J. Org. Chem.* **2008**, *73*, 1343-1353.
(337) Burgess, E. M.; Carithers, R.; McCullagh, L. *J. Am. Chem. Soc.* **1968**, *90*, 1923-1924.
(338) Evans, D. F. *J. Chem. Soc.* **1959**, 2003-2005.
(339) Kreilick, R. W. *J. Chem. Phys.* **1966**, *45*, 1922-1924.
(340) Kreilick, R. W. *J. Chem. Phys.* **1967**, *46*, 4260-4264.
(341) Schwarzhans, K. E. *Angew. Chem., Int. Ed. Engl.* **1970**, *9*, 946-953.
(342) Gillies, E.; Szarek, W. A.; Baird, M. C. *Can. J. Chem.* **1971**, *49*, 211-216.
(343) Petillo, P. A.; Defelippis, J.; Nelsen, S. F. *J. Org. Chem.* **1991**, *56*, 6496-6497.
(344) Machonkin, T. E.; Westler, W. M.; Markley, J. L. *Inorg. Chem.* **2005**, *44*, 779-797.
(345) Rastrelli, F.; Bagno, A. *Chem.–Eur. J.* **2009**, *15*, 7990-8004.
(346) Drexhage, K. H. *J. Res. Natl. Bur. Stand. Sec. A* **1976**, *80*, 421-428.
(347) Rurack, K.; Spieles, M. *Anal. Chem.* **2011**, *83*, 1232-1242.
(348) Würth, C.; Pauli, J.; Lochmann, C.; Spieles, M.; Resch-Genger, U. *Anal. Chem.* **2011**, *84*, 1345-1352.
(349) Bao, D. D.; Millare, B.; Xia, W.; Steyer, B. G.; Gerasimenko, A. A.; Ferreira, A.; Contreras, A.; Vullev, V. I. *J. Phys. Chem. A* **2009**, *113*, 1259-1267.
(350) Heckmann, A.; Lambert, C. *Unpublished results*.
(351) Verschoor-Kirss, M.; Kreisz, J.; Feighery, W.; Reiff, W. M.; Frommen, C. M.; Kirss, R. U. *J. Organomet. Chem.* **2009**, *694*, 3262-3269.
(352) Neunhöffer, O.; Heitmann, P. *Chem. Ber.* **1959**, *92*, 245-251.
(353) Prins, R. *J. Chem. Soc., Chem. Commun.* **1970**, 280-281.
(354) Prins, R. *Mol. Phys.* **1970**, *19*, 603-620.

(355) Haymond, S.; Zak, J. K.; Show, Y.; Butler, J. E.; Babcock, G. T.; Swain, G. M. *Anal. Chim. Acta* **2003**, *500*, 137-144.
(356) Quintal, S.; Fedi, S.; Barbetti, J.; Pinto, P.; Felix, V.; Drew, M. G. B.; Zanello, P.; Calhorda, M. J. *J. Organomet. Chem.* **2011**, *696*, 2142-2152.
(357) Gierschner, J.; Cornil, J.; Egelhaaf, H. J. *Adv. Mater.* **2007**, *19*, 173-191.
(358) Malagoli, M.; Bredas, J. L. *Chem. Phys. Lett.* **2000**, *327*, 13-17.
(359) de Leon, N. P.; Liang, W. J.; Gu, Q.; Park, H. *Nano Lett.* **2008**, *8*, 2963-2967.
(360) Kutala, V. K.; Villamena, F. A.; Ilangovan, G.; Maspoch, D.; Roques, N.; Veciana, J.; Rovira, C.; Kuppusamy, P. *J. Phys. Chem. B* **2008**, *112*, 158-167.
(361) Yordanov, N. D. *Appl. Magn. Reson.* **1996**, *10*, 339-350.
(362) Reitzenstein, D. *Dissertation* **2010**, *University of Würzburg*.
(363) Johns, G.; Ransom, C. J.; Reese, C. B. *Synthesis* **1976**, 515-516.

9 Table of Formulas

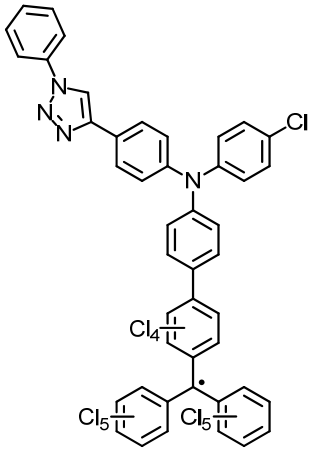

1

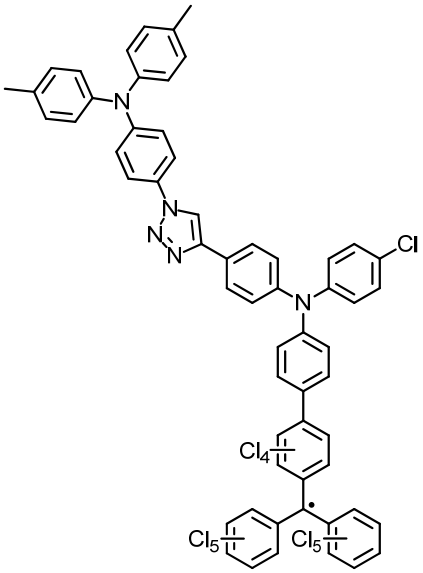

2

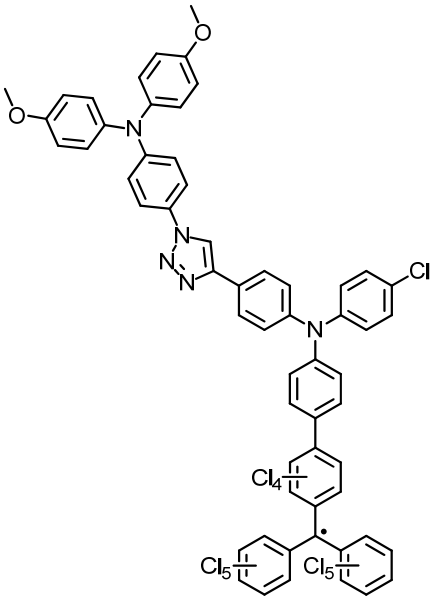

3

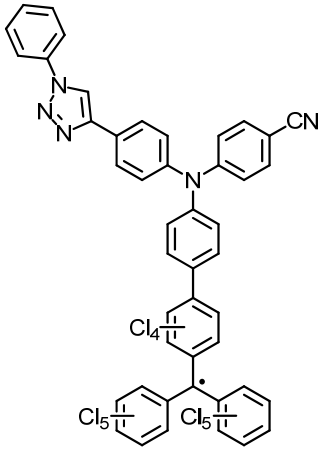

4

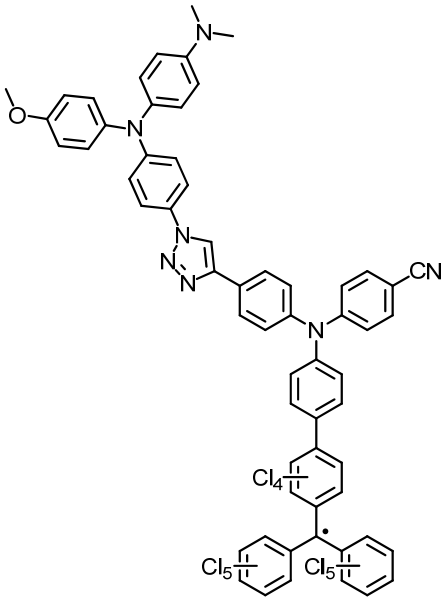

5

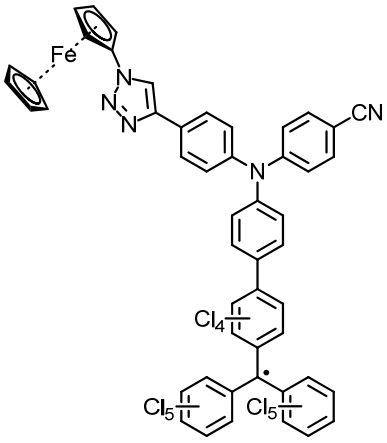

6

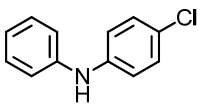

7

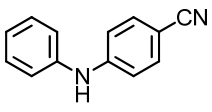

8

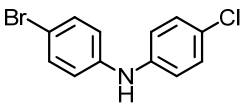

9

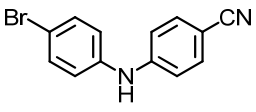

10

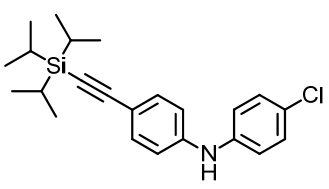

11

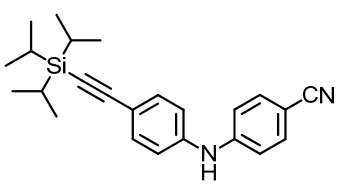

12

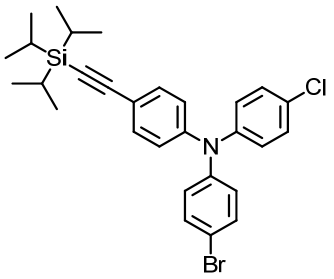

13

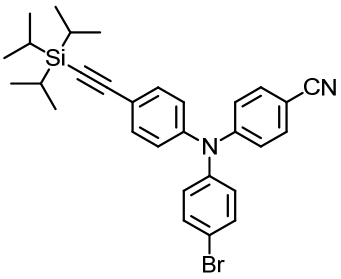

14

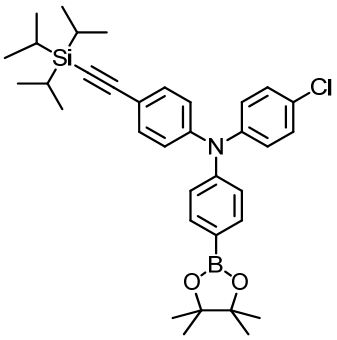

15

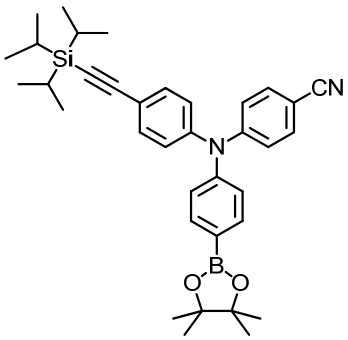

16

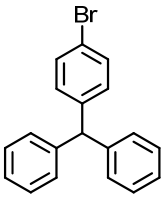

17

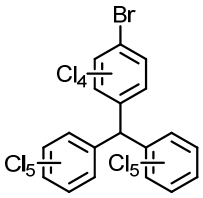

18

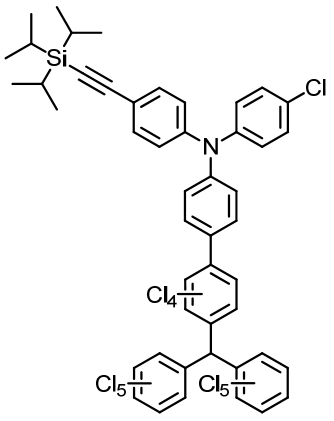

19

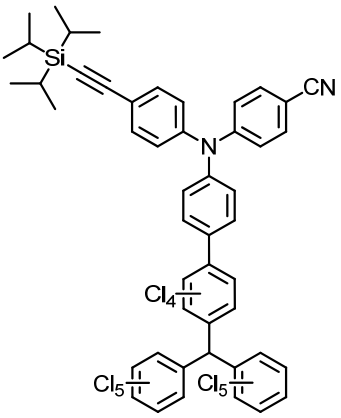

20

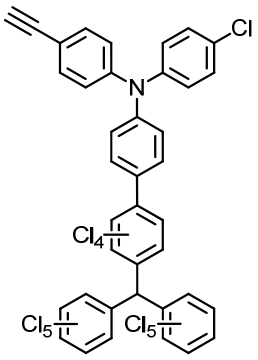

21

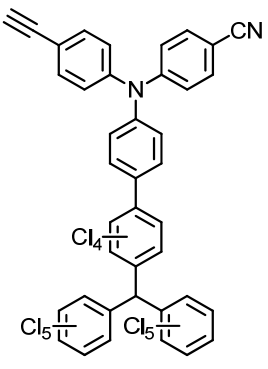

22

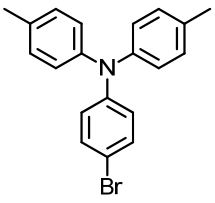

23

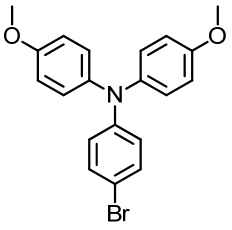

24

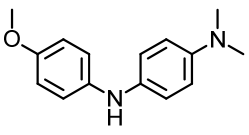

25

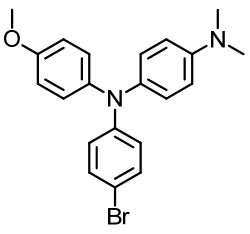

26

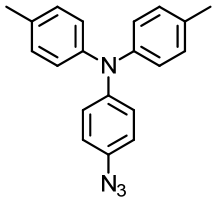

27

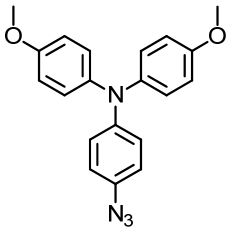

28

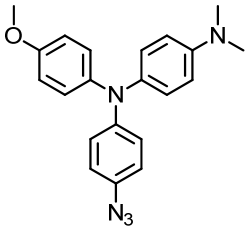

29

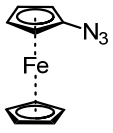

30

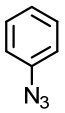

31

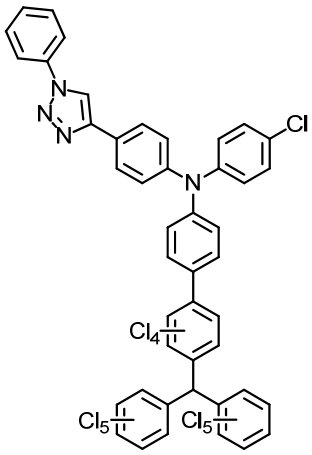

32

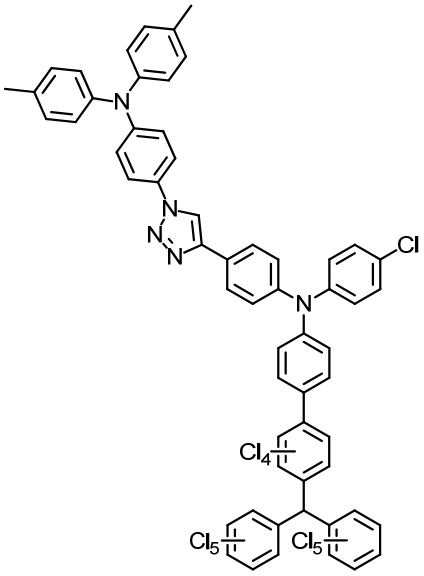

33

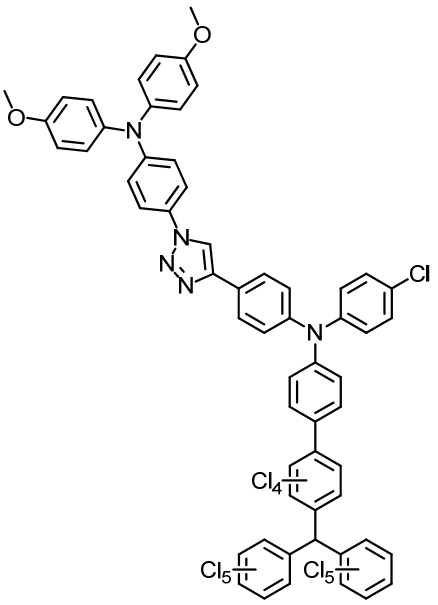

34

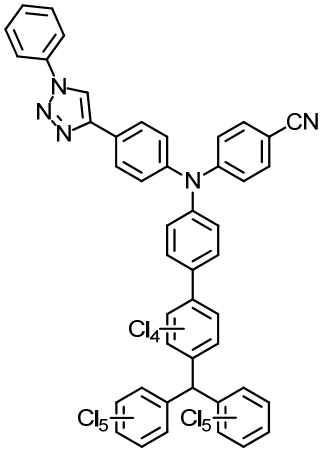

35

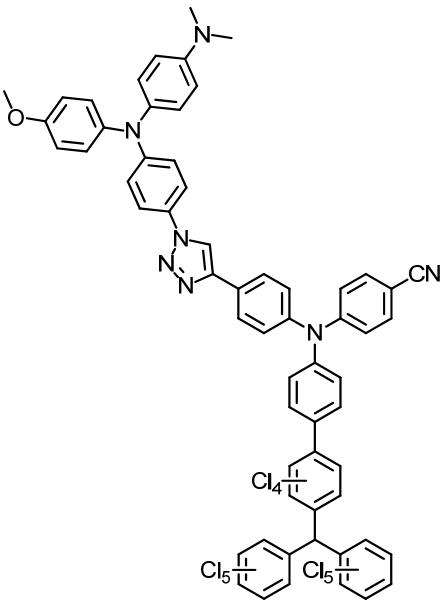

36

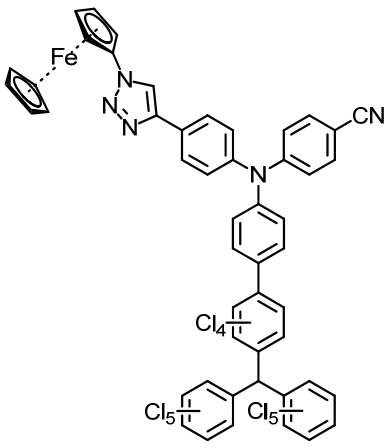

37

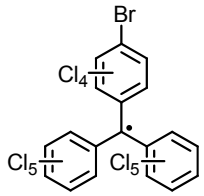

38

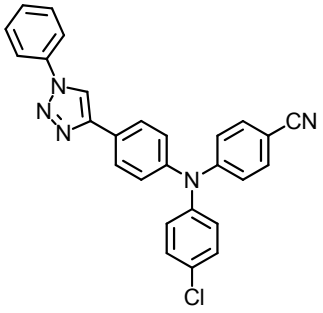

39

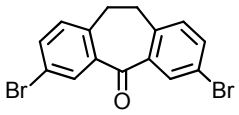

40

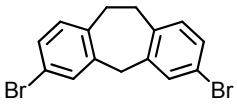

41

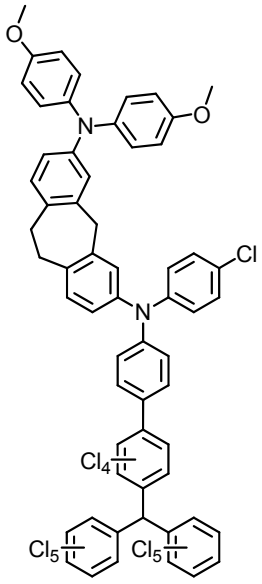

43

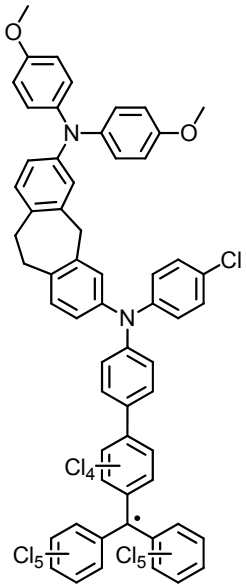

44

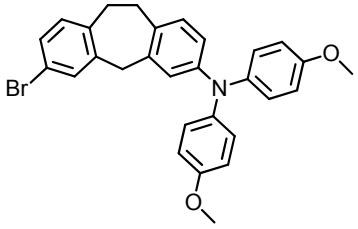

42

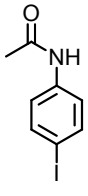

45

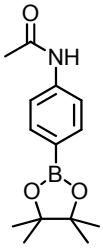

46

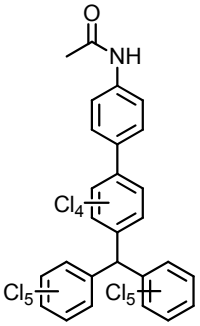

47

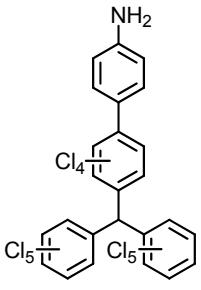

48

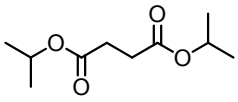

49

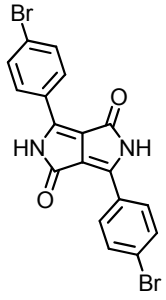

50

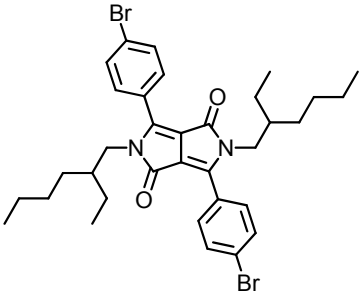

51

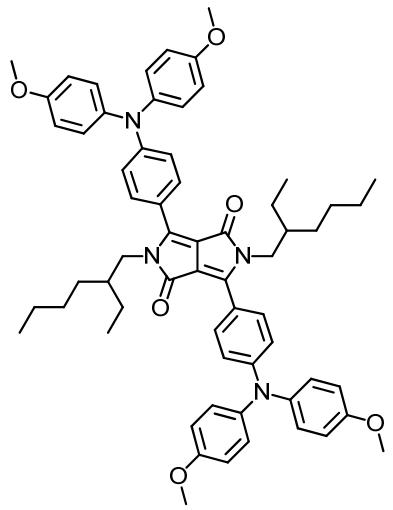

52

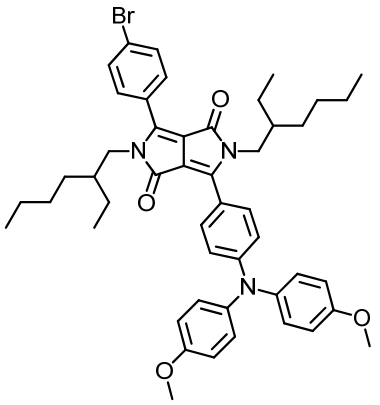

53

10 Zusammenfassung

Im Rahmen dieser Arbeit wurde eine Reihe von Redox-Kaskaden, Verbindungen **2**, **3**, **5** und **6** synthetisiert und hinsichtlich ihrer photophysikalischen und elektrochemischen Eigenschaften untersucht. In nahezu allen Kaskaden kamen der perchlorierte Triphenylmethyl(PCTM)-Radikal-Akzeptor (A) sowie zwei Triarylamin-Donoren (D1 und D2) zum Einsatz. Zusätzlich wurden eine Kaskade, bestehend aus einem Triarylamin-Donor (D1) und einem Ferrocen-Donor (D2), sowie zwei Referenzverbindungen **1** und **4**, mit dem perchlorierten Triphenylmethyl-Radikal-Akzeptor und einem Triarylamin-Donor hergestellt. Die gezielte Veränderung des Redoxpotentials der Triarylamine durch geeignete Wahl der Substituenten in *p*-Position ermöglichte den Aufbau eines gerichteten Redoxgradienten innerhalb der Kaskaden. Die Verknüpfung des PCTM-Radikal-Akzeptors A mit dem Triarylamin-Donor D1 wurde durch eine Biphenyl-Brücke erreicht, die mittels einer Pd-katalysierten Kreuz-Kupplung hergestellt wurde. Die nahezu rechtwinklige Orientierung der Ringe innerhalb der Biphenyl-Einheit garantiert hierbei eine kleine elektronische Kopplung zwischen A und D1. In den Kaskaden **2**, **3**, **5** und **6** wurde die Verknüpfung von D1 und D2 mit Hilfe einer 1,2,3-Triazol-Brücke bewerkstelligt, die mittels Click-Chemie aufgebaut wurde. Der PCTM-Radikal-Akzeptor wurde im letzten Schritt der Synthese durch Radikalisierung der entsprechenden *α*-H-Vorstufen erzeugt. Da in diesem Schritt während der ersten Reaktionsversuche keine zufriedenstellenden Ergebnisse erreicht werden konnten, wurde die Reaktion hinsichtlich Reaktanten, Lösungsmitteln sowie Reaktionsbedingungen optimiert um einen quantitativen Radikalisierungsprozess zu gewährleisten.

Die Absorptionsspektren der Verbindungen **1** – **6** zeigten sowohl die charakteristischen Banden der Triarylamine als auch des PCTM-Radikal-Akzeptors. Zusätzlich wies das Vorhandensein von IVCT-Banden im NIR-Bereich des Spektrums auf die Bevölkerung eines ^{2}CT-Zustandes zwischen A und D1 hin. Die IVCT-Banden wiesen eine schwache, unsystematische Abhängigkeit von der Lösungsmittelpolarität auf. Eine schwache bis mäßige Emission konnte für alle Verbindungen im NIR-Bereich in Cyclohexan beobachtet werden. Zuverlässlige Ergebnisse aus Messungen in polareren Lösungsmitteln konnten nicht erhalten werden, da die Emission hier deutlich schwächer und stark bathochrom verschoben war. Im Falle von **5** und **6** wurde die Fluoreszenz zusätzlich durch einen Loch-Transfer von D1 nach D2 gelöscht, der in einem ladungsgetrennten Zustand resultierte. Mittels Cyclovoltammetrie konnte der gerichtete Redoxgradient der Kaskaden bestätigt werden. Spektroelektrochemische Untersuchungen lieferten Ergebnisse hinsichtlich der spektroskopischen Eigenschaften der oxidierten und reduzierten Spezies aller Verbindungen.

Diese Ergebnisse wurden zur Interpretation der Transienten-Absorptionsspektroskopie benötigt, welche im ns- als auch im fs-Bereich durchgeführt wurde. Messungen im ns-Bereich

wurden im sichtbaren Bereich des Spektrums durchgeführt. Im Rahmen der Messungen im fs-Bereich wurden sowohl der sichtbare Bereich, als auch der NIR-Bereich untersucht. Spektren, die einzelnen Spezies zugeordnet werden können wurden mittels Entfaltung der Messungen erhalten. Allerdings war eine genaue Zuordnung der einzelnen Spektren zu bestimmten Spezies nicht immer möglich. Die Spektren der transienten Absorption zeigten jedoch, dass der gewünschte Loch-Transfer in den Kaskaden von D1 zu D2 stark von der Lösungsmittelpolarität und der Größe des Redoxgradienten abhängt. In stark polaren Solventien (Benzonitril) war die Population des ^{2}CS-Zustandes für alle Kaskaden zu beobachten. Dies steht im Gegensatz zu den Messungen in unpolaren Lösungsmitteln (Cyclohexan, Toluol), in denen der ^{2}CS-Zustand nur in Verbindungen bevölkert wurde, die einen Redox-Gradienten > 480 mV besitzen, was für **5** und **6** zutrifft. Die Prozesse der Ladungstrennung fanden für **1** – **6** im fs- bis ps-Bereich statt. Die Ladungsrekombination lag für alle Verbindungen im ps-Bereich, mit Ausnahme von Verbindung **5** in Benzonitril, die einen Wert von 3.0 ns aufwies. Die kurzen Zeiten für die Ladungsrekombination zeigen, dass weder Effekte durch Prozesse in der *Marcus*-invertierten Region noch Spin-Korrelation eine Rolle für die Ladungstransfer-Dynamik spielen. Aus diesem Grund, wird angenommen, dass die Dynamik größtenteils von der elektronischen Kopplung abhängig ist.

Appendix

Time Decay Curves (Emission Spectroscopy)

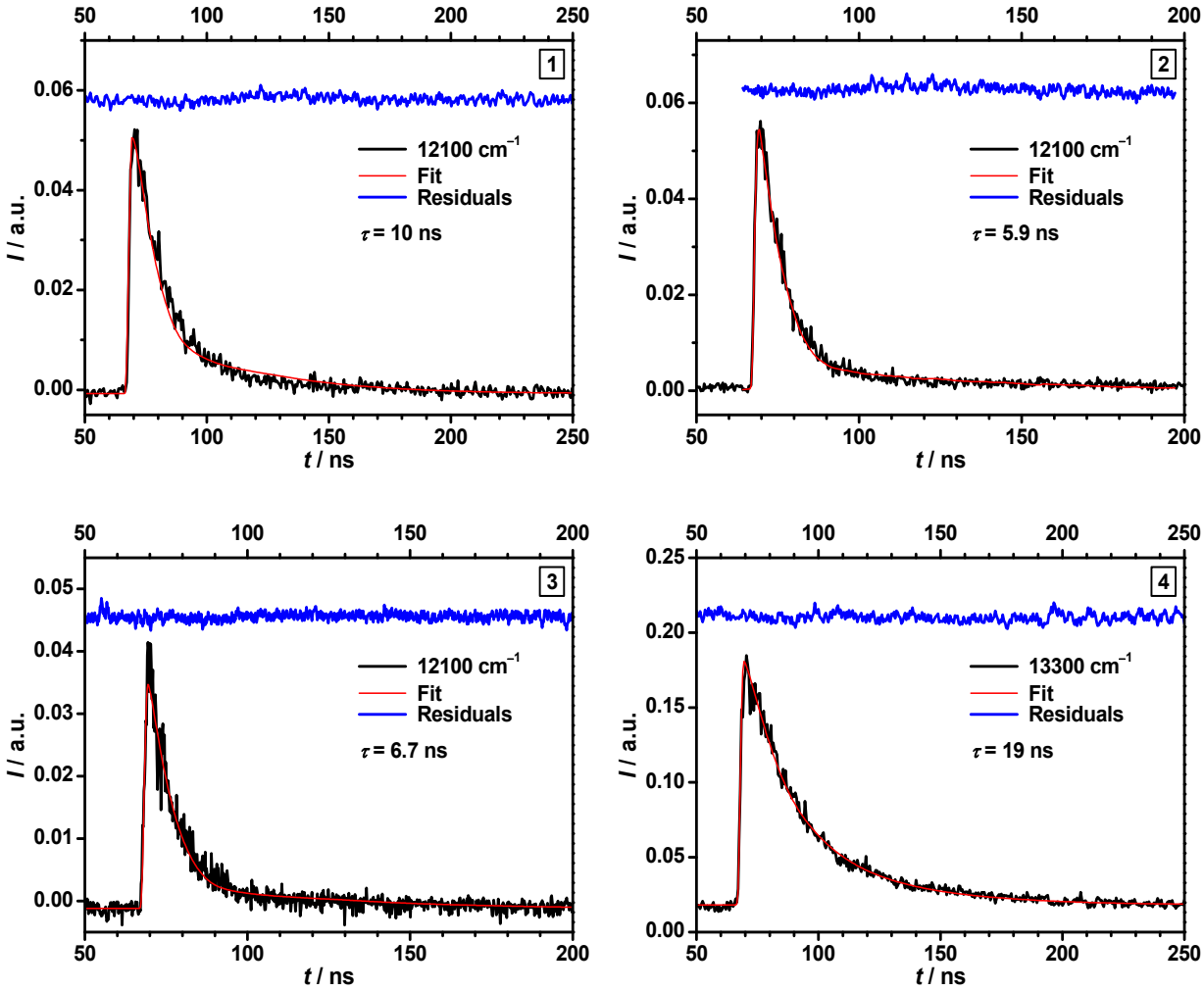

Figure A.1: Emission decay curves of compounds 1 – 4 and corresponding monoexponential fits. All measurements were performed in cyclohexane.

Time Decay Curves (ns-Transient Absorption Spectroscopy)

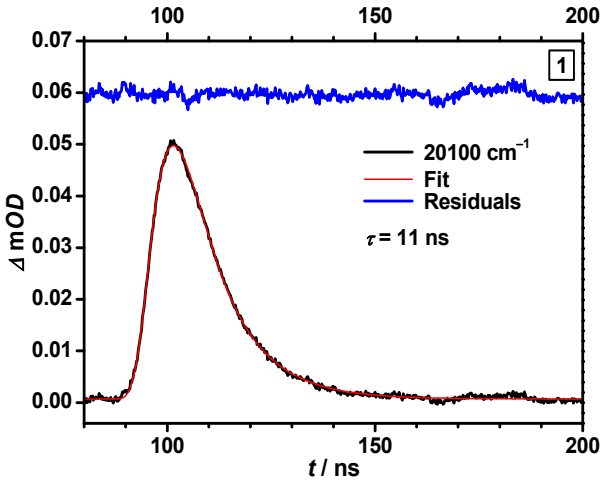

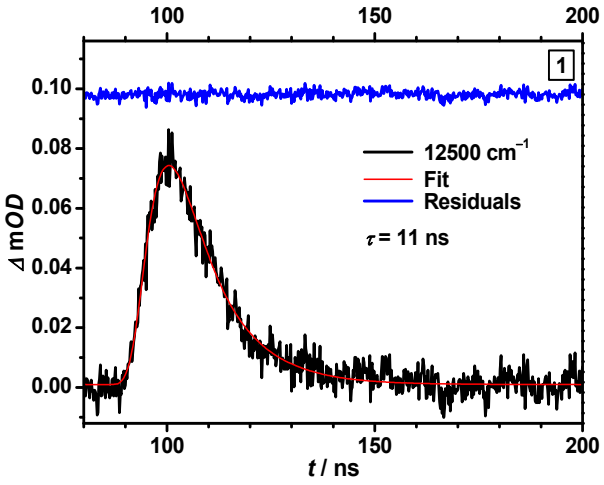

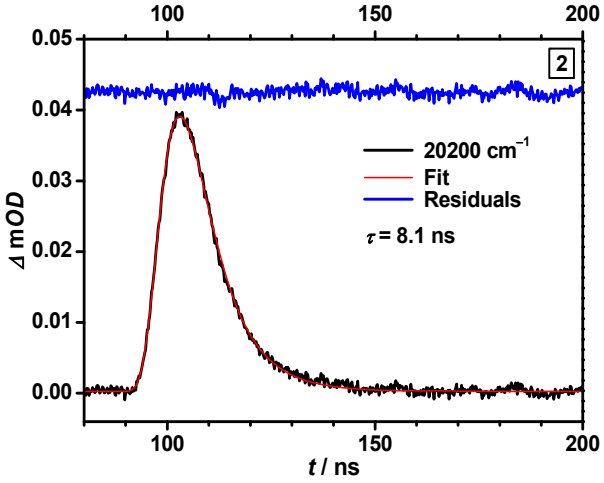

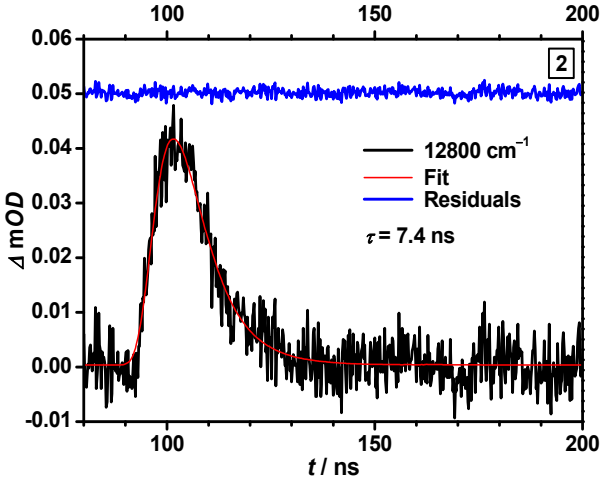

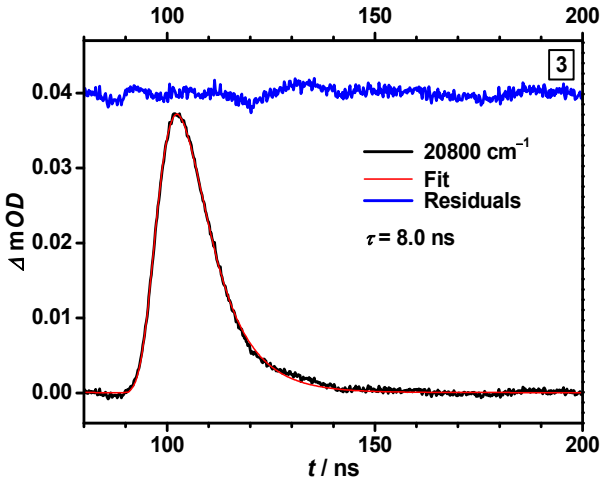

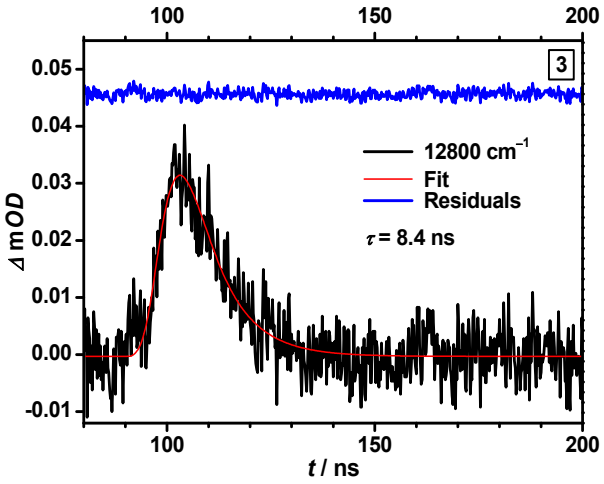

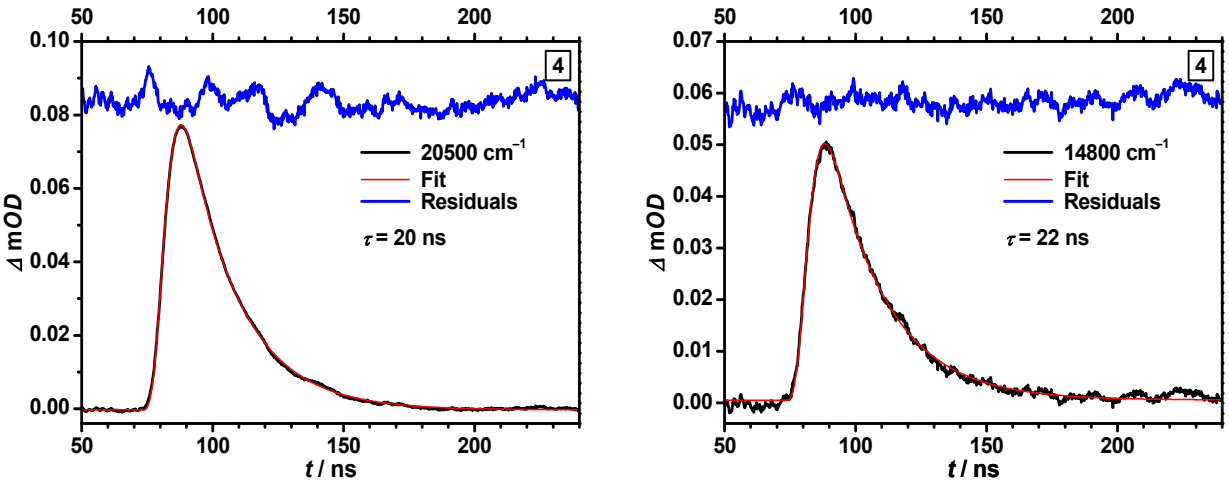

Figure A.2: Transient absorption decay curves of compounds 1 – 4 and corresponding monoexponential fits. All measurements were performed in cyclohexane.